MODELLING THE CIRCULATION AND SEDIMENT DISTRIBUTION IN THE ATHABASCA DELTA AREA

by

R. A. Harrington

Civil Engineering Department
Alberta Research Council

for

Research Management Division

Alberta Environment

RMD 81/23

September 1982

Alberta Research Council
Contribution Series No. 1183

TABLE OF CONTENTS

LIST OF TABLES

LIST OF FIGURES

Page

ABSTRACT

This project undertook an assessment of the potential for using satellite imagery to determine water quality parameters in the southwest end of Lake Athabasca and to provide a mathematical model capable of simulating the circulation patterns in this area of the lake. A substantial amount of field data was collected for calibration purposes and served to ellucidate some of the hydraulic characteristics of the study area.

The results indicated that water from the Athabasca River and its distributary channels could reach the north shore of the lake under conditions of moderately large inflow. It had been previously assumed that penetration of river water so far into the lake was unlikely. In addition, river water was found to extend up to at least 20 km northeast of the distributary channels. Water from the Embarras River and Fletcher Channel generally leaves the lake via the Chenal des Quatres Fourches while water from Big Point Channel generally discharges through the Riviere des Rochers.

Correlation of LANDSAT imagery with contemporaneous water quality data yielded a high correlation between suspended sediment concentrations and band 6 digital response values. No other water quality parameters were correlated with the raw LANDSAT data. Principal component analysis of the satellite data indicated a high correlation between suspended sediment and the first principal component, which emphasized the infrared bands. In addition, conductivity was well correlated with the third principal component, which emphasized the difference between the visible bands. This result could prove beneficial in analysing satellite imagery since conductivity is a useful parameter for differentiating between lake and river water.

A finite element model was developed which solves the vertically integrated momentum and continuity equations. Based on an implicit time stepping algorithm, the model was used to generate circulation patterns for an idealized representation of the study area.

ACKNOWLEDGEMENTS

This study was funded by Research Management Division, Alberta Environment and was undertaken as an extension of work previously completed jointly by Northwest Hydraulics Consultants Ltd. and the Alberta Research Council. Throughout the course of the work, advice and consultation were provided by Dr. B.R. Hammond and Mr. D.T. Sneddon of the Research Management Division of Alberta Environment.

Digital analysis of satellite imagery was carried out on a subcontract basis by Dr. G.D. Lodwick of the Division of Surveying Engineering of the University of Calgary with the assistance of Messrs. Steven Paine and Brian Baltis. The subcontractor's report was edited for inclusion herein by the author.

Mr. C.R. Neill of Northwest Hydraulics Consultants Ltd. provided input on a subcontract basis concerning portions of the interpretation of the satellite imagery.

Information and data were provided by the Water Survey of Canada offices in Calgary and Regina and by Technical Services Division, Alberta Environment. Mr. D. Hadler of Alberta Environment, Fort McMurray, provided equipment and logistical support for the winter dye test.

Special thanks are owed to Mr. Scott Flett and the staff of the Alberta Environment office, Fort Chipewyan, for the assistance provided throughout the course of the field operations.

The project could not have been successful without the efforts of T.P. Ridgway, J.H. Thompson, B. Trevor, P.M. Mostert, and G.D. Legge in collecting field data under conditions often less than ideal.

The report was typed by Ms. J. Merrithew and Mrs. A. Ellendt. Figures were drafted by the Drafting Department of the Alberta Research Council.

I. INTRODUCTION

Development of the Athabasca Oil Sands has resulted in concern regarding the environmental impact such development could have on the Athabasca River, the Peace-Athabasca Delta, and Lake Athabasca. The industrial development associated with oil sands exploitation will significantly increase the potential for the release of contaminants to the Athabasca River and the migration of such substances to the Athabasca Delta and Lake Athabasca. These areas are important both economically (due to the commercial fishery in Lake Athabasca and trapping in the surrounding area) and ecologically (the Peace-Athabasca Delta is a major water fowl staging area and supports several rare or endangered species). Knowledge of the system's response to such potentially adverse stimuli is necessary to assess the impact of various development scenarios on the system, to provide information to assess the adequacy of regulatory guidelines, or to implement appropriate countermeasures, if possible, as a result of an accidental contaminant release.

The spectrum of substances that could be introduced to the Athabasca River system is quite broad and the nature of their possible interactions with the environment is equally varied. Some contaminants may be either suspended or dissolved in the water while others may become attached to the sediment load. The extent to which chemical reaction of a contaminant introduced to the system could affect the impact on the system is largely unknown. Other factors to be ultimately considered are uptake by aquatic flora and fauna leading to increased contaminant concentration in higher levels of the food chain. In addition, loading may vary from gradual seepage from tailing ponds, for example, to sudden releases as could result from accidental spills.

The problem is further compounded by the complexity of the hydraulic system itself. The area comprises the Athabasca River and its several distributary channels in the delta, the southwest end of Lake Athabasca with its two outlet channels, and lakes Mamawi and Claire. The interdependancy of water levels and flow rates and the proximity of Lake Athabasca's inlet and outlet channels combine to present a complicated system to analyse or simulate.

As stated in the original proposal for this project, "Given the complex interactions possible in the system, in terms of both the hydraulics and contaminant-specific processes, it is recognized that the work proposed herein cannot address itself to all aspects of the problem". Previous work (Beltaos, 1978, 1979) has documented the mixing characteristics of the Athabasca River below Fort McMurray. Combined with recent advances in the understanding of longitudinal dispersion in rivers (Beltaos, 1980), it was determined that adequate information existed upstream of the delta area to characterize river-specific mixing processes. The complexity of the actual Athabasca delta area precluded its consideration in this study beyond more than a peripheral manner because of the short (one year) duration of the project. Therefore, attention was focused on the southwest end of Lake Athabasca, as shown in Figure 1. This area is of importance because once contaminants reach the lake it is presently unclear as to how they could be distributed or pass into the Slave River system. Therefore, knowledge of the circulation patterns and sediment distributed in the lake is necessary in order to better estimate the consequences of possible contaminant releases. This was also a logical extension of the work carried out in the previous year for the Alberta Oil Sands Environmental Research Program (AOSERP) (Neill, et al, 1981) which will be described subsequently.

1.1 OBJECTIVES

This project was undertaken to provide the first step in establishing a modelling and assessment capability in the Athabasca delta area and as such, was limited to the southwest end of Lake Athabasca. Two avenues were explored in order to provide these capabilities, with the objectives outlined in the contract being:

1. To provide a calibrated mathematical model capable of predicting the circulation patterns in the southwest end of Lake Athabasca and of indicating concentration distributions under various flow conditions.

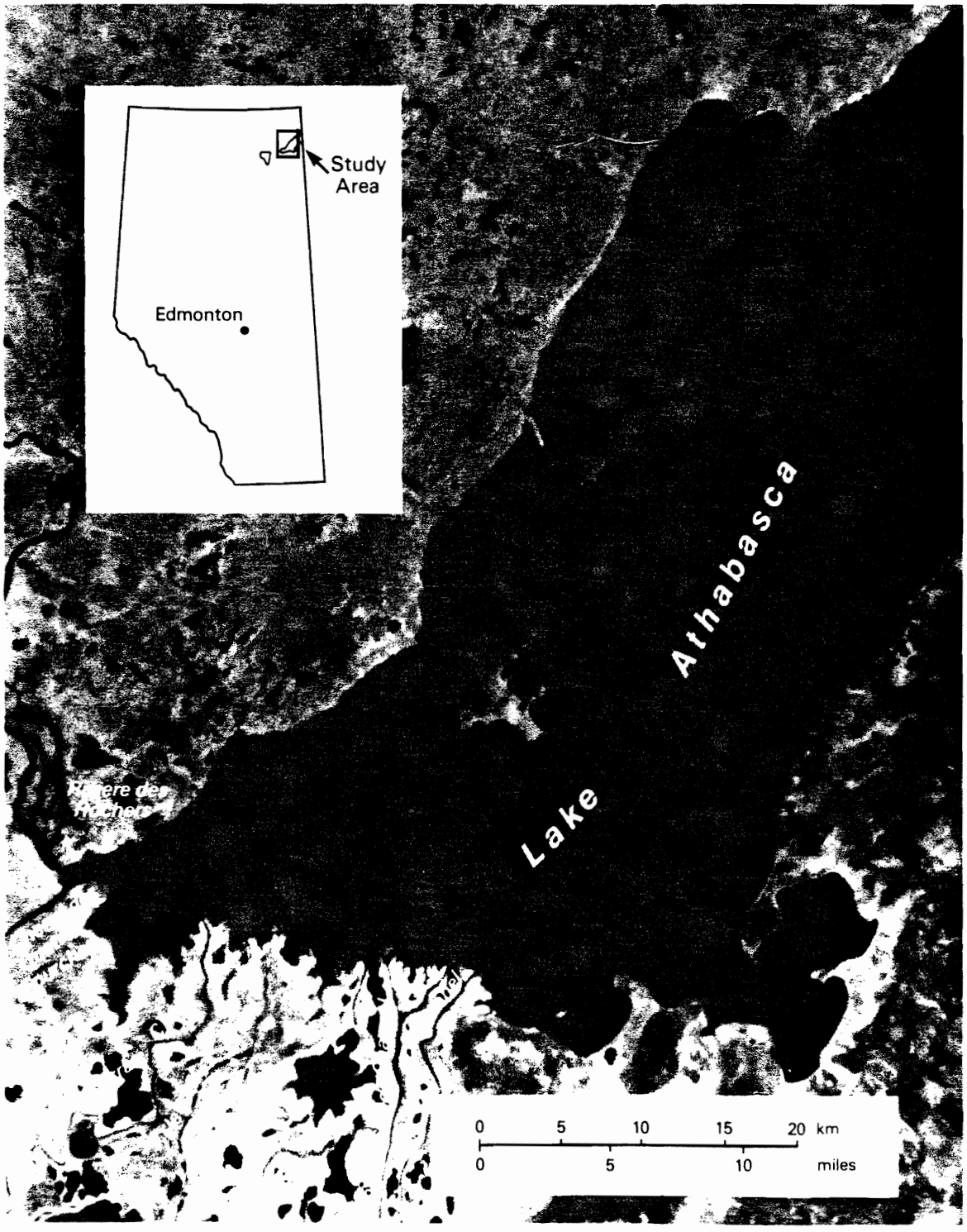

Figure 1. Location of Study Area

2. To relate LANDSAT imagery to water quality parameters, primarily suspended sediment concentrations.

There were three main components to the project, namely collection of field data, analysis of satellite imagery, and development of the mathematical model. Each component of the project will be discussed subsequently in the report.

1.2 SUMMARY OF RELATED STUDIES

Interest in the area, from the point of view of environmental impact, first arose as a result of construction of the Bennett Dam in British Columbia. Dam closure and the resulting regulation of the Peace River resulted in water levels being reduced in the delta area. The Peace-Athabasca Delta Symposium (1971) presented information related to the hydrologic, biologic and socio-economic impacts that arose due to the Peace River regulation. In depth studies were subsequently carried out under the auspices of the Peace-Athabasca Delta Project (1973) and remedial measures were implemented in an attempt to restore lake levels to their pre-regulation means. Further detailed studies have recently been completed as a result of the Slave River Hydro Feasibility Study (1982). All of these studies, as well as that of Sydor, et al (1979) contain some type of model for predicting water levels and flows in the delta area. Since these models are generally of the routing type, detailed circulation patterns in the southwest end of Lake Athabasca are not available. The work of Neill, et al (1981) was undertaken to describe how water and sediment from the Athabasca River are distributed through the delta system. The results included a detailed compilation of data relevant to the system and provided estimates of sediment loading and outflow. The potential of using satellite imagery for determining water quality and circulation patterns was also demonstrated. As a result of this work, the present project was undertaken to further investigate the potential utility of satellite imagery and to provide a mathematical model which could prove useful for detailed examination of processes in the lake.

2. FIELD STUDIES

Field studies were undertaken to provide water quality data contemporaneous with satellite overpasses, to obtain current data required for model calibration and to conduct mixing tests to determine mixing patterns and mixing coefficients. Analysis of previous LANDSAT imagery indicated that during the summer months there was a 25% probability of cloud free conditions during a satellite overpass. As a result, four summer field trips were scheduled such that sampling would coincide with either a LANDSAT 2 or a LANDSAT 3 overpass. In addition, one winter field trip was mounted to conduct a mixing test during ice-covered conditions.

The lake was sampled by boat on a four kilometer grid and samples were analysed in the field for pH, conductivity, temperature and dissolved oxygen using a Hydrolab System 8000 portable water quality device. Vertical profiles of water quality parameters were usually obtained. Samples were taken for subsequent sediment analysis at the surface, as well as 0.3 m and 1.0 m below the surface. Sediment analysis included total suspended solids, volatile (organic) suspended solids, total dissolved solids and volatile dissolved solids. Bed material samples were obtained during one field trip and analysed for grain size distribution. Wind speed and direction were measured at a height of 2 m using a hand held anemometer. Position on the lake was determined using a Motorola Miniranger III radar rangefinder which employed two remote stations and one master transceiver mounted in the sampling boat. The remotes were located on High Island and the top of Point Basse, which enabled coverage of almost the entire study area as shown in Figure 2. In those areas where the radar signal was blocked or where the range of the radar was exceeded, compass bearings were used for positioning. When conditions on the lake were favourable, velocity measurements were made at usually three vertical locations using a Marsh-McBirney model 201 electro-magnetic current meter. Depths were measured using a Raytheon echo sounder. These were the normal measurements carried out during the summer sampling period. Other miscellaneous measurements and the results of the dye tests are described

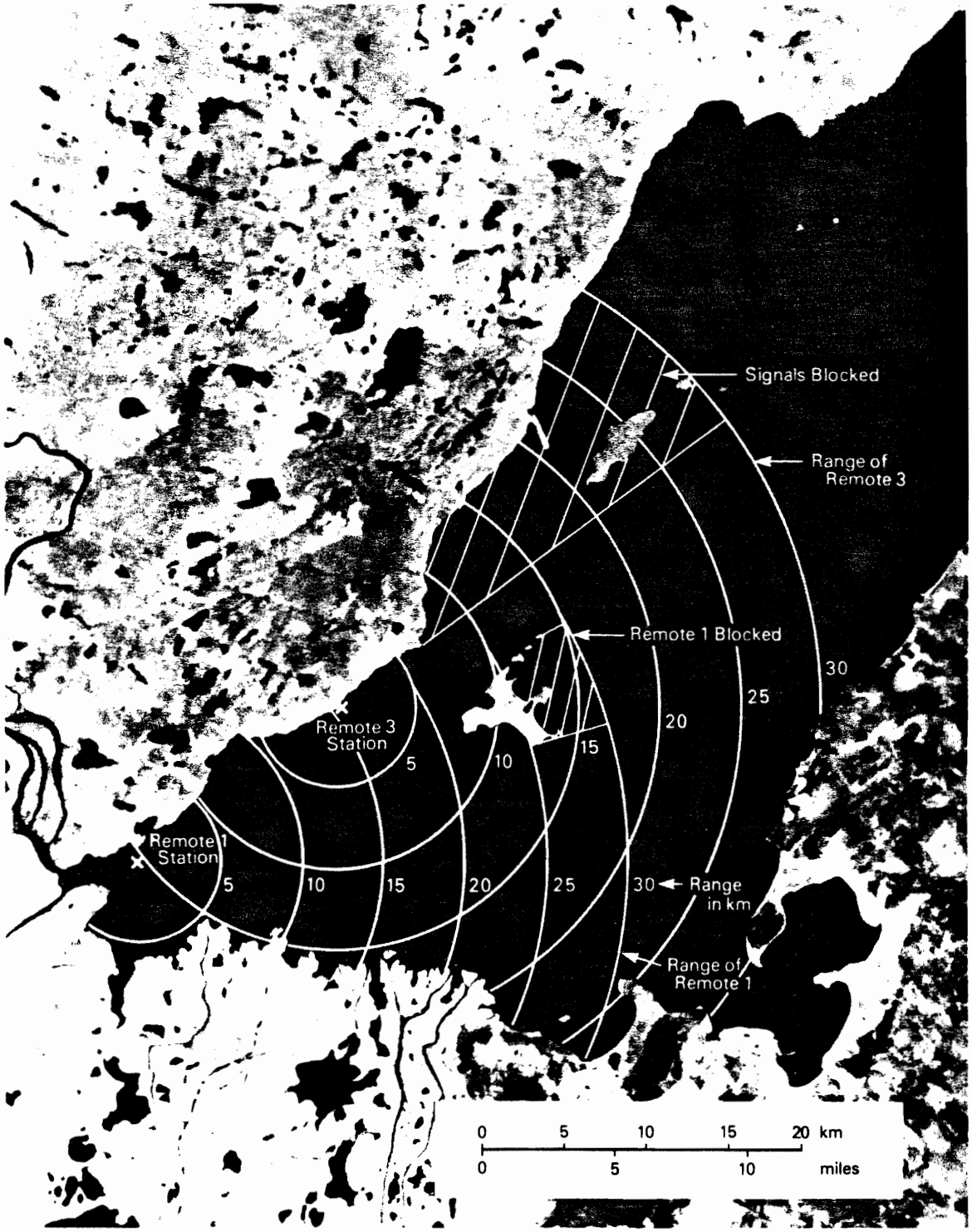

Figure 2. Radar Rangefinder Coverage of Study Area

subsequently. In this section, the results of the field studies are presented and an attempt is made to explain the finding in terms of circulation patterns.

2.1 JUNE 14-19, 1981 MEASUREMENTS

This trip was timed to coincide with a LANDSAT 2 overpass. Because of the northerly location of the study area and the convergence of the meridians of longitude, consecutive satellite passes provide overlapping coverage for three days. Therefore, LANDSAT 2 overpasses occurred on June 16, 17 and 18. Flows in the Athabasca River at Embarras Airport decreased from 1200 m^3/s on June 14 to 997 m^3/s on June 19. The peak flow at Embarras Airport was estimated at 1500 m^3/s on June 9 (Environment Canada, 1982) which represents a return period of under two years (Kellerhals, et al, 1972). Discharge measurements made by Alberta Environment indicated that the flow distribution in the distributary channels, after adjusting to total 100%, were Embarras River:6%, Fletcher Channel:16%, Goose Island Channel:34% and Big Point Channel:44%. These distributions are very similar to those reported by Neill, et al (1981). Inflow from the Fond du Lac River in Saskatchewan decreased from 400 m^3/s on June 12 to 387 m^3/s on June 19. Outflow on the Riviere des Rochers on June 29 was 1402 m^3/s and 252 m^3/s on the Chenal des Quatre Fourches although on June 9 the Chenal des Quatre Fourches was flowing toward the lake at a flow of 133 m^3/s. The difference in flows between the Slave River at Fitzgerald and the Peace River at Peace Point was approximately 1900 m^3/s during this trip so lake outflows exceeded inflow by a small amount. Fond du Lac inflow represented about 21% of the lake outflow while Athabasca River inflows contributed about 73% of outflow.

Water levels at Fort Chipewyan and Bustard Island as well as wind speeds are summarized in Table 1. The wind speeds are the average measured on the lake. In general, winds increased during the day and decreased at night. Results of the water quality sampling are shown in Figure 3 superimposed on a band 7 LANDSAT 2 image taken in August, 1981. An equipment malfunction prevented water quality

Date	June 16	June 17	June 18
Water Level, Fort Chipewyan (m)	208.89	208.84	208.87
Bustard Island (m)	208.91	208.88	208.90
Wind speed and direction at 2 m elevation (m/s)	6-N.E.	7-N.W.	7-W.

Table 1. Water levels and wind speeds, June 1981

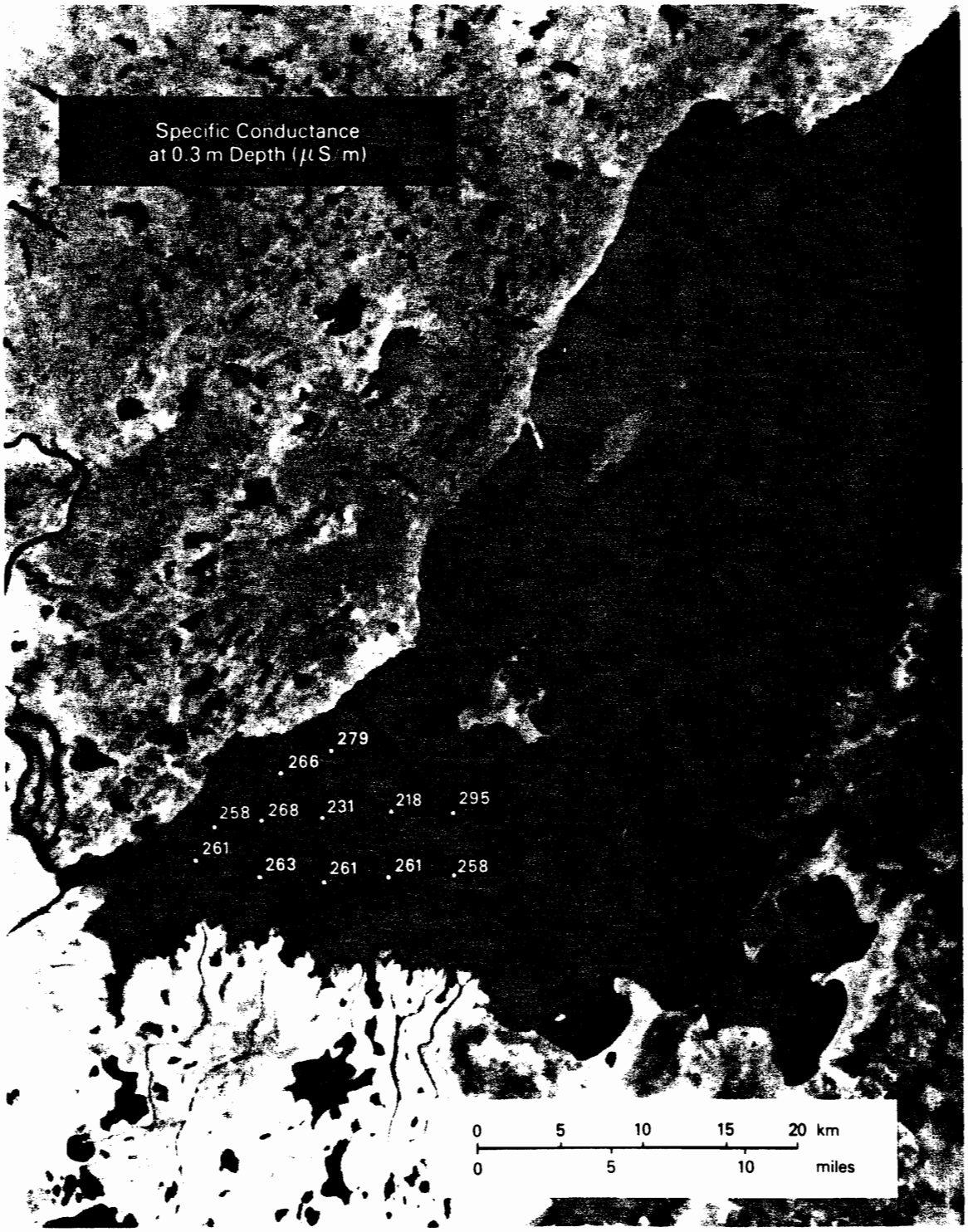

Figure 3. Water Quality Data, June, 1981
(continued in appendix)

measurements in the vicinity of Bustard Island. Values of pH averaged 7.76 with higher values along the delta front and lower values toward the north shore. Although the range in pH values was only 7.58 to 7.91, the variation may reflect the fact that water from the Athabasca River tends to be more alkaline than lake water typified by the Fond du Lac River inflow and consequently exhibits a higher pH.

The average temperature was 15.5° C ranging from 14.9° C to 16.9° C. Maximum temperatures occurred along the delta front and probably reflect the increased heating due to the shallow depths. The average dissolved oxygen level was 8.34 mg/L with a range of 8.15 to 8.95 mg/L. This is about 83% of the saturation level based on the average temperature. As with the previous measurements, higher values tended to occur along the delta front and are probably due to the fact that Athabasca River water would be expected to have higher dissolved oxygen levels than the lake water.

The conductivity data do not appear to exhibit any delineation between river and lake water. The average value was 261 µS/cm ranging from 218 to 295 µS/cm. This is in contrast with the results of Neill, et al (1981) and Seidner (1979) whose data indicated that specific conductance was useful in approximating the interface between lake and river water. Since outflow exceeded inflow, one might expect a clearer demarcation between the two water sources. However, the week before sampling, inflow averaged 1850 m^3/s while outflow averaged 1470 m^3/s. Under these circumstances it would be anticipated that river water could be found almost to the north shore and no large differentiation in water quality in the lake would be expected, especially since the Chenal des Quatre Fourches was flowing toward the lake. Since detention times average four days in the southwest end of the lake, it would not be unreasonable to expect river water which had reached the north shore to gradually become entrained in the outflow as the proportion of lake water in the outflow increased. The conductivity data of Figure 3, although limited in extent, tend to lend credence to this hypothesis since higher concentrations are found on the north shore, perhaps indicating gradual release of river water. The pH measurements also show high values along the delta, low values

in the central portion of the lake and intermediate values on the north shore which could be due to the gradual mixing of river and lake water on the north shore.

The suspended sediment data in Figure 3 indicate that sediment concentrations were relatively low, the maximum being only 201.8 mg/L. Neill, et al (1981) measured concentrations as high as 1980 mg/L although flows were also significantly higher. It was found that surface samples were invariably higher in concentration than any subsurface samples. This is contrary to what would be expected in quiescent water and must be attributable to wind effects. As shown in Table 1, the winds were relatively strong throughout the sampling period so it is possible that wind-induced turbulence prevented settling of the suspended load. The maximum concentration of 201.8 mg/L occurred off Big Point Channel approximately 5 km northeast of the outlet while concentrations in the dredged channel were in the order of 120 mg/L at the surface. Investigation of the mud flats east of Big Point Channel at the beginning of the sampling period indicated a fairly strong current across the mud flats in a generally northerly direction. Figure 4 shows this area and is taken from low level aerial photography flown in May 1980. Photography was flown by others in 1981 but, unfortunately, did not extend into the lake. However, the higher concentrations east of Big Point Channel are probably due to the flow across the mud flats picking up material. This type of flow across the entire delta front, combined with wind-induced turbulence, could account for the higher surface concentrations which were measured.

Sediment concentrations generally decreased further north into the lake and also decreased in a westerly direction. The decrease to the west along the delta front is probably due to the progressive westerly decrease in flow in the distributary channels. The exception to this pattern occurs along the north shore where surface concentrations increase to over 100 mg/L. This is probably due to sediment entrainment from islands and the sandy north shore caused by wind effects. Grain size analysis showed the median grain size in the sand range in the north shore samples. Although these data are limited, it seems reasonable to anticipate sediment contribution from the sandy shore deposits.

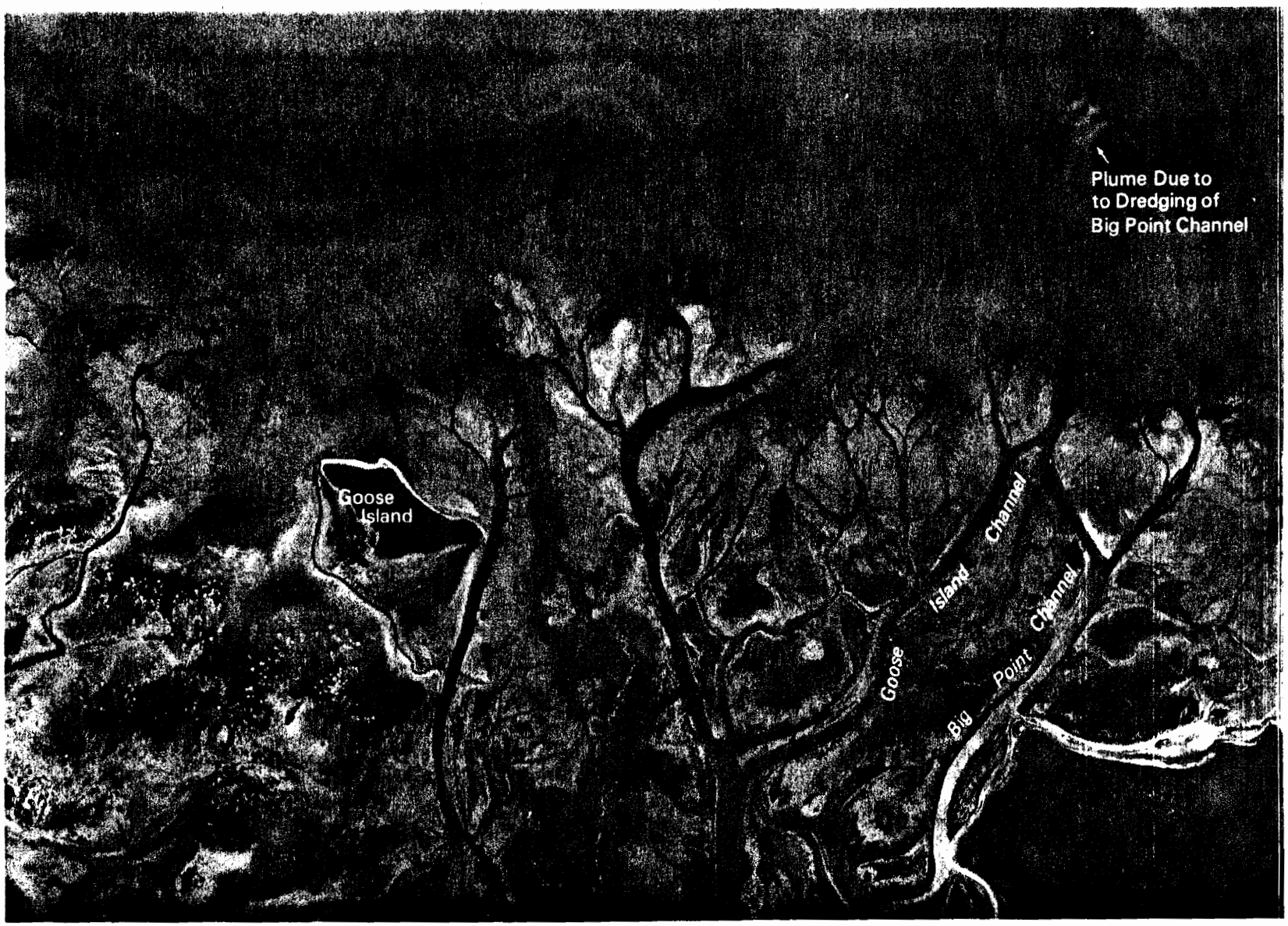

Figure 4. Athabasca Delta in Vicinity of Big Point Channel

In order to assess the penetration depth of the various LANDSAT sensors, Secchi depths were also measured. Three coloured Secchi discs were used. White was used to determine the standard Secchi depth. A green disc was used to determine the effective penetration of band 4, as described more fully in section 3, while a red disc was used to determine the penetration depth of band 5. In all cases no detectable difference in depth to extinction of visibility was noted and all were around 0.3 m. Wave action made these measurements difficult but the results do give an indication of the effective depths sampled by the band 4 and 5 LANDSAT sensors.

Unfortunately, cloud cover during the surveys precluded assessment of satellite imagery. However, Figure 5 shows two LANDSAT 3 band 5 images taken on June 9 and June 27, 1981, which straddle the sampling period. The June 9 image, when inflows exceed outflows, indicates a generally uniform tone to the lake. However, the June 27 image, when outflows exceed inflows, shows a somewhat lighter tone on the north shore, possibly indicative of higher sediment concentrations. Since this image postdates sampling by one week, it is difficult to be conclusive concerning the reasons for the tonal differences. As discussed subsequently, they may be due to a combination of grain size variation and variations in suspended sediment.

Wind and wave conditions precluded current measurements except at one point between Bustard Island and the north shore. A southwest current parallel to the north shore was measured at 0.08 m/s.

2.2 JULY 14-18, 1981 MEASUREMENTS

This trip was timed to coincide with LANDSAT 3 overpasses on July 14 and 15. Only two days of coverage were obtainable with LANDSAT 3 because the sensors producing the western quarter of the image were inoperative. The sensors on LANDSAT 3 had been turned off earlier but a request was made to reactivate the satellite for this project. Unfortunately, further problems with the sensors resulted in the system being turned off on July 13 and no notification was received until after the trip was complete. Evaluation of LANDSAT 2 imagery

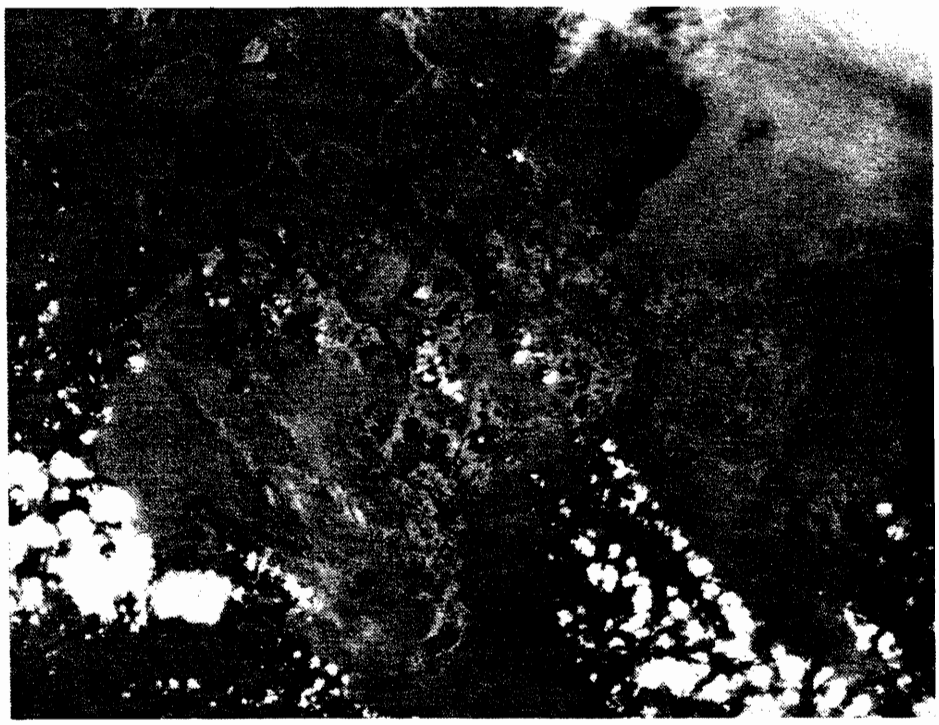

June 9, 1981

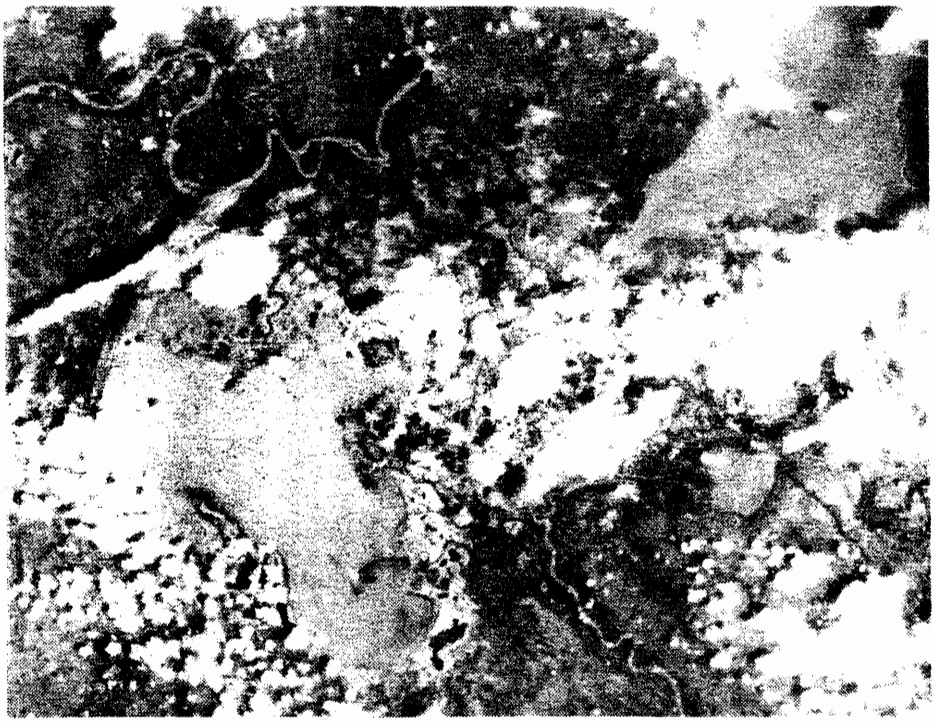

June 27, 1981

Figure 5. LANDSAT 3 Band 5 Images

for the week after the sampling showed cloud cover so no satellite coverage was available for this trip. In addition, winds had been variable so the applicability of later imagery is questionable.

Flows in the Athabasca River at Embarras Airport were estimated to have dropped from 1030 m^3/s on July 15 to 755 m^3/s on July 18. Measurements by Alberta Environment in the distributary channels indicated an inflow of approximately 916 m^3/s with the flow distribution being Embarras River:9%, Fletcher Channel:16%, Goose Island Channel:33% and Big Point Channel:42%. These flow distributions are very similar to those in June, 1981. Inflow from the Fond du Lac River was about 340 m^3/s giving a total inflow averaging 1256 m^3/s. Athabasca River water comprised approximately 73% of the inflow. The difference between flows in the Peace River at Peace Point and the Slave River at Fitzgerald averaged 1640 m^3/s while Alberta Environment gauging of the Riviere des Rochers and the Chenal des Quatres Fourches indicated an outflow of 1575 m^3/s. In this case, outflow exceeded inflow, as had been the case since the sampling in June, 1981. Table 2 shows the water levels at Fort Chipewyan and the wind speeds during the sampling period. No data are available for Bustard Island water levels.

Figure 6 shows the results of the water quality sampling. The temperature measurements indicated that heating of the upper layer of the lake had taken place. Surface temperatures were as high as 27.8°C 5 km northeast of Big Point Channel while temperatures were as low as 18.1°C 3 m below the surface 10 km east of Bustard Island. Temperature variations were greatest east of Bustard Island, showing the thermocline to be less than 1 m below the surface and a temperature differential of up to 8 C°. Temperature variations with depth were only about 1.2 C° to the west of Bustard Island, although caution must be used in interpreting these data. Sampling to the east and southeast of Bustard Island was done when winds were calm and air temperatures were above 30°C while the points south and west of Bustard Island were sampled in windy conditions. As the data of August 1981 will show, it does not appear that stratification in this area of the lake is stable since the wind induces fairly uniform vertical mixing.

Date	July 15	July 16	July 17	July 18
Water level, Fort Chipewyan (m)	208.96	208.88	208.80	208.98
Wind speed and direction (m/s)	5-N.E.	calm	4-S.W.	1-S.W. Changing to 10-N.E. in afternoon

Table 2. Water levels and wind speeds, July, 1981

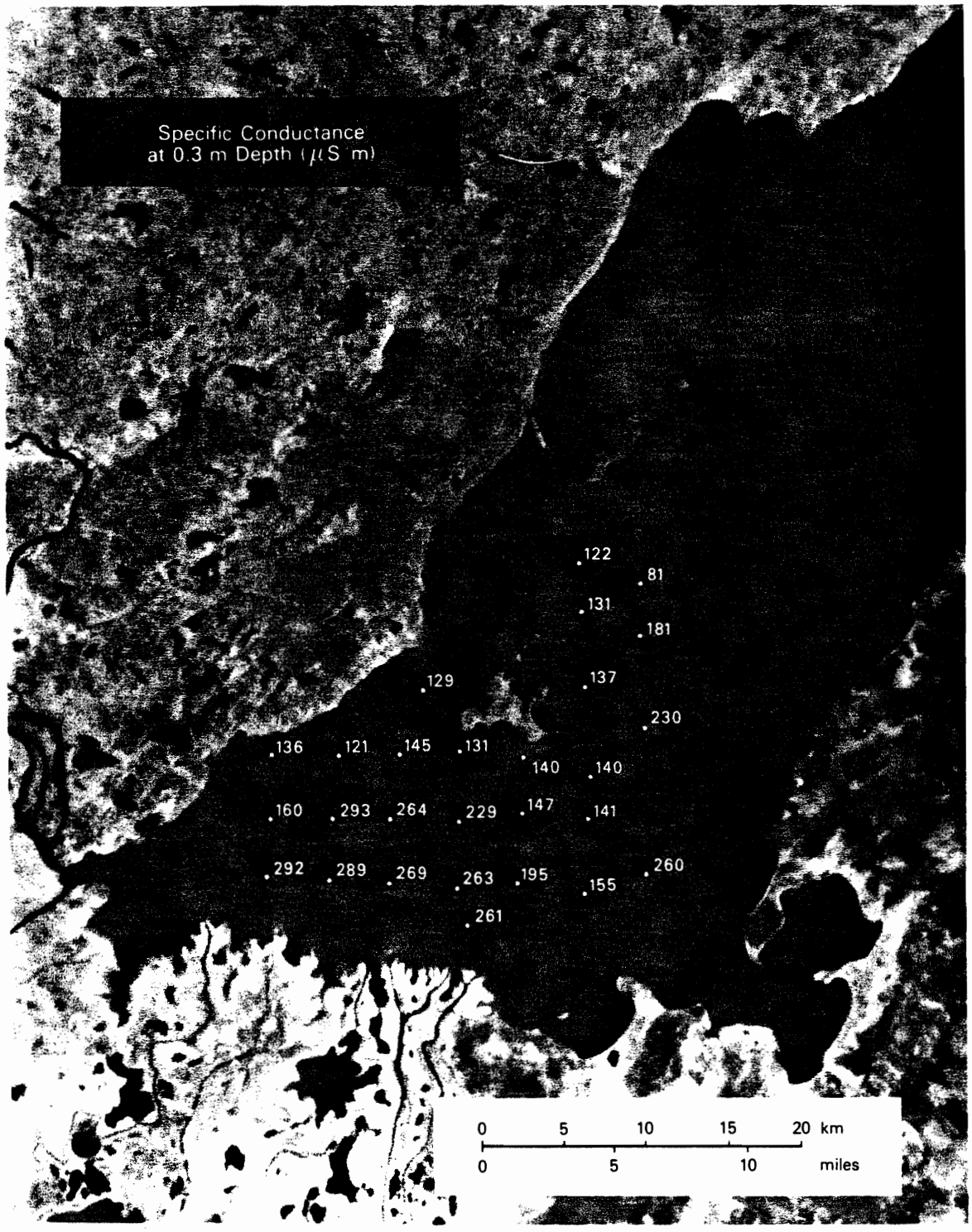

Figure 6. Water Quality Data, July ,1981
(continued in appendix)

This can be seen by comparing the data obtained on a calm day to those obtained during windy conditions. There appears to be no discernable pattern to the temperature measurements which would indicate the sources of water.

The dissolved oxygen data indicate a decrease with depth of about 0.4 mg/L for those sites where there appeared to be temperature stratification but there was otherwise no significant variation with depth. Values were typically 87% of saturation levels and no trends are evident in the data.

The pH values ranged from 7.21 to 8.04 with the smaller values generally occurring in the lake water. Values tended to decrease with depth. Some anomalies occurred at the sites furthest east and at one site 8 km southeast of Bustard Island where levels were as high as 7.78. Winds prior to July 14 had been sustained from the southwest so it is possible that river water had been forced out past Bustard Island. Northeast winds resumed on July 14 and lasted until July 15 so these anomalies could be a result of river water trapped on the east side of the main lake current.

The conductivity data also show higher values at the sampling sites furthest east of Bustard Island as well as at the site 8 km southeast of Bustard Island. River water exhibits a conductivity in the order of 280 µS/cm while the lake water is about 80 µS/cm. The anomalous sites have concentrations as high as 260 µS/cm and there appears to be little variation with depth. Otherwise, conductivity decreases to the north and appears to provide a good indication of the boundary between river and lake water. Since sampling was carried out on different days, the effects of wind can be seen and shows, as expected, that the Athabasca River water is found further to the north during periods of southwest winds but recedes when the winds are from the northeast.

Comparison of the conductivity data and the total dissolved solids data yields some unexpected results. Conductivity is a measure of a water's ability to pass an electric current and, therefore, is related to the number of ions in solution. Since the Athabasca River has more ionized species in solution than does Lake Athabasca water,

specific conductance is a good indicator for differentiating lake and river water. However, un-ionized species do not carry a current and therefore do not affect conductivity. Examples would be weak acids or bases or soluble organic material. During the July sampling, several very high dissolved solids concentrations were measured. Typical measurements in the lake were 120 mg/L but along the delta front in the shallows and in the small bay east of Big Point Channel values as high as 600 mg/L were obtained. The increase probably represents a larger proportion of dissolved organic material and could be related to increased biological activity in the shallow delta front during the summer. Further evidence of the fact that there is an increased proportion of dissolved organic material can be found in Neill, et al (1981) in their evaluation of LANDSAT imagery. Since organic material tends to absorb incoming radiation, the image received should be darker in areas of higher organic content. Satellite imagery frequently indicates fingers of darker water leaving the delta area. These effects could also be a result of local areas of ground water or swamp water discharge.

However, high dissolved solids concentrations were also found around the southwest end of Bustard Island. The results are not thought to be due to analytical error because of their consistency. Further, a plot of specific conductance against dissolved solids shown in Figure 7, excluding the three sites around Bustard Island, indicates a correlation coefficient of 0.841 but the correlation is only 0.116 when these three sites are included. There is no increase in conductivity at these three sites so the increased solids content must be due to some un-ionized matter, possibly organic. The source of the high concentrations is not clear. They could be due to circulation of water from the bays east of Big Point Channel in a counter clockwise direction during periods of southwest winds. Unfortunately, no satellite imagery is available with which to attempt to identify the possible source.

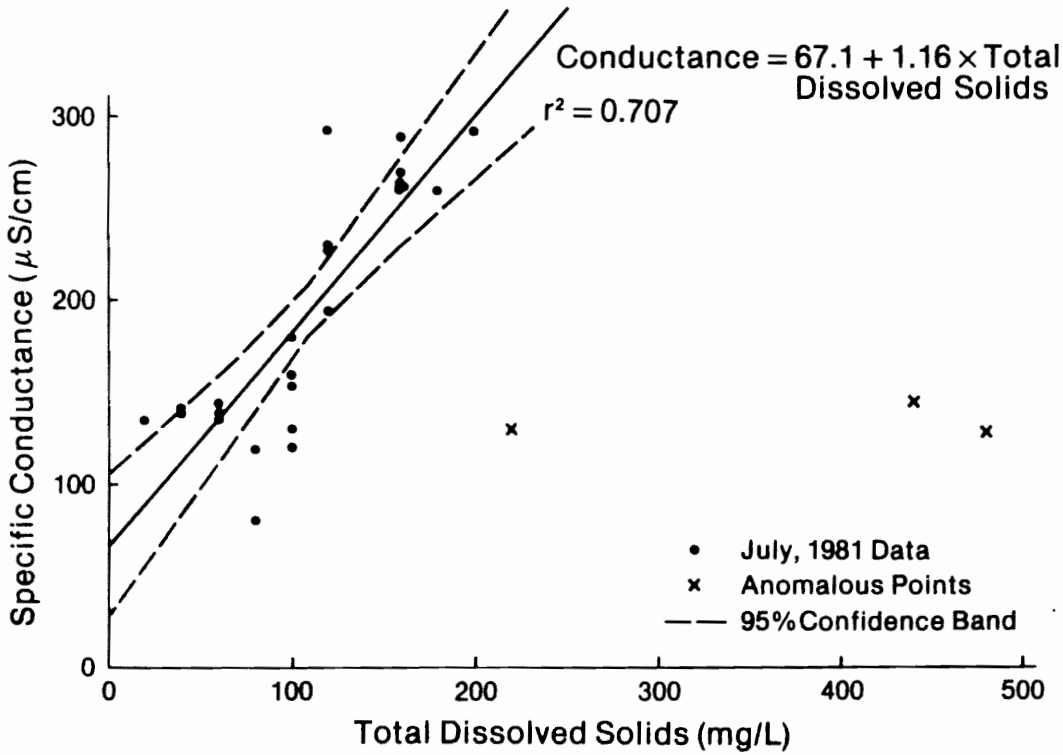
Conductance = 67.1 + 1.16 × Total Dissolved Solids
r² = 0.707
Specific Conductance (μS/cm)
Total Dissolved Solids (mg/L)
0
100
200
300
400
500
• July, 1981 Data
× Anomalous Points
—— 95% Confidence Band

Suspended sediment concentrations had decreased since June and showed a maximum of 130 mg/L 6 km north of Fletcher Channel and a minimum of 12.2 mg/L 4 km north of Goose Island. The data indicated an increase in concentration with depth. The sites furthest west, sampled on July 15, showed the highest concentrations, in the order of 100 mg/L. Winds during sampling were from the north east. These high concentrations could then be due to entrainment of course sediment from sandy shore deposits. The conductivity of the site with the highest concentration was only 160 µS/cm which indicates that the water was a mixture of lake and river water. Since the distributary channels had concentrations of only 40 mg/L, it appears that the source must be from other than the Athabasca River. Wind-induced entrainment from the bottom can probably be excluded as an explanation since the shallower water along the delta front does not show higher sediment concentrations.

Samples taken east of Bustard Island on July 16 during calm wind conditions showed variable levels of suspended sediment ranging from 12.9 mg/L to 41.5 mg/L. The lowest concentration was found southeast of Bustard Island in water originating from the Athabasca River, based on a conductivity of 260 µS/cm. Sediment concentrations at this site nearly doubled at a depth of 1 m. It appears that this river water could have been pushed out during the previous period of southwest winds and been trapped on the east shore as winds reversed. Water apparently originating from the Athabasca River was also found 8 km east of Bustard Island with sediment concentrations of 23.8 mg/L. Other sites in the area also showed relatively high suspended sediment concentrations although the water appeared to be lake water. This sediment could have originated from the shores of Bustard and Burntwood islands. It is difficult to be conclusive because sediment concentrations are all relatively small.

The volatile fraction of the suspended load was determined for all sites to determine the nature of the sediment and to determine if there were a significant variation in organic content which could affect the interpretation of satellite imagery. Organic content was consistently in the order of 10% of total suspended sediment concentration and there was no significant variation.

Current data, shown in Figure 8, could only be obtained to the south and east of Bustard Island due to wind conditions. A counter-clockwise current from Big Point Channel of about 0.03 m/s was detected which extended to about 6 km east of the outlet. Lake currents were also in the order of 0.03 m/s.

2.3 AUGUST 8-12, 1981 MEASUREMENTS

This trip was timed to coincide with LANDSAT 2 overpasses on August 9, 10, and 11, 1981. Flows in the Athabasca River at Embarras Airport decreased from 1210 m^3/s on August 8 to 1000 m^3/s on August 11. During this period, Fond du Lac River inflows decreased from 311 to 302 m^3/s. Alberta Environment gauging indicated an inflow from the Athabasca River of 979 m^3/s with the distribution being Embarras River: 6%, Fletcher Channel:16%, Goose Island Channel:34% and Big Point Channel: 44%. The flow distribution in the distributary channels had remained relatively constant all summer. Outflow based on the difference in flows between the Slave River at Fitzgerald and the Peace River at Peace Point averaged 1590 m^3/s while Alberta Environment measured an outflow of 1448 m^3/s. Outflows exceeded inflows and the proportion of Athabasca River water in the outflow had apparently declined to about 65%. Water levels at Fort Chipewyan and wind speeds on the lake are shown in Table 3.

Results of the water quality sampling are shown in Figure 9. The pH data ranged from 6.94 at a 4 m depth east of Bustard Island to 8.37 northeast of High Island. In contrast to previous sampling, there is no apparent pattern to the variations. Temperatures were in the order of 24.0°C with a maximum vertical variation of 2.6 C°. There was no strong stratification at any sampling site and no patterns were evident. Similarly, dissolved oxygen levels showed no systemic horizontal variations and ranged from 6.32 mg/L at a 4 m depth to 8.02 mg/L at the surface. Some depletion at depth was evident in the deeper water east of Bustard Island.

Winds had been fairly steady from the south and southwest prior to and during the sampling. The conductivity data show that

Figure 8. Current Data, July 1981

Figure 8. Continued

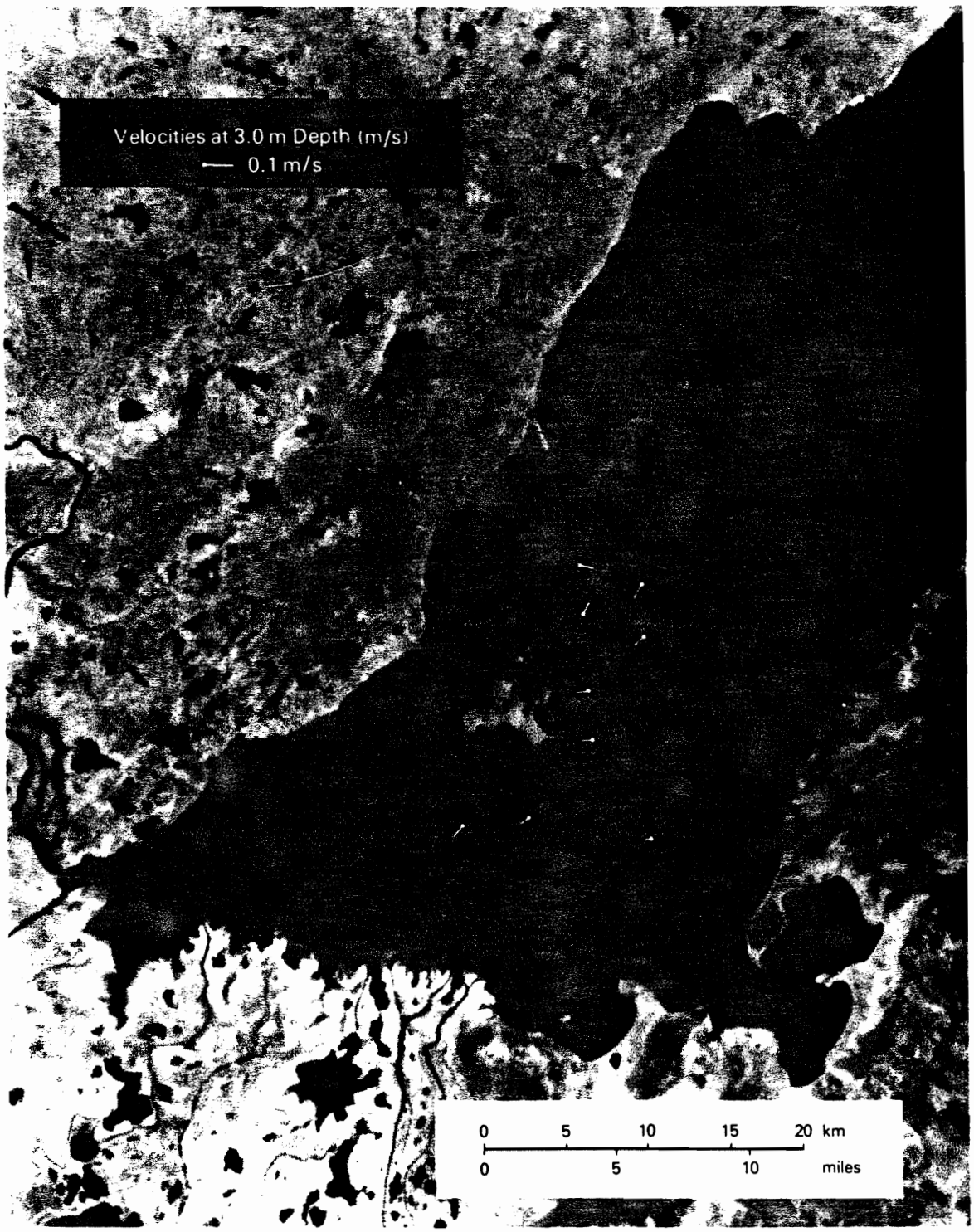

Figure 8. Conclusion

Date	Aug. 8	Aug. 9	Aug. 10	Aug. 11
Water level, Fort Chipewyan (m)	208.78	208.73	208.72	208.77
Wind speed and direction at 2 m elevation (m/s)	3.5-S.W.	8-S.	4-S.W.	8-S.W.

Table 3. Water levels and wind speeds, August, 1981

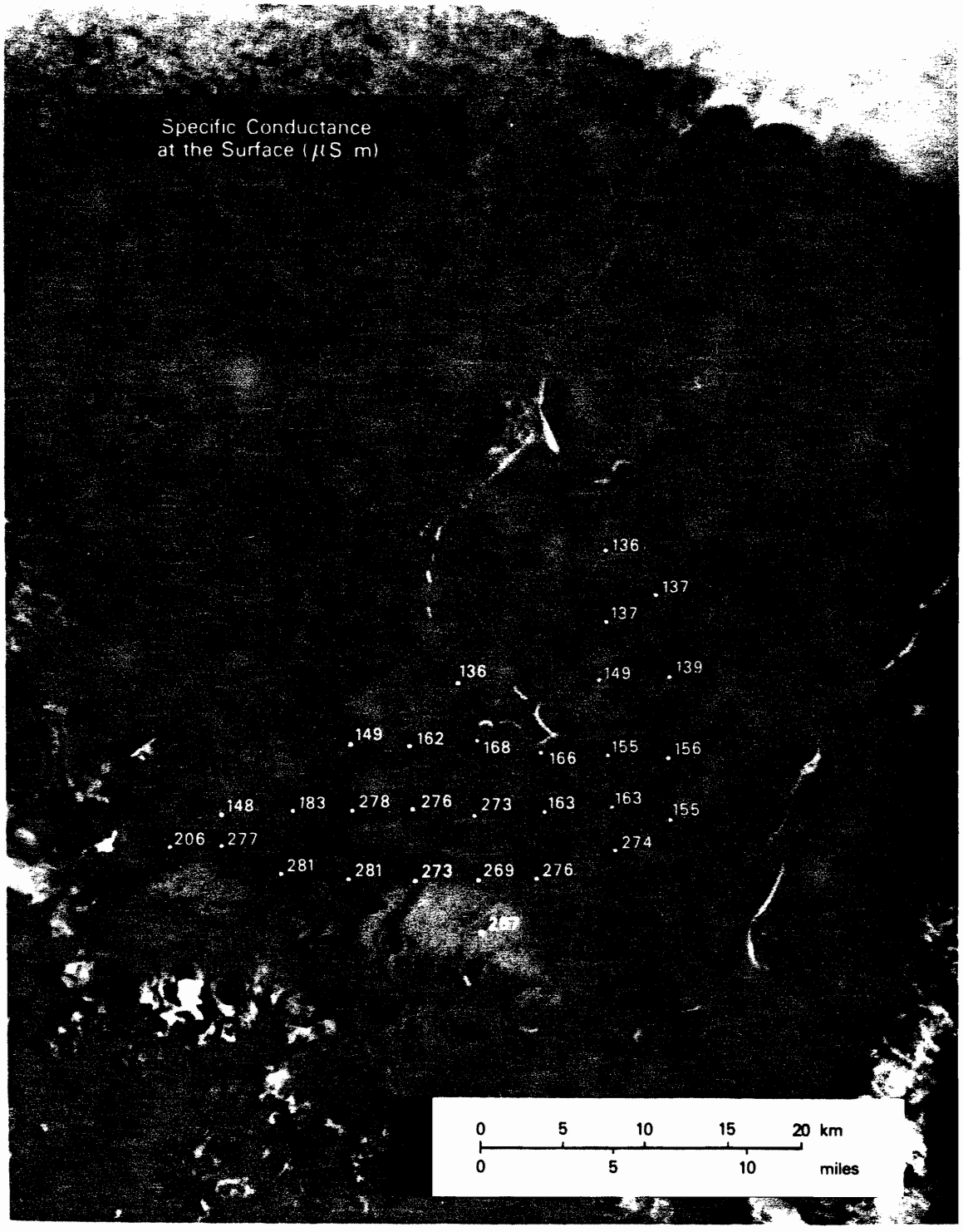

Figure 9. Water Quality Data, August, 1981
(continued in appendix)

river water was found up to 8 km north of the delta front and up to 8 km northeast of Big Point Channel. In contrast to previous sampling, no river water was found east of Bustard Island. However, lake water generally has a conductivity in the order of 80 µS/cm. The water east of Bustard Island had levels around 140 µS/cm which could mean that river water had moved northeast and mixed with the lake water. Assuming that river and lake water have conductivities of 270 and 80 µS/cm respectively, the water east of Bustard Island was 32% river water.

Water quality profiles in the inlet and outlet channels are shown in Figure 10. It is evident that lateral variation in water quality existed in the Riviere des Rochers with increasing proportions of river water further south. The discharge weighted mean fraction of river water in the Rochers is 53%. The Chenal des Quatres Fourches was essentially 100% river water which shows that the total fraction of river water in the outflow was 60%. However, river inflow was about 68% of outflow so river water could have moved to the northeast to gradually mix with the lake water. In contrast, Neill, et al (1981) found that, for a much higher inflow, the Rochers comprised almost 100% river water. Therefore, as river inflows decline, the Rochers draws a larger fraction of lake water.

Suspended sediment concentrations were approximately 100 mg/L in Big Point Channel but were much lower elsewhere. East of Bustard Island, concentrations were about 4 mg/L while on the north shore, concentrations were up to 17 mg/L. Organic content was more variable than the previous sampling, averaging 15% in the area north of the delta and ranging from 0 to 100% east of Bustard Island. This high variability could be due to the low sediment concentrations which provides a larger margin for analytical error.

The dissolved solids concentrations were variable and, as shown in Figure 11, show no correlation with conductivity. The organic content is equally varied. No extremely high concentrations were measured although marginally higher concentrations were found south of Bustard Island. No conclusions were drawn from these data.

Bed samples were collected and analysed for grain size distribution. Figure 12 shows these data and the results indicate

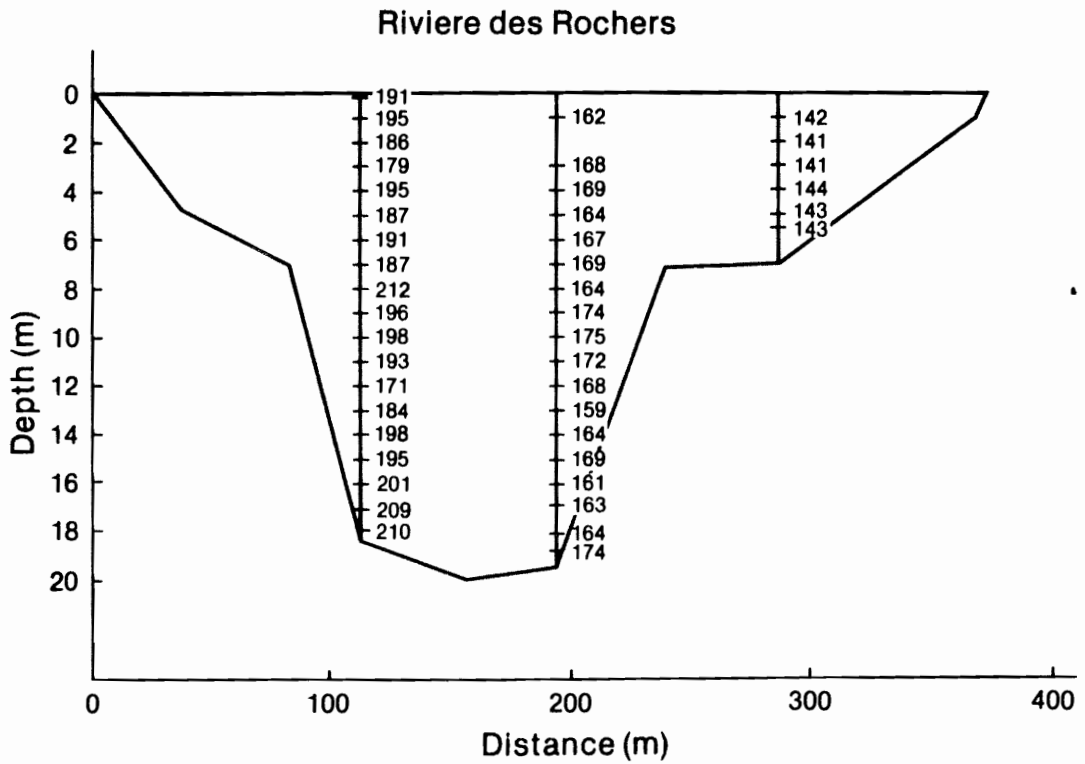
Riviere des Rochers
Depth (m)
0
2
4
6
8
10
12
14
16
18
20
191
195
186
179
195
187
191
187
212
196
198
193
171
184
198
195
201
209
210
162
168
169
164
167
169
164
174
175
172
168
159
164
169
161
163
164
174
142
141
141
144
143
143
0
100
200
300
400
Distance (m)

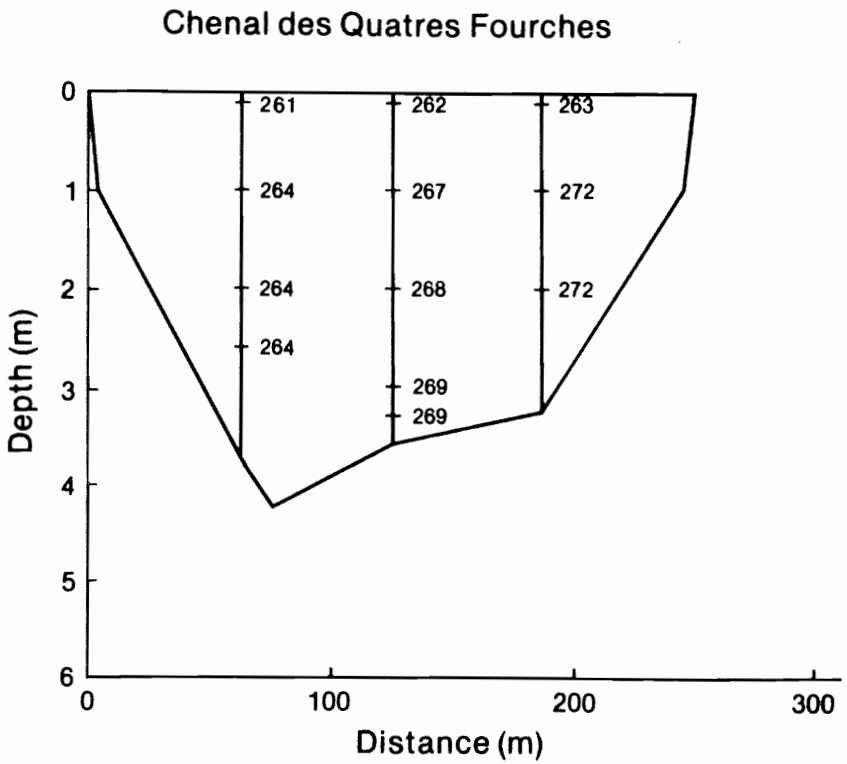
Chenal des Quatres Fourches
Depth (m)
0
1
2
3
4
5
6
261
264
264
264
262
267
268
269
269
263
272
272
0
100
200
300
Distance (m)

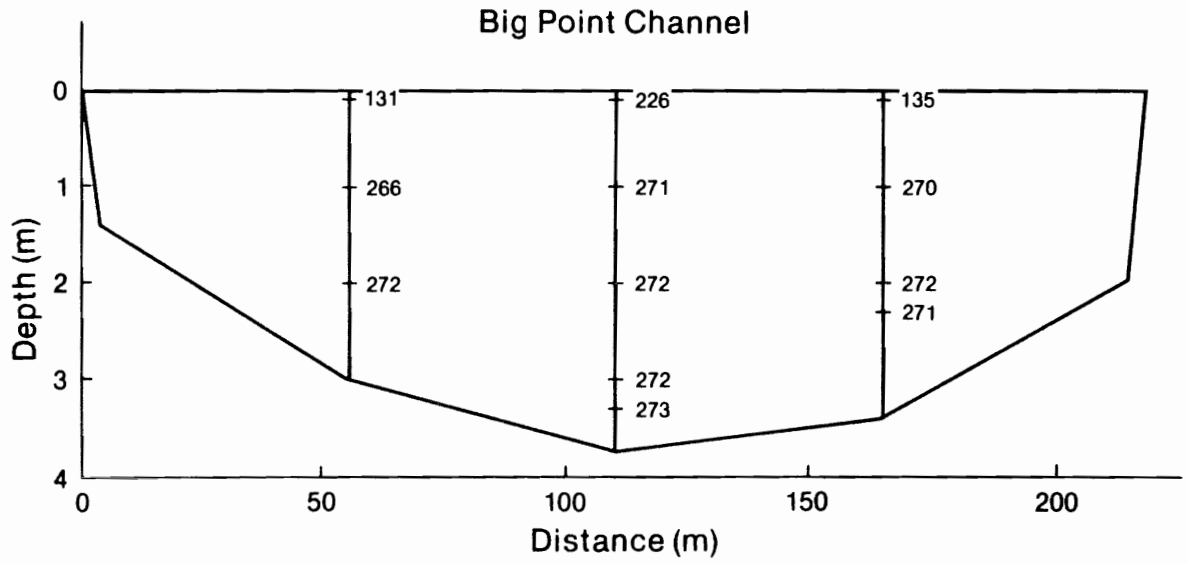
Big Point Channel
Depth (m)
0
1
2
3
4
131
266
272
226
271
272
272
273
135
270
272
271
0
50
100
150
200
Distance (m)

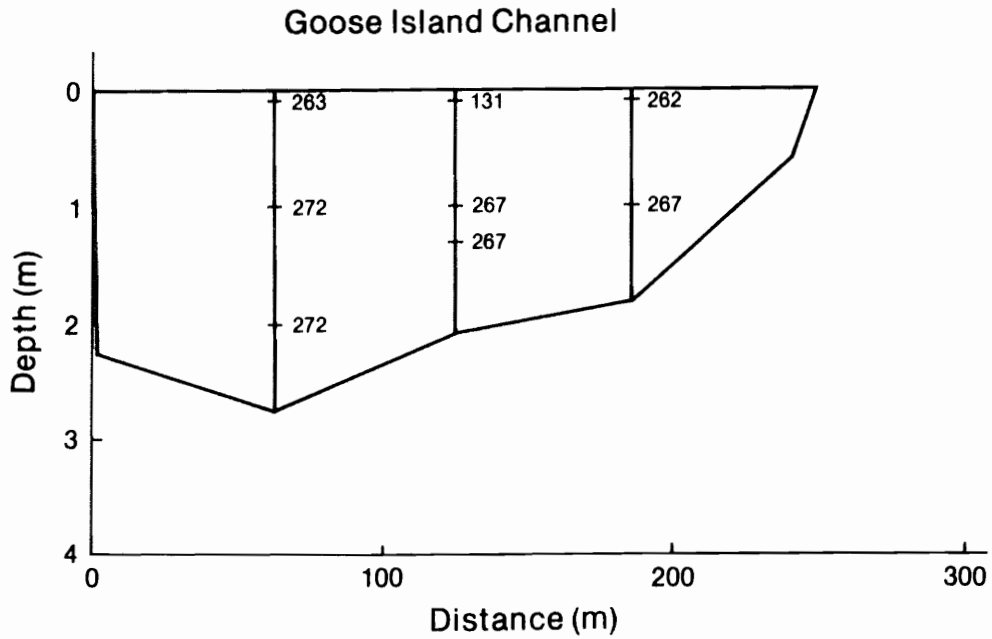
Goose Island Channel
Depth (m)
0
1
2
3
4
263
272
272
131
267
267
262
267
0
100
200
300
Distance (m)

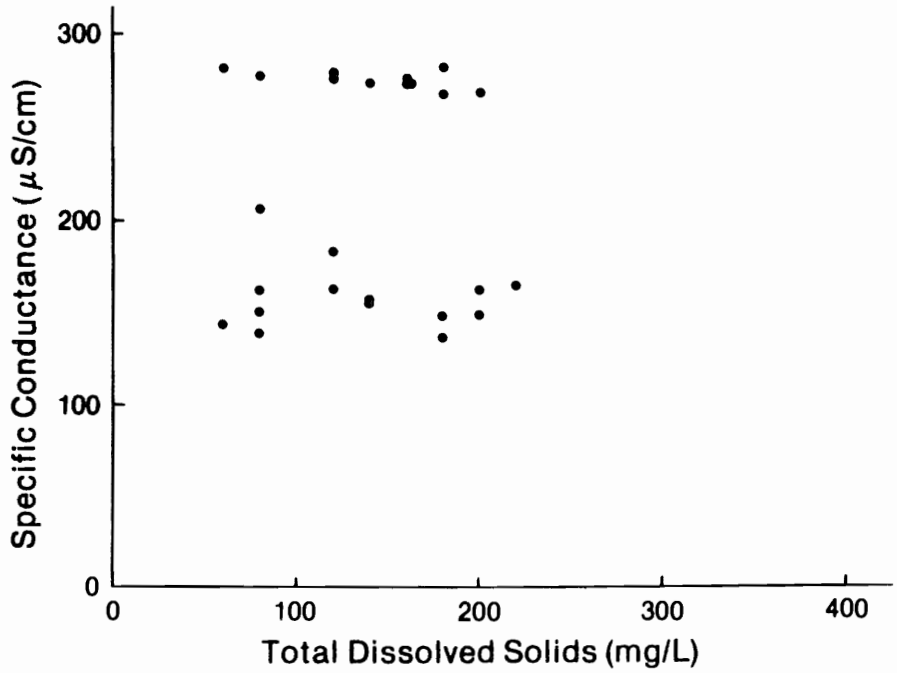
Specific Conductance (μS/cm)
300
200
100
0
0
100
200
300
400
Total Dissolved Solids (mg/L)

a decrease in material size north of the delta front but sizes along the north shore and in the vicinity of Bustard and Burntwood islands tend to increase. This variation is probably due to near shore sediment sorting processes.

Current data are shown in Figure 13 and indicate fairly strong currents of 0.15 m/s along the north shore with weaker currents of 0.04 m/s north of the delta.

Satellite coverage was available for all three days of overpass. Band 5 images are presented in Figure 14 for the overpasses on August 9, 10 and 11. Sampling took place on August 8 east and south of Bustard Island with light south winds. High south winds on August 9 prevented sampling. Winds moderated on August 10 and sampling was done west of Bustard Island. It is probable that conditions east of Bustard Island on this date were similar to those on August 8 so the total data set can be compared to the August 10 image. The tonal patterns are similar to the sediment distribution although the plume along the north shore appears brighter than that further south. This could be due to the fact that the sediment along the north shore had generally larger grain sizes which could affect the reflected signal. There is evidence of a plume along the south shore originating at the William River. The movement of river water from Big Point Channel and Goose Island Channel to the northeast is evident and comparison of the August 9 and 10 images shows the retraction of river water as winds decreased. Also evident is the improved delineation of the north shore lake current as winds decreased. On August 11, strong southwest winds prevented sampling. The image for this date shows the marked eastward movement of river water from Goose island Channel and Big Point Channel although both the Fletcher Channel and Embarras River are discharging westward to the Chenal des Quatres Fourches. The wind effects are also clearly seen in Mamawi Lake. Further comparison of the satellite imagery and water quality data will be discussed in section 3.

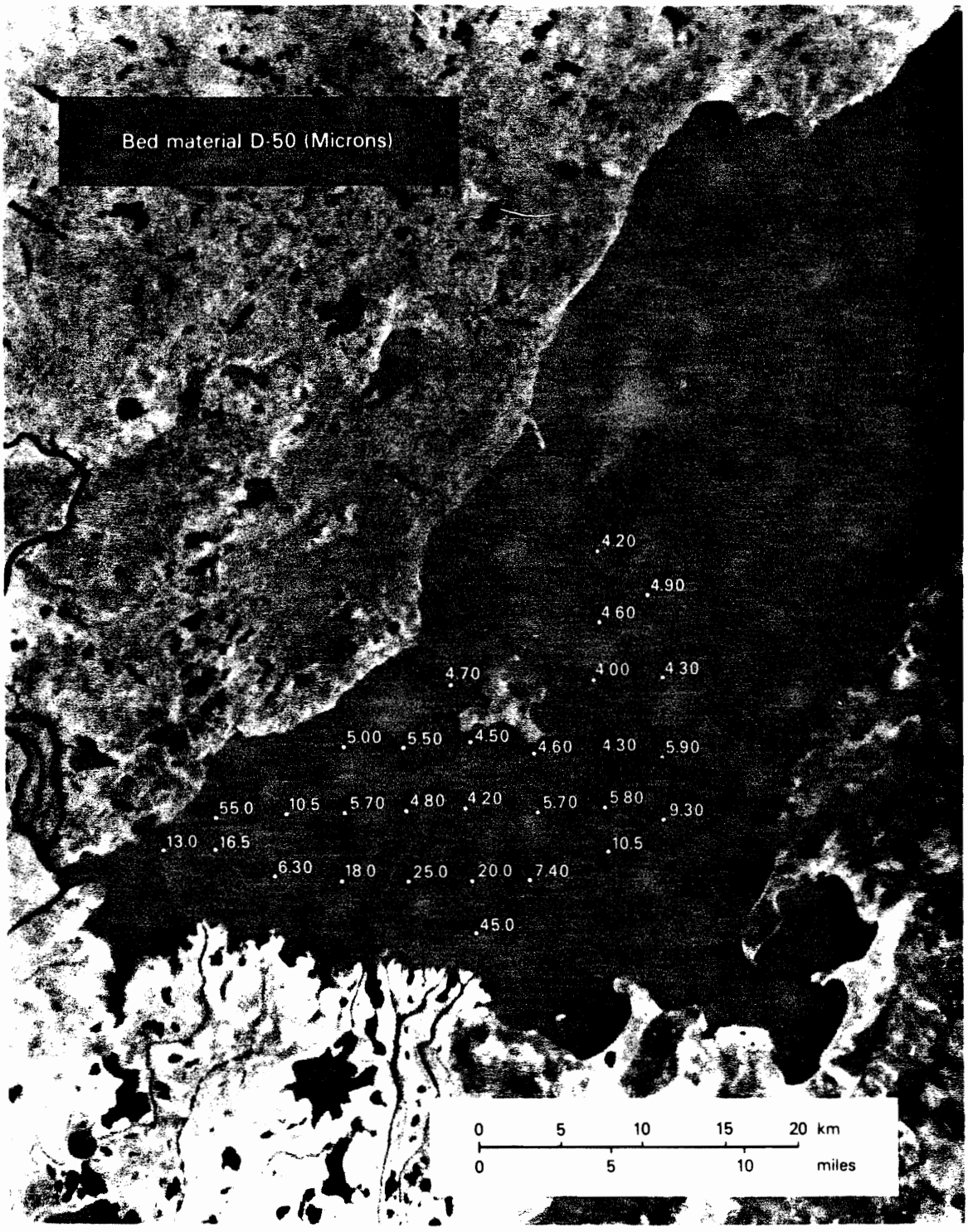
Bed material D-50 (Microns)
4.20
4.90
4.60
4.70
4.00
4.30
5.00
5.50
4.50
4.60
4.30
5.90
55.0
10.5
5.70
4.80
4.20
5.70
5.80
9.30
13.0
16.5
10.5
6.30
18.0
25.0
20.0
7.40
45.0
0 5 10 15 20 km
0 5 10 miles

Figure 12.

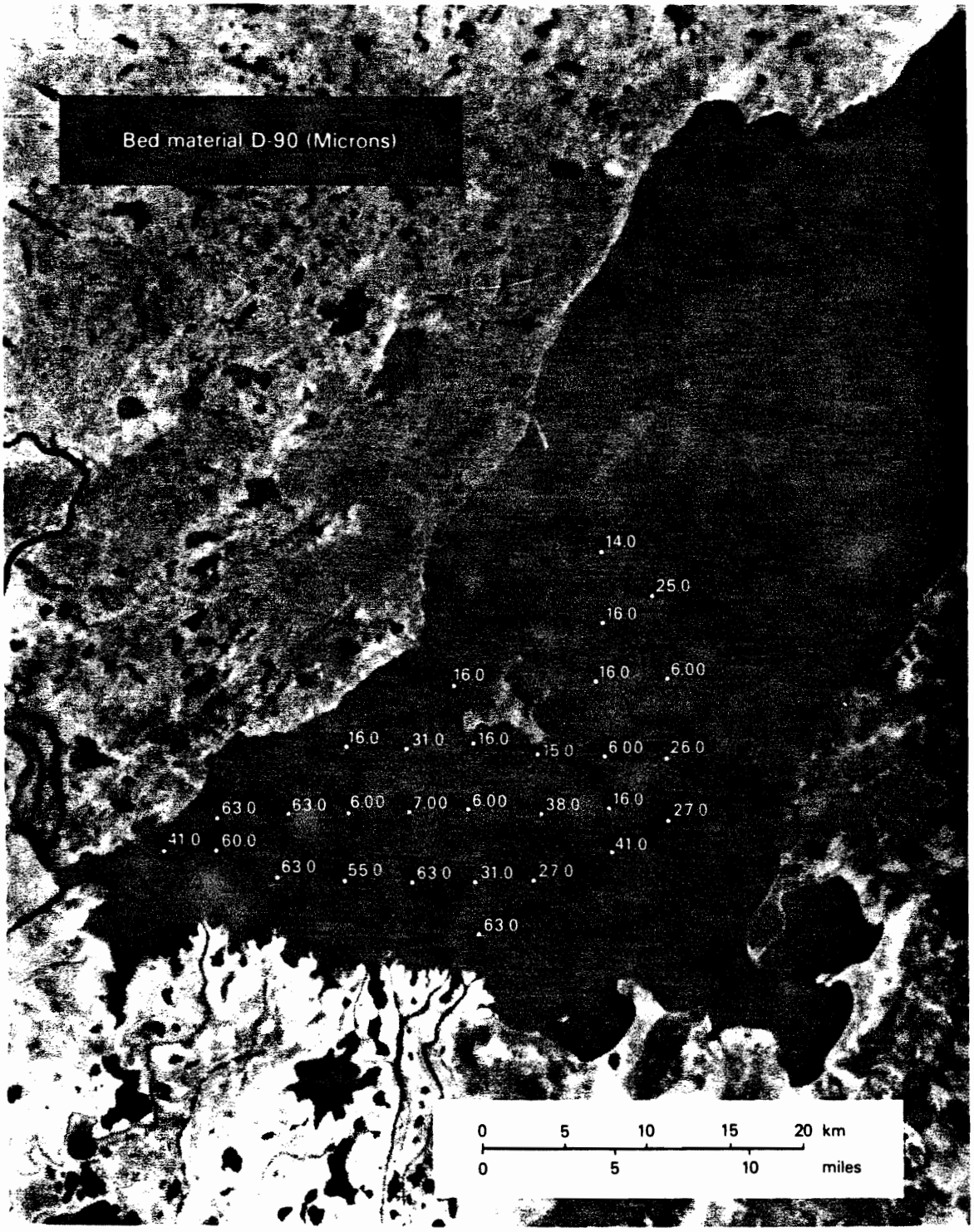

Figure 12. Conclusion

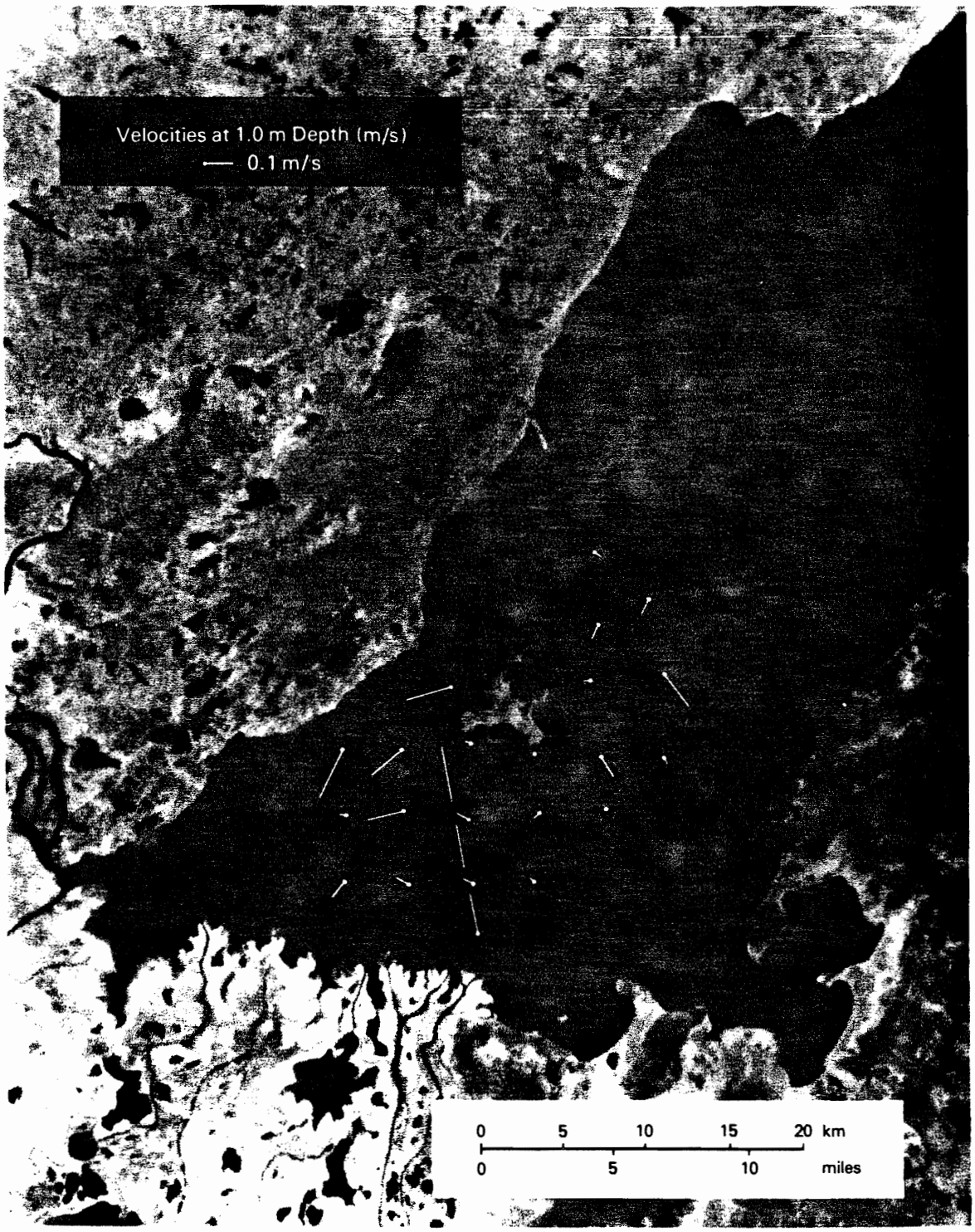

Figure 13. Current Data, August 1981

Figure 13. Continued

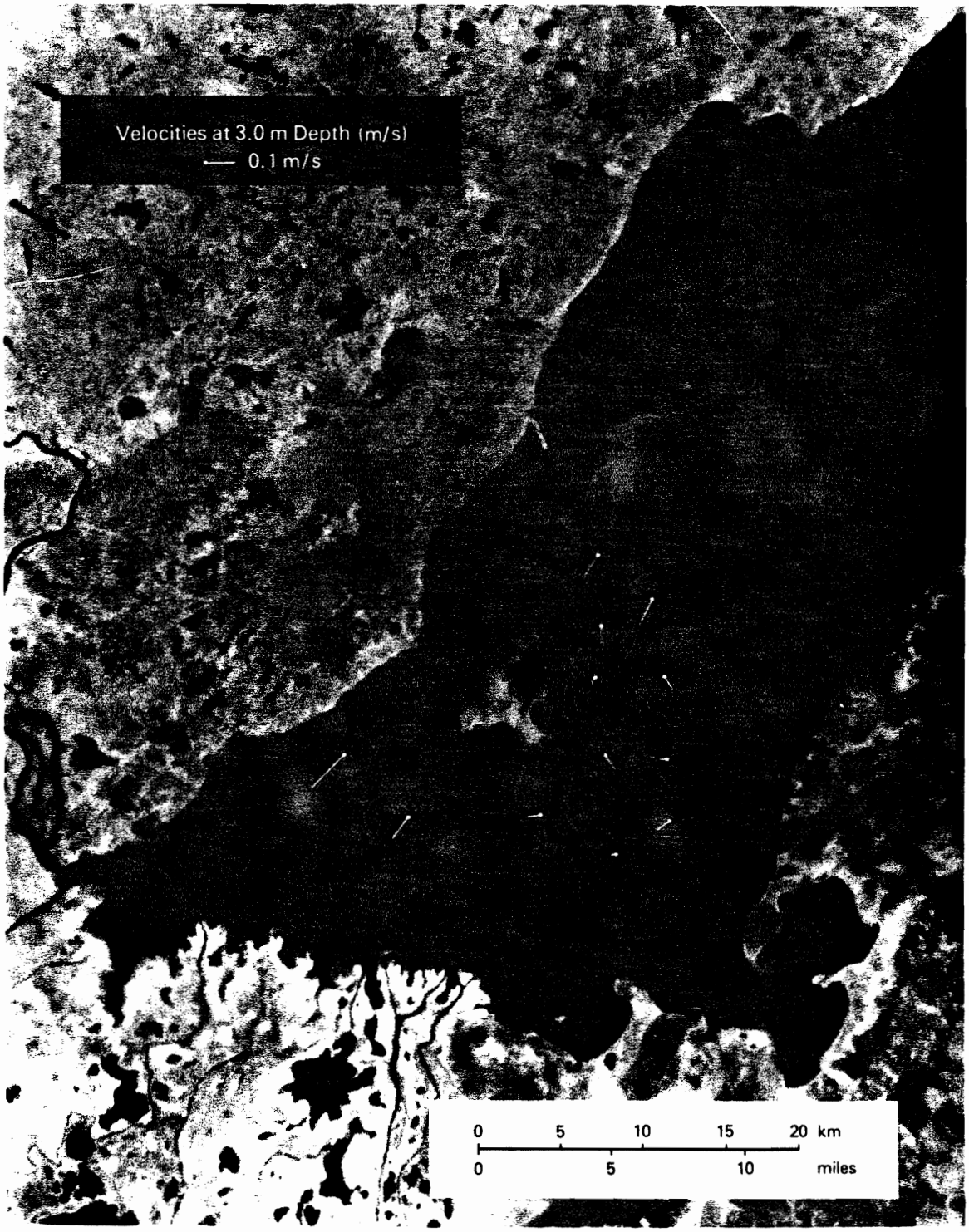

Figure 13. Conclusion

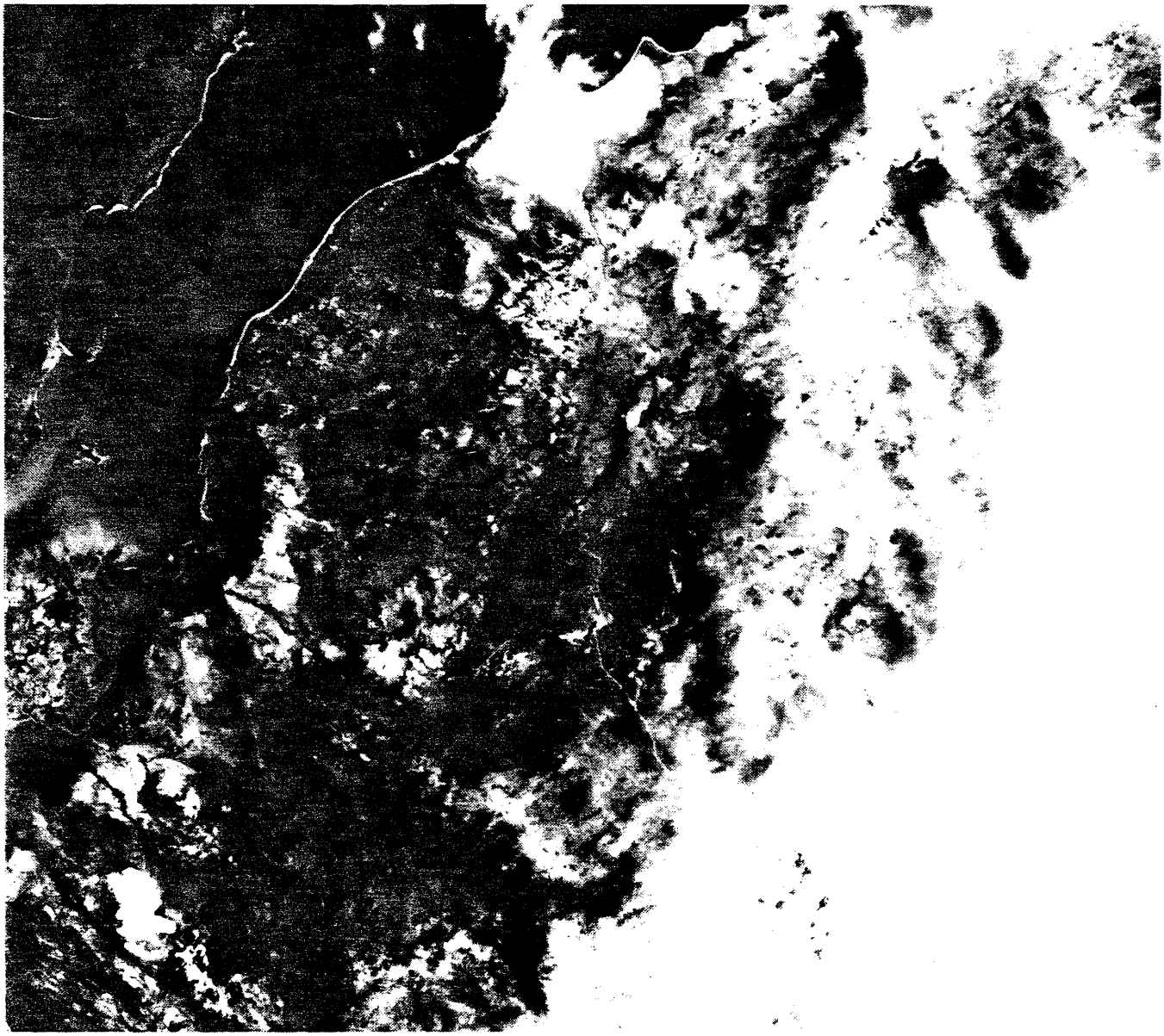

August 9, 1981

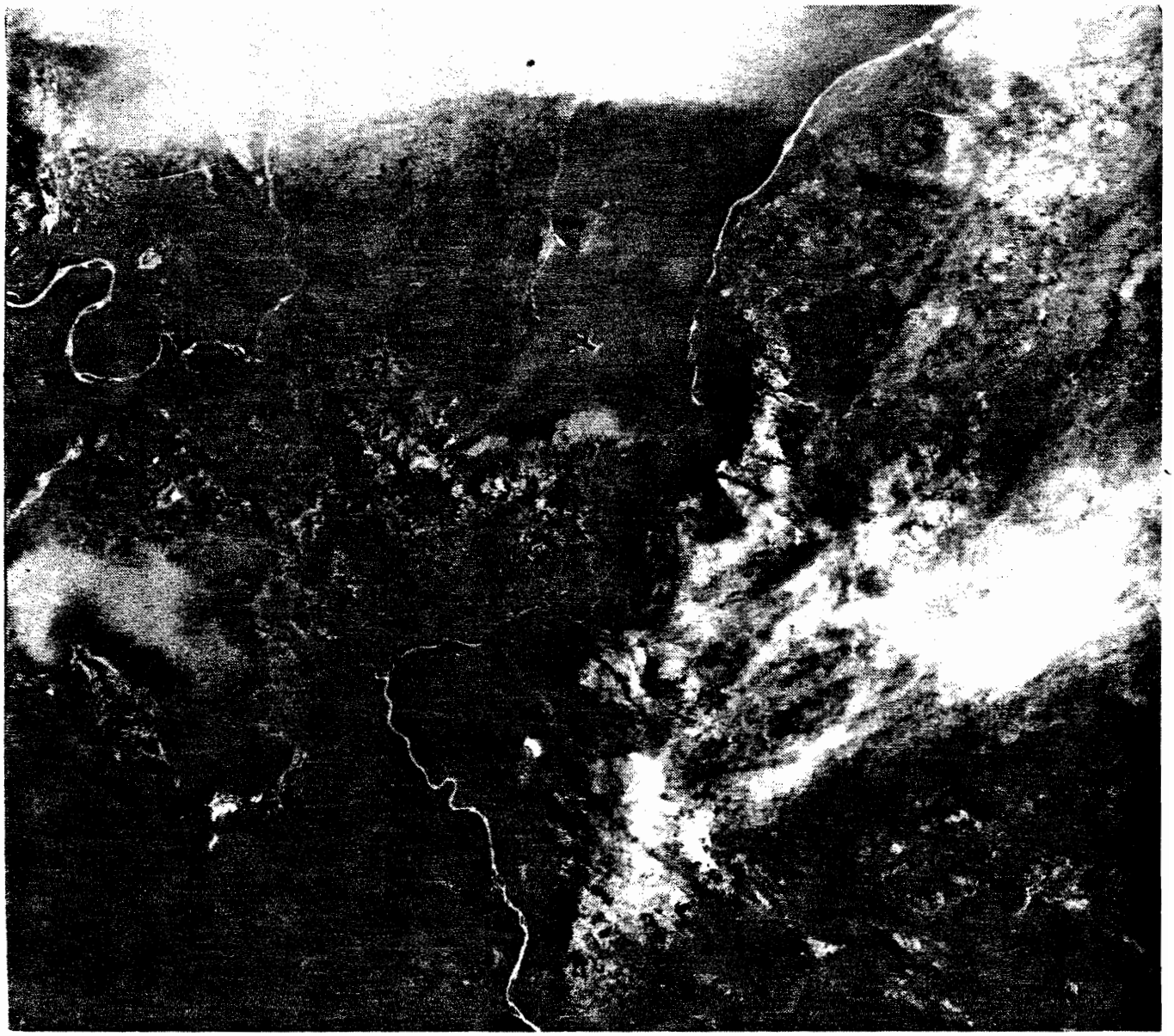

August 10, 1981

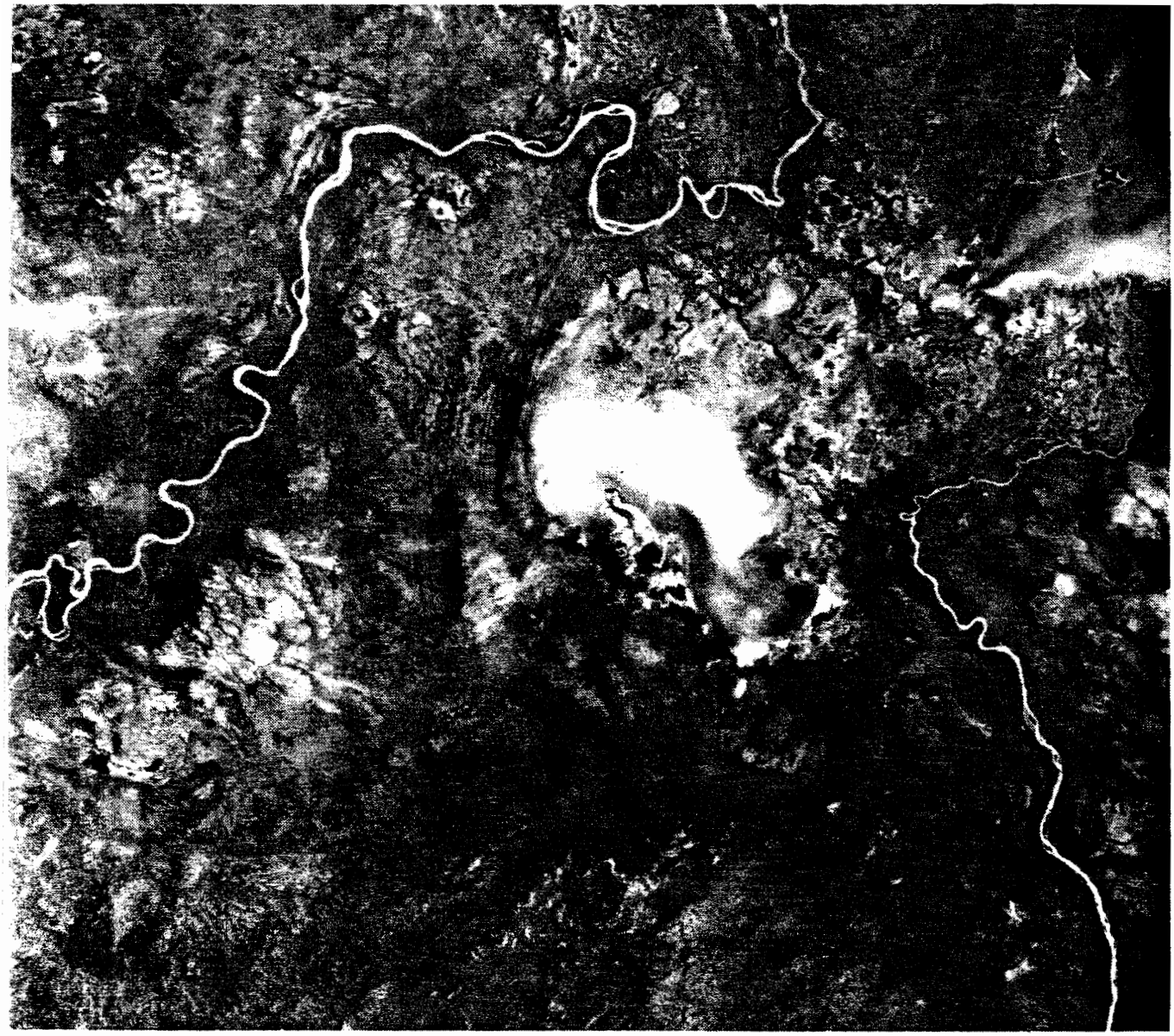

August 11, 1981

BAND 5

2.4 SEPTEMBER 11-17, 1981 MEASUREMENTS

This trip was timed to coincide with LANDSAT 2 overpasses on September 14, 15 and 16. The objective was to carry out two dye tests which had been prevented previously due to equipment malfuctions. Flows in the Athabasca River at Embarras Airport declined from 557 m^3/s on September 11 to 507 m^3/s on September 16. Flows in the Fond du Lac River were relatively steady around 253 m^3/s giving an average inflow of 780 m^3/s. The outflow, based on Peace River and Slave River flows, averaged 1270 m^3/s. The only flow data from Alberta Environment indicated a discharge of 220 m^3/s in the Chenal des Quatre Fourches. Winds and water levels are shown in Table 4.

Minimal water quality sampling was carried out due to minor equipment breakdowns and wind conditions. Operations were further hampered by dense forest fire smoke which reduced visibility to under 10 m at times and prevented satellite coverage. It was decided to proceed with the dye tests in spite of the lack of satellite coverage. One test comprised dye injection in Goose Island Channel and the second injection was made south of Bustard Island. It was hoped that by monitoring the dye clouds, the circulation patterns of river and lake water would be clarified. Permission to carry out the tests was granted by Standards and Approvals Division, Alberta Environment.

A 15 kg slug of 20% Rhodamine WT fluorescent dye mixed with 8 L of methanol was injected at 14:25 hrs. on September 15. The methanol was added to ensure neutral buoyancy of the tracer. The injection location is shown in Figure 15. Measurements of fluorescence were made with a Turner Designs Model 10-000 fluorometer capable of detecting concentrations as low as 0.01 µg/L. Continuous sampling was accomplished by mounting a small pump outboard of the sampling boat and using the flow-through mode of the fluorometer. Results were recorded on an Esterline-Angus model M5413B three channel chart recorder and were later digitized.

Once the dye had entered Big Point Channel it became evident that the dye cloud was going to be moved westward across the delta front where the shallow depths would prevent sampling. Longitudinal and lateral profiles were made as long as depths permitted access by boat.

Date	Sept. 11	Sept. 12	Sept. 13	Sept. 14	Sept. 15	Sept. 16
Water level, Fort Chipewyan (m)	208.56	208.47	208.25	208.29	208.28	208.20
Wind speed and direction at 2 m elevation (m/s)	8-W.	8-W.	calm	3-S.E.	6-S.E.	7-S.W.

Table 4. Water levels and wind speeds, September 1981.

Figure 15. Location of Channel Injection Site

These results are shown in Figure 16. The maximum concentration was 50 µg/L on the west side of the dredged channel. The dye cloud then moved west across the delta front. This occurred two hours after injection. Continuous traverses were made across the delta measuring fluorescence in hope of finding the dye as it entered deeper water. No dye was found. It appears that, under the prevailing wind conditions (southeast winds), all the flow from Goose Island Channel, after merging with Big Point Channel, moves across the delta front rather than into the lake. This could also be due to the larger proportion of lake water in the outflow resulting in relatively stronger lake crossflows. Because of deteriorating weather conditions, it was decided to proceed with the second injection the next day rather than monitor the outlet channels in an attempt to detect the dye as it left the lake.

A second 15 kg slug of 20% Rhodamine WT dye mixed with 7 L of methanol was injected 4.5 km south and 2.0 km east of the southwest end of Bustard Island at 11:57 hrs on September 16. Figure 17 shows the location of the injection site. Both longitudinal and lateral traverses of the dye cloud were carried out. The measured contours are shown in Figure 18. The dye was tracked for 8 hrs at which time it had moved 2 km in a northwest direction and had a surface area of approximately 70,000 m^2. The maximum concentration at this time was 45 µg/L. The average velocity of the dye cloud was about 0.075 m/s. This velocity is somewhat larger than those previously measured in this area of the lake and is likely due to the southeast winds. By this time, dense forest fire smoke had reduced visibility to under 10 m so operations were curtailed in the interest of safety. The next day the lake was traversed along the anticipated path of the dye cloud for 7 hrs. but no dye was detected. Based on the apparent velocity, three days should have elapsed before the dye left the lake. However, currents previously measured along the north shore were as high as 0.15 m/s which, once the dye entered this current, would have reduced the detention time by one half. The southeast winds could have increased the surface velocities and further reduced the detention time.

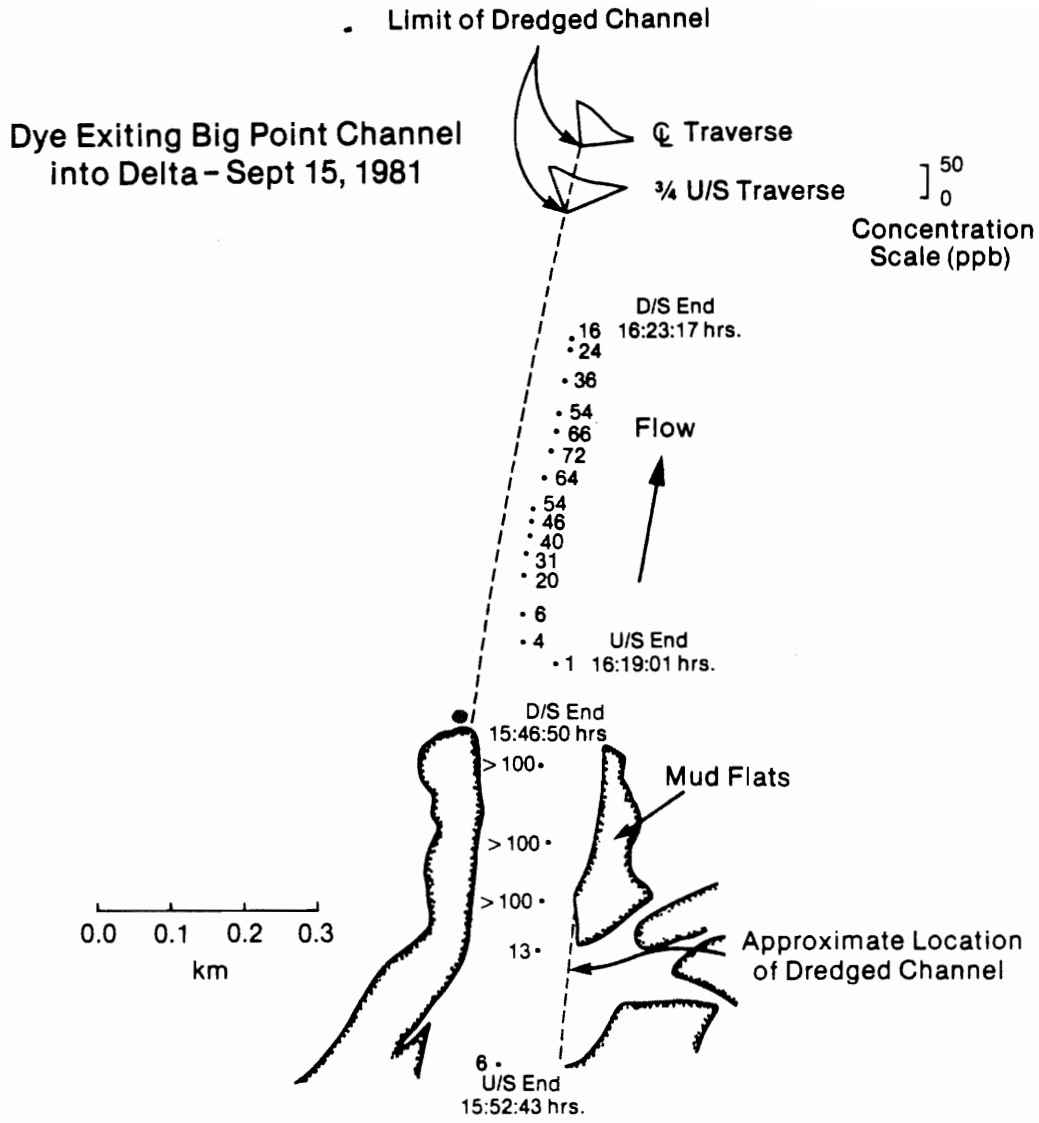
Limit of Dredged Channel
Dye Exiting Big Point Channel into Delta - Sept 15, 1981
℄ Traverse
¾ U/S Traverse
50
0
Concentration Scale (ppb)
D/S End 16:23:17 hrs.
16
24
36
54
66
72
64
54
46
40
31
20
6
4
1
U/S End 16:19:01 hrs.
Flow
D/S End 15:46:50 hrs
> 100
> 100
> 100
13
6
U/S End 15:52:43 hrs.
Mud Flats
Approximate Location of Dredged Channel
0.0 0.1 0.2 0.3
km

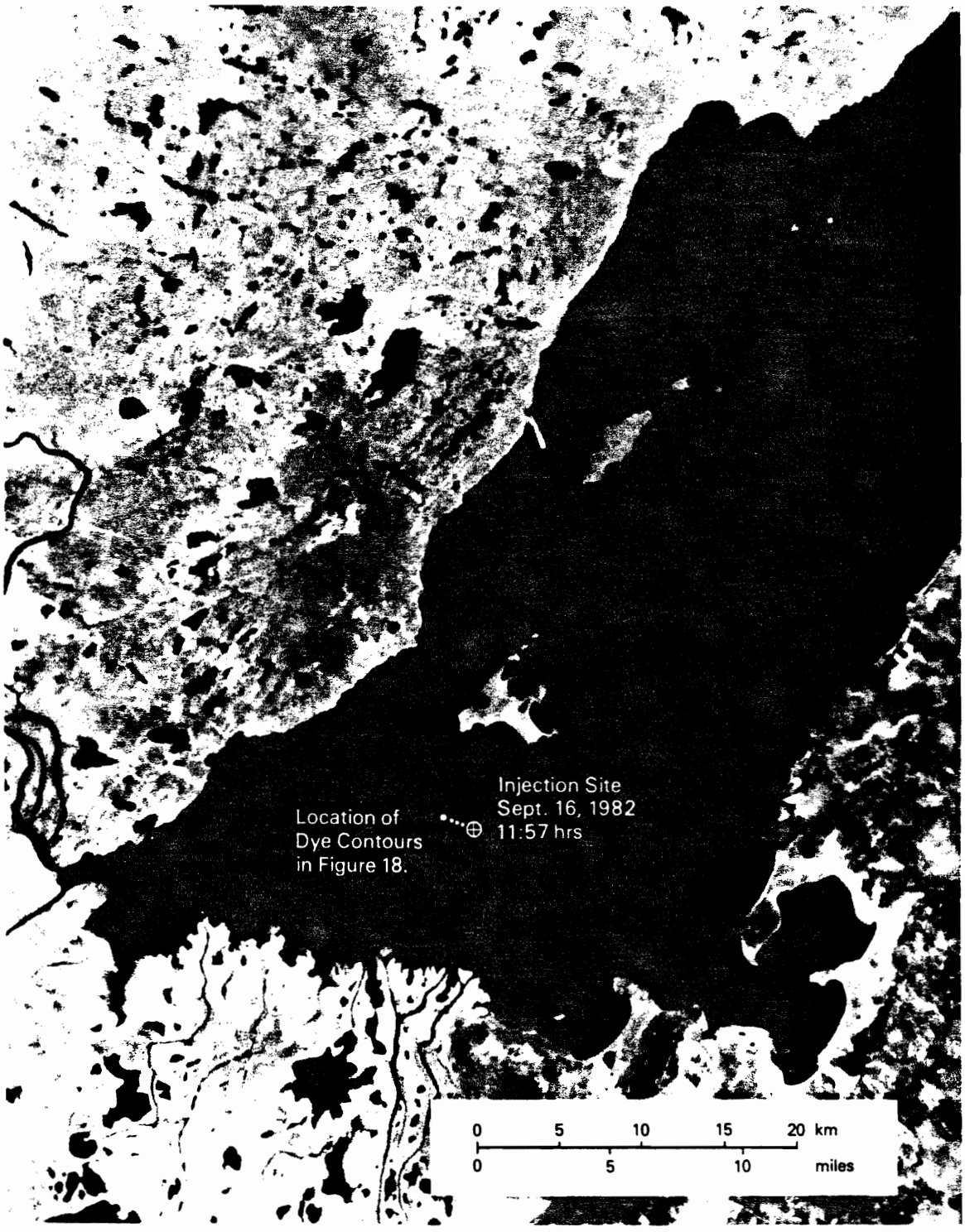

Figure 17. Location of Lake Injection Site

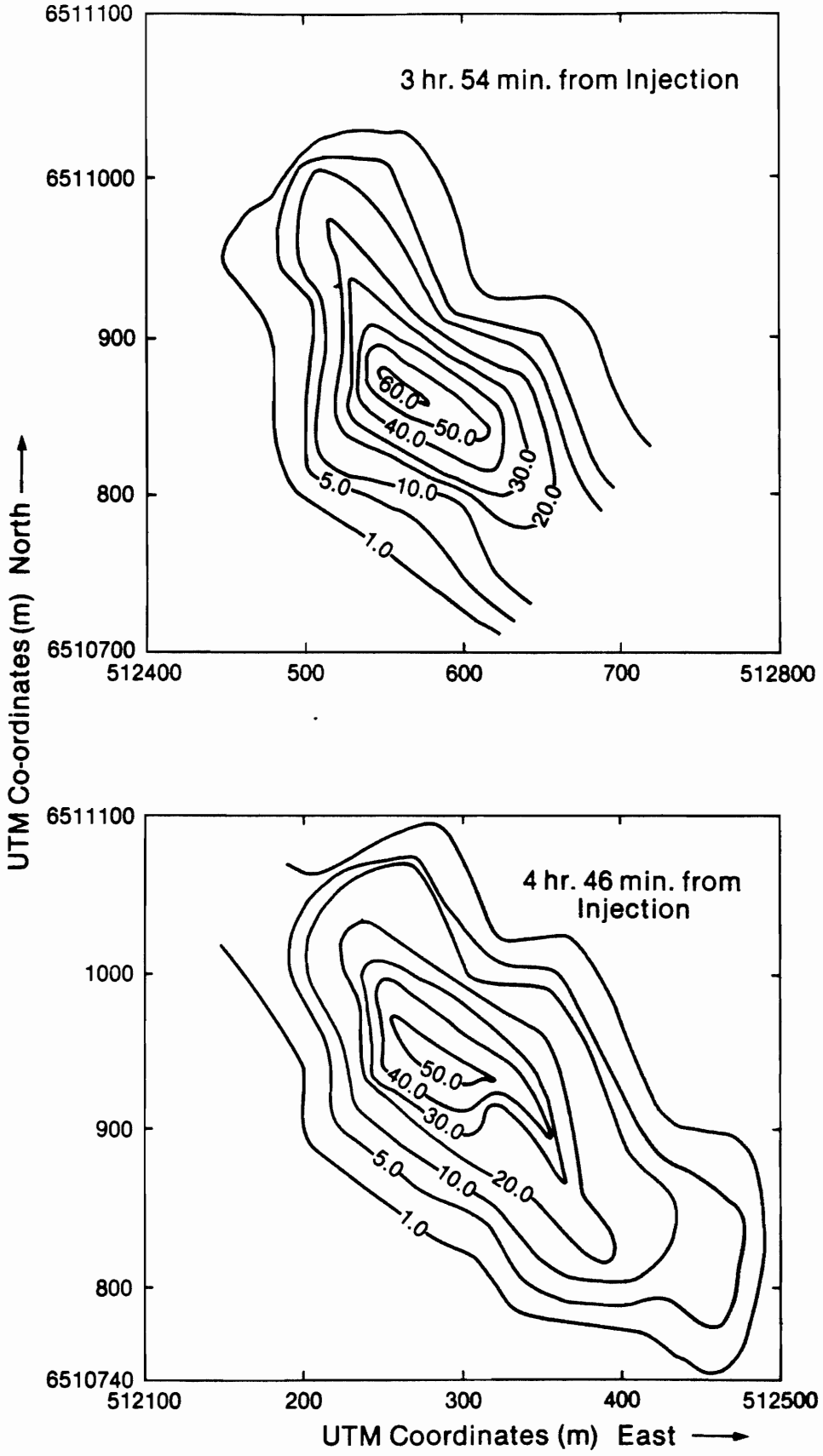
3 hr. 54 min. from Injection
6511100
6511000
900
800
6510700
512400
500
600
700
512800
60.0
50.0
40.0
30.0
20.0
10.0
5.0
1.0
4 hr. 46 min. from Injection
6511100
1000
900
800
6510740
512100
200
300
400
512500
50.0
40.0
30.0
20.0
10.0
5.0
1.0
UTM Co-ordinates (m) North
UTM Coordinates (m) East

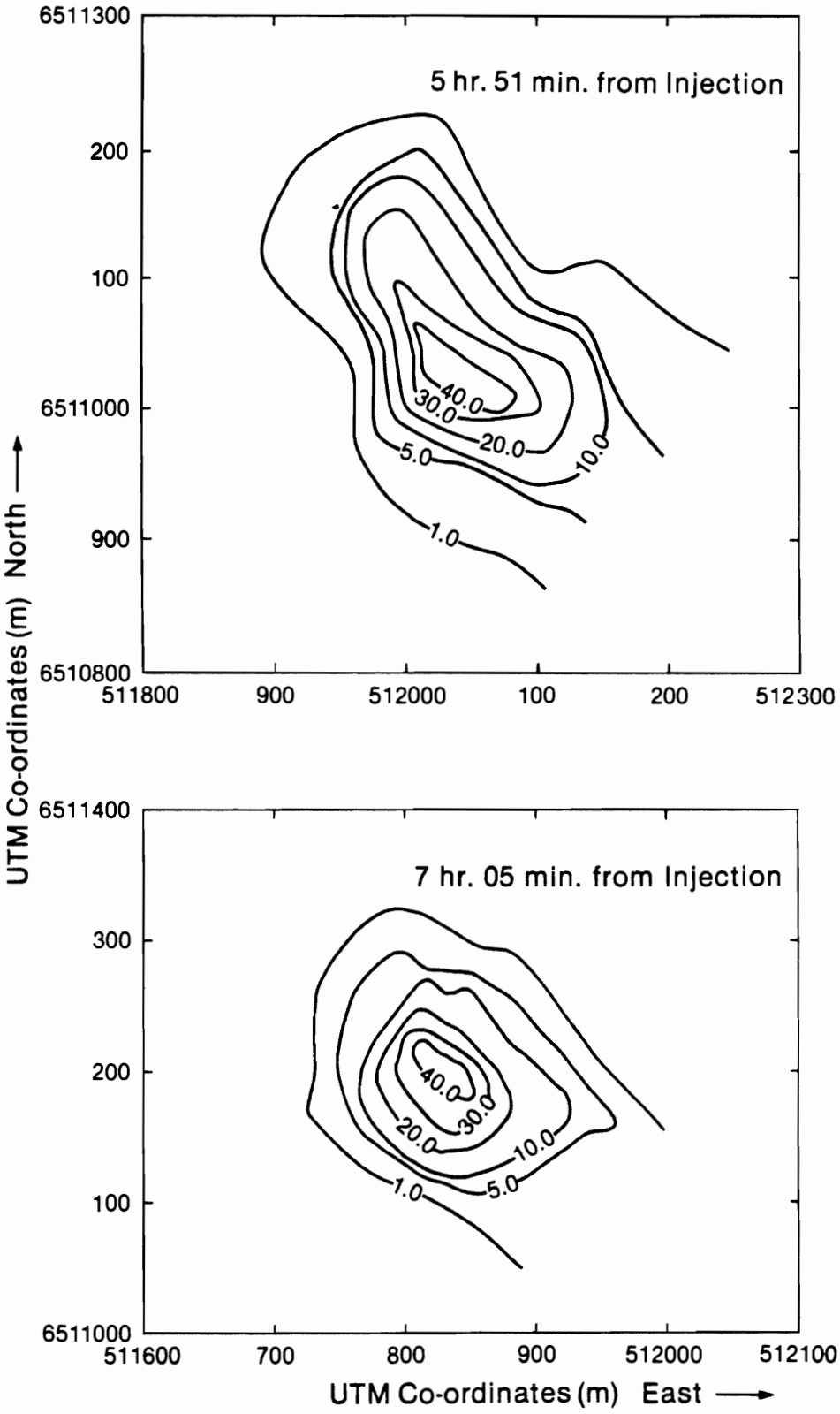
5 hr. 51 min. from Injection
6511300
200
100
6511000
900
6510800
511800
900
512000
100
200
512300
40.0
30.0
20.0
10.0
5.0
1.0
7 hr. 05 min. from Injection
6511400
300
200
100
6511000
511600
700
800
900
512000
512100
40.0
30.0
20.0
10.0
5.0
1.0
UTM Co-ordinates (m) North
UTM Co-ordinates (m) East

The mixing, or spread, of the dye cloud is characterized by the variance of the concentration distribution. If x is the longitudinal direction and y the lateral direction, the variances s_x^2 and s_y^2 are defined by

$$s_x^2 = \frac{\int_{-\infty}^{\infty} x^2 \, c \, dx}{\int_{-\infty}^{\infty} c \, dx} - \left(\frac{\int_{-\infty}^{\infty} x \, c \, dx}{\int_{-\infty}^{\infty} c \, dx} \right)^2$$

and

$$s_y^2 = \frac{\int_{-\infty}^{\infty} y^2 \, c \, dy}{\int_{-\infty}^{\infty} c \, dy} - \left(\frac{\int_{-\infty}^{\infty} x \, c \, dy}{\int_{-\infty}^{\infty} c \, dy} \right)^2$$

where c is the dye concentration. The dye cloud was typically elongated in the longitudinal direction so the calculation of s_x^2 and s_y^2 is made along the major and minor axes of the cloud. A mixing coefficient in each direction can be calculated from the rate of growth of variance(Fischer, et al, 1979) from the relationships

$$\varepsilon_x = \frac{1}{2} \frac{ds_x^2}{dt}$$

$$\varepsilon_y = \frac{1}{2} \frac{ds_y^2}{dt}$$

where ε_x and ε_y are the mixing coefficients in the x and y directions and t is time. Figure 19 shows a plot of s_y^2 versus t for the lake mixing test. The data indicate a lateral mixing coefficient of 0.016 m^2/s. Figure 20 shows the longitudinal variance plotted with time. There is considerable scatter in these data, probably due to sampling difficulties due to waves during the longitudinal profiles. The longitudinal mixing coefficient, based on the first two data points,

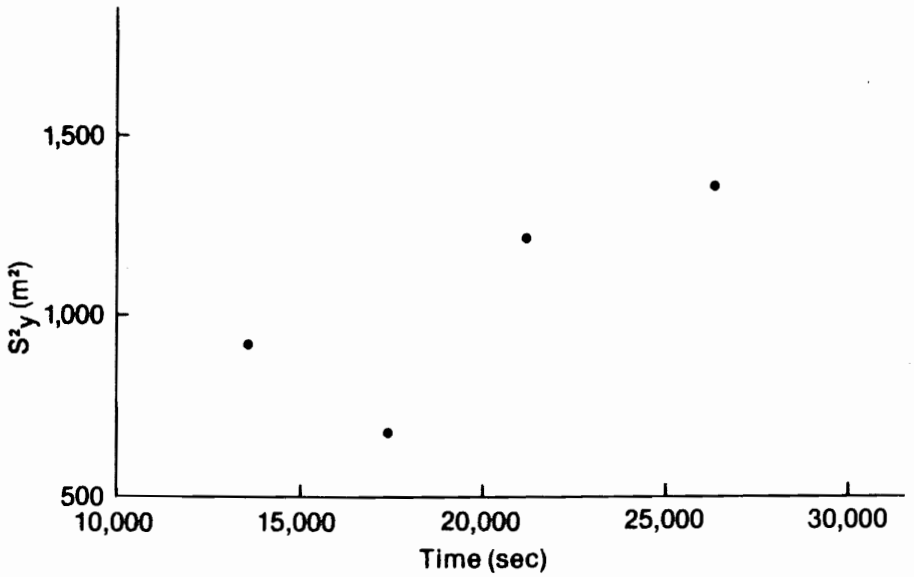

S^2_y Versus t, Lake Mixing Test, September 1981

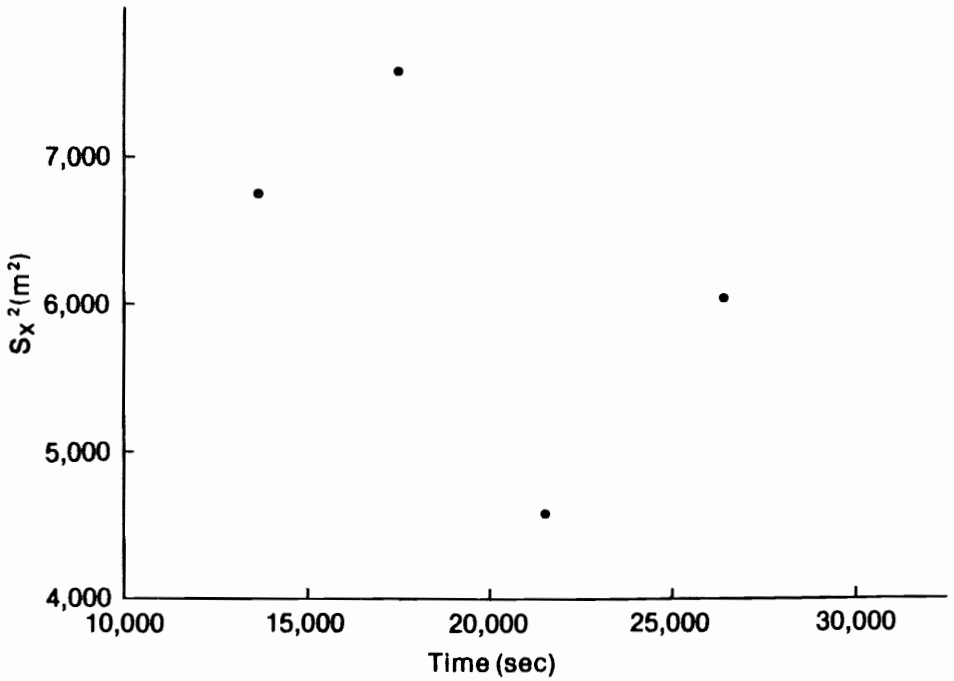

S_X^2 Versus t, Lake Mixing Test, September 1981

is estimated around 0.24 m^2/s. These values are of the same order as those determined by Neill, et al (1981). Recovery ratios for the dye were about 70% for the first three traverses and 40% for the last traverse. The relatively low recovery is probably due to poor definition of the low concentrations around the edges of the dye cloud. The uncertainty in this area also affects the variance calculations and accounts for some of the scatter in Figures 19 and 20.

Although it was not possible to track the dye from either injection to the lake outlet, some characteristics of the mixing patterns in the lake were clarified. For example, as river flows decline over the summer, river water does not extend as far north, which is obvious. However, most of the flow from the Embarras River, Fletcher Channel and Goose Island Channel, which represents about 56% of the Athabasca River discharge, moves west across the delta front. The August data further indicate that most of the river water in the Rochers probably originates from Big Point Channel. Under conditions of west or southwest winds, the Goose Island Channel flow may move further into the lake. Mixing characteristics will be discussed further in section 4.

2.5 FEBRUARY 24 - MARCH 4, 1982 MEASUREMENTS

This trip was undertaken in order to conduct a dye test under ice-covered conditions. Flow in the Athabsca River at Embarras Airport was estimated at 98 m^3/s, which is well below the February mean of 169 m^3/s reported by Neill, et al (1981) and is the lowest flow of record since 1958 (Environment Canada, 1979). Flow in the Fond du Lac River was estimated at 128 m^3/s, which is also below the February mean of 201 m^3/s. Flow measurements by Alberta Environment indicated that of the four main distributary channels, only Big Point Channel had any detectable currents, these being in the order of 0.06 m/s. Of the outlet channels, only the Riviere des Rochers had any measurable flow. Based on the work of Lipsett and Harrington (1981), outflow in the Rochers was estimated at 200 m^3/s. Throughout the test, temperatures were extremely low and hampered operations. Daytime highs rarely exceeded $-30^{\circ}C$ and nighttime lows were always below $-40^{\circ}C$. North winds of up to 6 m/s were common.

Since it was anticipated that sampling would be carried out over a 24 hr. period, a base camp was established by a crew of four people on the ice 5 km southwest of Bustard Island on February 24. On February 25 the injection site was drilled 3.5 km south and 1 km east of the southwest end of Bustard Island as shown in Figure 21. In addition, a line of sampling sites was established for 5 km north of the base camp and spaced every 250 m. At 1600 hrs. on February 26 a 15 kg slug of Rhodamine WT dye mixed with methanol was injected under the ice. Ice thickness on the lake averaged 0.8 m while the depth of water below the ice averaged 1.2 m. Velocities were measured at all sampling sites and ranged from 0.015 m/s to 0.035 m/s with the average velocity being 0.025 m/s. The direction of flow was generally west to southwest. Water quality measurements indicated dissolved oxygen levels in the lake of 10 mg/L and a temperature of 0.4^{o}C. Specific conductance was 112 μS/cm, indicative of predominantly lake water and the pH was 7.27. The outflow, based on the mean depth and velocity, and assuming a flow width of 8 km, was estimated at 240 m^3/s which is reasonably close to the estimated flow in the Rochers.

Sampling for dye started on February 27. Samples were taken in a 2 km arc around the injection site to cover the expected trajectory of the dye, as well as along the sampling line north of the base camp. Samples were taken just below the ice, just above the bed and at two intermediate points. The samples were prevented from freezing and returned to the base camp for fluorescence analyses. Sampling was carried out every three hours until March 1. No samples exhibited any trace of dye. To check that the dye had not remained in the injection hole or frozen to the underside of the ice, the injection site was redrilled and no significant quantities of dye were found. On March 1, two people were dispatched to Fort Chipewyan to monitor the outlet channel in the event that the dye had missed all the sampling sites. Sampling at the outlet was maintained at 2 to 4 hr. intervals for the duration of the test. On each of March 2, 3 and 4, a crew returned to the sampling site and worked its way back to Fort Chipewyan collecting samples for analyses. No dye was found in any samples. On March 4 operations were terminated.

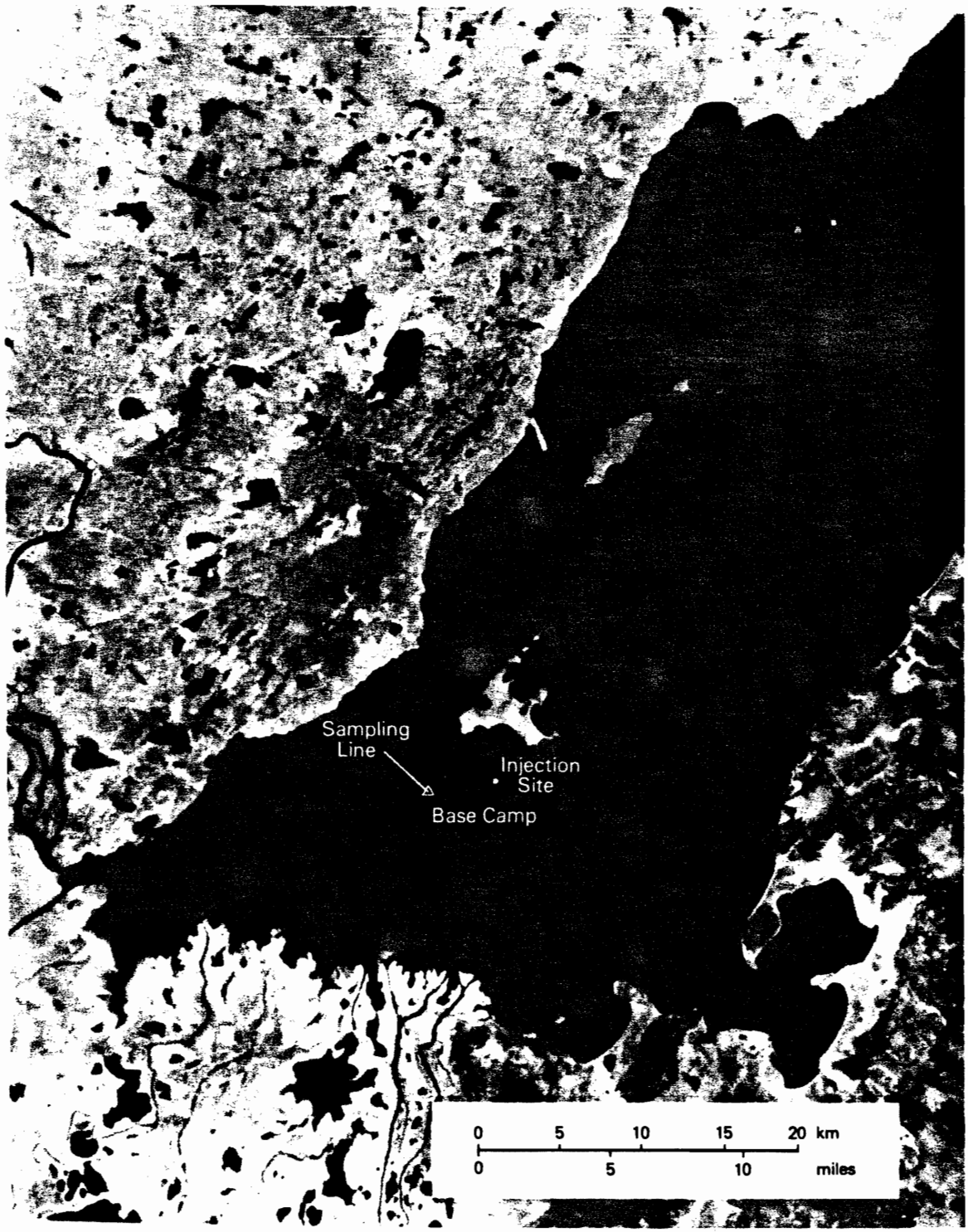

Figure 21. Location of Winter Injection Site

The results of this test were disappointing in that no dye was recovered. There are two possible explanations for not having recovered the dye. One is that the low velocities inhibited spreading of the dye cloud to the extent that none of the sampling holes intersected the dye's path. This possibility is unlikely, however, since the location and approximate size of the cloud can be estimated from the summer dye test and the mean velocities. The lateral dispersion coefficient from the summer data was 0.016 m^2/s. If it is assumed that the winter conditions had a mixing coefficient of only one third of this value, the variance of the concentration distribution can be estimated from the relationship.

$$2\ \varepsilon_y\ dt = ds^2$$

Measurable dye concentrations should be found over a width of approximately 6 s, which, after only two days travel time, is about 250 m. Since this was the spacing of the main sampling line, it is unlikely that the dye cloud missed the sampling holes. Further, after two days, the dye would have moved approximately 4 km which would put it at the location of the main sampling line. Since sampling was carried out for over three days and included several auxiliary sampling sites, it seems unlikely that the dye was missed. The second, and more likely explanation is that the dye simply sank as a result of the low velocities. Although methanol had been mixed with the dye prior to injection, the stoichiometric quantity was reduced somewhat to ensure that the dye was not buoyant and could not freeze or stick to the underside of the ice.

2.6 SUMMARY OF FIELD STUDIES

As previously stated, the field studies were undertaken to achieve two goals, the first being collection of water quality data contemporaneous with LANDSAT overpasses and the second to acquire data that could be used in calibration of a mathematical model. To varying degrees, both objectives were satisfied. The initial assessment of 25% probability of success in obtaining simultaneous satellite coverage and lake sampling was correct and only one set of data was suitable

for detailed comparison to satellite data. The remaining data did prove useful in assessing the circulation patterns in the lake and provided further insight to the sources of sediment and the degree to which lake and river water could intermix. The current data were not as extensive as initially planned but wind and wave conditions precluded any additional measurements. The mixing tests provided information concerning the mixing coefficients in the lake and the mixing characteristics in various parts of the lake. The extremely low flows during the winter test rendered those results least satisfactory in terms of meeting the test objectives.

3. ANALYSIS OF SATELLITE IMAGERY

This phase of the project was undertaken to assess the utility of using remotely sensed satellite imagery for evaluating water quality and inferring circulation patterns. The work of Neill, et al (1981) has demonstrated the potential of using this technique and part of this project's objectives was to gather additional data and more fully investigate the potential for quantitative interpretation.

3.1 LANDSAT IMAGERY

The satellite imagery analysed in this study were obtained from LANDSAT satellites. These satellites (LANDSAT 2 and LANDSAT 3) each operate on 18 day cycles with a nine day phase difference. Thus, overpass of a particular site occurs every nine days. In addition, as previously stated, the northerly location of the study area results in overlapping coverage for three days.

The LANDSAT satellites employ multi spectral scanners (MSS) which sense the electro magnetic energy which is reflected from or emitted by the target body. The energy reflected from a water body comprises three components: some energy is reflected from the water surface; energy not absorbed by the water may be reflected from the bottom; and energy may be reflected from suspended particles. Since the LANDSAT MSS receive this energy in four separate wavelength bands, the nature of the signal received by each band varies. Band 4 (0.5-0.6 μm) and band 5(0.6-0.7 μm) receive energy in the visible range while band 6(0.7-0.8 μm) is in the near infrared range and band 7 (0.8-1.1 μm) is in the infrared range.

Energy in the band 7 wavelengths is almost completely absorbed in the top one or two centimetres of the water so the scanners receive no reflected signal unless there is floating or exposed surface material to provide reflection. As will be discussed, this band was used to delineate the land-water interface for later analysis. Energy in the band 6 range penetrates to a greater depth before it is totally absorbed and can, therefore, be used in analysing near surface sediments.

Bands 4 and 5 exhibit larger and more variable depth penetration. Factors affecting the depth penetration include the concentration of suspended sediments, in that higher concentrations reduce the penetration depth. Bartolucci, et al (1977) show that the penetration depth is about 0.30 m at sediment concentrations of 100 mg/L. These results are similar to the concentrations and Secchi depths measured in June. Blanchard and Leamer (1973) indicate that band 5 is probably most useful for discerning variations in suspended sediment although they point out that the nature of the spectral response depends on the sediment type. For example, red and black sediments can exhibit reversals in response at high concentrations. They suggest for suspended sediment concentrations above 75 mg/L, detection of sediment may not be feasible, although this limit is a function of sediment type. On the other hand, Ritchie, et al (1976) suggest that band 6 is the best spectral region for detecting sediment and their data included sediment concentrations up to 350 mg/L. In addition, LANDSAT data have been used sucessfully to observe the occurence of estuarine fronts (Klemas and Polis, 1977), the occurence of internal waves (Apel, Charnell and Blackwell, 1974) and to map the distribution of water containing industrial waste (Klemas, Bartlett and Philpot, 1978).

Products available from LANDSAT data include both paper copies and computer compatible tapes (CCT). Black and white pictures for each MSS band are available in various scales. In addition, colour composites can be obtained. The C1 composite is produced by combining band 4 with a blue filter, band 5 with a green filter and band 7 with a red filter. This composite is useful in assessing sediment patterns and results in clear water appearing dark blue and sediment laden water appearing lighter blue or grey. The C2 composite is not as useful for sediment analysis and comprises band 5 (green filter), band 6 (red filter) and band 7 (blue filter). Other colour composites are available on special request. The CCT product contains the digital recording of the measured response of each MSS band. Each picture element (pixel) covers a ground area of 80 m x 80 m and the entire image covers an area approximately 185 km x 185 km. Each pixel has associated with it a number from 0-255 for each band, with the larger number indicating

a higher value of reflected energy. This product is well-suited to quantitative analysis, as described by Lodwick (1979).

3.2 IMAGE ANALYSIS

As previously discussed, satellite coverage and lake sampling were obtained simultaneously only once, in August. Ideally, sampling should occur within a few hours of overpass. However, the size of the area to be sampled and the inability to venture onto the lake on some days prevented such sampling to occur. Satellite overpass occurred on August 9, 10 and 11 while sampling was carried out on August 8 and 10. Because conditions on August 8 and 10 were similar, it was decided to use the entire data set in analysis of the August 10 imagery. Obviously this will introduce some measure of error to the results and they should be interpreted with these facts in mind.

The main constituents of the image analysis phase of the project were as follows. The LANDSAT image was enhanced using principal components analysis (Lodwick, 1979). This reduced the complexity of the LANDSAT 4 band multivariate data set. The image was then rectified to the ground using a third order polynomial modelling technique and spatial resection to ground control points (Lodwick, 1978). The ground-truth data were then compared to the LANDSAT data using a simple linear regression algorithm and computing the correlation coefficients. A principal components analysis was also performed on the groundtruth data and this was then compared to the enhanced LANDSAT data using the same linear regression algorithm as above.

The data used in the comparison to the satellite imagery were:

(1) conductivity at the surface,
(2) pH at the surface,
(3) suspended organics at the surface (mg/L),
(4) bed material D_{50} (μm)
(5) bed material D_{90} (μm)
(6) total suspended sediment at the surface (mg/L),
(7) total suspended sediment at 0.3 m depth (mg/L),

(8) total suspended sediment at 1.0 m depth (mg/L),

(9) total dissolved solids at the surface (mg/L),

(10) total dissolved solids at 0.3 m depth (mg/L) and

(11) total dissolved solids at 1.0 m depth (mg/L).

LANDSAT 2 images of Lake Athabasca were obtained for August 9, 10 and 11, 1981. Copies of the imagery for bands 4 to 7 and a C1 composite are shown in Figure 22. The August 10 image used for analysis is 2239217500 of track 46 frame 19. Time of overpass was 1750 GMT or 1050 MST. Perusal of the original photographic imagery shows clear sedimentation patterns in the lake.

Another feature which shows up clearly on the imagery is the effect of haze. At the time of overpass there was much smoke in the atmosphere due to the effects of forest fires. Because the atmosphere selectively scatters the shorter wavelengths of light, LANDSAT band 4 (0.5 to 0.6 μm) will contain the highest component of scattered light, and band 7 (0.8 to 1.1 μm) the least. This effect to the north of Lake Athabasca can be clearly seen in Figure 22.

As well as the photographic imagery, a magnetic tape containing digital information from all four bands was obtained. This enabled the analytical manipulation of the LANDSAT data.

The computer system used for the enhancement has been described in Lodwick (1981). The system was developed at the University of New South Wales and is available for use on the Honeywell 66/80 computer at The University of Calgary. A schematic of the system is given in Figure 23. The computer programs are written in Fortran and carry out the following procedures:

(1) reformatting the original Canada Centre for Remote Sensing (CCRS) tapes for the Honeywell computer, and selection and storage of a 600 x 600 pixel study area,

(2) presentation and display of the data and results by shadeprints, characterprints and video displays,

(3) correction of the data by use of image statistics,

(4) calculation of principal components and scores,

(5) geometric rectification of the image section by least-squares reduction,

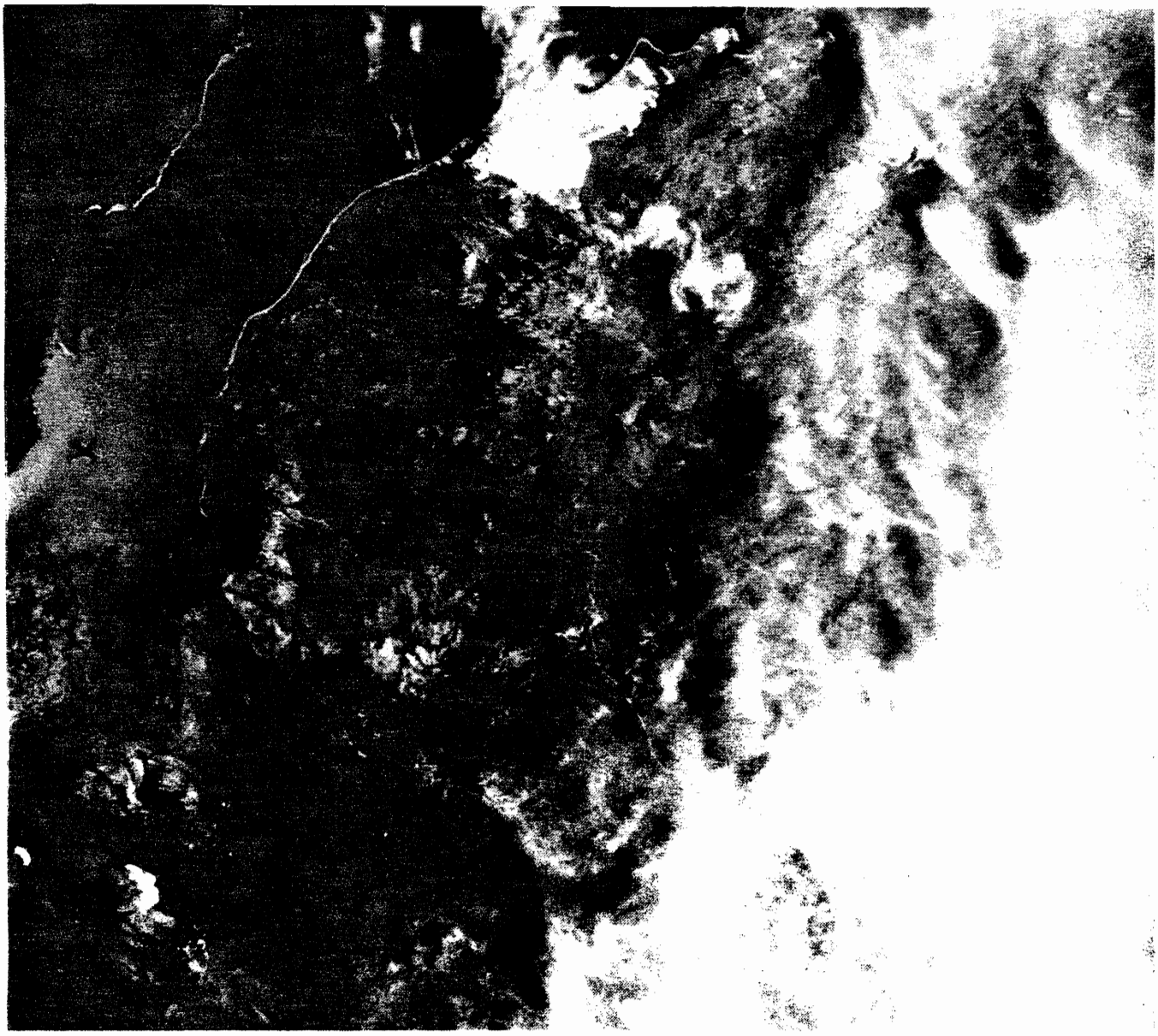

August 9, 1981

August 10, 1981

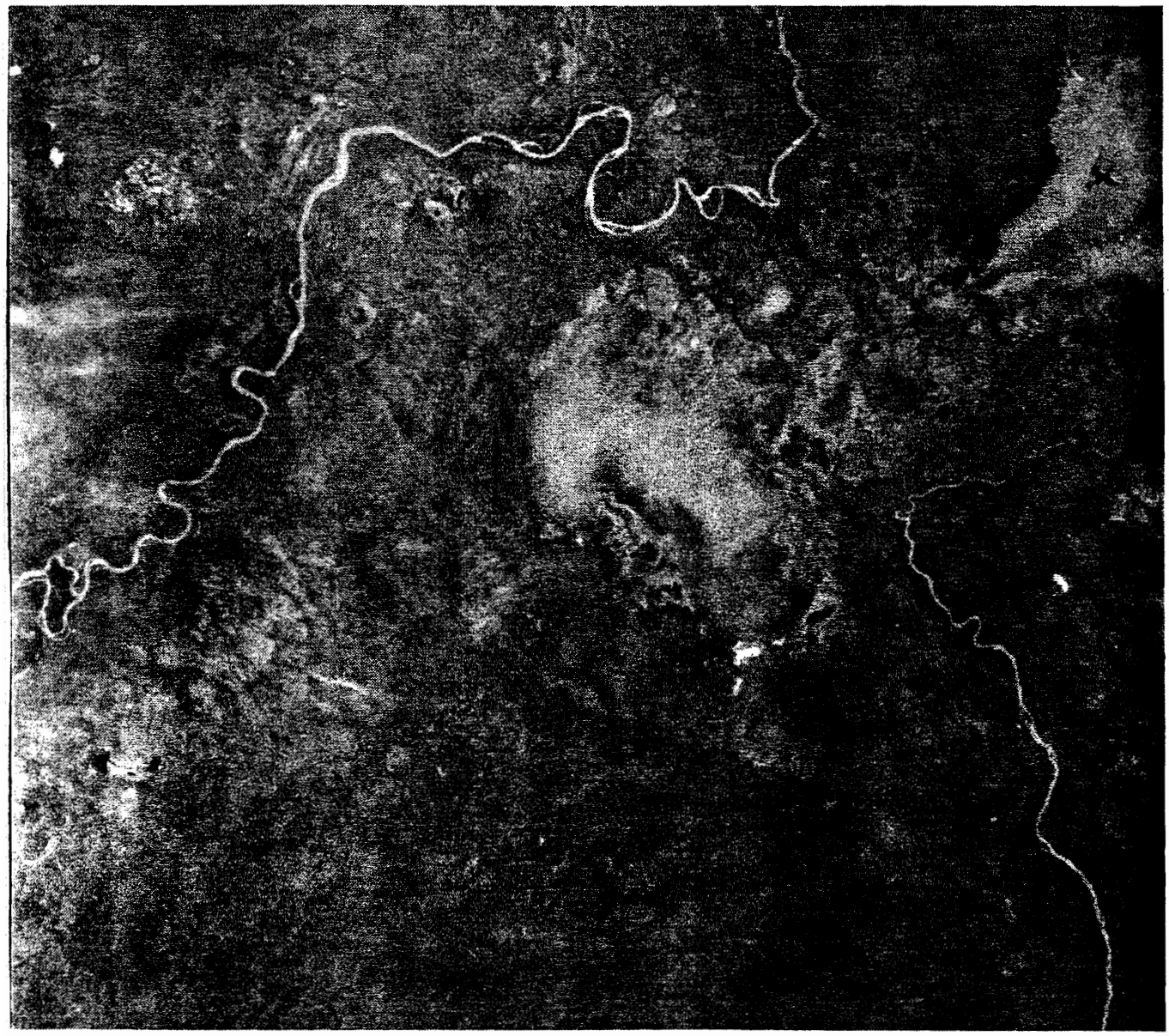

August 11, 1981

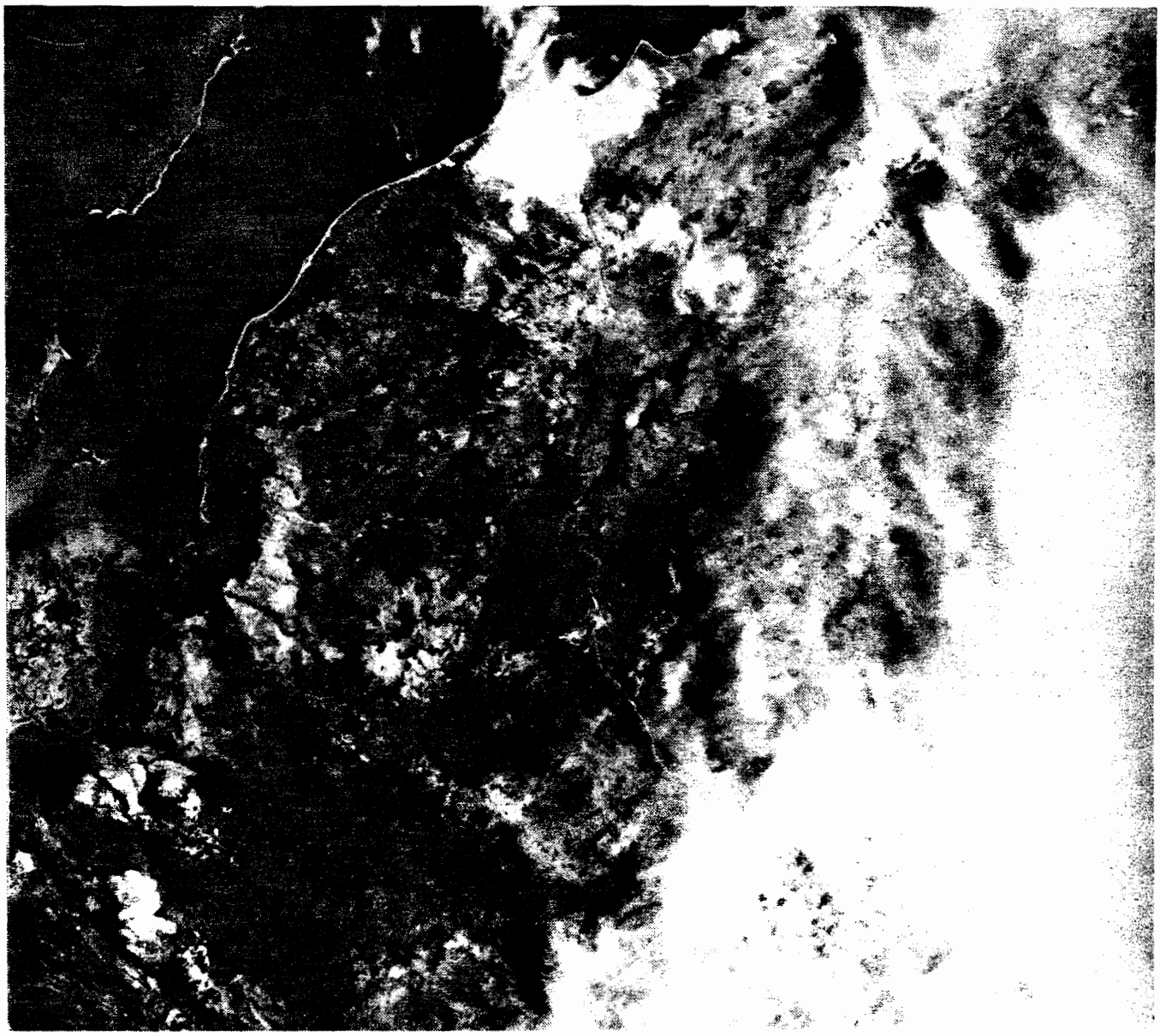

August 9, 1981

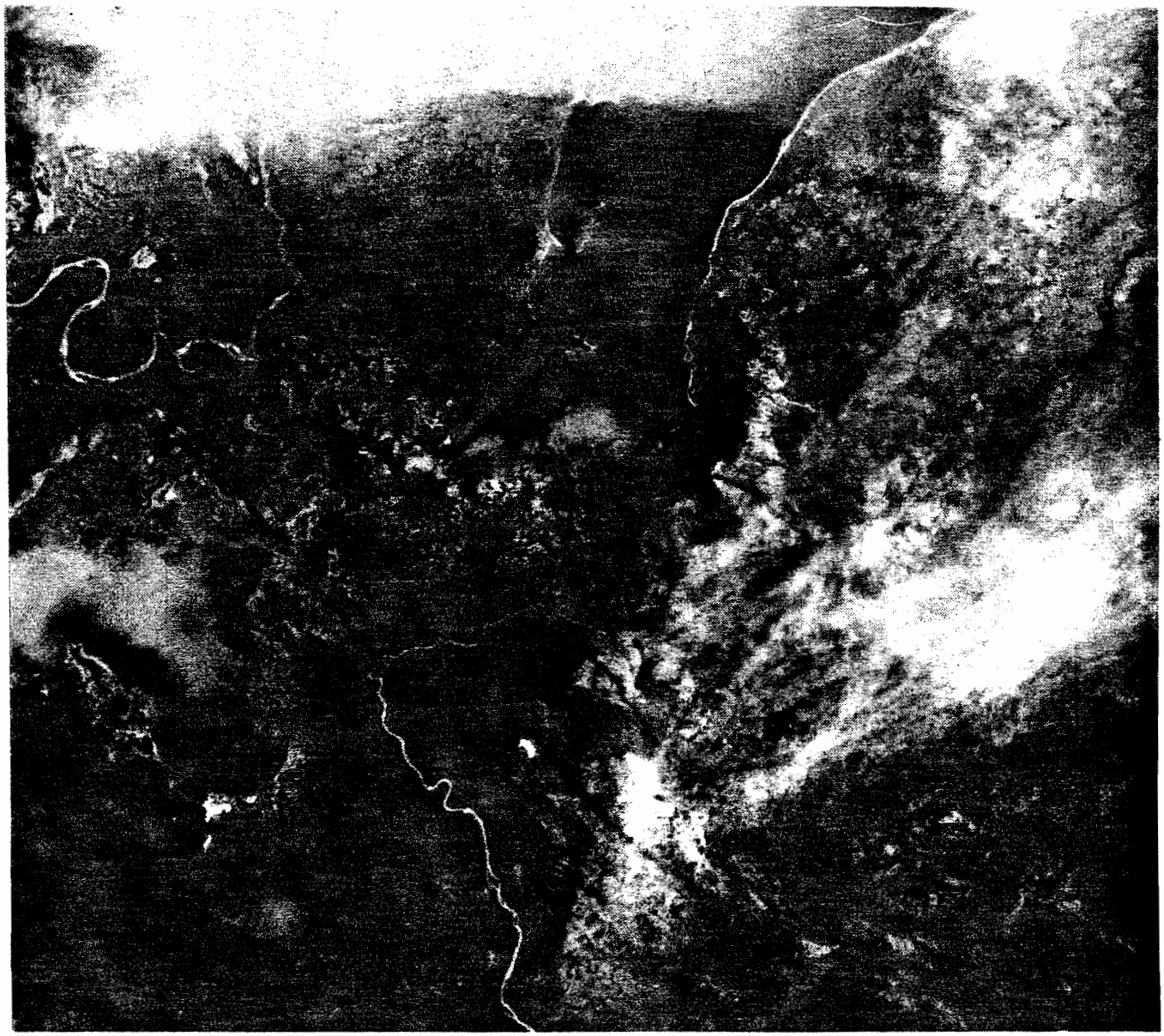

August 10, 1981

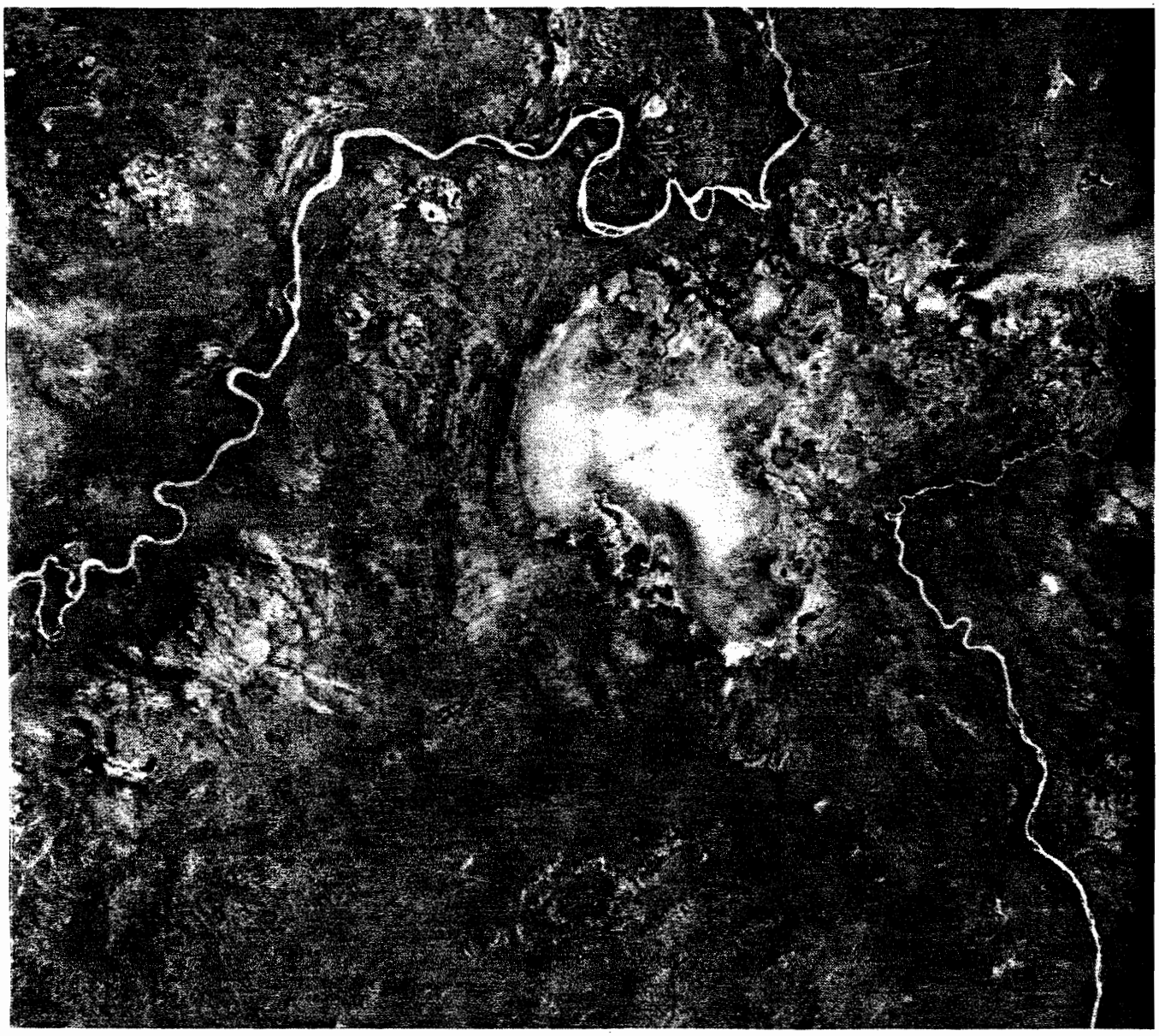

August 11, 1981

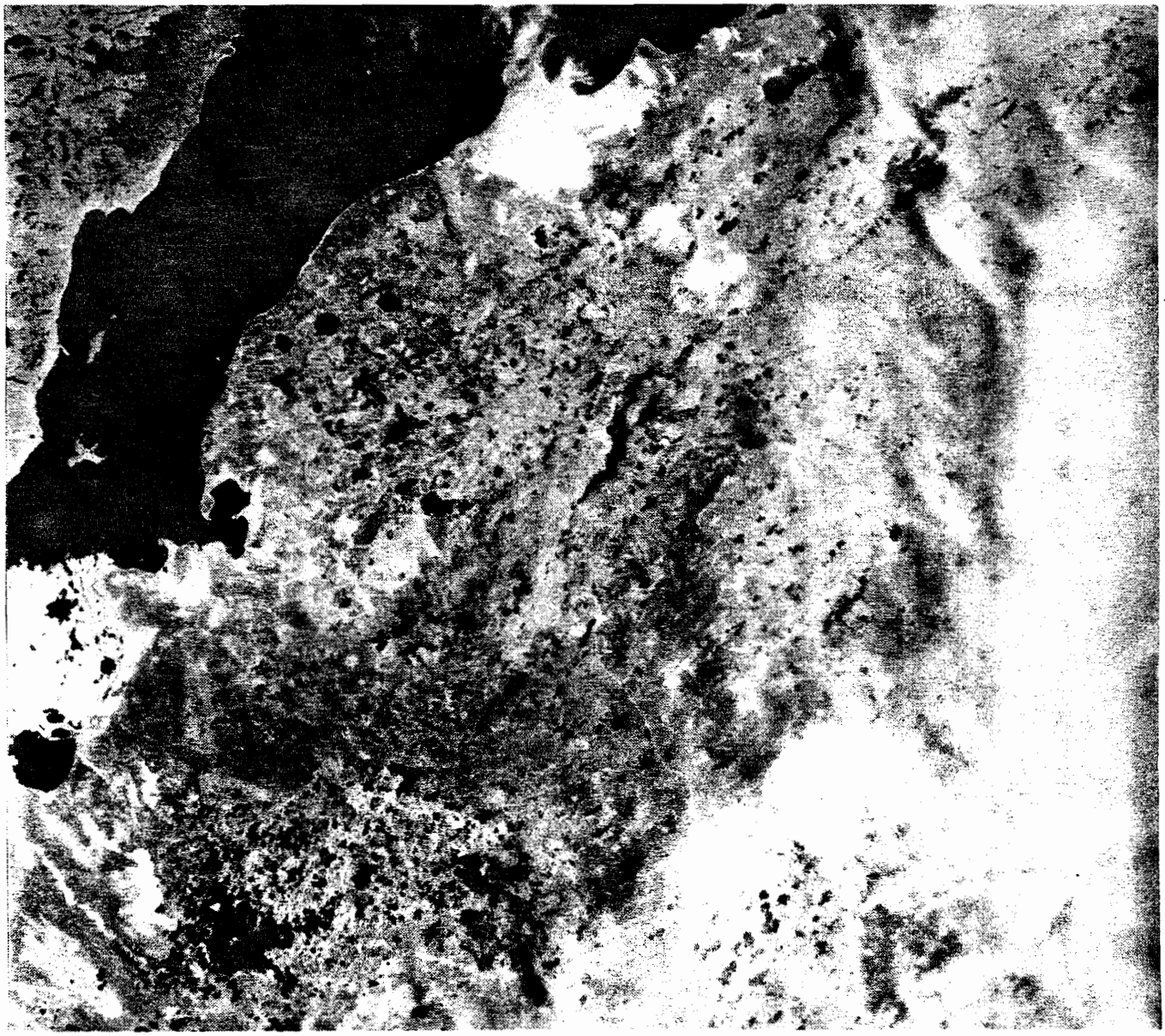

August 9, 1981

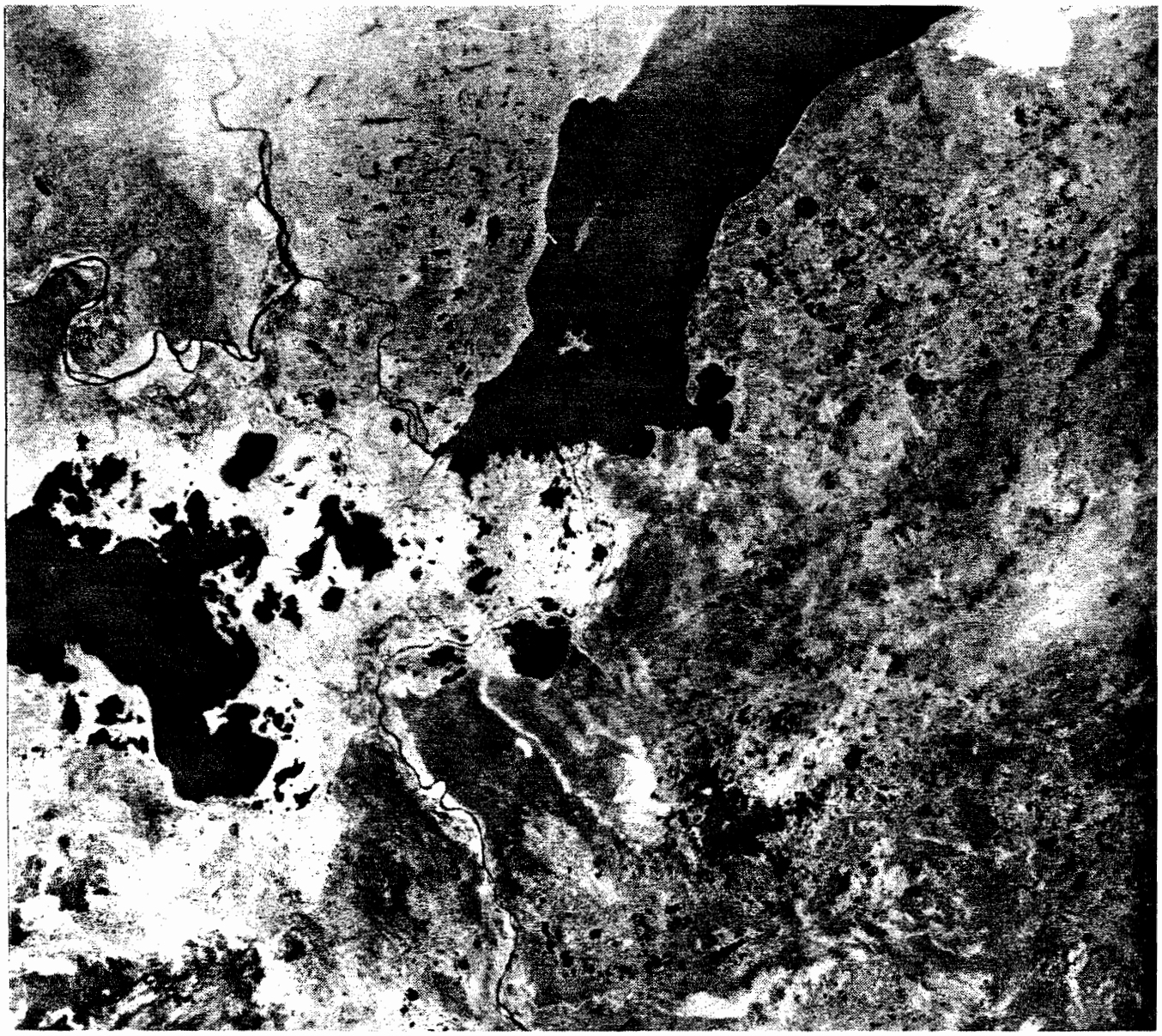

August 10, 1981

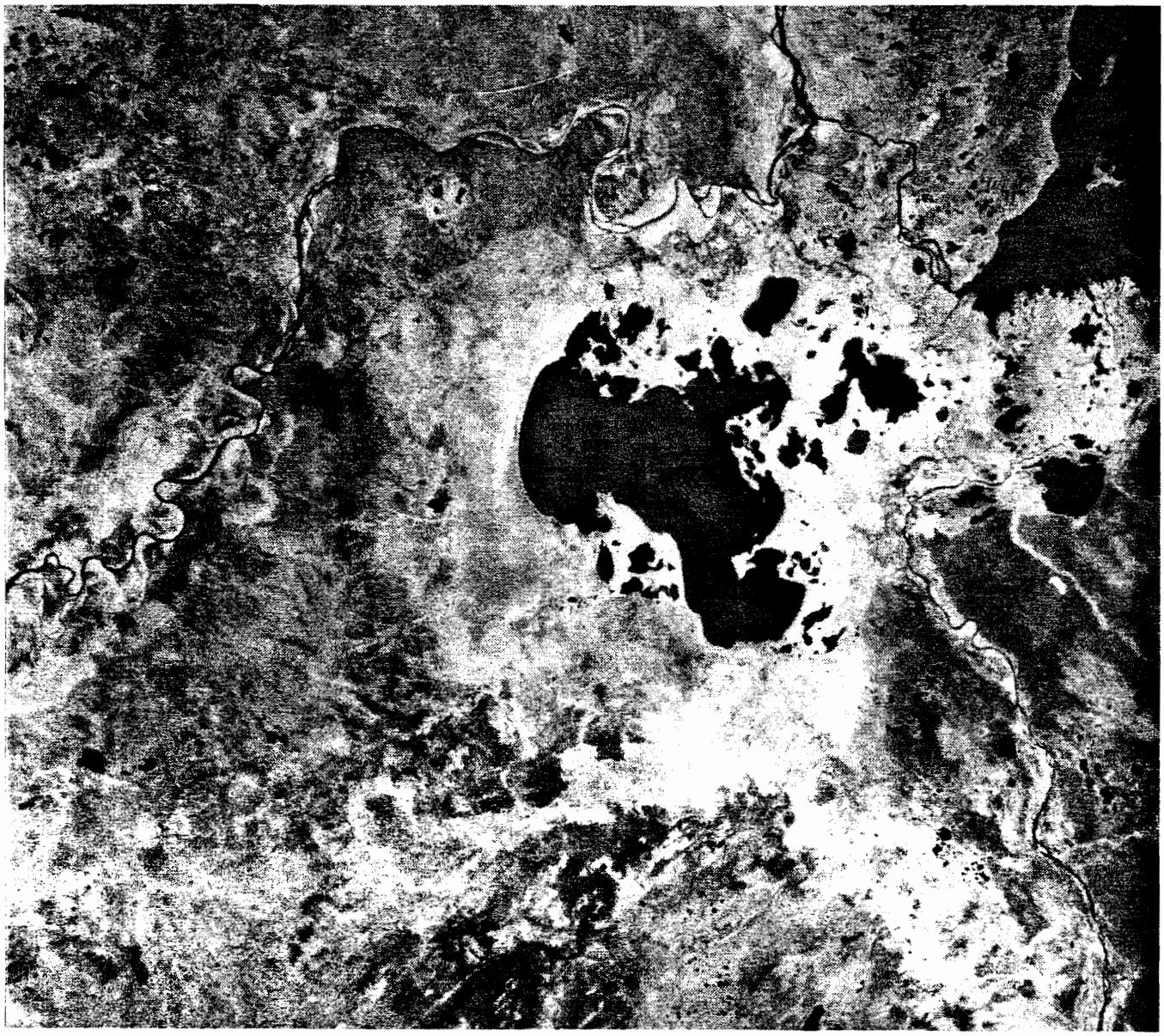

August 11, 1981

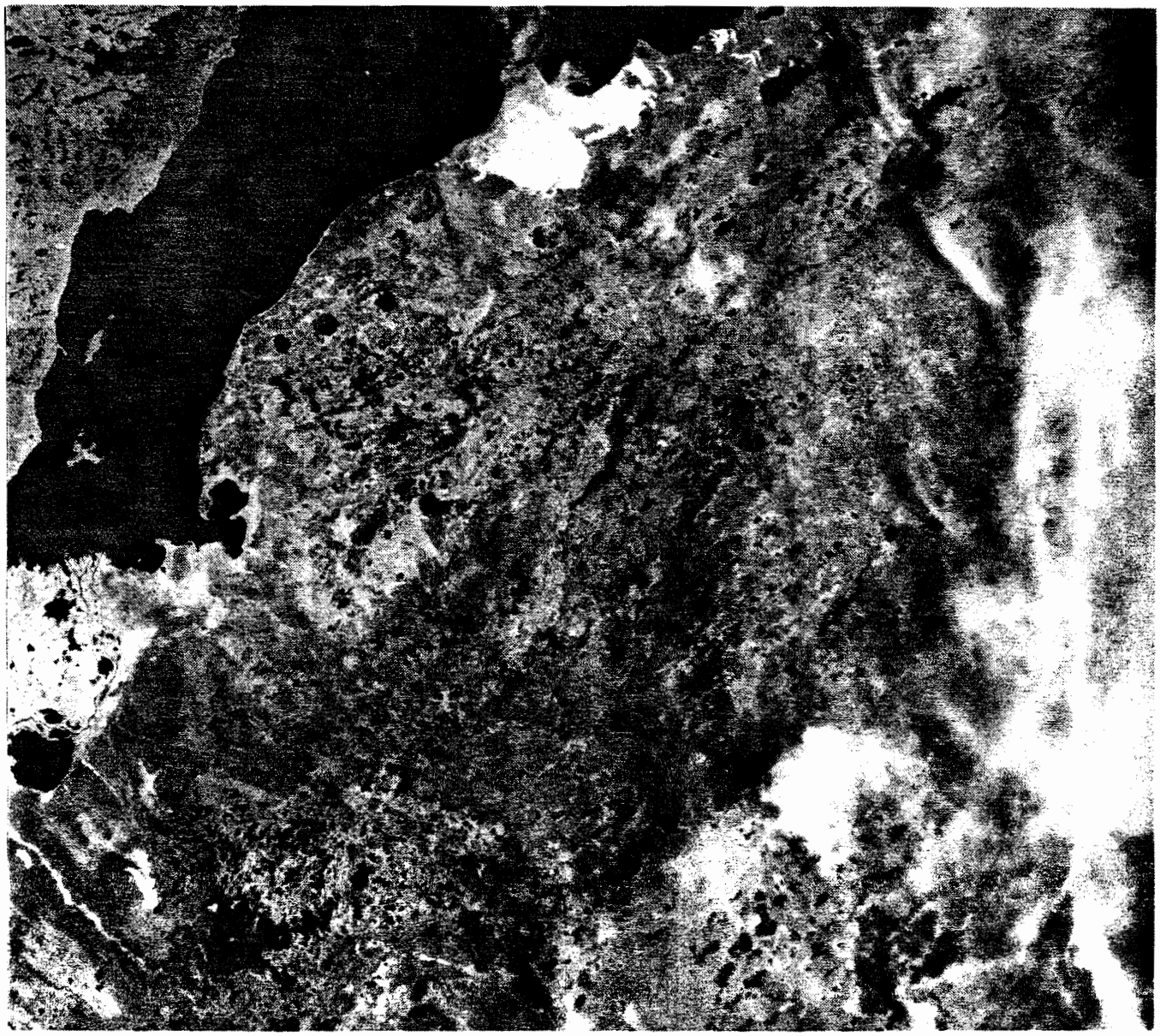

August 9, 1981

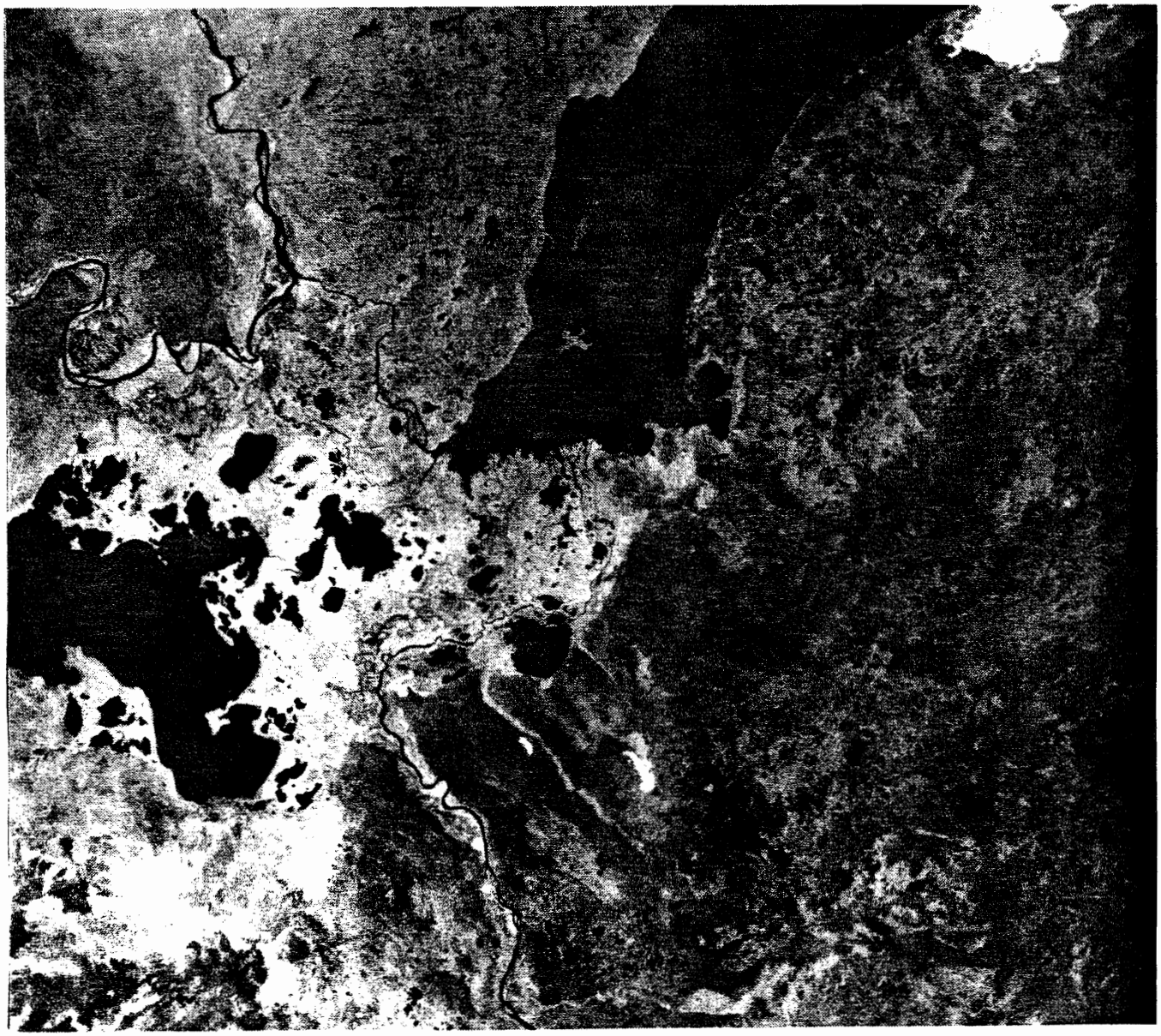

August 10, 1981

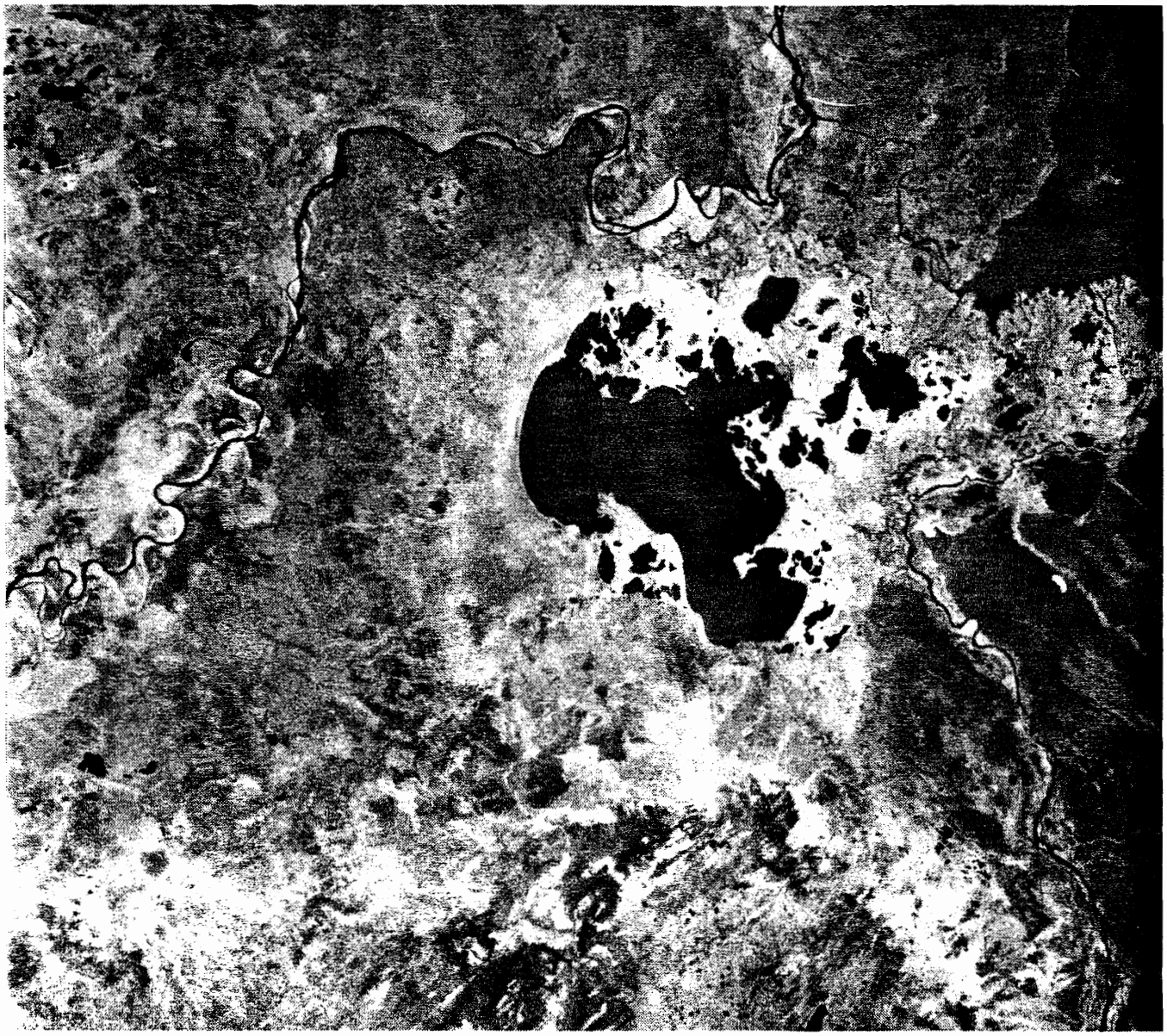

August 11, 1981

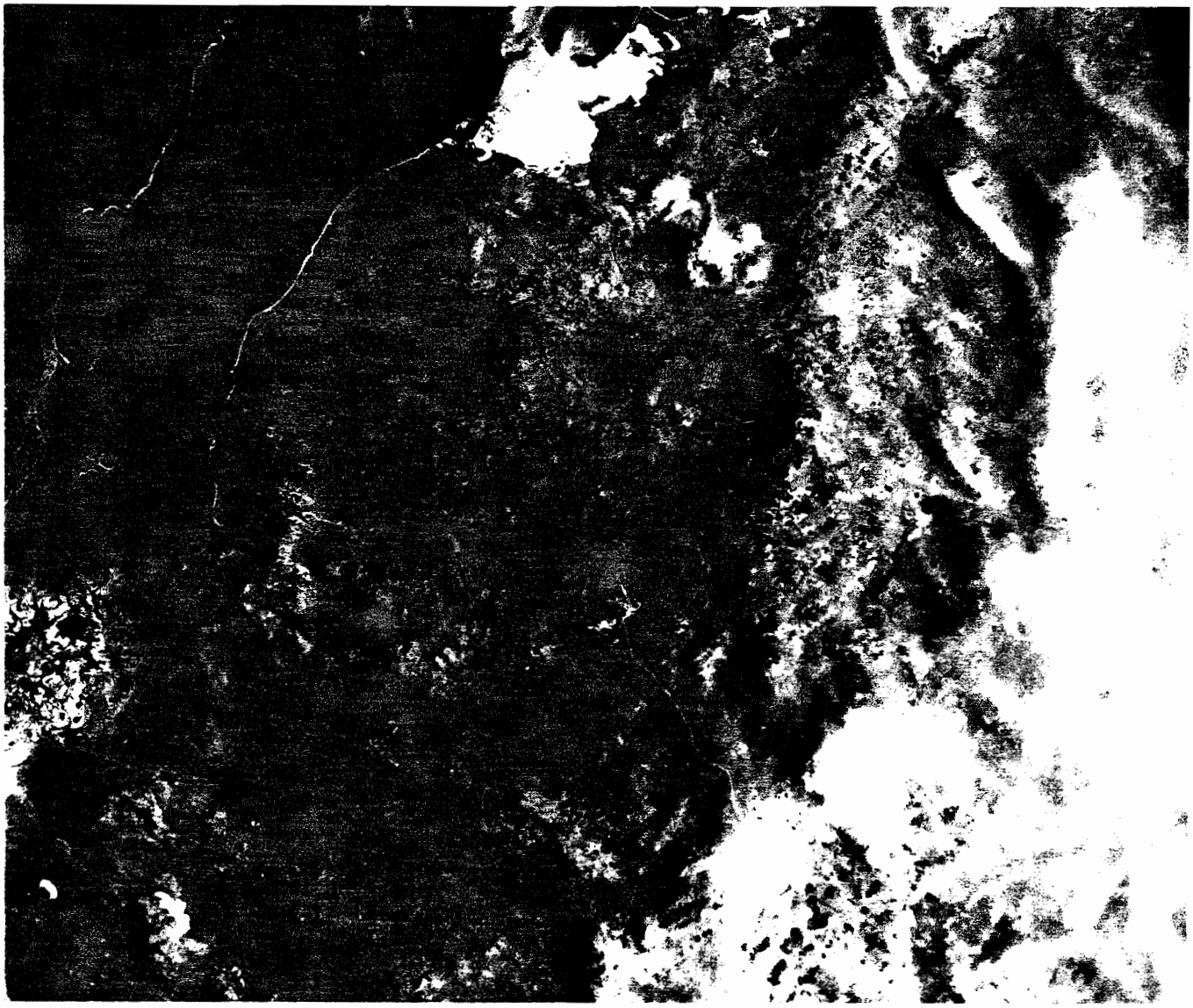

August 9, 1981

August 10, 1981

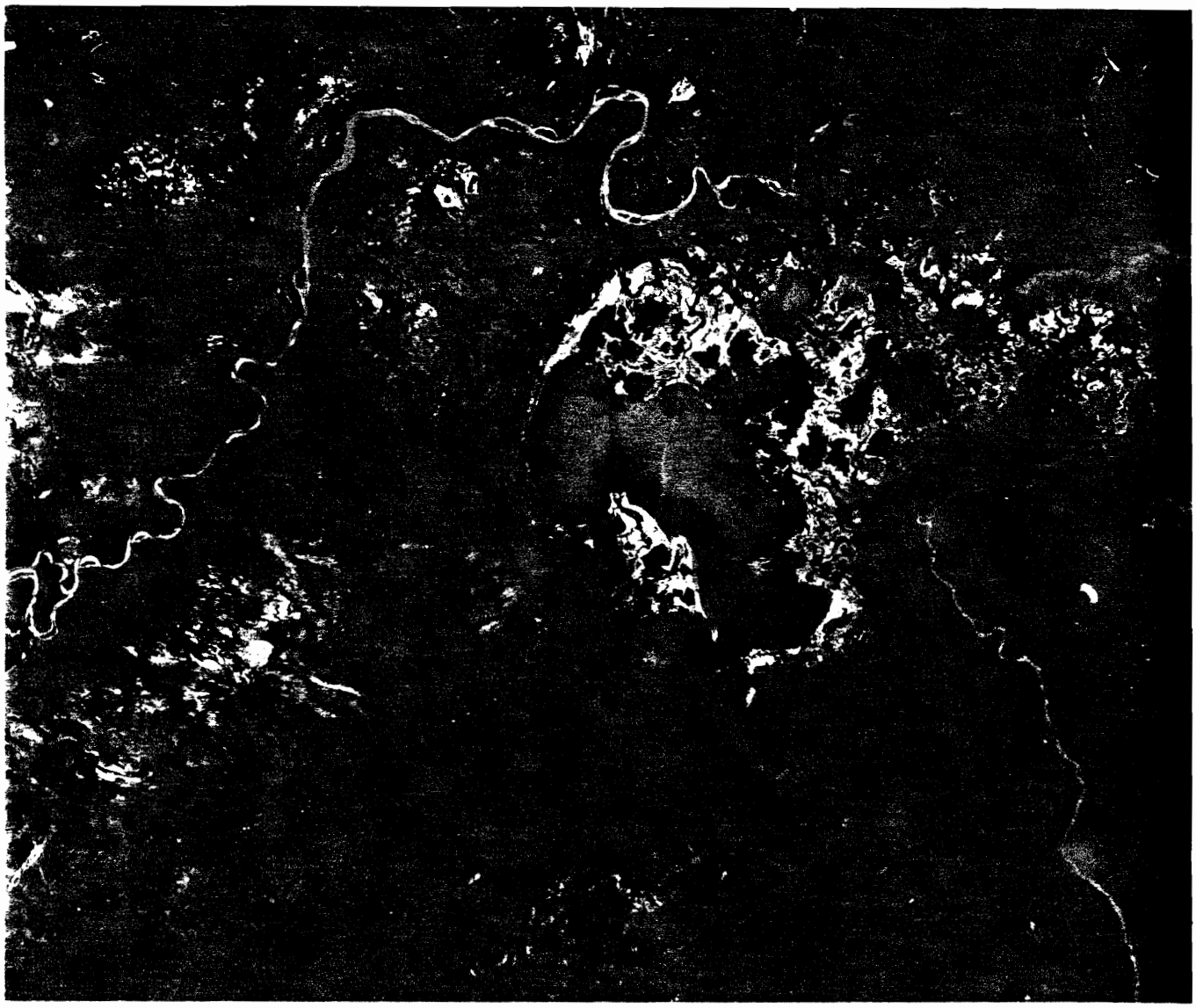

August 11, 1981

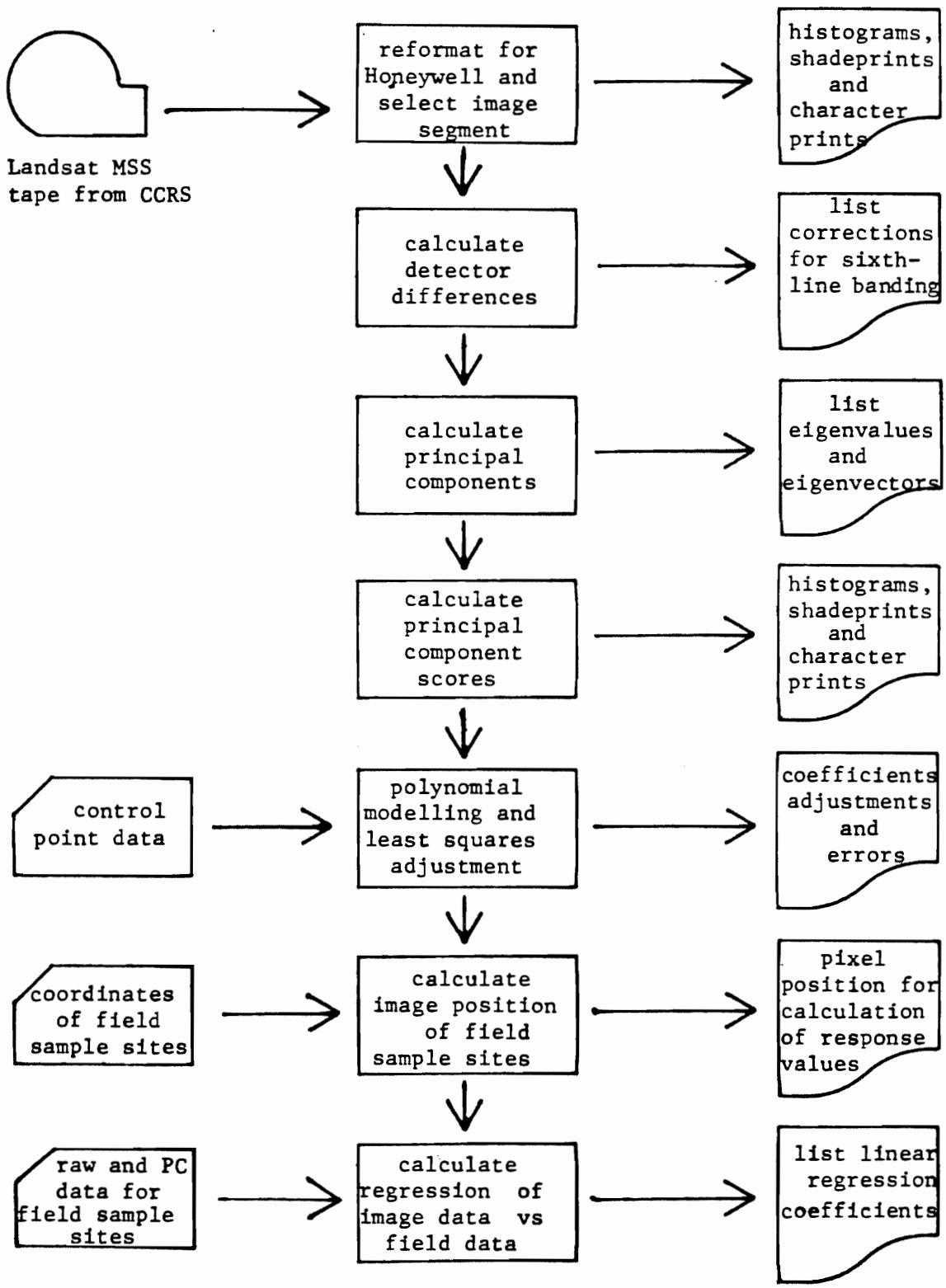

Figure 23: Computer System

(6) calculation of image position and response levels of specific field sites in the image,

(7) correlation of the response values with field data.

The 600 x 600 pixel image segment selected for detailed study is situated at the southwest end of Lake Athabasca. Its position is marked on band 7 of the August 10 image in Figure 22. Shadeprints for bands 4 and 7 produced from the CCT for this segment are shown in Figure 24. Note again, the clear sedimentation features discernable in band 4 as compared to band 7.

For the image segment, histograms of the response levels for all four bands were produced. These are displayed graphically in Figure 25. Here there are two aspects to note. First of all, for band 6 and 7, the form of the distribution is bimodal. The node of higher response values corresponds to the more brightly reflecting land surface, whereas the other node corresponds to the highly absorbent water surface. Second, saturation has not occurred for any of the bands. Also, there is a good measure of discrimination in the response values. In band 7 for example, there is a dynamic range in the water node of around 35 pixel response values.

One of the requirements, however, to carry out a meaningful principal components analysis is that the form of the response distributions should be symmetrical. As indicated above, for the infrared bands, there is a bimodal distribution, formed because of the two disparate componets, water and land. An initial step was, therefore, carried out to separate these two components. This was done on the basis of the band 7 response values. A cut-off was set in each program whereby only those pixels with a band 7 value less than or equal to 35 were considered in the analysis. Figure 26 displays all these lower values as black and higher values as white. It can clearly be seen how well the land-water interface is delineated based on the band 7 data.

The only video data correction that had to be considered in this study was to account for sixth-line banding. Other effects which may occur (e.g. atmospheric scatter, or haze) are substantially eliminated by the enhancement process itself, which standardizes the

Band 4

Band 7

FIGURE 24.

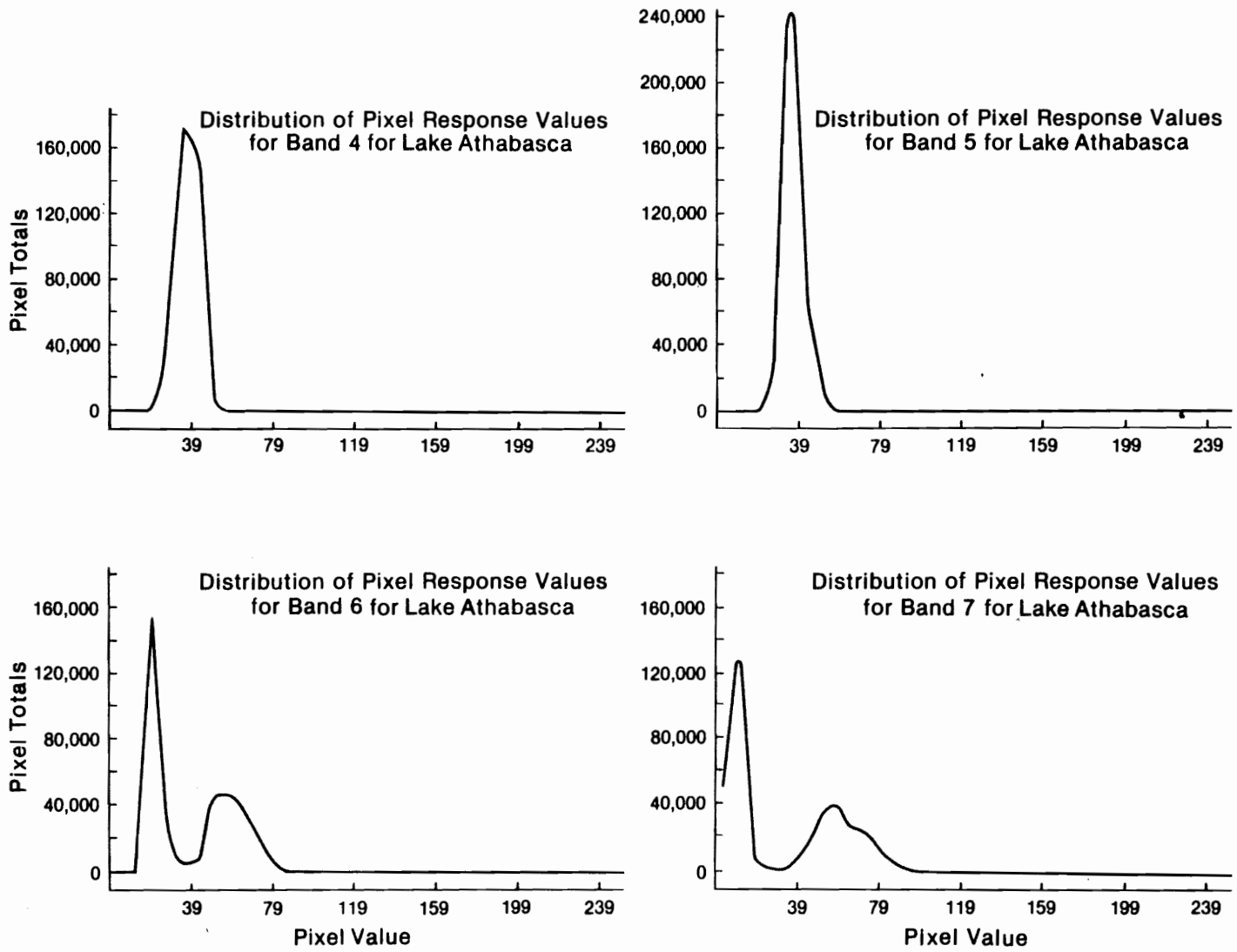
Distribution of Pixel Response Values
for Band 4 for Lake Athabasca
Pixel Totals
160,000
120,000
80,000
40,000
0
39
79
119
159
199
239
Distribution of Pixel Response Values
for Band 5 for Lake Athabasca
240,000
200,000
160,000
120,000
80,000
40,000
0
39
79
119
159
199
239
Distribution of Pixel Response Values
for Band 6 for Lake Athabasca
Pixel Totals
160,000
120,000
80,000
40,000
0
39
79
119
159
199
239
Pixel Value
Distribution of Pixel Response Values
for Band 7 for Lake Athabasca
160,000
120,000
80,000
40,000
0
39
79
119
159
199
239
Pixel Value

Figure 21

data. The effect of sixth-line banding can be seen in Figure 24. This shows the band 7 response values for the image segment. A striping effect can be seen across the lake surface in the across track (or sensing) direction and is due to the fact that each band is sampled by a six sensor array. Because the segment measures approximately 15 cm in the along track direction (corresponding to 600 lines or 100 swaths) each band will appear to be around 1.5 mm wide on the image.

Correction for sixth-line banding involves an analysis of the whole image segment, by calculating the means and standard deviations for each of the four detectors for each of the six lines. The philosophy behind this method of correction is that, for a large enough segment (in this case, 196376 pixels for the water surface, giving over 32000 values for each of the six lines) the average response levels recorded should be the same. The formula for adjustment is:

$$P_c = S \times (P_o - m_i) / S_i + M$$

where

P_c = corrected pixel value
P_o = original pixel value
M = mean of the whole data set
S = standard deviation of the whole data set
m_i = mean of the data set for band i
S_i = standard deviation of the data set for band i

The detector differences are quite small. Both the means and the standard deviations for individual lines are shown in Table 5. For the means, the largest difference for the band is less that 0.4 (measured on a scale 0 to 255) whereas the maximum difference for a band for the standard deviation (equal to S/S_i) ranges from 0.950 to 1.042.

Despite the fact that striping was removed using this statistical approach, the important conclusion from this analysis is that sensor calibration differences are quite small as compared to the dynamic range of the response values.

Sensor means	Band 4	Band 5	Band 6	Band 7
line 1	40.811	36.763	22.347	9.296
line 2	41.006	36.844	22.776	9.375
line 3	40.981	36.856	22.585	9.210
line 4	40.902	36.761	22.632	9.667
line 5	40.780	36.497	22.817	9.512
line 6	40.626	36.948	23.102	9.583
averages	40.851	36.778	22.709	9.440
Sensor SD's				
line 1	4.831	4.325	4.307	4.262
line 2	5.086	4.524	4.215	4.287
line 3	4.791	4.584	4.190	4.272
line 4	4.757	4.432	4.350	4.292
line 5	4.968	4.641	4.602	4.645
line 6	4.791	4.555	4.623	4.489
averages	4.874	4.514	4.391	4.380

Table 5: Sensor Means and Standard Deviations for the 24 Detectors for the Lake Athabasca Image Segment

Detailed investigation of LANDSAT data requires analysis of a 4 band data set. Principal components analysis (PCA) is useful for this purpose because it can usually reduce the spatial complexity of multivariate problems. (A theoretical discussion on the use of multivariate techniques in the earth sciences is given by Davis (1973)). The technique involves an orthonormal transformation which produces a rotation of the image data set but individual points retain their relative positions through the transformation. The method involves setting up a variance-covariance matrix and recalculating scores for the samples along the principal components (or eigenvectors) which represent new variables. These new variables, identical in number to the original ones, are linearly independent and the total variance calculated for the scores is identical to the variance in the original bands. However with LANDSAT data, because of the high correlation between the original bands, the first (PC1) and second principal components (PC2) typically account for more than 95 per cent of the original variance. Thus the original spectral position of a particular data element can be defined in terms of a vector in two dimensions with negligible loss of information, and this can be compared to those of other elements.

For Lake Athabasca, both the non-standardized and standardized components were calculated. Standardization is carried out simply by adjusting the distribution of each band to a mean of zero and a standard deviation of one. In this way bands which have a greater dynamic range (usually bands 6 and 7) will not contribute a disproportionate amount of the variance. The eigenvalues and eigenvectors in both standardized and non-standardized form are given in Table 6.

As indicated above, when a PCA is performed on LANDSAT data, the first and second principal components together usually contain over 95 per cent of the information from all four bands of the original data. This is due to the high degree of correlation between the original spectral bands. However, these results are typical for LANDSAT images involving mostly land and vegetation (Lodwick, 1977). In contrast, the results of the standardized data for this study showed that PC1 contained 47% of the total variance, PC2 almost 38%, PC3 over 12% and PC4 around 3%. The non-standardized values were similar.

Non-Standardized Data

Eigenvalues

36.4075	44.1%
33.0447	40.0%
10.6638	12.9%
2.4725	3.0%

Eigenvectors

-0.0015	0.3440	0.7014	0.6243
-0.7675	-0.5839	0.0544	0.2588
0.6320	-0.6499	-0.0527	0.4188
-0.1074	0.3439	-0.7088	0.6065

Standardized Data

Eigenvalues

1.8814	47.0%
1.4967	37.4%
0.4946	12.4%
0.1273	3.2%

Eigenvectors

0.0336	-0.3005	-0.7043	-0.6423
-0.7131	-0.6530	0.0122	0.2549
-0.6889	0.5960	0.0817	-0.4044
-0.1257	0.3580	-0.7051	0.5991

Table 6: Eigenvalues and Eigenvectors for the Lake Athabasca Image Segment

In both methods, the form of the transformations is also of interest. PC1 can be seen to be emphasizing bands 6 and 7 as shown in Table 6 since the weighting of each band to the principal component is the corresponding value of the eigenvector. These bands represent the infrared part of the spectrum, and together contribute approximately 90 per cent of the information contained in PC1. (Their contribution is calculated by squaring the appropriate coefficients in the eigenvector.) Similarly, PC2 can be seen to be emphasizing bands 4 and 5 which represent the visible end of the spectrum. These bands contribute over 90 per cent of the information contained in PC2. With PC3, bands 4 and 5, which contribute over 80 per cent of the information, have different signs. Therefore PC3 is emphasizing the difference between the two visible bands. In the same way PC4 emphasizes the difference between the two infrared bands, but is much less important because it contains only around 3 per cent of the total variance.

The scores for each component were calculated and the data displayed by means of histograms and shadeprints. Shadeprints for PC1, PC2, PC3 and PC4 scores are shown in Figure 27.

Imagery rectification involved spatial resection to ground control points using cubic polynomials. Image rectification using polynomials has been discussed by Derouchie and Forrest (1974) and Wong (1975). The particular method used in this system has been outlined by Lodwick (1978) and Trinder and Smith (1979). With this approach certain known geometric errors need to be taken into account before rectification. There are the swath discontinuous errors (sensor delay and earth rotation). The swath continuous errors (e.g. non-linear mirror velocity) and the global continuous errors (e.g. roll, pitch, yaw) are fully accommodated by the modelling procedure.

Usually control points comprise naturally occurring features that are clearly identifiable in the image, although methods have been reported for producing artificial control points by generating identifiable landmarks imaged by the satellite at the time of overpass (e.g. Evans (1974), Evans (1976), McCloy (1977), and Thomas, Allcock and Child (1979)). However, as Forrest (1970) points out, the control points need not be points on the earth's surface that have been precisely surveyed. The important requirements are that the location

FIGURE 27 Pc

PC3 + PC4

accuracy be commensurate with the scale of the mapping to be done from the image, and that the control points be easily and uniquely identifiable.

Overall, 23 points were identified for control using a character print of band 7, because it best delineates the land/water interface. Twenty six control points were originally selected. However three were deleted because of problems with identification. Points were identified from both 1 : 50 000 topographic mapping and a 1 : 250 000 topographic map of the area.

The polynomial equations used for the modelling are:

$$E = a_0 + a_1x + a_2x^2 + a_3x^3 + a_4y + a_5y^2 + a_6y^3 + a_7xy + a_8x^2y + a_9xy^2$$

$$N = b_0 + b_1x + b_2x^2 + b_3x^3 + b_4y + b_5y^2 + b_6y^3 + b_7xy + b_8x^2y + b_9xy^2$$

where

E and N are East and North coordinates

x and y are pixel column and row coordinates

and a_0 to a_9, b_0 to b_9 are the transformation parameters

These third order polynomials are solved by a least-squares procedure, both ground and image coordinates being considered subject to error. Appropriate variances are assigned to the image coordinates according to the estimated accuracy of measurement, and to the ground coordinates according to the assigned map accuracies and estimated pointing errors. Because the computer program allows a selected proportion of the error to be allocated to the ground data, the adjusted ground control values are likely to be better approximations of the actual positions that the original estimates.

Twenty three control points gives a redundant solution for the resection problem so that a statistical determination of the fit and the reliability of the control points can be determined. In fact, at the end of the adjustment process the root mean square (rms) accuracy of the fit of ground control was 50 metres in X and 48 metres in Y. This reduced level of accuracy is probably due to the smaller scale of the base maps used for control point selection. Interestingly, the

quality of control points scaled off the 1 : 250 000 map was better than the quality of control points scaled off the 1 : 50 000 topo map. Once the parameters for the cubic polynomials are calculated, the ground coordinates for all pixel centres can be calculated directly.

The ground coordinates of the 29 data sites were read off the 1 : 50 000 topographic map and their corresponding pixels were calculated. The reflectance values for each band for each of the 29 ground-truth sites were calculated to be the mean of the reflectance values in the 3 x 3 pixel area surrounding the corresponding ground-truth pixel.

3.3 COMPARISON OF IMAGE AND SITE DATA

To compare the LANDSAT data to the groundtruth data, a simple linear regression algorithm was used. From this, correlation coefficients were computed, which measured the linear relationship between the LANDSAT data and the groundtruth data. Prior to the comparison, however, a PCA was also performed on the groundtruth data, using the standardized variance-covariance matrix for the 11 sets of groundtruth data. Standardization removes the units associated with the raw data, making each parameter contribute equally to the result. This facilitates the mathematical manipulations involved in doing the PCA. (Standardization also has the effect of making the variance of each data-element equal to unity, therefore the variance of the data set, equal to the trace of the variance-covariance matrix, is equal to 11.) The eigenvalues and eigenvectors of the standardized field data set are given in Table 7, from which the contribution of each variable to the principal components can be seen.

Table 8 shows the calculated correlations between the raw field data and the individual LANDSAT bands. The only strong correlation which exists is between total suspended sediment and band 6 responses. Correlation coefficients for band 6 are 0.87, 0.80 and 0.84 for suspended sediment at the surface, 0.3 m and 1.0 m depths respectively. These relationships account for from 63% to 75% of the

STANDARDIZED DATA

Eigenvalues

4.5648	2.0176	1.3795	0.8763	0.7810	0.6192	0.3805	0.2189	0.1337	0.0217	0.0068
41.5%	18.4%	12.4%	8.0%	7.1%	5.6%	3.5%	2.0%	1.2%	0.2%	0.1%

Eigenvectors

-0.2102	0.0629	-0.3706	-0.2891	-0.2683	-0.4486	-0.4305	-0.4366	-0.0754	-0.2001	-0.1899
0.0958	0.2004	-0.0455	0.3357	0.3493	0.0237	0.0797	0.0192	-0.3907	-0.5272	-0.5254
0.4398	0.6239	-0.1602	0.1849	0.3023	-0.1457	-0.2064	-0.2002	0.0629	0.2458	0.3127
-0.3289	0.3443	0.1701	0.0950	0.0442	0.0058	0.0341	-0.0065	0.7920	-0.2876	-0.1484
0.5544	0.2929	-0.0532	-0.4203	-0.4891	0.1550	0.2111	0.1914	0.0800	-0.1734	-0.2158
0.5069	-0.5381	-0.1645	0.4404	-0.1130	-0.0666	-0.1682	-0.1421	0.3807	-0.1134	-0.0953
-0.1454	-0.0500	-0.8639	-0.0843	0.2212	0.1998	0.1972	0.2641	0.1486	0.0023	0.0582
-0.1958	0.2049	-0.1332	0.5364	-0.5857	0.0107	0.1139	0.0829	-0.1873	-0.2336	0.4019
-0.1400	0.1624	-0.1011	0.3035	-0.2604	0.1260	-0.0209	-0.0174	-0.0020	0.6520	-0.5850
0.0382	-0.0384	-0.0174	0.0361	0.0294	-0.7018	0.6925	-0.0562	0.0414	0.1240	-0.0474
0.0158	0.0191	0.0395	0.0416	0.0022	-0.4472	-0.3999	0.7949	0.0122	0.0304	-0.0565

Table 7: Eigenvalues and eigenvectors for the Lake Athabasca Site Data

Site Data (Observations)	Landsat Data (bands)	Correlation Coefficient
1	4	-.2904
1	5	0.2771
1	6	0.3201
1	7	-.1715
2	4	-.3465
2	5	-.2925
2	6	-.2089
2	7	0.0390
3	4	0.3160
3	5	0.5616
3	6	0.6326
3	7	-.2897
4	4	-.0904
4	5	0.2710
4	6	0.3555
4	7	-.2902
5	4	-.0409
5	5	0.1415
5	6	0.2693
5	7	-.2093
6	4	0.1960
6	5	0.6951
6	6	0.8655
6	7	-.5523
7	4	0.1372
7	5	0.5821
7	6	0.7965
7	7	-.5818
8	4	0.1711
8	5	0.6225
8	6	0.8399
8	7	-.5648
9	4	0.3567
9	5	0.3865
9	6	0.2774
9	7	0.1380
10	4	0.3079
10	5	0.4739
10	6	0.4393
10	7	0.0212
11	4	0.2950
11	5	0.3899
11	6	0.3746
11	7	-.0445

Table 8: Correlation coefficients between the raw site data and the raw Landsat data

variance observed in the measured data. While the band 5 correlations with suspended sediment (0.58-0.70) are significant at the 95% confidence level, they do not explain over 50% of the variance. This is interesting bacause examination of the bands 5 and 6 images of Figure 22 tends to imply that band 5 would be more useful in interpretation of sediment patterns. These results are consistent with those of Ritchie, et al (1976) who indicated that a more consistent relationship between reflectance and sediment was observed in band 6. Another interesting, but perhaps unimportant, feature concerns the band 7 correlations with total suspended sediment which range from -0.55 to -0.58. Although the correlations only explain from 31% to 34% of the variance, they are significant at the 95% confidence level. The interesting feature is that the relationships indicate a decrease in reflectance with increasing concentration. There is no apparent reason for this to occur and could be strictly a result of the low correlations and the fact that sampling was not truly synoptic. No other relationships in Table 8 explain over 50% of the variance and the only other significant correlations are between suspended organics and bands 5 and 6, which is expected since the organics are a subset of the total suspended concentrations. Thus the only band which shows a strong correlation with any of the measured water quality parameters is band 6 and it is correlated to suspended sediment. There is a weaker correlation between band 5 and suspended sediment.

Table 9 shows the relationships between the raw field data and the LANDSAT principal components. There are two strong correlations evident here. The total suspended data show correlations of from -0.84 to -0.77 with PC1 which accounts for from 59% to 70% of the variance. Note that the negative correlation is due to the negative values in the eigenvectors of Table 6. The main contributions to PC1 are band 6 (50%) and band 7 (41%) with band 5 contributing only 9% and band 4 being negligible. This reflects the strong correlation between band 6 and the suspended sediment data previously derived. The other strong correlation is between PC3 and conductivity, with a coefficient of 0.83, which explains 68% of the variation. This principal component emphasizes the difference between band 4 (47% contribution) and band 5 (36%) with some contribution of band 7 (16%) and

Site Data (Observations)	Landsat Data (PC Scores)	Correlation Coefficient
1	1	-.3494
1	2	0.1722
1	3	0.8267
1	4	0.2085
2	1	0.2217
2	2	0.4967
2	3	0.2061
2	4	0.1489
3	1	-.6411
3	2	-.2272
3	3	0.3644
3	4	-.2576
4	1	-.3112
4	2	0.0181
4	3	0.4266
4	4	-.2164
5	1	-.2183
5	2	0.0636
5	3	0.3351
5	4	-.2169
6	1	-.8368
6	2	-.3520
6	3	0.5754
6	4	-.4956
7	1	-.7665
7	2	-.2609
7	3	0.4552
7	4	-.4801
8	1	-.7992
8	2	-.3155
8	3	0.4745
8	4	-.5110
9	1	-.2976
9	2	-.3473
9	3	0.0790
9	4	0.0943
10	1	-.4473
10	2	-.3807
10	3	0.2987
10	4	-.1377
11	1	-.3680
11	2	-.2797
11	3	0.2488
11	4	-.0993

Table 9: Correlation Coefficients Between the raw site data and the Landsat PC scores

negligible contribution from band 6. This relationship is interesting because conductivity did not correlate well with any single LANDSAT band. Further, PC3 contains the same bands that are used in a C1 composite. Comparison of Figure 22 and 27 shows the similarity between PC3 and the C1 composite. PC2 reflects primarily band 4 (51%) and band 5 (43%) with a small contribution from band 7 (6%) and shows no strong correlation with any of the raw data. PC4 also shows no correlation with the raw data, although this component accounts for only 3% of the information content.

Table 10 shows the relationship between the principal components of the field data and the four LANDSAT bands. As seen in Table 6, PC1 has 71% of its contribution from the suspended sediment data. A correlation coefficient of 0.83 exists between PC1 and band 6, accounting for 68% of the variance. In contrast, only 45% of the variance is explained by the correlation of 0.67 between PC1 and band 5. None of the other principal components show a dominant contribution from any particular water quality parameter or a significant relationship to any one LANDSAT band.

Table 11 shows the correlation between the field and LANDSAT principal components. A coefficient of 0.80 is found between the field PC1 (mainly sediment data) and the LANDSAT PC1 (bands 6 and 7). There is no significant correlation between the field PC1 and LANDSAT PC2 (bands 4 and 5) and, although the field PC1 and LANDSAT PC3 correlation is significant at the 95% level, it only accounts for 36% of the variance. There are no other relationships of any significance.

These results indicate that there is a strong correlation between the field and LANDSAT data sets. The sediment data seems to correlate best with either band 6 or the LANDSAT PC1. The advantage of using principal components analysis becomes evident when the field conductivity correlations are examined. No relationships exist with the individual LANDSAT bands but PC3 shows a strong correlation with conductivity. Although the principal component analysis cannot change the amount of information in the original data, the orthonormal transformation effectively maximizes the information's distribution. The principal component analysis is not as fruitful when applied to the

Site Data (PC Scores)	Landsat Data (Bands)	Correlation Coefficient
1	4	-.1905
1	5	-.6709
1	6	-.8274
1	7	0.4795
2	4	-.4183
2	5	-.3155
2	6	-.1853
2	7	-.1957
3	4	-.2762
3	5	-.1202
3	6	-.1362
3	7	0.1634
4	4	0.1863
4	5	0.0720
4	6	0.0433
4	7	0.0793
5	4	-.2464
5	5	0.0784
5	6	0.1467
5	7	-.1623
6	4	-.0453
6	5	0.1682
6	6	0.0074
6	7	0.1332
7	4	-.0528
7	5	-.0051
7	6	0.1019
7	7	-.1701
8	4	-.1477
8	5	-.0589
8	6	0.0190
8	7	-.2578
9	4	-.0494
9	5	0.1288
9	6	0.1084
9	7	0.0493
10	4	-.1423
10	5	-.2543
10	6	-.1683
10	7	0.0496
11	4	-.1463
11	5	-.2318
11	6	-.0111
11	7	0.1158

Table 10: Correlation coefficients between the site PC scores and the raw Landsat data

Site Data (PC Scores)	Landsat Data (PC Scores)	Correlation Coefficient
1	1	0.8002
1	2	0.2904
1	3	-.6006
1	4	0.4087
2	1	0.2173
2	2	0.4244
2	3	0.0733
2	4	-.0414
3	1	0.1365
3	2	0.3491
3	3	0.4234
3	4	0.2852
4	1	-.0376
4	2	-.0563
4	3	-.1369
4	4	0.0233
5	1	-.1905
5	2	0.1616
5	3	0.3768
5	4	0.1661
6	1	-.0415
6	2	-.1170
6	3	0.2393
6	4	0.3107
7	1	-.0399
7	2	-.1863
7	3	-.0813
7	4	-.2686
8	1	0.0213
8	2	0.1126
8	3	-.0487
8	4	-.1983
9	1	-.1073
9	2	-.1335
9	3	0.0736
9	4	-.1737
10	1	0.1540
10	2	0.2020
10	3	-.2996
10	4	0.1909
11	1	0.1075
11	2	0.1821
11	3	-.1978
11	4	-.0427

Table 11: Correlation Coefficients Between the site PC scores and the Landsat PC scores

field data. Only PC1 shows a dominant contribution from any one water quality parameter and the contribution of conductivity, which is effective in delineating lake and river water, is not predominant in any principal component.

3.4 DISCUSSION OF RESULTS

The spectral response of water varies with wavelength, according to the energy - matter interactions taking place. For water bodies, the interactions are a result of the nature of the water itself and are further affected by the various conditions of the water.

An indication of the relationship between wavelength and water penetration using satellite sensing has been shown in some of the work with LANDSAT 1 data. Lepley, Foster and Everett (1975) estimated depth penetration for clear water to be 10 metres for band 4, 3 metres for band 5, 1 metre for band 6 and only 10 cm for band 7.

In the natural world, water bodies are usually not clear but contain a variety of organic and inorganic materials, some of which are in suspension. These materials cause scattering and absorption of incident energy and consequently cause significant variations in the transmission of energy through water. Specht, et al (1973) showed that transmittance of water in bays could be reduced as much as tenfold over ocean water, at certain wavelengths.

The shadeprint of PC1 (in Figure 27) shows what appear to be distinct sedimentation patterns similar to those seen on the black and white LANDSAT images and the C1 colour composite. Because the first principal component is emphasizing infrared bands 6 and 7, depth penetration can be expected to be no more than 0.1 to 0.5 m. Therefore, what is likely being seen is sedimentation in the surface layers of the water. The response is most marked where the distributaries from the Athabasca River enter the lake. Dark channels are clearly apparent where lower sedimentation occurs, as can be seen by comparison to the suspended sediment data of Figure 9.

The shadeprint of PC2 is similar to that of PC1, except that the smaller lakes surrounding Lake Athabasca are darker and so

less reflective, possibly indicating lower sediment levels. This effect could also be due to absorption by organic bottom material. For example, the bay west of the Embarras River appears grey, as does Richardson Lake, the bay east of Big Point Channel and several areas along the delta front. These areas are all shallow (under one metre) so penetration of bands 4 and 5 should reach the bottom and result in a stronger reflected signal. The lack of return could be due to absorption by organic material. Dark tones on the C1 composite are found in the same areas. The change in response of the pond on Bustard Island between PC1 and PC2 indicates that there are distinct bottom effects in these shallow areas which apparently decrease the response values for bands 4 and 5. Also the sedimentation pattern in the lake is generally more extensive. Since PC2 emphasizes the visible bands, likely penetration in this case can be expected to be no more than a few metres. Thus PC2 is highlighting sedimentation down to deeper levels than PC1. Because the shadeprint of PC2 corresponds closely with that of PC1, it could be inferred that sediment near the surface of the water also corresponds closely to the sediment at deeper levels. Another specific difference on the shadeprint between PC1 and PC2 is that the responses to the northeast of Bustard Island appear more dense for PC2 than for PC1. This possibly indicates more sediment in this area at deeper levels in the lake, which, in fact, can be seen to some extent in Figure 9.

However, PC2, which emphasizes bands 4 and 5, did not correlate well with the total suspended sediments. Even though the shadeprints of PC1 and PC2 appear similar, the quantitative response values at the sample sites must differ significantly. One possibility is that the poor correlation may be due to the fact that the total suspended sediments were only taken to a depth of 1.0 m and bands 4 and 5 may penetrate even sediment laden water for several metres. In particular, because many of the sites are located in shallow water, and complete penetration may occur, the PC2 scores may be corrupted by bottom effects.

PC3, which correlates with conductivity, very clearly indentifies the area where the Athabasca River enters the lake. The uniform pattern that covered almost the entire study area in PC1 and PC2 is gone.

Since PC3 emphasizes the difference between the two visible bands, bands 4 and 5, this pattern could indicate an area where the response exhibits some variation with depth. For example, the pond on Bustard Island and the small lakes to the north appear dark, indicating little difference between bands 4 and 5. The bay west of the Embarras River and Richardson Lake, however, both show higher PC3 responses. The reason for this is unclear, but could be indicative of the relative penetration depth of these two bands. The correlation with conductivity could be due to the different depth penetrating characteristics of lake and river water associated with their respective sediment loads.

This analysis has demonstrated that the LANDSAT data and selected water quality parameters, primarily suspended sediment, correlate quite well. Principal component analysis indicated that additional relationships existed between conductivity and PC3. Because of the short project duration and lack of additional synoptic data, verification of the relationships on an independent data set was not possible. Surprisingly, band 5 data did not correlate very well with the water quality data, although this may be due to the fact that the field data were only quasi-contemporaneous with the LANDSAT overpass.

As a result of this work, it is possible to review the analysis of LANDSAT imagery undertaken by Neill, et al (1981) and provide additional information concerning some of the questions and interpretive difficulties which were presented. The imagery assessed is reproduced in Figure 28. The 26 August 1973 C1 composite shows a sharp and distinct boundary between lake and river water. Winds were westerly and inflows were similar to those in August 1981 although outflows were nearly double those experienced in 1981. The possibility that the muddy blue tone of the inflow was a result of contamination of river water by sources other than sediment was investigated with Pollution Control Division of Alberta Environment (Masuda, personal communication). There were no records of any spills or unusual releases around the time of the imagery, so this possibility was discounted. It is likely that the tonal differences simply indicate the boundary between lake and river water. The sharpness of the boundary is probably due to the

combined effect of high lake outflow and west winds. There are some similarities to the August 1981 imagery in that the river water seems to be seen entering only the Chenal des Quatres Fourches.

The 22 May 1974 C1 composite showed apparent river water penetrating almost to the north shore. Based on the June 1981 data, it now seems evident that, particularly for high inflow relative to outflow, more distant penetration of river water into the lake occurs and that penetration to the north shore is possible.

The 2 August 1974 band 5 image showed apparently high turbidity levels in Lake Athabasca whose origins were unclear. It now appears that this turbidity originates from erosion of islands and local sand or till areas along the shoreline.

The C1 composite of 1/2 July 1975 raised questions concerning the bands of dark water originating in Old Fort Bay and in various locations along the delta front. While the sources are not completely clear, it seems from the July 1981 data that part of the explanation has to do with high volatile dissolved solids concentrations. The sources along the delta may be due to swamp water or groundwater discharge. The water in Old Fort Bay could also be due to inflows originating on the Canadian Shield from the Harrison and Old Fort rivers. The 13 September 1978 C1 composite raised a similar question concerning the reason for the darker water at the east end of the delta. Rather than being a wind effect, this difference in tone appears to be due to differing water quality parameters.

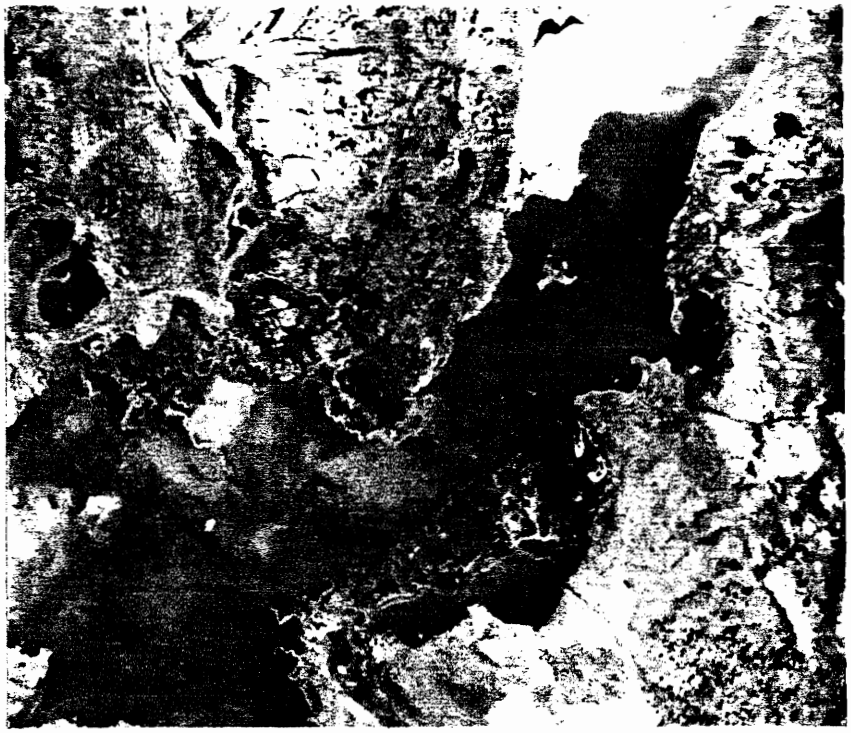

May 22, 1974

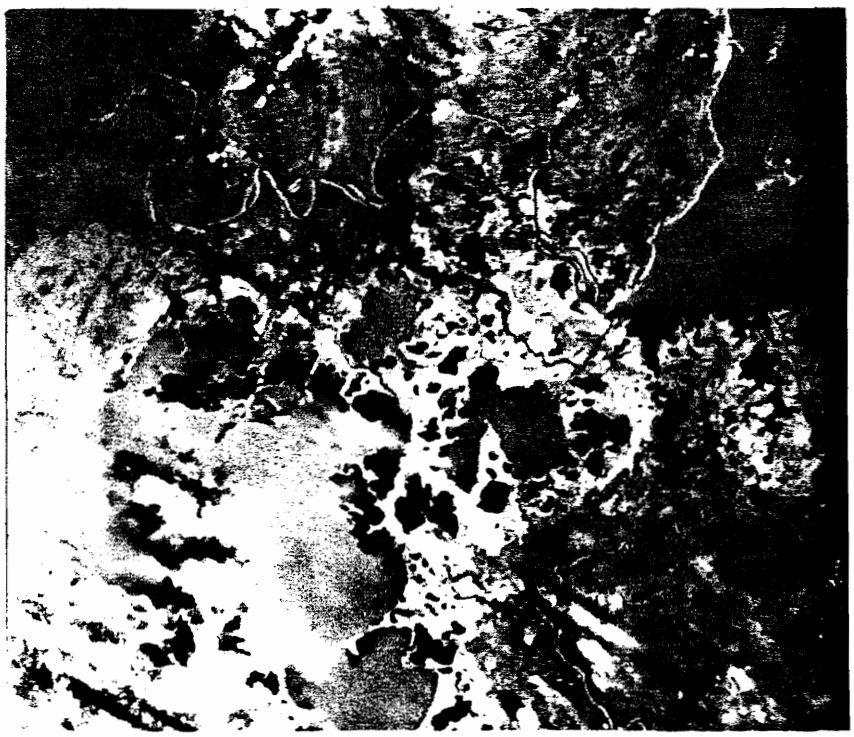

August 26, 1973

August 2, 1974

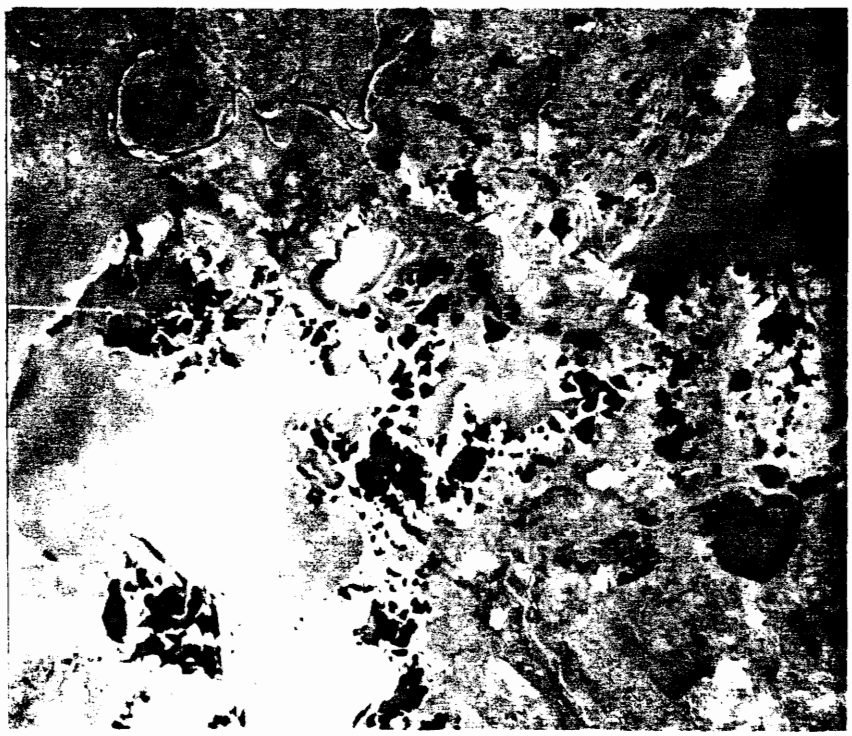

July 1, 1975

July 2, 1975

September 13, 1978

4. MATHEMATICAL MODELLING

The previous section has indicated that it is possible to discern some features of the mixing and circulation characteristics in the southwest end of Lake Athabasca from satellite imagery. However, in order to evaluate these characteristics in a more detailed or quantitative manner, some type of modelling capability is required. As previously described, various models for the study area have been developed but they are generally of the routing type. For example, the model of Sydor et al (1979) is of the reach-node type, whereby a number of reaches are inter connected at specified nodes and the routing computations are performed at each node. This type of model is well-suited for riverine systems because the reaches (in this case, the river channels) are usually uniquely defined. However, for lake systems, this approach is unrealistic because the flow pattern is predetermined by the reach-node layout. Thus, the modelling phase of this project was undertaken to investigate the feasibility of employing more sophisticated modelling techniques.

4.1 THEORETICAL DEVELOPMENT

Mathematical description of the circulation in bodies of water is governed by the principles of conservation of mass and momentum. The three dimensional set of differential equations describing such motion is complex and generally defies analytical or numerical solution for all but the simplest situations which often find little practical utility. A solution to these equations can be determined in some cases by physical modelling, although the shallowness of the area of interest to this study would require such scale distortion that physical modelling is probably not feasible. (Descriptions of physical modelling may be found in Yalin (1971) and ASCE (1978, 1980)). In order to reduce the complexity of the mathematical problem, simplifying assumptions are sought which also preserve the main features of the system under consideration. The shallowness of the southwest end of Lake Athabasca lends itself to consideration of only horizontal motions, which is to say that variations in the vertical direction are neglected. A description

of the development of the vertically integrated momentum and continuity equations can be found in Ippen (1966) or Simons (1980). These equations can be written as

$$\frac{\partial q_x}{\partial t} + u\frac{\partial q_x}{\partial x} + v\frac{\partial q_x}{\partial y} - fq_y + gh\frac{\partial \eta}{\partial x} - \tau_x^s + \tau_x^b$$

$$- \frac{\partial}{\partial x}\varepsilon_x \frac{\partial q_x}{\partial x} - \frac{\partial}{\partial x}\varepsilon_{xy}\left(\frac{\partial q_x}{\partial y} + \frac{\partial q_y}{\partial x}\right) = 0 \quad \text{(x momentum)}$$

$$\frac{\partial q_y}{\partial t} + u\frac{\partial q_y}{\partial x} + v\frac{\partial q_y}{\partial y} + fq_x + gh\frac{\partial \eta}{\partial y} - \tau_y^s + \tau_y^b$$

$$- \frac{\partial}{\partial y}\varepsilon_y \frac{\partial q_y}{\partial y} - \frac{\partial}{\partial y}\varepsilon_{xy}\left(\frac{\partial q_x}{\partial y} + \frac{\partial q_y}{\partial x}\right) = 0 \quad \text{(y momentum)}$$

$$\frac{\partial \eta}{\partial t} + \frac{\partial q_x}{\partial x} + \frac{\partial q_y}{\partial y} = 0 \quad \text{(continuity)}$$

The terms appearing above are:

x, y: co-ordinate directions where x is east and y is north,

h: total depth of flow (m),

η: water surface elevation above some datum (m),

q_x, q_y: vertically integrated velocities or flow intensity ($m^3/s/m$) in the x and y directions,

u,v: vertically averaged velocities (m/s) (e.g. $u = q_x/h$) in the x and y directions,

f: Coriolis coefficient, (s^{-1}), equal to $2\omega \sin\phi$ where ω = angular velocity of the earth and ϕ = latitude, (for Lake Athabasca, $f \simeq 0.000124$)

g: gravitational acceleration (9.81 m/s^2),

ε_x, ε_y, ε_{xy}: turbulent eddy viscosities (m^2/s),

τ_x^s, τ_y^s: wind shear at the surface,

τ_x^b, τ_y^b: bottom shear, and

t: time.

The surface shear is defined as

$$\tau_x^s = \gamma^2 \frac{\rho_a}{\rho} (w_x^2 + w_y^2)^{1/2} w_x$$

where γ^2 is a coefficient approximately equal to 0.0026 (Pollack, 1960) ρ_a and ρ are the densities of air and water respectively and w_x and w_y are the wind velocities in the x and y directions at the standard anemometer height. The value of τ_y^s is similarly defined. The bed stress is defined using the Manning equation as

$$\tau_x^b = \frac{gn^2(q_x^2 + q_y^2)^{1/2} q_x}{h^{10/3}}$$

where n is Manning's roughness coefficient. The value of τ_y^b is similarly defined.

The above equations were derived by making the assumption that the pressure is hydrostatic and that density variations are negligible. These assumptions are not unreasonable given the shallow depths of the study area. Further, since no vertical stratification exists, dealing with vertically-integrated velocities is appropriate. Turbulence has been accounted for by use of an eddy viscosity approach wherein the turbulent and spatial deviation from the mean velocity are represented by an apparent eddy viscosity. Although more sophisticated approaches are available (Leschziner and Rodi, 1979) which involve another pair of differential equations describing the turbulence characteristics, the eddy viscosity formulation was deemed appropriate for this initial work.

It is instructive to examine the relative magnitudes of some of the terms of the momentum equation to determine if further simplification is possible. In particular, the convective terms (i.e. $u \frac{\partial q_x}{\partial x}$) are examined since their inclusion often poses difficulties in solving the equations. One measure of their relative

importance is the Rossby number, R, defined as

$$R = \frac{V}{fL}$$

where V is a typical velocity and L is a typical horizontal length scale. The Rossby number is the ratio of convective (or inertial) forces to Coriolis forces and a value much greater than unity (i.e. 10) indicates a dominance of inertial forces while a value much less than unity (i.e. 0.01) indicates a dominance by Coriolis forces. Typical values for Lake Athabasca are V = 0.03 m/s and L = 10 km giving a value for R of 0.02. This would imply that the convective terms could possibly be neglected. However, in the vicinity of the distributary channels, velocities can be an order of magnitude larger than that used above so, in this area, both convective and Coriolis forces can be significant.

Since the above equations cannot be solved analytically, the objective is to obtain a numerical solution using a mathematical model.

4.2 MATHEMATICAL MODEL

There are generally two types of mathematical models available for solution of the equations of motion, these being finite difference models and finite element models. Finite difference methods involve overlaying the region of interest in which a solution is to be obtained by a (usually) regularly spaced mesh of grid points. The derivatives in the governing equations are then approximated by the values of the independent variables at each grid point. For example, a derivative such as $\frac{\partial f}{\partial x}$, with f any unknown variable, could be approximated as $(f_{i+1} - f_i)/\Delta x$ where f_{i+1} and f_i are values of f at grid points i+1 and i and Δx is the grid spacing. Finite difference models have been popular for some time (see, for example, Leendertse (1967) or Ponce and Yabusaki (1981)) but do suffer from some drawbacks, as described in Wang (1975) for example. The main drawback appears to be the fact that a regular grid must be used. This poses difficulties in dealing with the irregular boundaries usually encountered in natural systems.

More recently, the finite element method has been employed to analyse circulation problems, for example, in Niemeyer (1979), Walters and Cheng (1980) and Wang (1975). The finite element method involves subdividing the domain of interest into discrete elements. Within each element, the solution is assumed to follow some predetermined distribution, i.e. linear, parabolic etc. The residual so created is then weighted and the contribution of each element is summed. The resulting integro-differential equations yield a system of linear equations which may then be solved using standard numerical techniques. The advantage of the method lies in the relative ease with which boundaries can be defined and in the straightforward method in which boundary conditions can be applied. This type of model was investigated in this project, based on a model developed by Harrington et al (1978).

Figure 29 shows an idealized solution domain partially subdivided into elements. Linear triangles are used as elements mainly because of their relative simplicity, which results in a linear variation of the solution field within the element. This variation of a variable, say p, at any point x, y within the element can be described as a linear function of the nodal co-ordinates, such that

$$p = [(a_i+b_ix+c_iy)p_i + (a_j+b_jx+c_jy)p_j + (a_k+b_kx+c_ky)p_k]/2\Delta$$

The parameters a, b and c, above are defined at the nodes i, j and k such that

$$a_i = x_k y_j - x_j y_k$$

$$b_i = y_k - y_j$$

$$c_i = x_j - x_k$$

and the values for nodes j and k are obtained by a cyclic permutation, as shown in Figure 30. The area of the triangular element is Δ and p_i, p_j and p_k are the values of p at the nodes. The above equation can be written more compactly as

$$p = \langle N \rangle \{p\}$$

where <N> is a row vector, called the shape function, given by

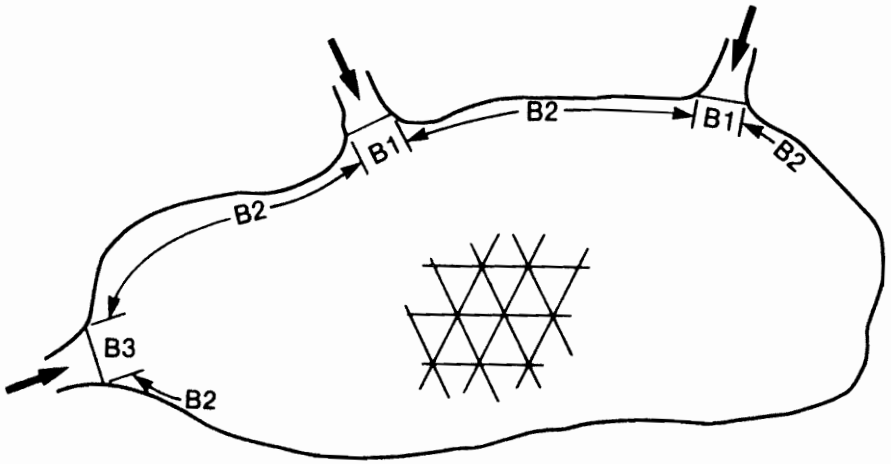

Discretization of Solution Domain

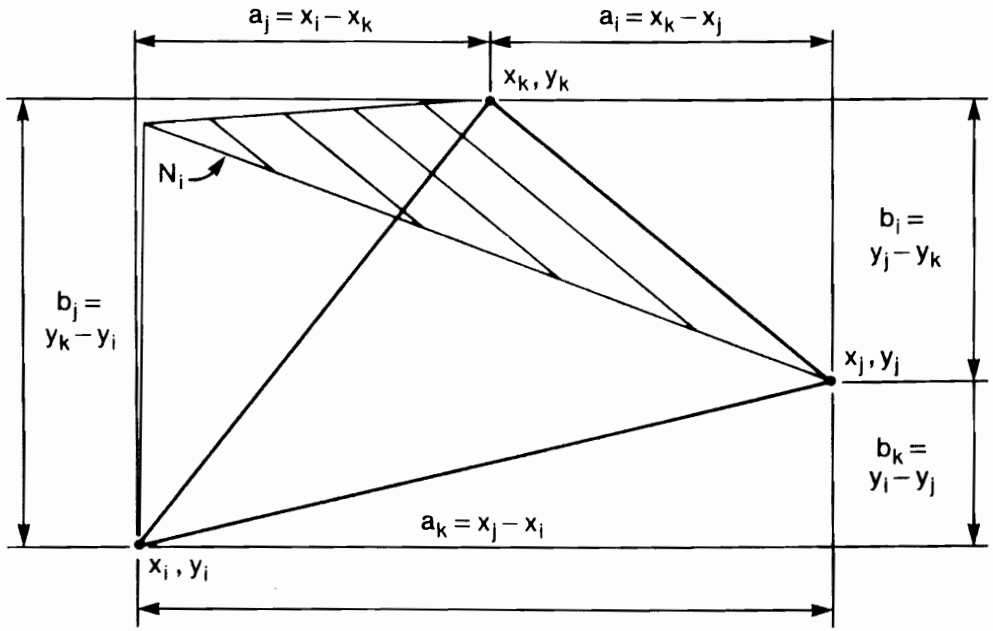

A Typical Element

$$<N> = <(a_i+b_i x+c_i y)\ (a_j+b_j+c_j y)\ (a_k+b_k+c_k y)>/2\Delta$$

and {p} is a column vector of the nodal values of p. This formulation thus permits description of the variation of p within an element given the nodal values of p.

In order to obtain a solution to the momentum and continuity equations, the element-wise continuous function describing the intra-element variation is substituted into these equations and a residual is formed. For example, let L represent the differential operator (i.e. the original equations) so that the governing equations may be written as $L(q_x, q_y, \eta) = 0$

For briefness, denote ψ as the set of nodal values of q_x, q_y, η. Using the shape function and the nodal values of ψ, substitution of the approximate solution $<N>\{\psi\}$ into L yields

$$L(<N>\{\psi\}>) = R$$

where R is the residual created due to the approximation. The residual is then weighted in some fashion, integrated over the element and set equal to zero. Using the Galerkin method of weighted residuals (Crandall, 1956), the weighting function is chosen to be the shape function <N>. Summing the contribution of each element yields

$$\Sigma_{ne} \int\int <N>' L(<N>\{\psi\})\ d\Delta = 0$$

where ne is the number of elements, $d\Delta$ indicates integration over an element and a superscript prime denotes the transpose. The integration yields a set of simultaneous equations which may then be solved for $\{\psi\}$.

In order that $L(<N>\{\psi\})$ is an admissable solution, the values of ψ and its derivatives of one order less than those appearing in L must be continuous across element boundaries (Zienkiewcz (1971)). Thus, the second order terms in the momentum equation are integrated by parts.

Noting that <N> is only a function of x and y so, for example, $\frac{\partial q_x}{\partial x} = \frac{\partial <N>}{\partial x}\{q_x\}$ and that $\{q_x\}$, $\{q_y\}$ and $\{\eta\}$ are only functions of t such that $\frac{\partial q_x}{\partial t} = <N> \frac{\partial \{q_x\}}{\partial t}$, the finite element formulation can be written as

x momentum

$$\sum_{n_e} \int\int \Bigg[\langle N\rangle' \langle N\rangle \frac{\partial\{q_x\}}{\partial t} + \langle N\rangle' \overline{\langle N\rangle\{u\}} \frac{\partial\langle N\rangle}{\partial x} \{q_x\}$$

$$+ \langle N\rangle' \overline{\langle N\rangle\{v\}} \frac{\partial\langle N\rangle}{\partial y} \{q_x\} - f\langle N\rangle' \langle N\rangle \{q_y\} +$$

$$g \langle N\rangle' \langle N\rangle\{h\} \frac{\partial\langle N\rangle}{\partial x} \{\eta\} - \langle N\rangle' \langle N\rangle\{\tau_x{}^s\} + \langle N\rangle' \langle N\rangle\{\tau_x{}^b\}$$

$$+ \frac{\partial\langle N\rangle}{\partial x} \varepsilon_x \frac{\partial\langle N\rangle}{\partial x} \{q_x\} + \frac{\partial\langle N\rangle}{\partial y} \varepsilon_{xy} \left(\frac{\partial\langle N\rangle}{\partial y} \{q_x\} + \frac{\partial\langle N\rangle}{\partial x} \{q_y\}\right) \Bigg] d\Delta$$

$$= \sum_{n_e} \oint \left[\langle N\rangle' \varepsilon_x \frac{\partial\langle N\rangle}{\partial x} \{q_x\} \ell_x + \langle N\rangle' \varepsilon_{xy} \left(\frac{\partial\langle N\rangle}{\partial x} \{q_y\} + \frac{\partial\langle N\rangle}{\partial y} \{q_x\}\right) \ell_x \right] ds$$

y momentum

$$\sum_{n_e} \iint \Bigg[\langle N\rangle' \langle N\rangle \frac{\partial\{q_y\}}{\partial t} + \langle N\rangle' \overline{\langle N\rangle\{u\}} \frac{\partial\langle N\rangle}{\partial x} \{q_y\}$$

$$+ \langle N\rangle' \langle N\rangle\{v\} \frac{\partial\langle N\rangle}{\partial y} \{q_y\} + f \langle N\rangle' \langle N\rangle\{q_x\} +$$

$$g \langle N\rangle' \langle N\rangle\{h\} \frac{\partial\langle N\rangle}{\partial y} \{\eta\} - \langle N\rangle' \langle N\rangle \{\tau_y{}^s\} + \langle N\rangle' \langle N\rangle \{\tau_y{}^b\}$$

$$+ \frac{\partial\langle N\rangle'}{\partial y} \varepsilon_y \frac{\partial\langle N\rangle}{\partial y}\{q_y\} + \frac{\partial\langle N\rangle'}{\partial x} \varepsilon_{xy} \left(\frac{\partial\langle N\rangle}{\partial y}\{q_x\} + \frac{\partial\langle N\rangle}{\partial x}\{q_y\}\right) \Bigg] d\Delta$$

$$= \sum_{n_e} \oint \left[\langle N\rangle' \varepsilon_y \frac{\partial\langle N\rangle}{\partial y} \{q_y\}\ell_y + \langle N\rangle' \varepsilon_{xy} \left(\frac{\partial\langle N\rangle}{\partial x} \{q_y\} + \frac{\partial\langle N\rangle}{\partial y} \{q_x\}\right) \ell_y \right] ds$$

continuity

$$\sum_{n_e} \iint \left[\langle N\rangle' \langle N\rangle \frac{\partial\{\eta\}}{\partial t} - \frac{\partial\langle N\rangle'}{\partial x} \langle N\rangle \{q_x\} - \frac{\partial\langle N\rangle'}{\partial y} \langle N\rangle \{q_y\} \right] d\Delta$$

$$= \sum_{n_e} \oint \langle N\rangle' \langle N\rangle\{q_n\}\, ds$$

In these equations, ℓ_x and ℓ_y are the direction cosines of the outward normal, ds signifies integration over a boundary and q_n is the inflow normal to a boundary side. The overbars indicate values which must be linearized in some way, as discussed subsequently.

Using linear elements, the above integrals can be readily evaluated. For example, direct integration yields

$$\iint \langle N \rangle' \langle N \rangle \, d\Delta = \frac{\Delta}{12} \begin{bmatrix} 2 & 1 & 1 \\ 1 & 2 & 1 \\ 1 & 1 & 2 \end{bmatrix} \quad \text{and}$$

$$\iint \frac{\partial \langle N \rangle'}{\partial x} \langle N \rangle \, d\Delta = \frac{1}{6} \begin{bmatrix} b_1 & b_1 & b_1 \\ b_2 & b_2 & b_2 \\ b_3 & b_3 & b_3 \end{bmatrix}$$

The advantage of using the flow intensity representation as opposed to a velocity formulation is manifested in the continuity equation which is rendered linear in the finite element formulation. Further, integration by parts of the spatial derivatives in the continuity equation results in a line integral which allows for easy application of boundary conditions. Because evaluation of the line integral on internal segments yields equal but opposite contributions from adjoining elements, the only non-zero contribution comes from the external boundaries of the solution domain. Thus, flow boundaries are easily treated by specifying the discharge integral of the continuity equation at flow boundaries, designated as B1 in Figure 29.

The integrals are calculated for each element and the contribution of each element is summed or assembled. (See Martin and Carey (1973) for a complete description of the mechanics of evaluation and assembly.) The result is a system of simultaneous equations which can be written as

$$[P]\{\dot{\psi}\} + [K]\{\psi\} = \{F\}$$

where $[P]$ is the mass matrix containing the assemblage of the integral of $\langle N \rangle' \langle N \rangle$ and $\{\dot{\psi}\}$ is the time derivative of $\{\psi\}$. The vector $\{F\}$ contains the wind stress terms and the known flow values along the boundary.

The surface integrals along boundary segment B2 in Figure 29 in the momentum equations are neglected since, as described by Walters and Cheng (1980), their contribution is negligible. The matrix $[K]$ contains all the other terms appearing in the formulation.

A solution is achieved by approximating $\{\dot{\psi}\}$ by a finite difference in time such that the result is

$$[P]\{\psi\}_{t+\Delta t} + \Delta t\,[K]\{\psi\}_{t+\Delta t} = \Delta t\,\{F\}_{t+\frac{\Delta t}{2}} + [P]\{\psi\}_{t}$$

The matrix $[K]$ is nonlinear because of the contribution of the convective and bed stress terms in the momentum equations. Linearization is achieved by using an initial estimate of $u_{t+\Delta t}$ and $v_{t+\Delta t}$ to evaluate $[K]$ and iterating until successive iterates of $\{\psi\}_{t+\Delta t}$ do not differ significantly. The initial estimate of u and v is obtaining using a predictor based on substituting finite difference approximations into an Adams Bashford second order predictor (Conte and de Bour, 1965) to give

$$u_{t+\Delta t} = 2.25\,u_t - 1.5\,u_{t-\Delta t} + 0.25\,u_{t-2\Delta t}$$

This scheme is implemented after two time steps, a simple linear extrapolation being used initially. Using the values of u and v at time t has resulted in instability, necessitating extrapolation.
The fully implicit system then becomes

$$[A]\{\psi\}_{t+\Delta t} = \{F'\}$$

where $[A] = [P] + \Delta t\,[K]$ and
$[F] = \Delta t\,\{F\}_{t+\Delta t/2} + [P]\{\psi\}_{t}$

Since successive iterates of $\{\psi\}$ may be of the same order of magnitude, significant numerical error may accrue. It is, therefore, advantageous to solve for the correction to $\{\psi\}_{t+\Delta t}$ using a Newton Raphson procedure such that

$$[A]\{\delta\psi\} = \{\delta F'\}$$

where $\{\delta\psi\} = \{\psi\}' - \{\psi\}^{o}$,

$\{\delta F\} = \{F'\}^{1} - \{F'\}^{o}$

and the superscript indicates the iteration number. Solution is obtained by means of Gauss elimination. The iteration continues until the normalized error is less than a specified tolerance, typically 0.1%, with the error, e, defined as

$$e = \left| \frac{\Sigma(\delta\psi)^2}{\Sigma(\psi)^2_{t+\Delta t}} \right|^{\frac{1}{2}}$$

A separate error is calculated for flow intensity and water surface elevation since the momentum equations typically require more iterations than does the continuity equation and a better indication of relative error is achieved using separate error calculations.

The implicit time integration scheme can shown to be stable for a simple linear system defined by

$$\frac{dy}{dt} + y = 0$$

by substituting $(y_{t+1} - y_t)/\Delta t$ for the time derivative and y_{t+1} for y to yield

$$y_{t+1}\,(1 + \Delta t) - y_t = 0$$

Assuming a solution of the form $y_{t+1} = \lambda y_t$, stability is assured if $|\lambda| < 1$. Substitution yields

$$\lambda = \frac{1}{1+\Delta t}$$

which is unconditionally stable. However, nonlinear instability can arise due to short wavelength or sub grid size noise. This noise is damped to some extent by the eddy viscosity terms but because of the lack of reliable field estimates of appropriate values of eddy viscosity, a second damping technique is incorporated (Ponce, 1981; Wang, 1976).

This method is a smoothing technique whereby each nodal value, say f, is smoothed to f' based on the area A_i of the elements surrounding the node, the average value, f_i, of f within each element and the distance, x_i, to the centroid of each element such that

$$f' = \alpha f + (1 - \alpha) \left[\sum_n f_i A_i/x_i\right] / \left[\sum_n A_i/x_i\right]$$

where n is the number of elements surrounding the node and α is a weighting factor of the order of 0.99. This scheme has the disadvantage that it lacks any basis in the physics of the flow phenomenon but is a velocity averaging mechanism which produces a numerical eddy viscosity which is a function of the spatial discretization of the solution domain.

The solution is marched in time upon specification of the initial and boundary conditions. Initial conditions often take the form of a flat water surface and zero velocities throughout the domain for lack of other information. Boundary conditions include specification of the water surface elevation on a portion of the boundary, designated B3 in Figure 29. Flows are specified on inflow boundaries as previously described. On land boundaries, shown as B2 in Figure 29, the flow is tangential to the boundary. This poses some difficulties when linear triangles are used because discontinuities arise when the natural boundaries are curved. As shown in Figure 31, the discontinuity results in flow leaving one side of the discontinuity and entering the other side. To minimize this effect, an average direction of the outward normal is specified such that the flow leaving is balanced by the flow entering. This angle is given by the relationship

$$\tan \theta = \frac{L_1 - L_2 \cos \phi}{L_2 \sin \phi}$$

where L_1 and L_2 are the lengths of the element sides at the discontinuity and L_1 the upstream boundary segment when the solution domain is to the left of the direction of advance. The angles θ and ϕ are defined in Figure 31. The flow is made tangential using the method of Gray (1976).

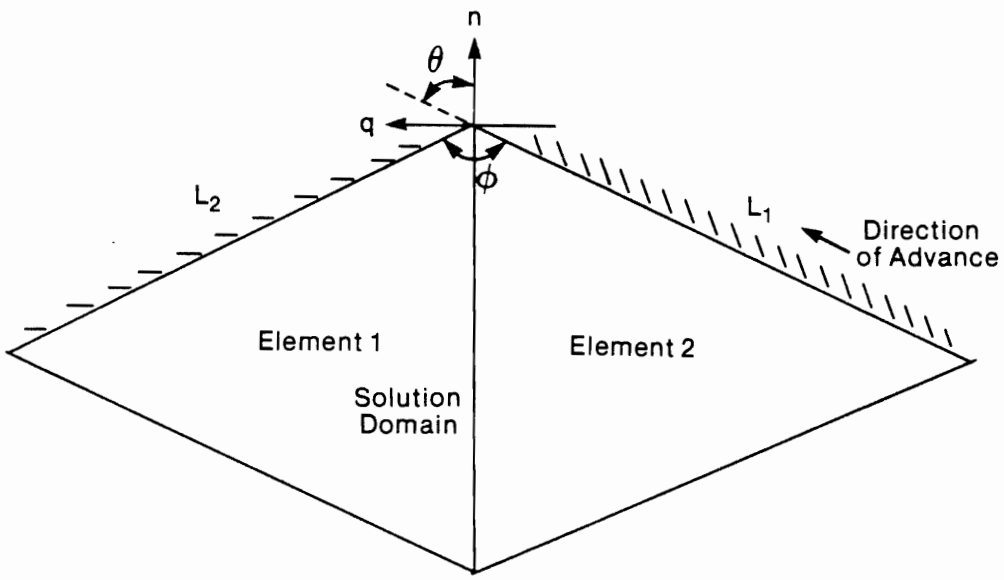
n
θ
q
ϕ
L2
L1
Direction
of Advance
Element 1
Element 2
Solution
Domain

Thus, if β is the angle of the outward normal from the x axis, the calculated values of q^*_x and q^*_y are adjusted such that the flow is tangential to the boundary using the relationships

$$q_x = q^*_x \sin^2 \beta - q^*_y \sin \beta \cos \beta$$

$$q_y = q^*_x \sin \beta \cos \beta + q^*_y \cos^2 \beta$$

4.3 MODEL APPLICATION

The model was first applied to simplified examples to ensure that there were no programming errors and to assess the stability and continuity of the model. The first example comprises a rectangular basin closed at one end and subject to a sinusoidal water level variation at the other. The analytical solution for this case (Ippen, 1966) is given by

$$\eta = \frac{a \cos \left[\omega(x - L)/\sqrt{gH}\right] \cos \left[\omega t\right]}{\cos \left[\omega L/\sqrt{gH}\right]}$$

$$q_x = \frac{a\sqrt{gH} \sin \left[\omega(x-L)/\sqrt{gH}\right] \sin \left[\omega t\right]}{\cos \left[\omega L/\sqrt{gH}\right]}$$

where a is the amplitude of the water level variation, ω is the frequency of excitation, H is the undisturbed depth and L is the basin length. The conditions used in the testing were a = 0.1 m, period = 200 s, L = 160 m and H = 5 m. The tests were carried with the channel aligned along both the x and y axes to ensure there were no programming errors. The results are shown in Figure 32, in which a time step of 10 s was employed. Initial conditions were zero velocities and a flat water surface. After two cycles, the solution repeated itself and showed no signs of instability even after ten cycles of computation. The results were identical for channel alignment along both axes. Some phase shift is evident and is due to the relatively short period of the forcing function. Similar phase shifts are reported by Partridge

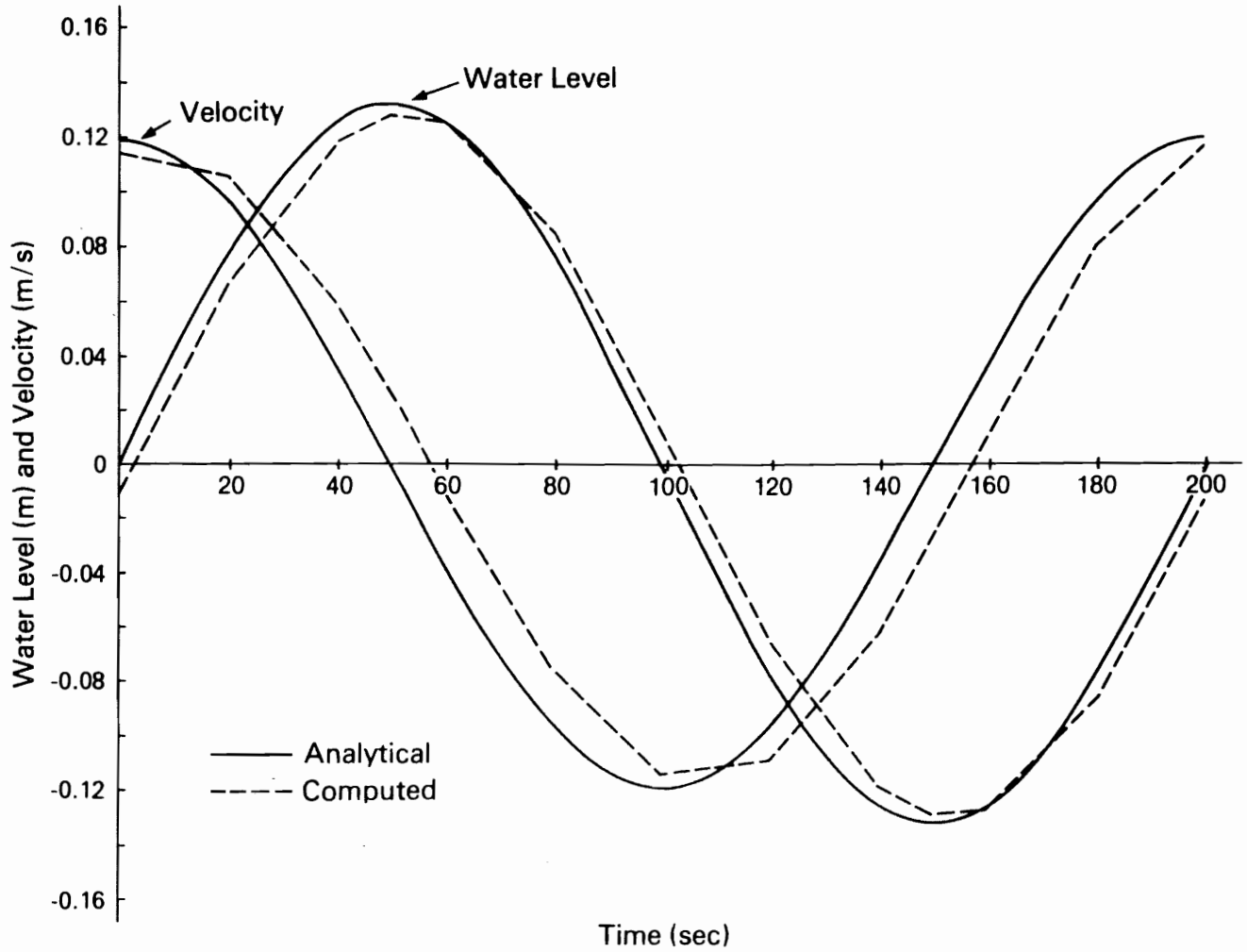
0.16
0.12
0.08
0.04
0
-0.04
-0.08
-0.12
-0.16
20
40
60
80
100
120
140
160
180
200
Water Level
Velocity
Analytical
Computed
Water Level (m) and Velocity (m/s)
Time (sec)

and Brebbia (1976) and Wang (1975) and reflect primarily the violation of the assumptions underlying the analytical solution because of the relatively steep water surface slopes induced by the short oscillation period.

The second test involved calculation of flow continuity for the 40% contraction shown in Figure 33. Flow is from the wide end of the channel to the narrow end. The width changes from 20 m to 12 m and the depth at the outlet is 1.0 m. The discharge was specified at 12 m^3/s. The solution was calculated until a quasi steady state was achieved and the amount of flow passing each tranverse section was calculated. These amounts, normalized with the specified discharge, are shown in Figure 33. Continuity violations did not exceed 5% at any one section and overall continuity was within 2%. These tests were considered to have verified the model integrity, although for production purposes, further testing would be desirable using more complex configurations, for example those described by Lynch and Gray (1979).

The model was applied to the southwest end of Lake Athabasca using an idealized discretization shown in Figure 34. This limited lay-out was used because time constraints did not permit detailed analysis. As a result, the boundary conditions, because of the proximity of the boundaries to the area of interest, affect the results to some extent. The conditions simulated were similar to those encountered during the June 1981 field trip. The flow from the main body of Lake Athabasca was set at 300 m^3/s distributed uniformly along the upstream boundary. A discharge of 900 m^3/s was applied at the location of Big Point Channel and 300 m^3/s at the location of the Embarras River. An outflow of 1500 m^3/s was specified at the downstream end. A uniform depth of 3 m was assumed.

Figure 35 shows the calculated velocity vectors for a north-east wind of 8.5 m/s imposed on the system. Strong currents directed towards the outlet and a suppression of the penetration of the Big Point Channel discharge is evident. However, boundary effects are evident, particularly at the east end of the study area where the interaction of the lake inflow and the Big Point Channel discharge are not properly developed due to the proximity of the boundary.

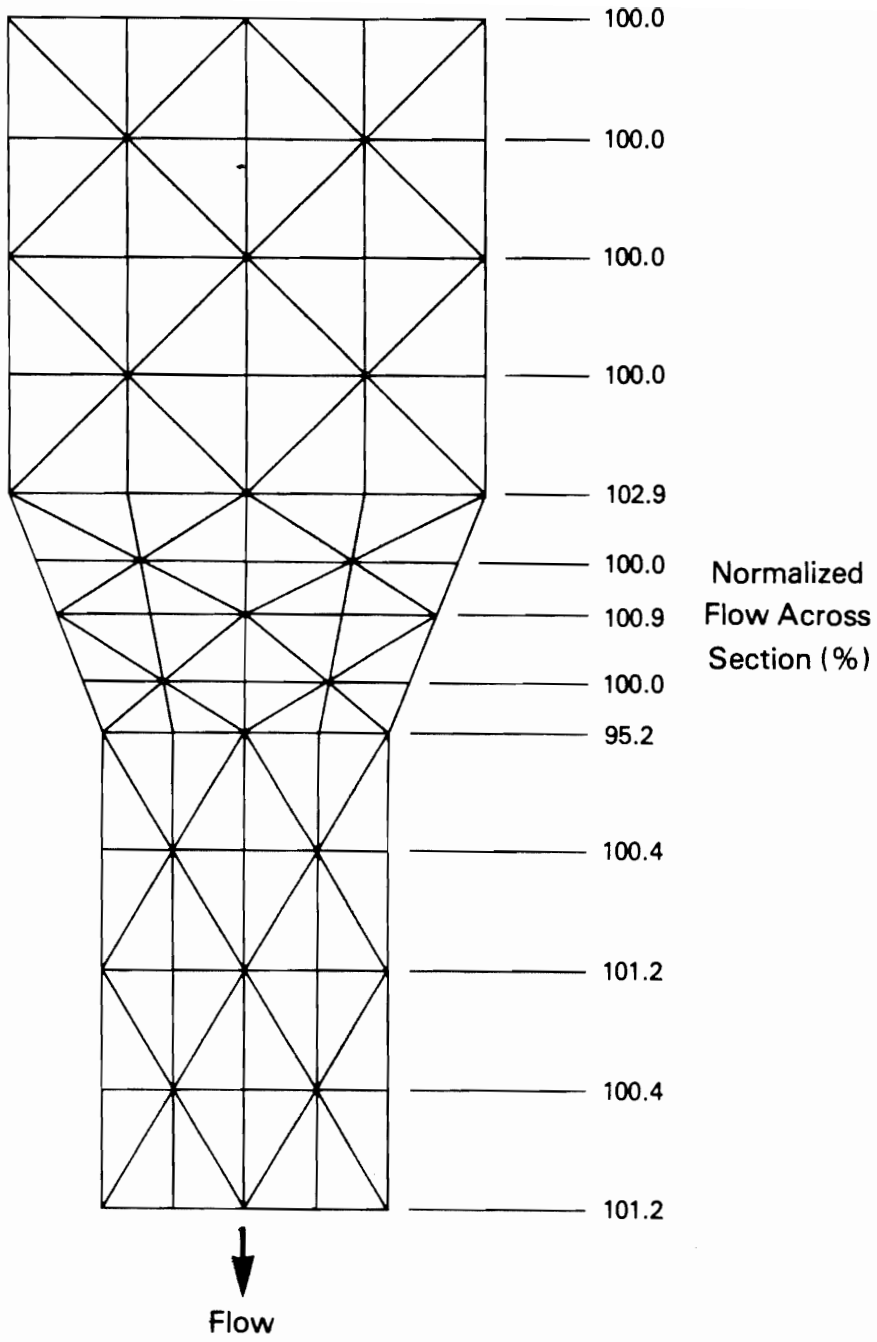
100.0
100.0
100.0
100.0
102.9
100.0
100.9
100.0
95.2
100.4
101.2
100.4
101.2
Normalized
Flow Across
Section (%)
Flow

Figure 34. Discretization of Lake Athabasca

Figure 35. Model Results, Northeast Wind

Figure 36 shows the model results for a southeast wind of 8.5 m/s. The movement of water from Big Point Channel in a westerly direction along the delta front is evident and the flow pattern is qualitatively similar to that encountered during the September dye test. The calculated velocities are somewhat higher than those observed in September but the wind speed of 8.5 m/s used in the model is also larger than that of 6 m/s measured in September. The model did not reproduce the stronger north shore current but this is thought to be a result of the use of a uniform inflow across the lake boundary.

In an effort to reduce the effect of the boundary conditions on the calculated results, the grid was extended past Bustard Island. The lake inflow was altered so the flow distribution varied linearly from zero to Old Fort Bay at the south east corner to a maximum near Burntwood Island and retained the total inflow of 300 m^3/s. The model was run with no wind and the results are shown in Figure 37. The most obvious difference between the measured and observed results is the clockwise circulation around Bustard Island. This is due to insufficient inflow from the lake at the northern part of the lake boundary to suppress the deflection of currents from the north shore. In addition, a portion of the lake was excluded from the simulation and it appears that further refinement of the lake inflow distribution is necessary. The counter clockwise circulation east of Big Point Channel which was observed during July and August was reproduced as was penetration of river water to the north shore. There are some indications of possible instability in the western end of the lake which could be due to the strong gradients which exist and the inability of the relatively coarse grid to resolve them.

For application purposes, further verification of the model should be undertaken to completely test and verify all the options. Since the model was developed as a research tool, some programming inefficiencies may exist which should be examined prior to production run implementation.

Figure 36. Model Results, Southeast Wind

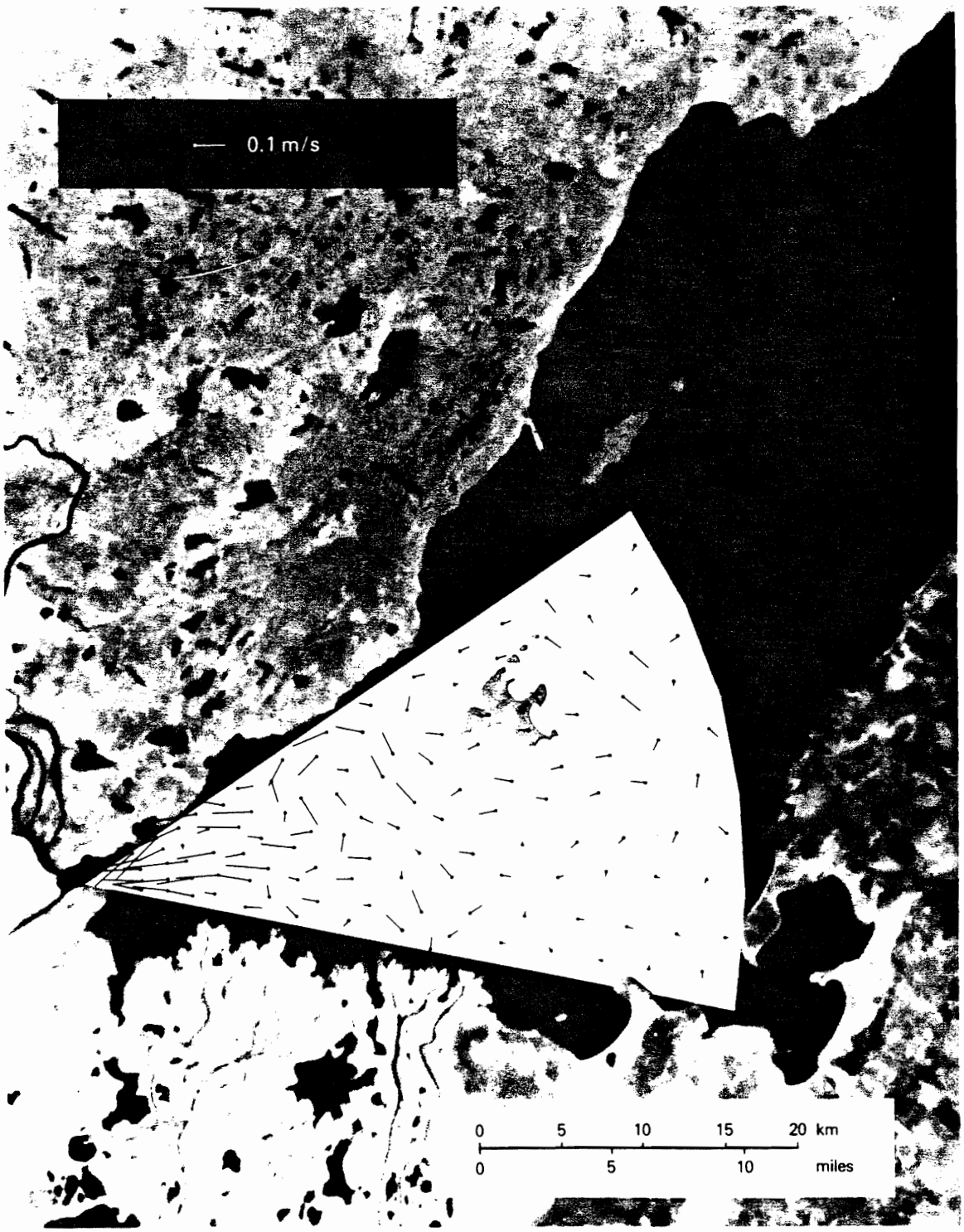

Figure 37. Model Results, No Wind

5. CONCLUSIONS AND RECOMMENDATIONS

This project was undertaken to evaluate the use of LANDSAT imagery for discerning water quality variations and to implement a mathematical circulation model of the southwest end of Lake Athabasca. To achieve these objectives considerable field data were acquired which provided clarification of some of the aspects of the circulation characteristics of the study area. The conclusions can be grouped into three categories: 1) circulation patterns and water quality; 2) satellite imagery and 3) mathematical modelling.

5.1 CIRCULATION PATTERNS AND WATER QUALITY

This study has indicated that water from the Athabasca River distributary channels can extend further into the southwest end of Lake Athabasca than had been previously thought. For moderately high inflow to outflow ratios, river water can reach the north shore of the lake. In addition, river water was found up to 20 km northeast of Big Point Channel. The results also indicated that the Embarras River and Fletcher Channel water was found primarily in the Chenal des Quatre Fourches while the Riviere des Rochers tended to comprise water from Big Point Channel and lake water. In terms of environmental impact, the extent of influence from contaminants introduced via the Athabasca River can be better delineated as a result of this work.

The winter work was undertaken under conditions of very low flow so extrapolation of the findings to more normal conditions is tenuous. It was found that of the distributary channels, only Big Point Channel had any measurable discharge and that lake currents were very low. Thus, mixing of any contaminant introduced to the system would be suppressed. The manner in which contaminants were distributed among the delta channels would play a large role in determining how they would pass through the system.

The results also indicated that more sediment is derived from shoreline sand and till deposits than was previously thought.

As a result, some aspects of interpreting satellite imagery were clarified. It was found that the volatile fraction of the suspended sediment was relatively small, indicating that the organic content probably does not significantly affect the water quality.

The water quality data indicated that the southwest end of Lake Athabasca does not exhibit any stable stratification. No evidence of significant oxygen depletion was found and no diminution of pH values was observed.

5.2 SATELLITE IMAGERY

The results of the study indicated that only suspended sediment concentration correlated well with the LANDSAT data. Band 6 provided the highest correlation while band 5 did not correlate very well with the raw satellite data. Principal component analysis of the digital satellite data indicated that PC1, which emphasizes bands 6 and 7, correlated well with suspended sediment. In addition, PC3, emphasizing the difference between bands 4 and 5, was strongly related to conductivity. In addition, PC3 showed similarities to the C1 colour composite. Thus, it appears that PC3 could prove useful in determining the distribution of river water in the study area. Because only one set of field data was available during a satellite overpass, it was not possible to do any verification analysis with an independent data set.

As a result of these findings, some interpretive questions raised in a previous study were resolved.

5.3 MATHEMATICAL MODELLING

A finite element model capable of solving the vertically integrated momentum and continuity equations was developed. Application of the model to an idealized representation of the southwest end of Lake Athabasca yielded results similar to those observed in the field. The model results could be used as input to a mixing model to predict concentration fields in the study area.

5.4 RECOMMENDATIONS

As a result of this study, the following recommendations for further work are presented. Since LANDSAT imagery has been shown to correlate well with suspended sediment and conductivity, verification of the relations presented herein could be undertaken. Additional contemporaneous water quality data would be valuable to achieve proper verification. These data could be collected either by remote samplers or field crews. The number of water quality parameters measured could be greatly reduced based on the results of this work. Application of the techniques presented in this study could be made to water bodies in other, more easily accessible, areas of the province.

Further mathematical model development could be undertaken. Interfacing with existing routing models could provide better definition of boundary conditions. Development or application of a mixing model could be carried out to provide detailed descriptions of concentration fields.

To assess winter conditions, sampling under the ice could be undertaken to measure currents and conductivity in order to provide better definition of the degree to which lake and river water intermix.

6. REFERENCES CITED

ASCE. 1978. Verification of mathematical and physical models in hydraulic engineering. 887 pp.

ASCE. 1980. Computer and physical modelling in hydraulic engineering. 492 pp.

Apel, J.R., R.L. Charnell, and R.J. Blackwell. 1974. Ocean Internal Waves off the North American and African Coasts from ERTS-1, Proceedings Ninth International Symposium on Remote Sensing of Environment, Ann Arbor, Michigan, 15-19 April, 1974.

Bartolucci, L.A., B.F. Robinson and L.F. Silva. 1977. Field measurement of the spectral response of natural waters. Photogrammetric Engineering and Remote Sensing, Vol. 43, No. 5. pp. 595-598.

Beltaos, S. 1978. Tranverse mixing in natural streams. Transportation and Surface Water Engineering Division Report No. SWE-78/03, Alberta Research Council. 52 pp.

Beltaos, S. 1979. Mixing characteristics of the Athabasca River below Fort McMurray - winter conditions. Prep. for the Alberta Oil Sands Environmental Research Program by Transportation and Surface Water Engineering Division, Alberta Research Council. AOSERP Report 40. 110 pp.

Beltaos, S. 1980. Longitudinal dispersion in rivers. Journal of the Hydraulics Division, American Society of Civil Engineers. Vol. 106, No. HY1. pp. 151-172.

Blanchard, B.J. and R.W. Leamer. 1973. Spectral reflectance of water containing suspended sediment. Remote sensing and water resources management, Proc. #17. American Water Resources Association, June. pp. 339-347.

Conte, S.D. and C. Debour. 1965. Elementary numerical analysis. McGraw-Hill. 396 pp.

Crandall, S.H. 1956. Engineering Analysis, McGraw-Hill. 417 pp.

Davis, J.C. 1973. Statistics and Data Analysis in Geology. John Wiley and Sons Inc., New York, 550 pp.

Derouchie, W. F. and R.B. Forrest. 1974. Potential Positioning Accuracy of ERTS-1 MSS Images, paper presented at ACSM-ASP Convention, St. Louis, Missouri, March 1974.

Environment Canada. 1979. Histroical Streamflow Summary. Alberta. Inland Waters Directorate, Water Resources Branch, Water Survey of Canada. Ottawa. 434 pp.

Environment Canada. 1982. Surface Water Data. Alberta. Inland Waters Directorate, Water Resources Branch, Water Survey of Canada. Ottawa. 253 pp.

Evans, W.E. 1974. Marking ERTS Images with a Small Mirror Reflector, Photogrammetric Engineering. Vol. 40, No. 6. pp. 665-671.

Evans, W.E. 1976. Effect of Sun Angle, Atmospheric Attenuation and Turbulence on Mirror Beacons for LANDSAT Image Control, U.S. Department of Commerce, NTIS, Report No. PB-255 404.

Fischer, H.B., E.J. List, R.C.Y. Koh, J. Imberger and N.H. Brooks. 1979. Mixing in inland and coastal waters. Academic Press. 483 pp.

Forrest, R.B. 1970. Mapping From Space Images, Bendix Technical Journal Earth Resources Exploration. Vol. 3, No. 2 pp. 40-47.

Gray, W.G. 1976. An efficient finite element scheme for two-dimensional surface water computation. Finite Elements in Water Sources. Pentech Press. pp. 4.33-4.49.

Harrington, R.A., N. Kouwen and G.J. Farquhar. 1978. Behaviour of a hydrodynamic finite element model. Finite Elements in Water Resources. Pentech Press. pp. 2.43-2.60.

Ippen, A.T. (ed). 1966. Estuary and coastline hydrodynamics. McGraw-Hill 744 pp.

Kellerhalls, R. 1971. Factors controlling the level of Lake Athabasca. Proceedings of the Peace-Athabasca Delta Symposium, University of Alberta, Edmonton. pp. 57-109.

Kellerhals, R., C.R. Neill and D.I. Bray 1972. Hydraulic and geomorphic characteristics of rivers in Alberta. River Engineering and Surface Hydrology Report 72-1. Research Council of Alberta. Edmonton. 52 pp.

Klemas, V., D.S. Bartlett, W.D. Philpot, G.R. Davis, R.H. Rogers, and L. Reed. 1974. Application of Ecological, Geological and Oceanographic ERTS-1 Imagery to Delaware's Coastal Resources Management, Final Report September 1972, June 1974, Delaware University.

Klemas, V., D.S. Bartlett, and W.D. Philpot. 1978. Remote Sensing of Coastal Environment and Resources, Proceedings Coastal Mapping Symposium. Rockville, Maryland.

Klemas, V. and D.F. Polis. 1977. Remote Sensing of Estuarine Fronts and Their Effects on Pollutants, Photogrammetric Engineering and Remote Sensing. Vol. 43, No. 5. pp. 599-612.

Leendertse, J.J. 1967. Aspects of a computational model for long-period water wave propogation. The Rand Corporation, Report No. RM 5294 PR.

Lepley, L.K., K.E. Foster, and L.G. Everett. 1975. Water Quality Monitoring of Reservoirs on the Colorado River Utilizing ERTS-1 Imagery, in Remote Sensing and Water Resources Management, Thomson, K.P.B., R.L. Lane, and S.C. Csallany, (eds.), Proceedings American Water Resources Association. No. 17, Urbana, Ill. pp. 105-111.

Leschziner, M.A. and W. Rodi. 1979. Calculation of strongly curved open channel flow, Journal of the Hydraulics Division, ASCE. Vol. 105, No. HY5. pp. 1297-1314.

Lipsett, A.W. and R.A. Harrington. 1981. Evaluation of ice bridges in the Fort Chipewyan area. Transportation and Surface Water Engineering Department Report 81-1. Alberta Research Council. 76 pp.

Lodwick, G.D. 1977. A Computer Analysis of ERTS Data and its Role in Terrain Classification for Engineering, Proceedings International Conference on Computer Applications in Developing Countries, Bangkok, Thailand, 1977, A.I.T. Bangkok, Thailand. pp. 653-668.

Lodwick, G.D. 1978. Between Scene Registration Accuracy in LANDSAT Time Sequencing, Proceedings Twelfth International Symposium on Remote Sensing of Environment, Manilla, Philipines, 1978, ERIM, Ann Arbor, Michigan. pp. 1461-1470.

Lodwick, G.D. 1979. Measuring Ecological Changes in Multitemporal LANDSAT Data Using Principal Components, Proceedings Thirteenth International Symposium on Remote Sensing of Environment, University of Michigan, 1979, ERIM, Ann Arbor, Michigan. pp. 1131-1141.

Lodwick, G.D. 1981. A Computer System for Monitoring Environmental Changes in Multitemporal LANDSAT Data, Canadian Journal of Remote Sensing. Vol. 7, No. 1. pp. 24-33, July 1981.

Lynch, D.R. and W.G. Gray. 1979. Analytical solutions for computer flow model testing. Journal of the Hydraulics Division, ASCE. Vol. 104, No. HY10. pp. 1409-1428.

Martin, H.C. and G.F. Carey. 1973. Introduction to finite element analysis. McGraw-Hill. 386 pp.

McCloy, K.R. 1977. Geometric Fitting of LANDSAT Imagery, Bulletin of the Remote Sensing Association of Australia. Vol. 3, No. 1. pp. 6-19.

Neill, C.R., B.J. Evans, and A.W. Lipsett. 1981. Circulation of water and sediment in the Athabasca delta area. Prep. for the Alberta Oil Sands Environmental Research Program by Northwest Hydraulic Consultants Ltd. and the Alberta Research Council. AOSERP Report 123. 182 pp.

Niemeyer, G. 1979. Long wave model independent of stability criteria. Journal of the Waterway, Port, Coastal Ocean Engineering Division, ASCE. Vol. 105, No. WW1. pp. 51-65.

Partridge, P.W. and C.A. Brebbia. 1976. Quadratic finite elements in shallow water problems. Journal of the Hydraulics Division, ASCE. Vol. 102, No. HY9. pp. 1299-1313.

Peace-Athabasca Delta Project. 1973. Technical Report and Appendices. Edmonton. 4 Vols.

Peace-Athabasca Delta Symposium. 1971. University of Alberta. Edmonton. 359 pp.

Pollack, M.J. 1960. Wind set-up and shear stress coefficient in Chesapeake Bay. Journal of Geophysical Research. Vol. 65, No. 10. pp. 3383-3389.

Ponce, V.M. and S.B. Yabusaki. 1981. Modelling circulation in depth-averaged flow. Journal of the Hydraulics Division, ASCE. Vol. 107, No. HY11. pp. 1501-1518.

Ritchie, C.R., F.R. Schiebe, and J.R. McHenry. 1976. Remote sensing of suspended sediment in surface waters. Photogrammetric Engineering and Remote Sensing. Vol. 42, No. 12. pp. 1539-1545.

Seidner, R. 1979. Regional water quality of the AOSERP study area. Draft report, Alberta Oil Sands Environmental Research Program, Project HY2-8-1.

Simons, T.J. 1980. Circulation models of lakes and inland seas. Canadian Bulletin of Fisheries and Aquatic Sciences. Department of Fisheries and Oceans. Ottawa. 146 pp.

Slave River Hydro Feasibility Study. 1982. Technical Report and Appendices. Alberta Environment.

Specht, M.R., D. Needler, and N.L. Fritz. 1973. New Colour Film for Water-Photography Penetration, Photogrammetric Engineering. Vol. 39, No. 4. pp. 359-369.

Sydor, M., A. Debour, and T. Cheng. 1979. Developing a mathematical flow simulation model for the Peace-Athabasca Delta. Draft report, Environment Canada and Alberta Environment. 22 pp. and appendices.

Thomas, I.L., G.M. Allcock, and R.C. Child. 1979. Cartography from LANDSAT - New Zealand Experiments in Marking LANDSAT Imagery with Solar Reflectors, paper presented at 49th ANZAAS Congress, University of Auckland, New Zealand, January 1979.

Trinder, J.C. and C.J.H. Smith. 1979. Rectification of LANDSAT Digital Imagery, Australian Journal of Geodesy, Photogrammetry and Surveying. No. 30. pp. 15-30.

Walters, R.A. and R.T. Cheng. 1980. Accuracy of an estuarine hydrodynamic model using smooth elements. Water Resources Research. Vol. 16, No. 1. pp. 187-195.

Wang, H.P. 1976. Multi-levelled finite element hydrodynamic model of Block Island Sound. Finite Elements in Water Resources. Pentech Press. pp. 4.69-4.93.

Wang, J.D. 1975. Mathematical modelling of near coastal circulation. Ph. D. Thesis, Massachusetts Institute of Technology. 272 pp.

Wong, K.W. 1975. Geometric and Cartographic Accuracy of ERTS-1 Imagery, Photogrammetric Engineering and Remote Sensing. Vol. 41, No. 5. pp. 621-635.

Yalin, M.S. 1971. Theory of Hydraulic Models. MacMillan. 266 pp.

Zienkiewicz, O.C. 1971. The finite element method in engineering science. McGraw-Hill. 787 pp.

7. APPENDIX

7.1 FIELD DATA

The detailed field measurements are presented as a continuation of the figures presented in chapter 2.

Figure 3. Water Quality Data, June, 1981
(continued from text)

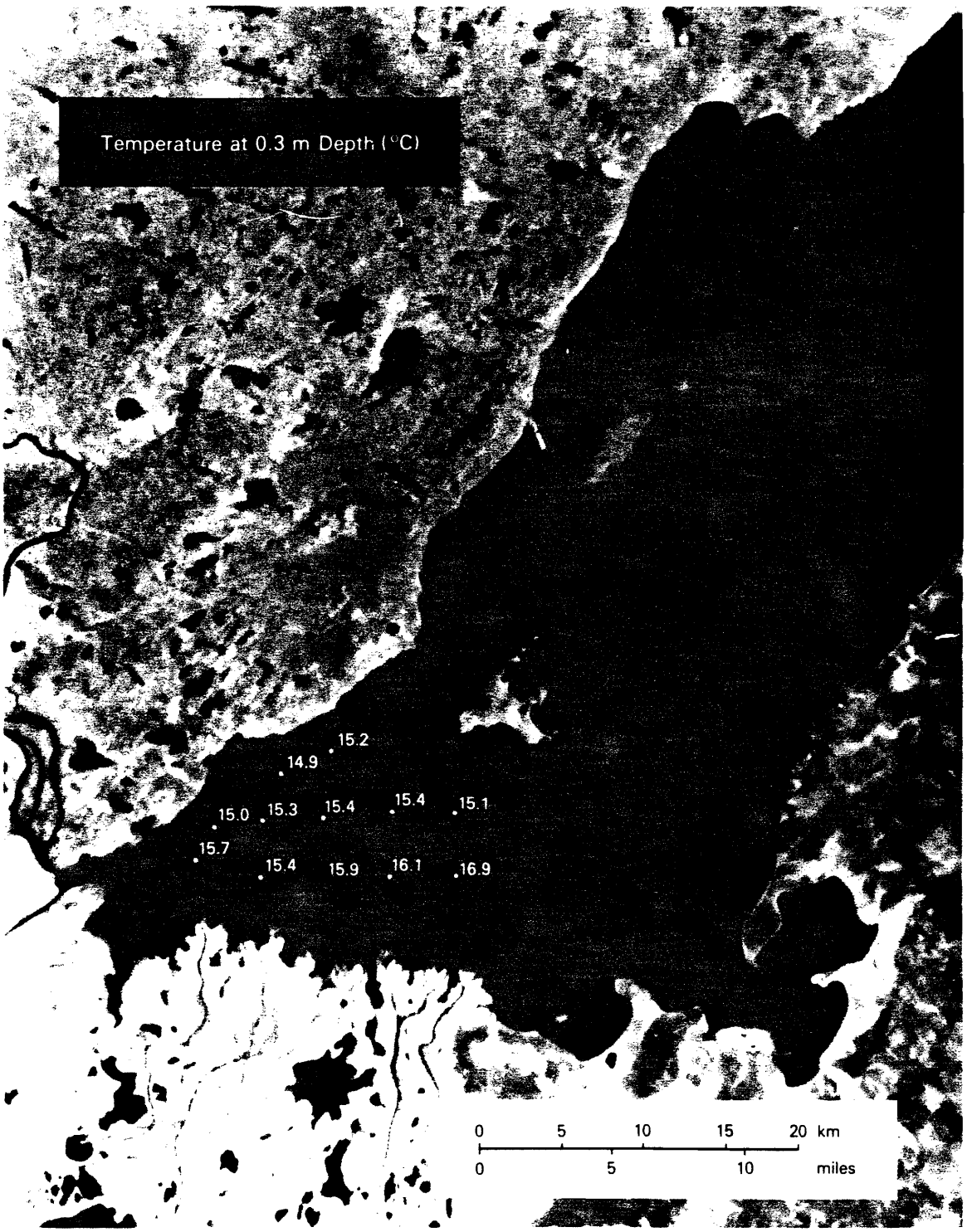

Figure 3. Continued

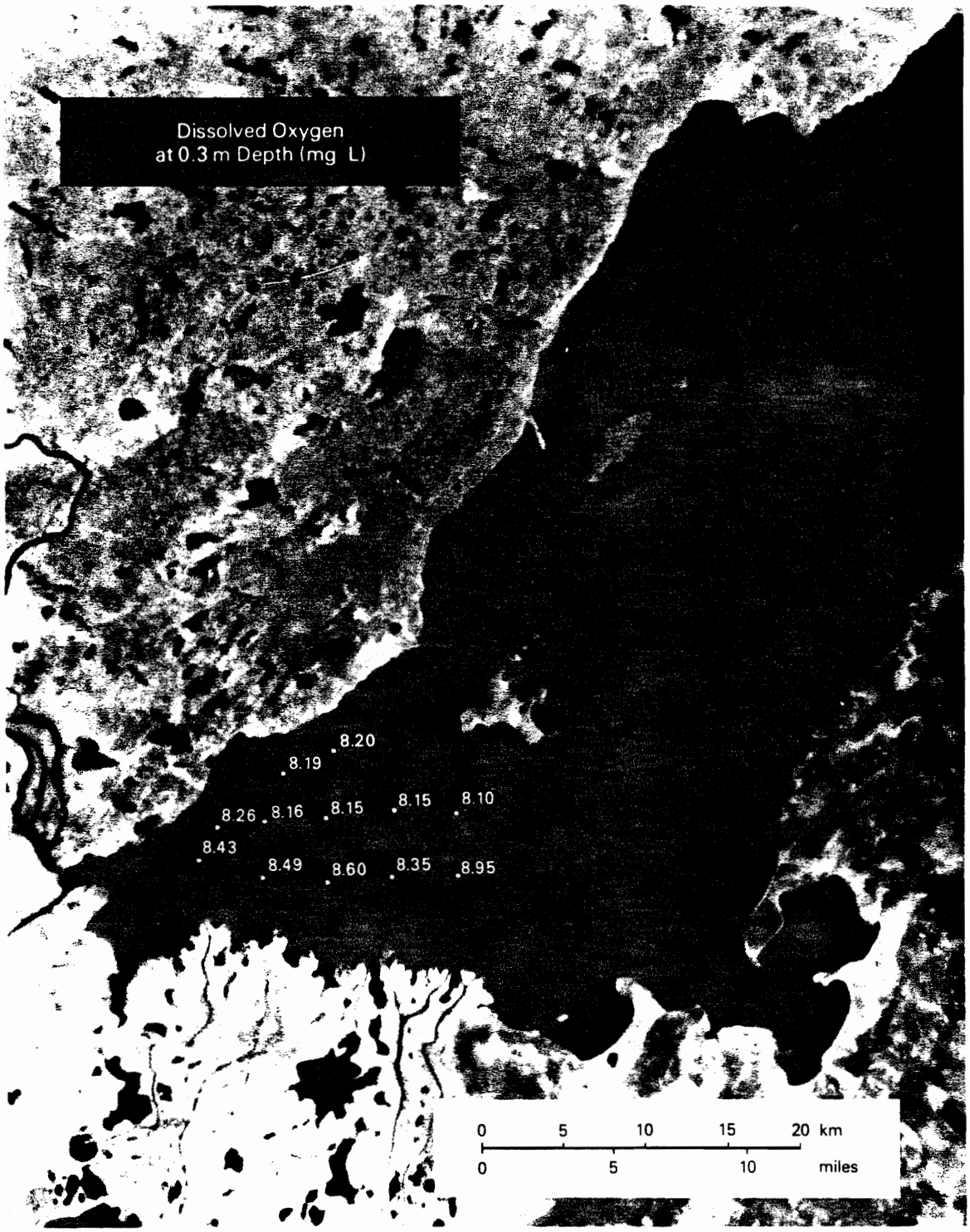

Figure 3. Continued

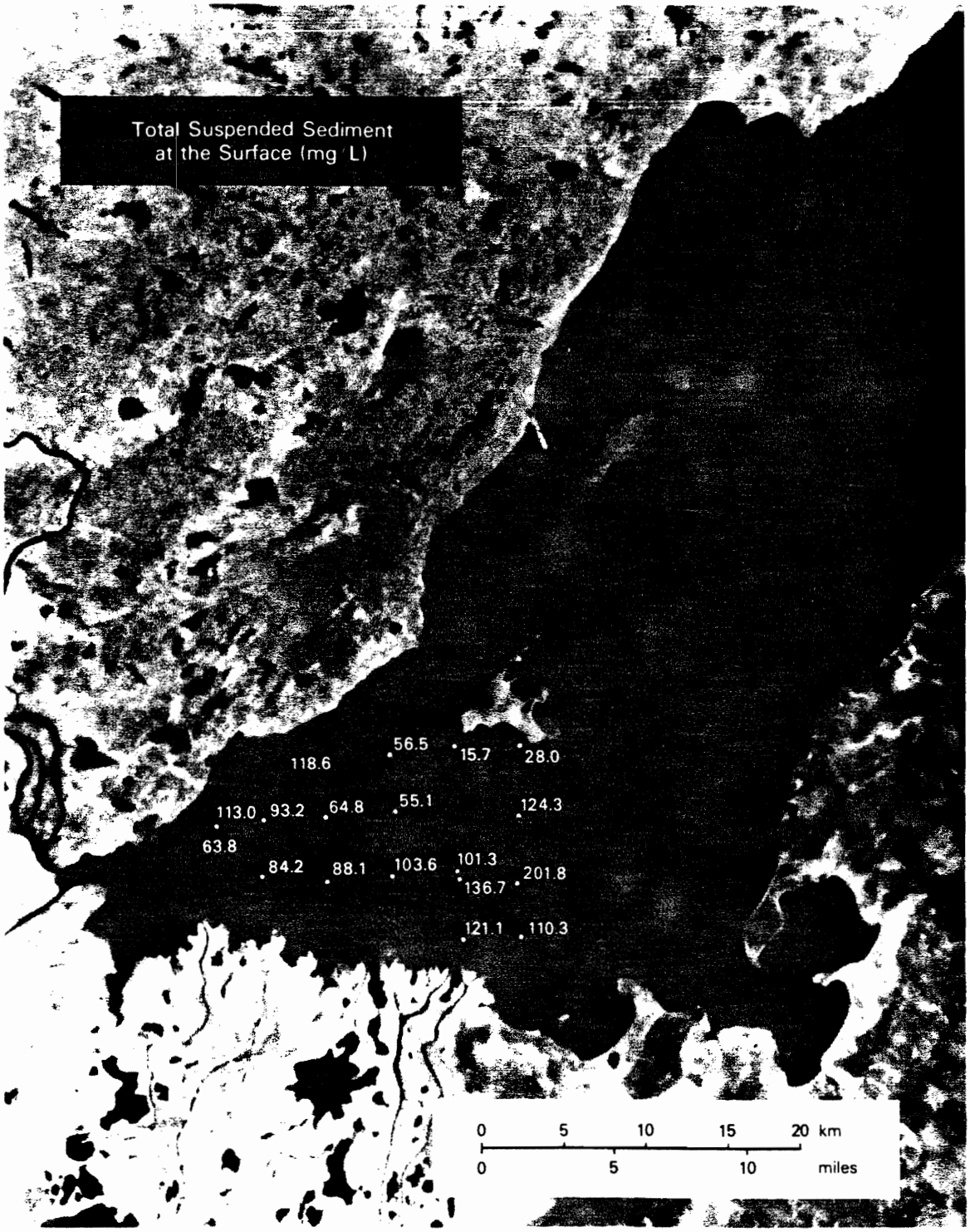

Figure 3. Continued

Figure 3. Continued

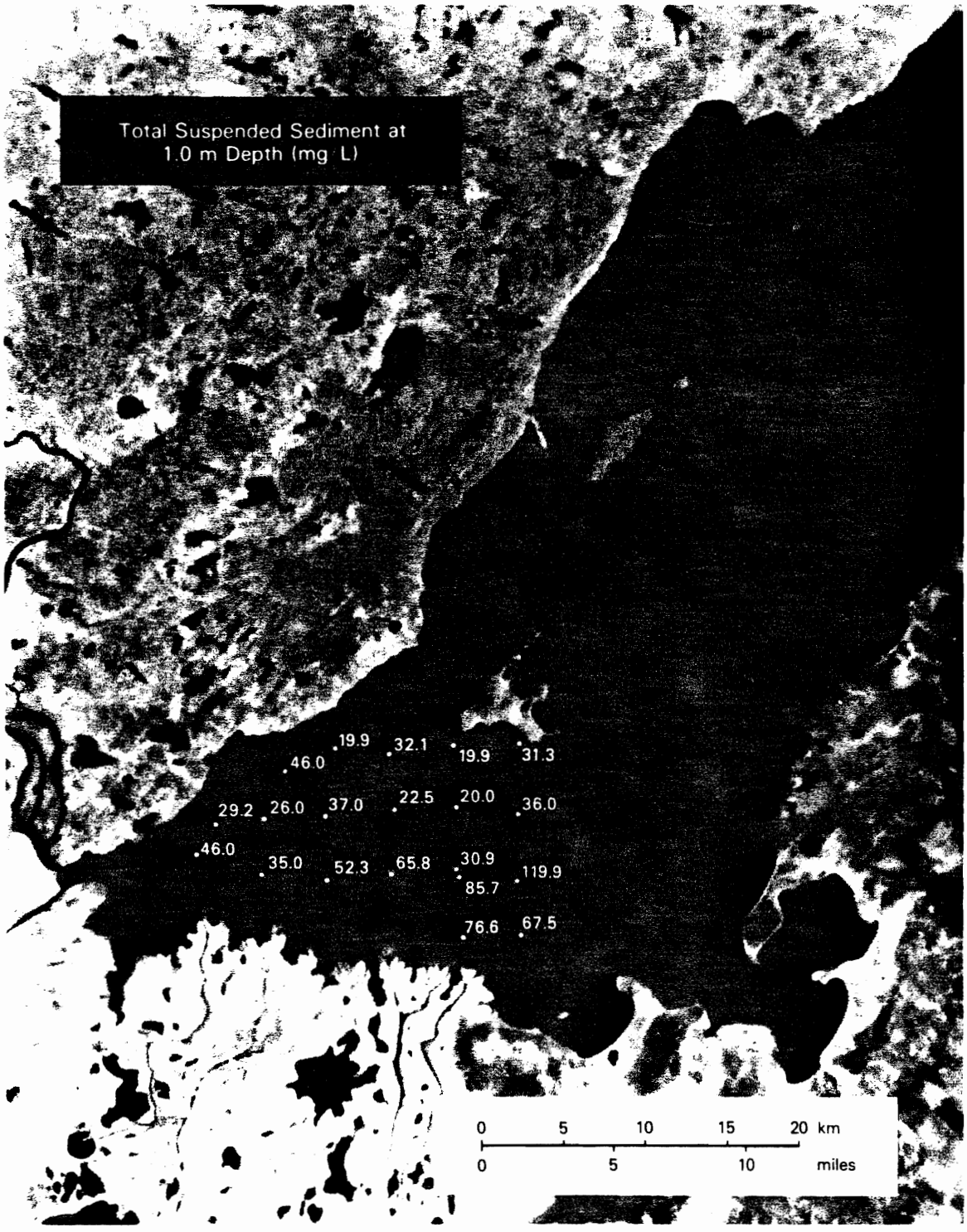

Figure 3. Continued

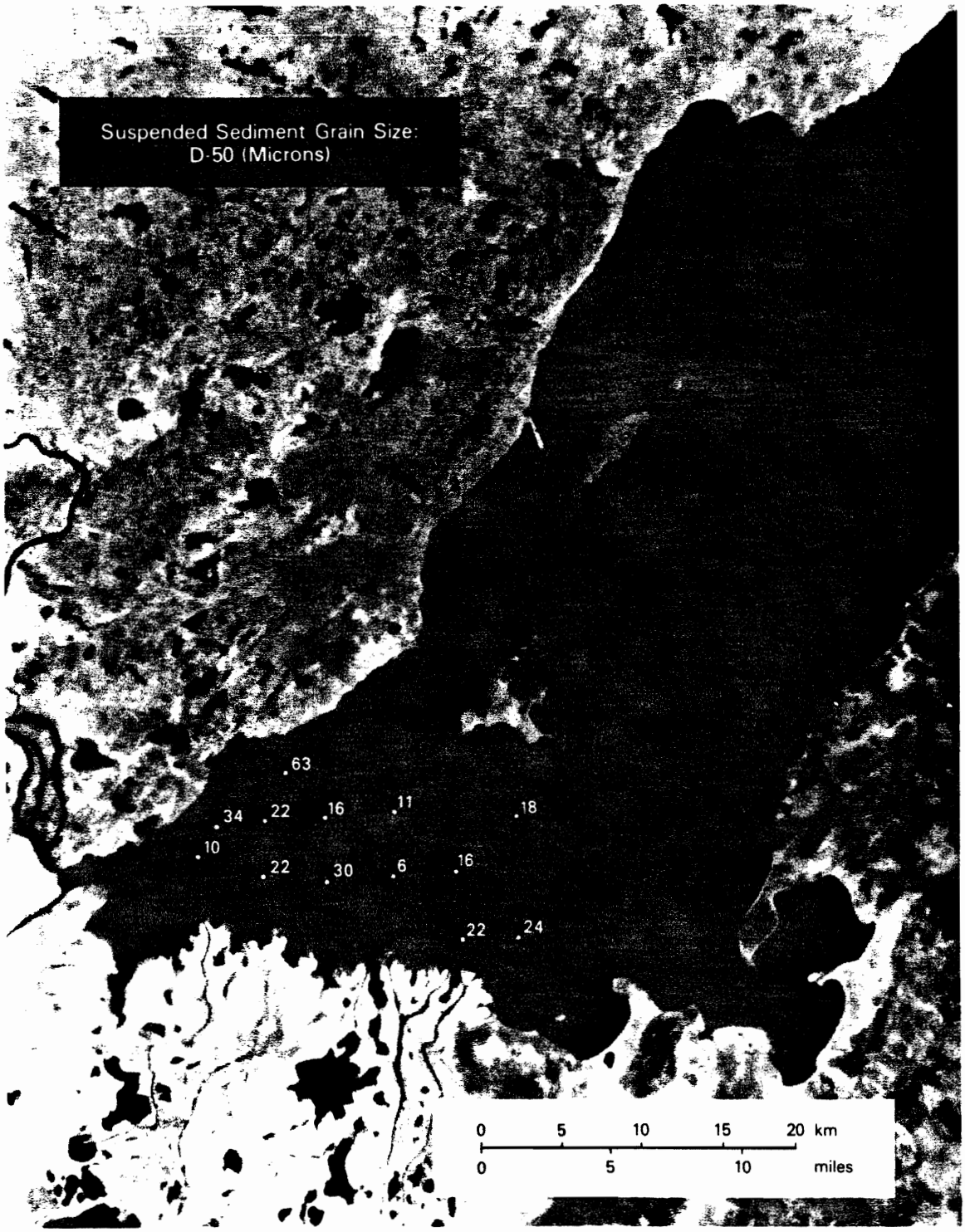

Figure 3. Conclusion

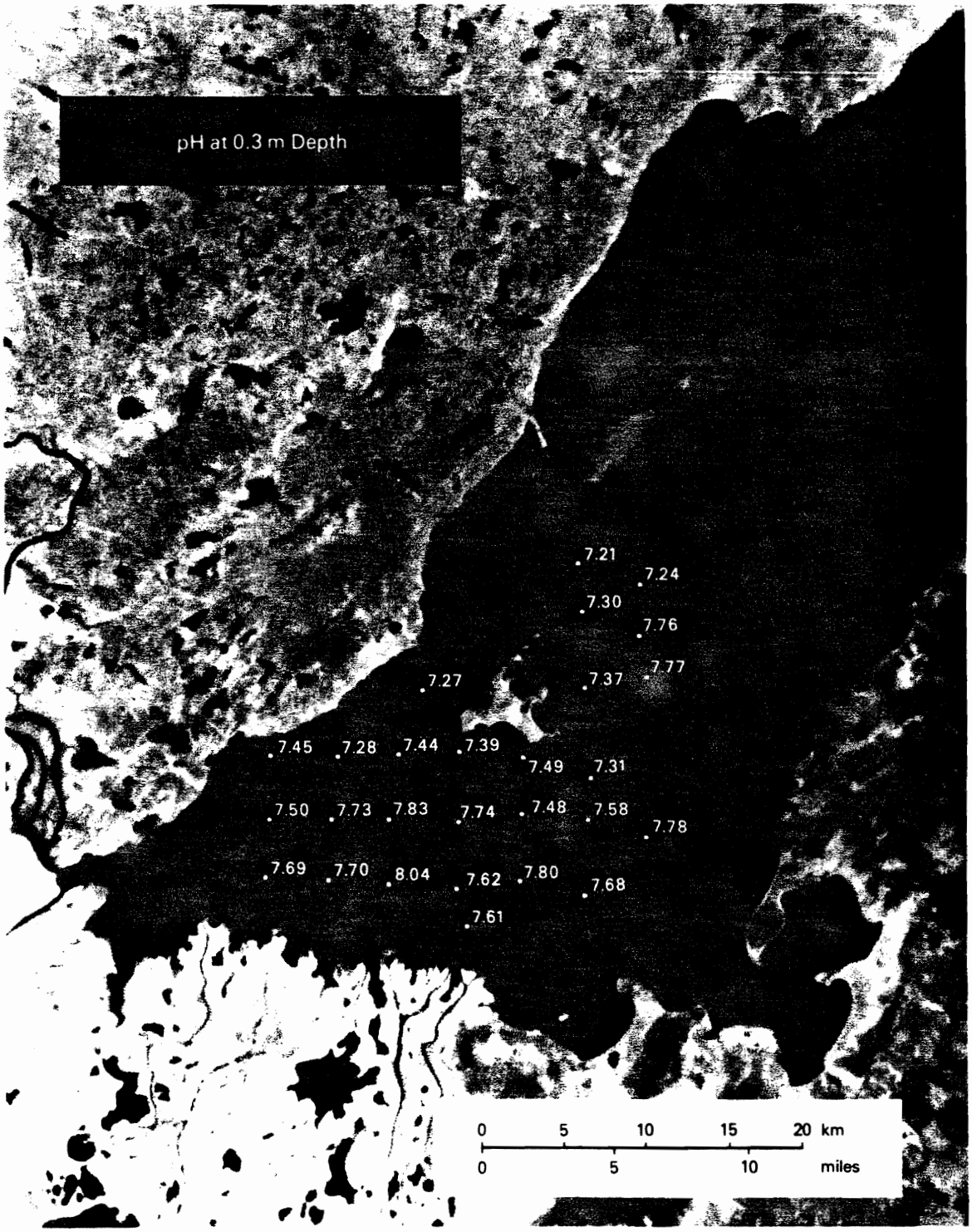

Figure 6. Water Quality Data, July, 1981
(continued from text)

Figure 6. Continued

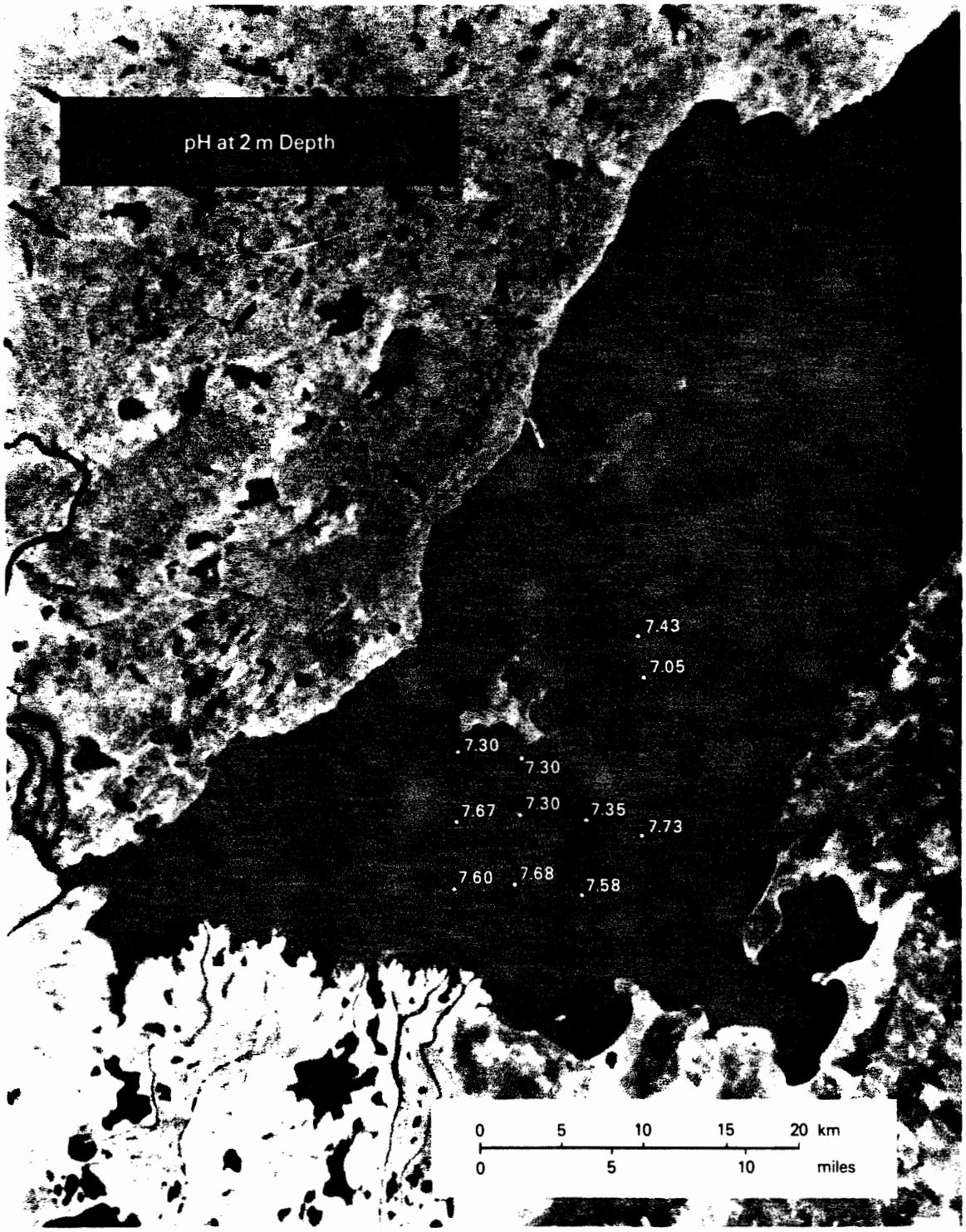

Figure 6. Continued

Figure 6. Continued

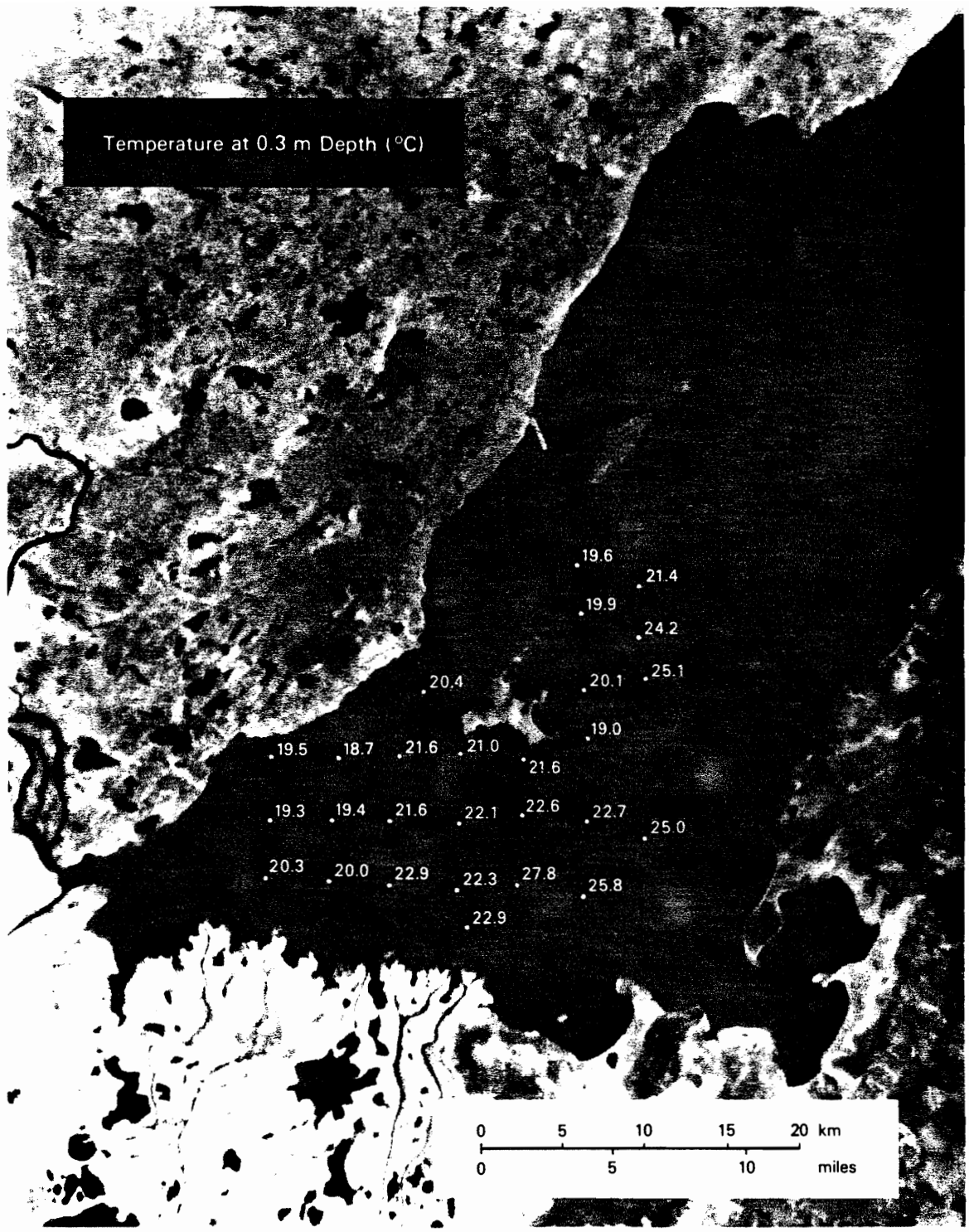

Figure 6. Continued

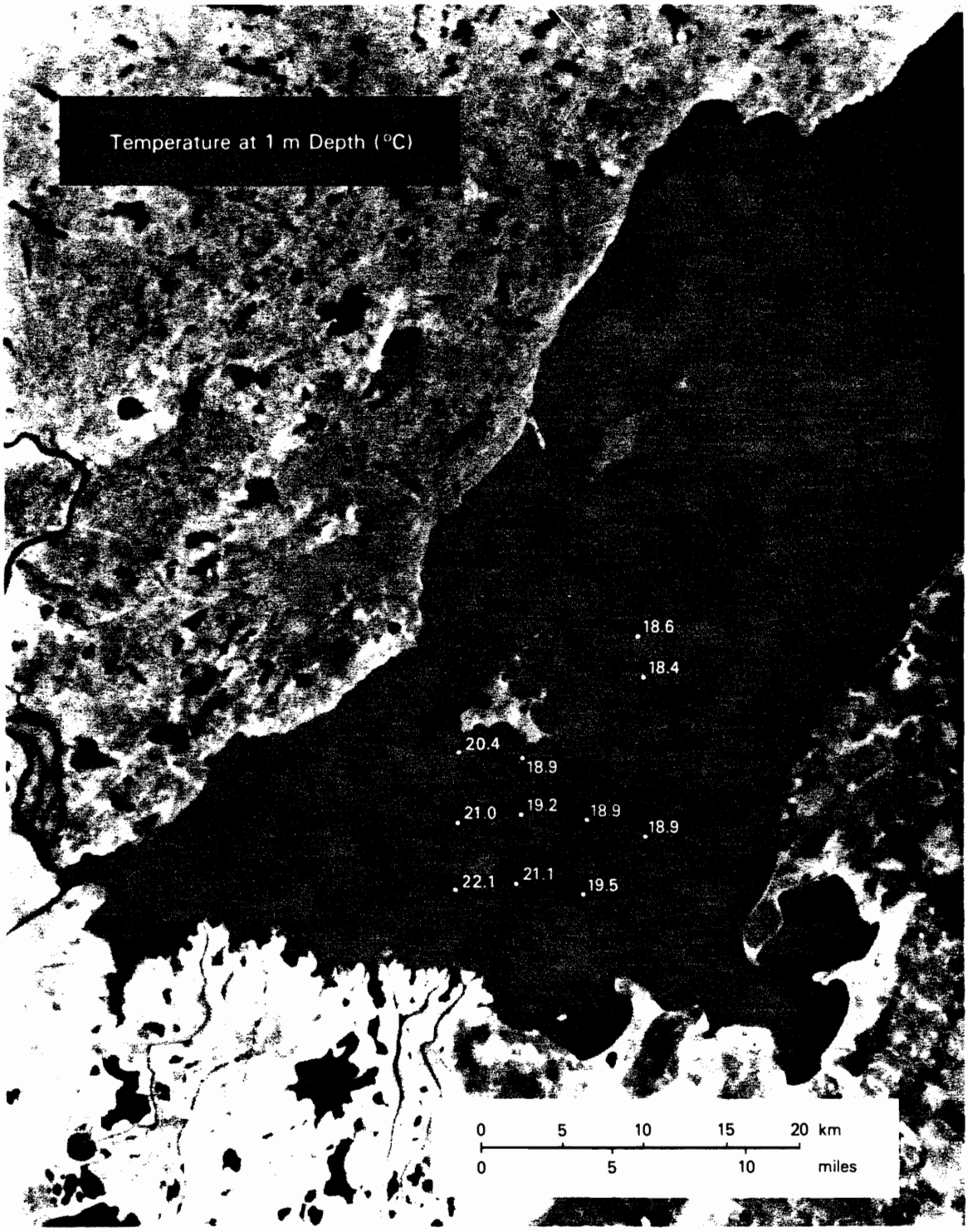

Figure 6. Continued

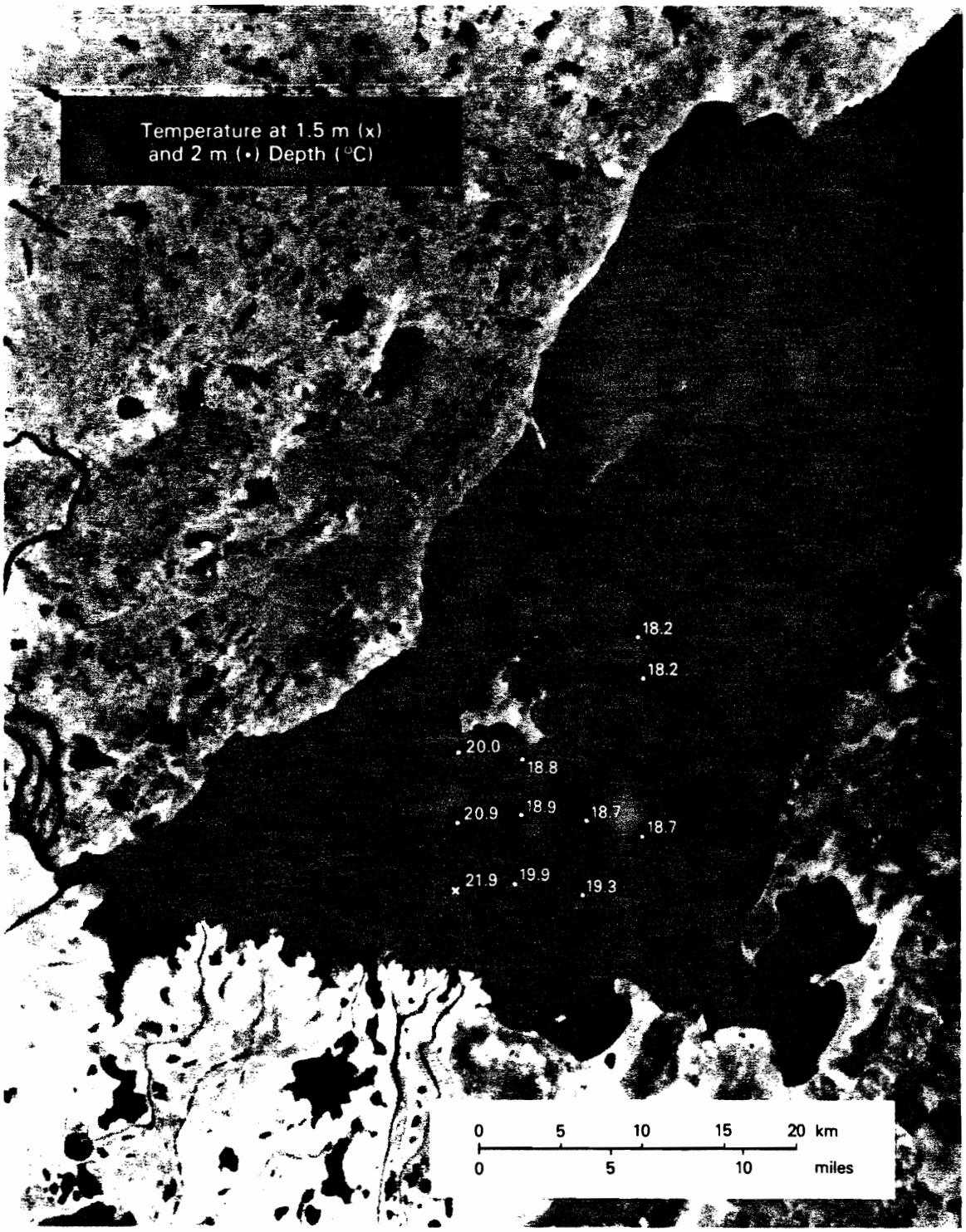

Figure 6. Continued

Figure 6. Continued

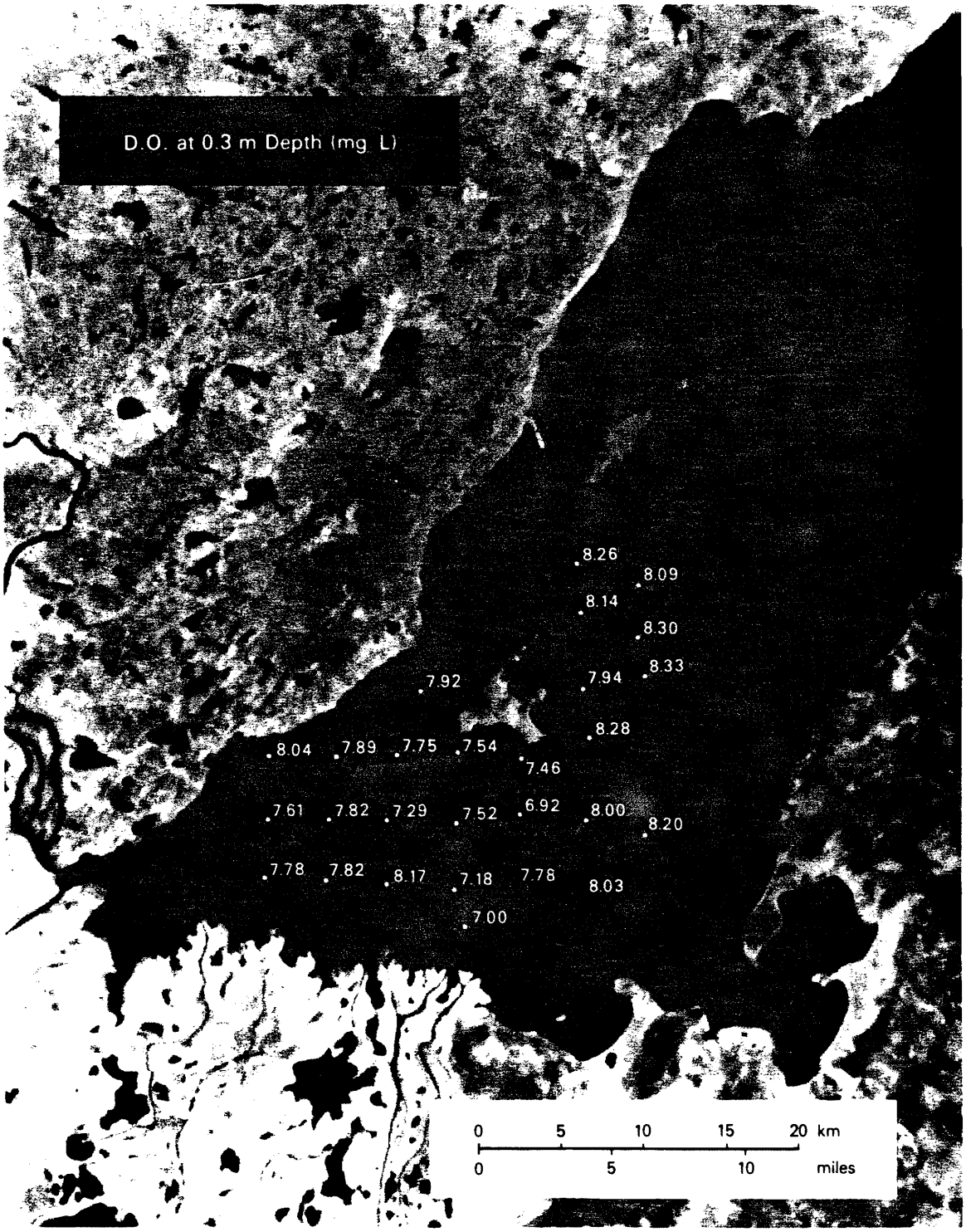

Figure 6. Continued

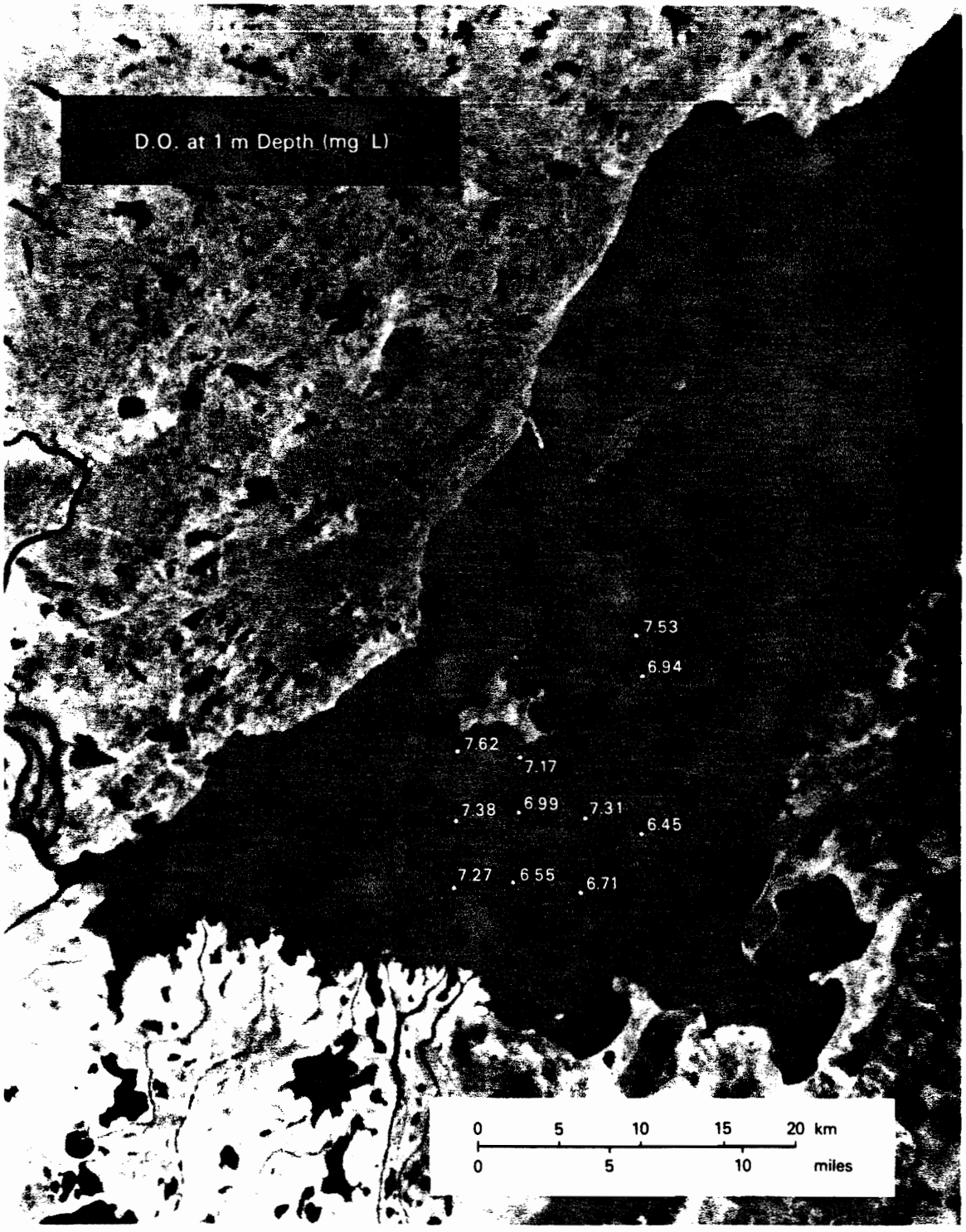

Figure 6. Continued

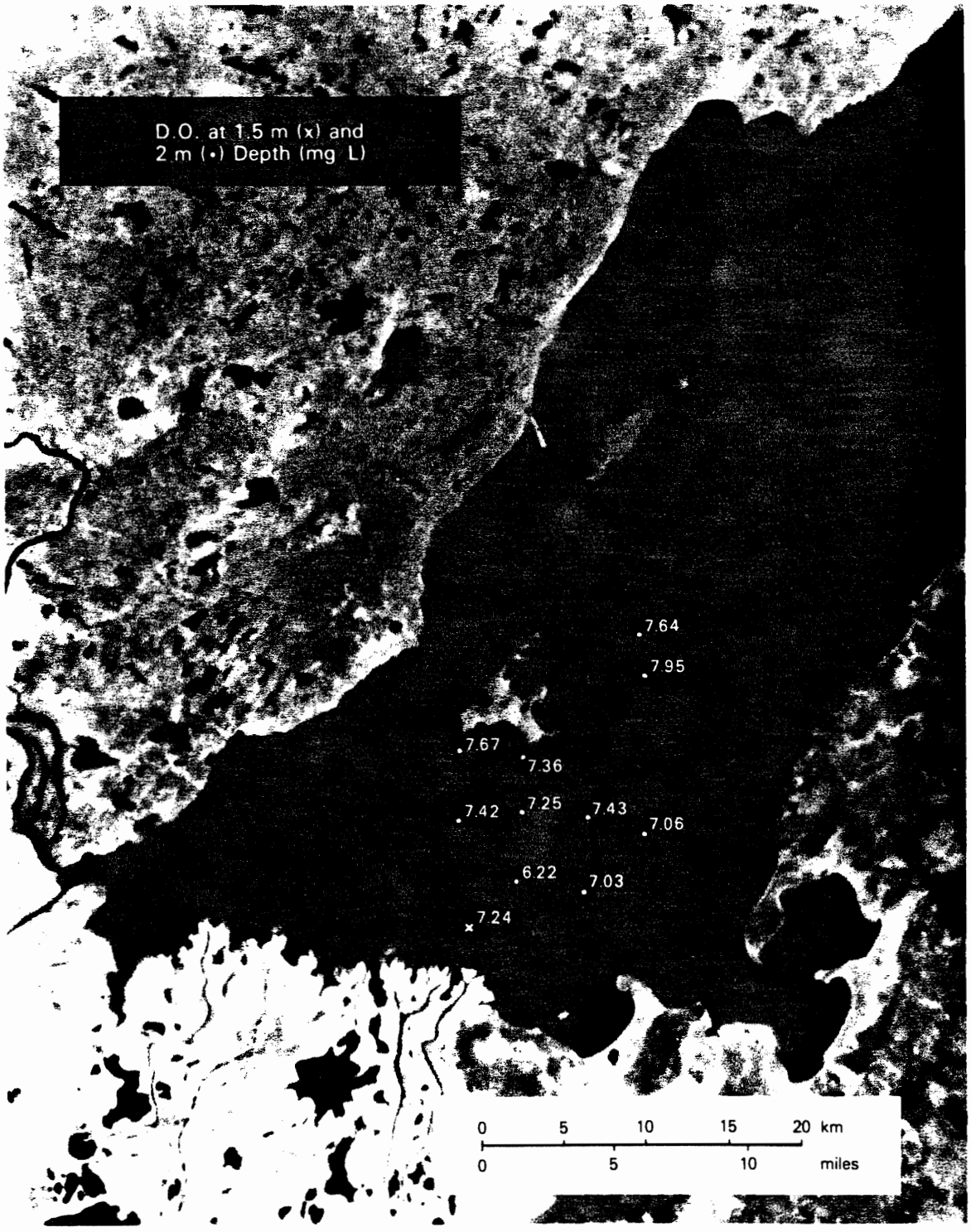

Figure 6. Continued

Figure 6. Continued

Figure 6. Continued

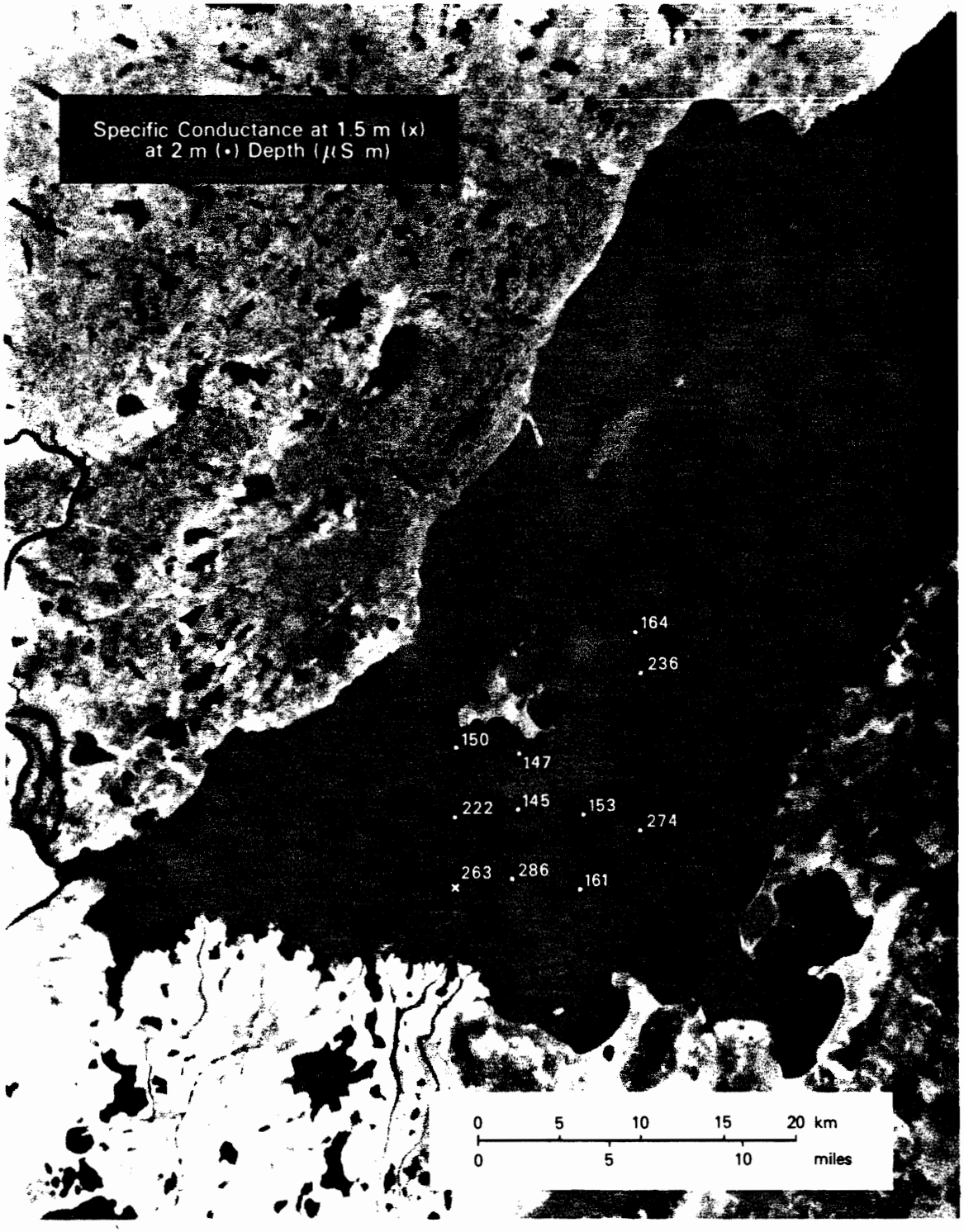

Figure 6. Continued

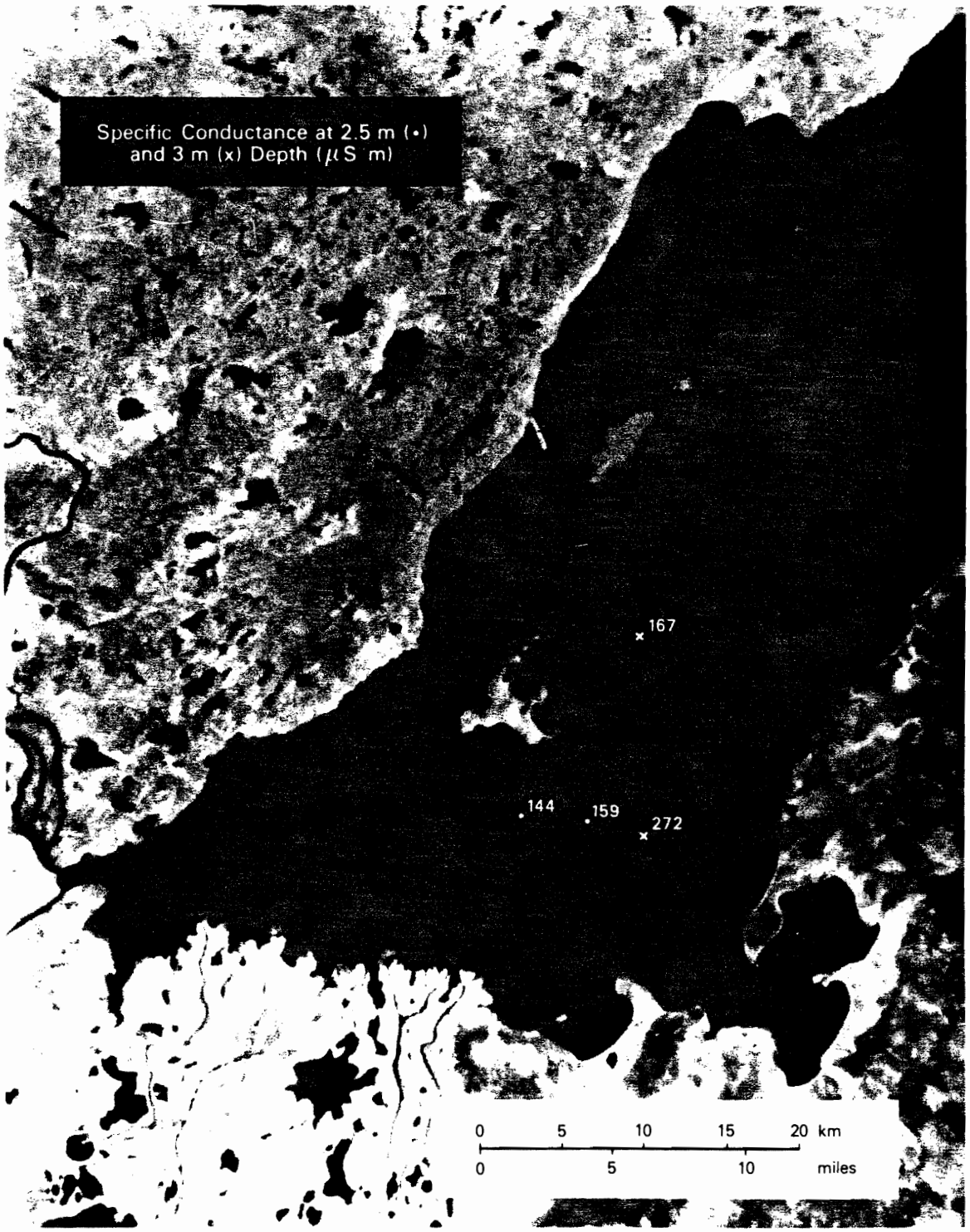

Figure 6. Continued

Figure 6. Continued

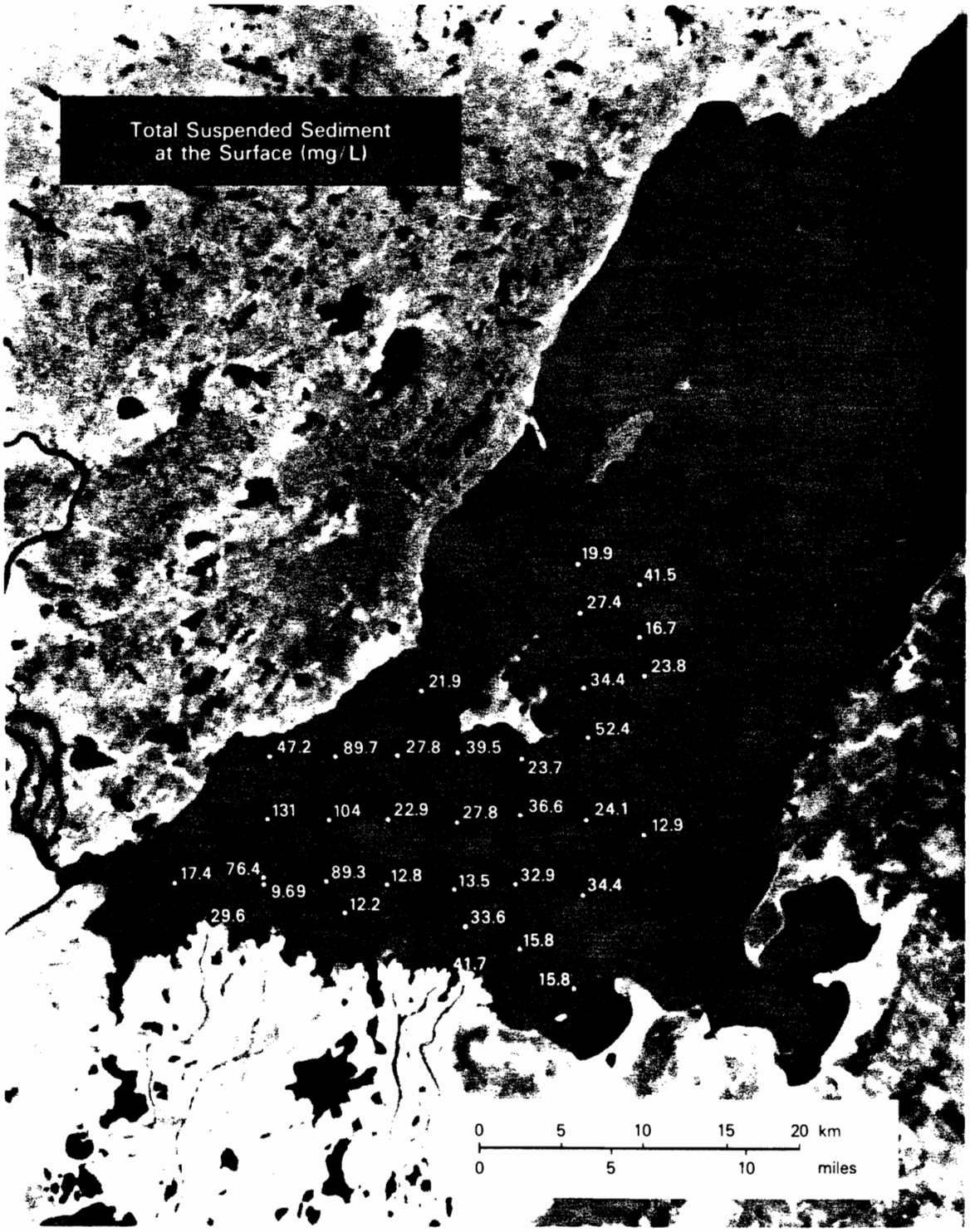

Figure 6. Continued

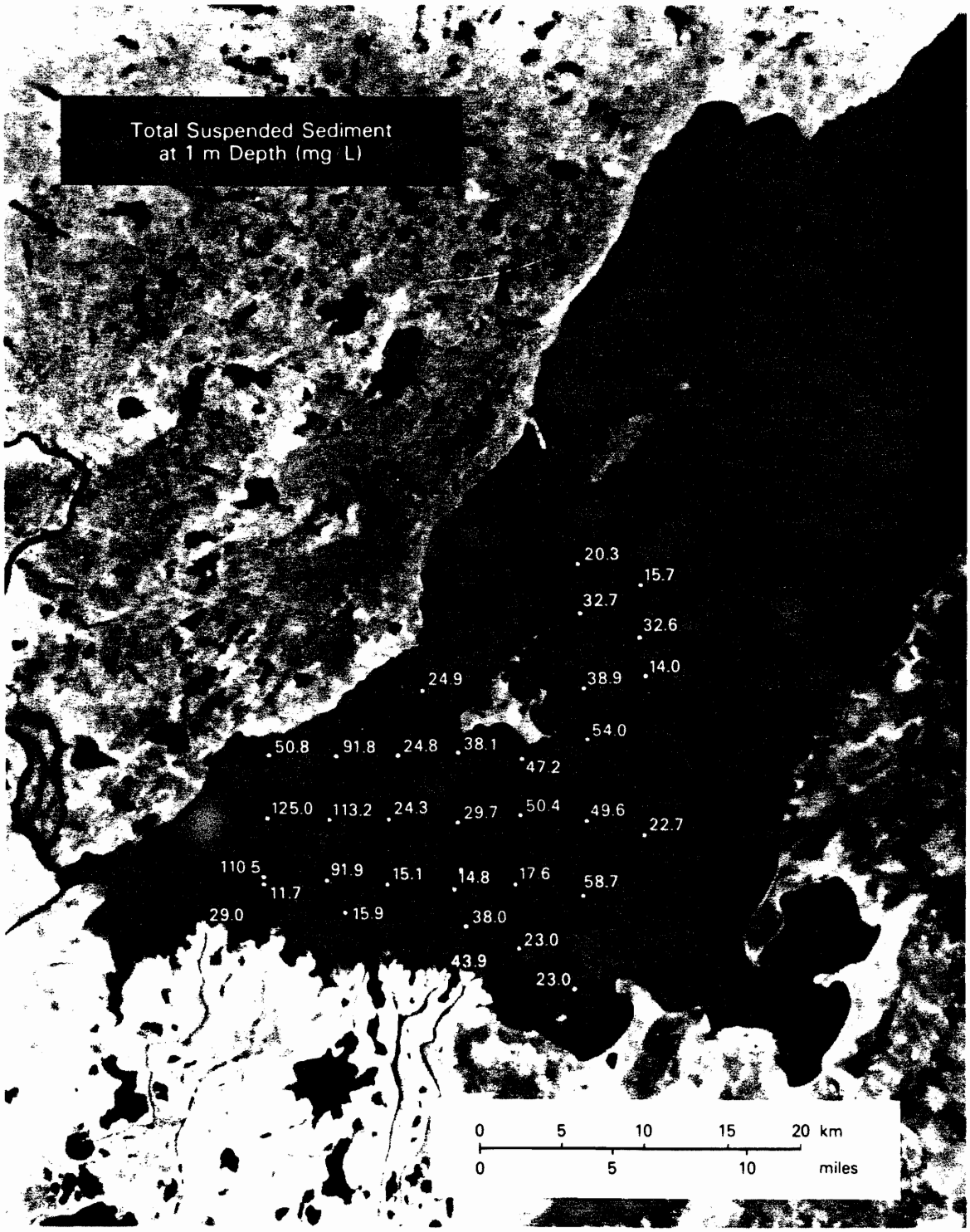

Figure 6. Continued

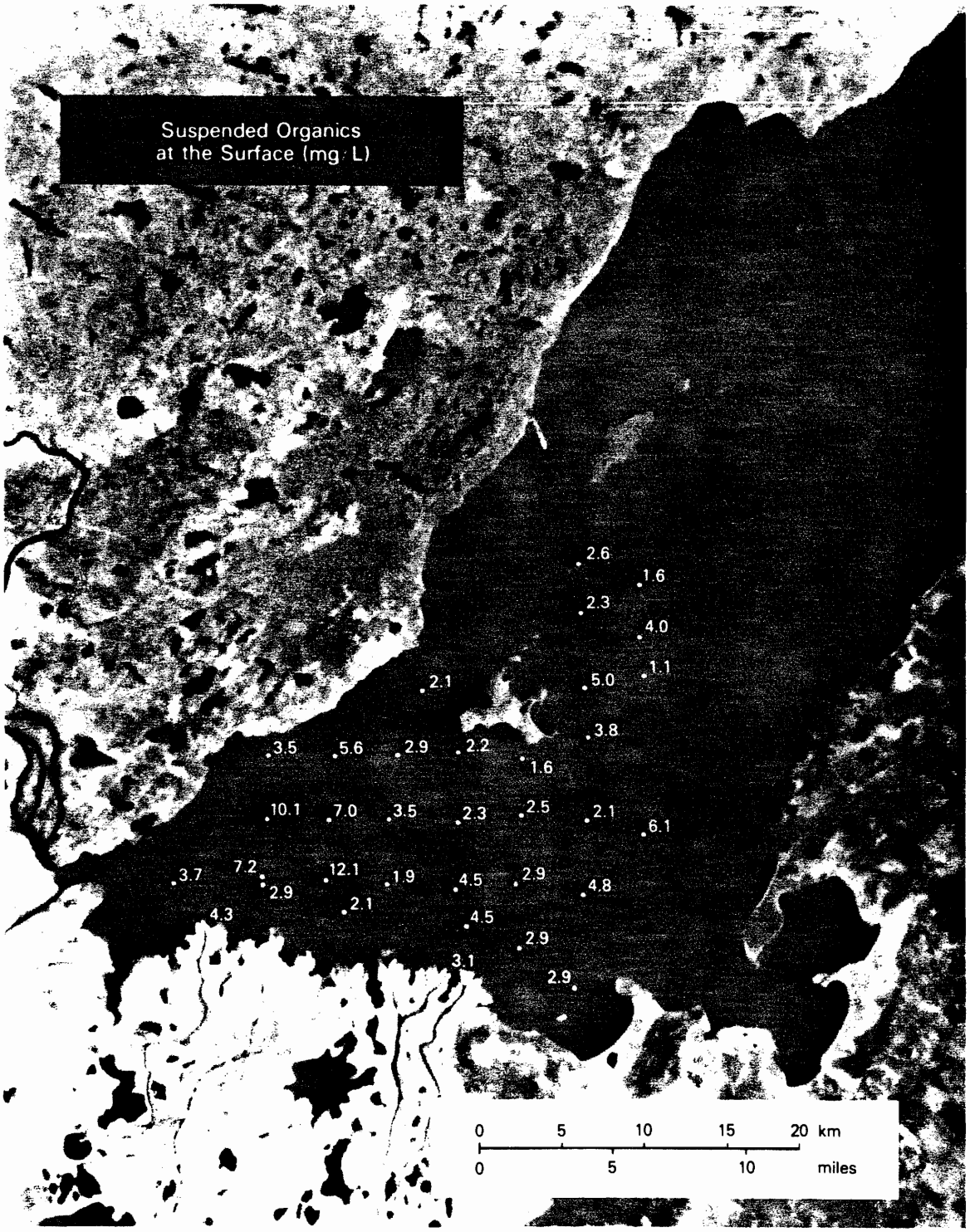

Figure 6. Continued

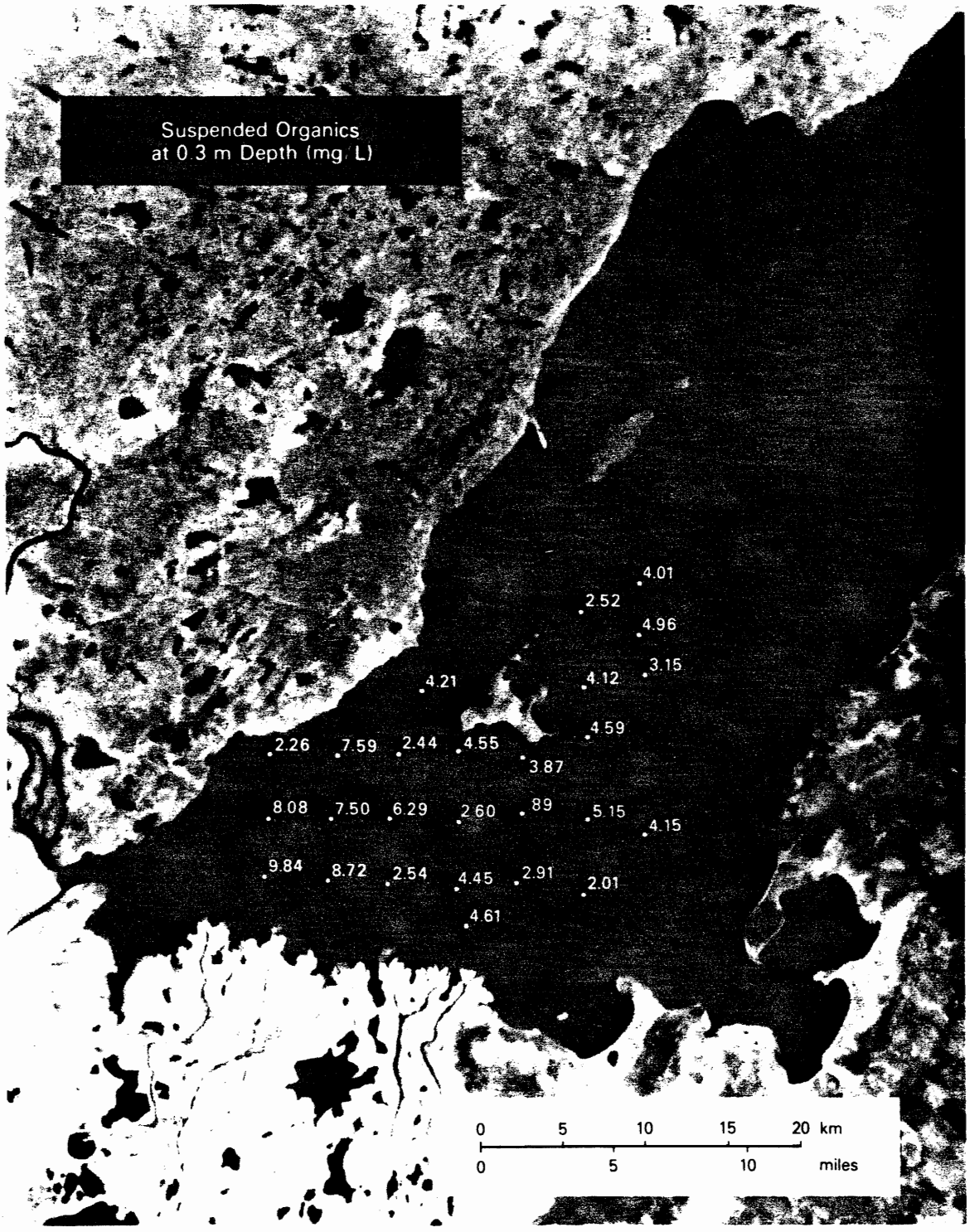

Figure 6. Continued

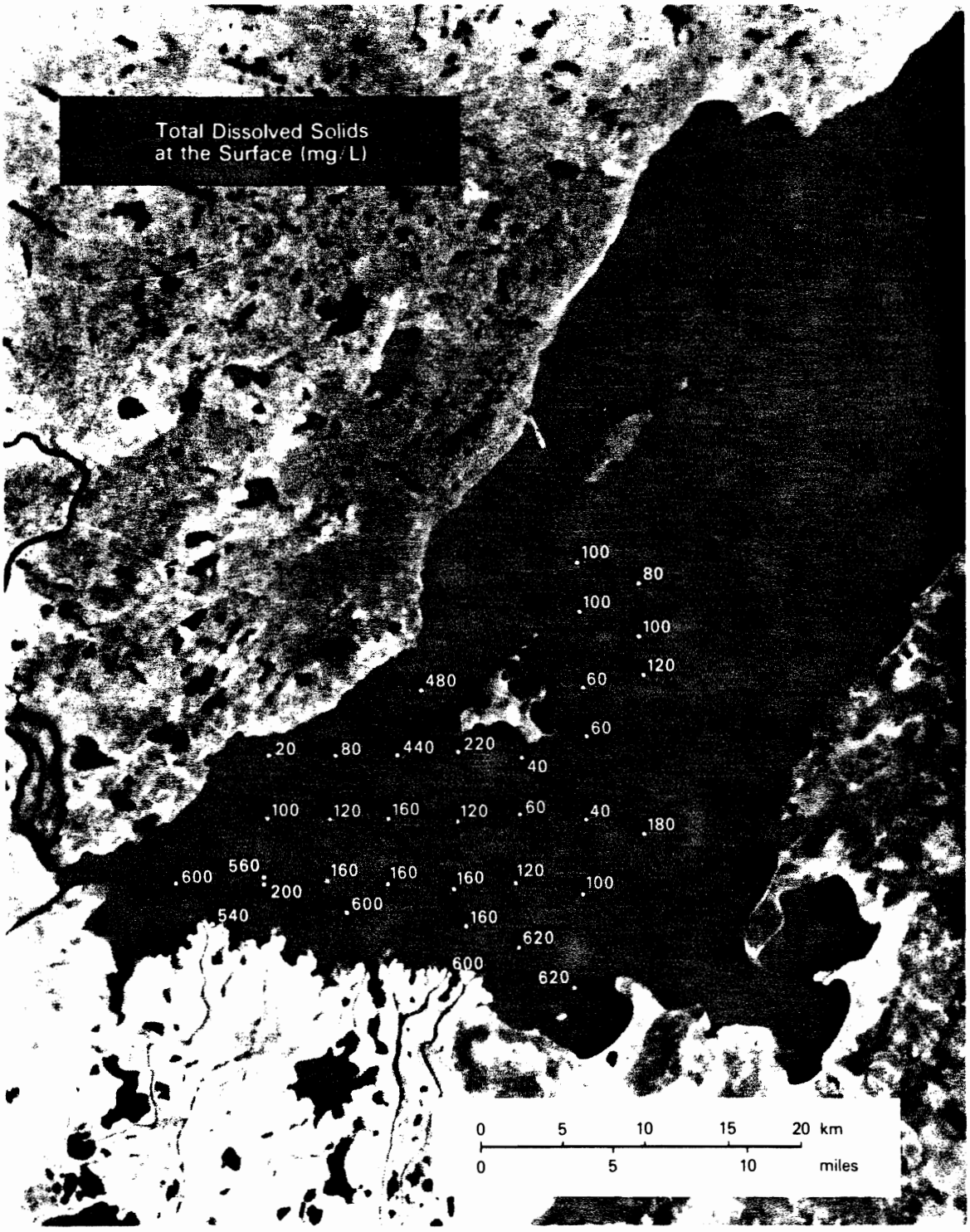

Figure 6. Continued

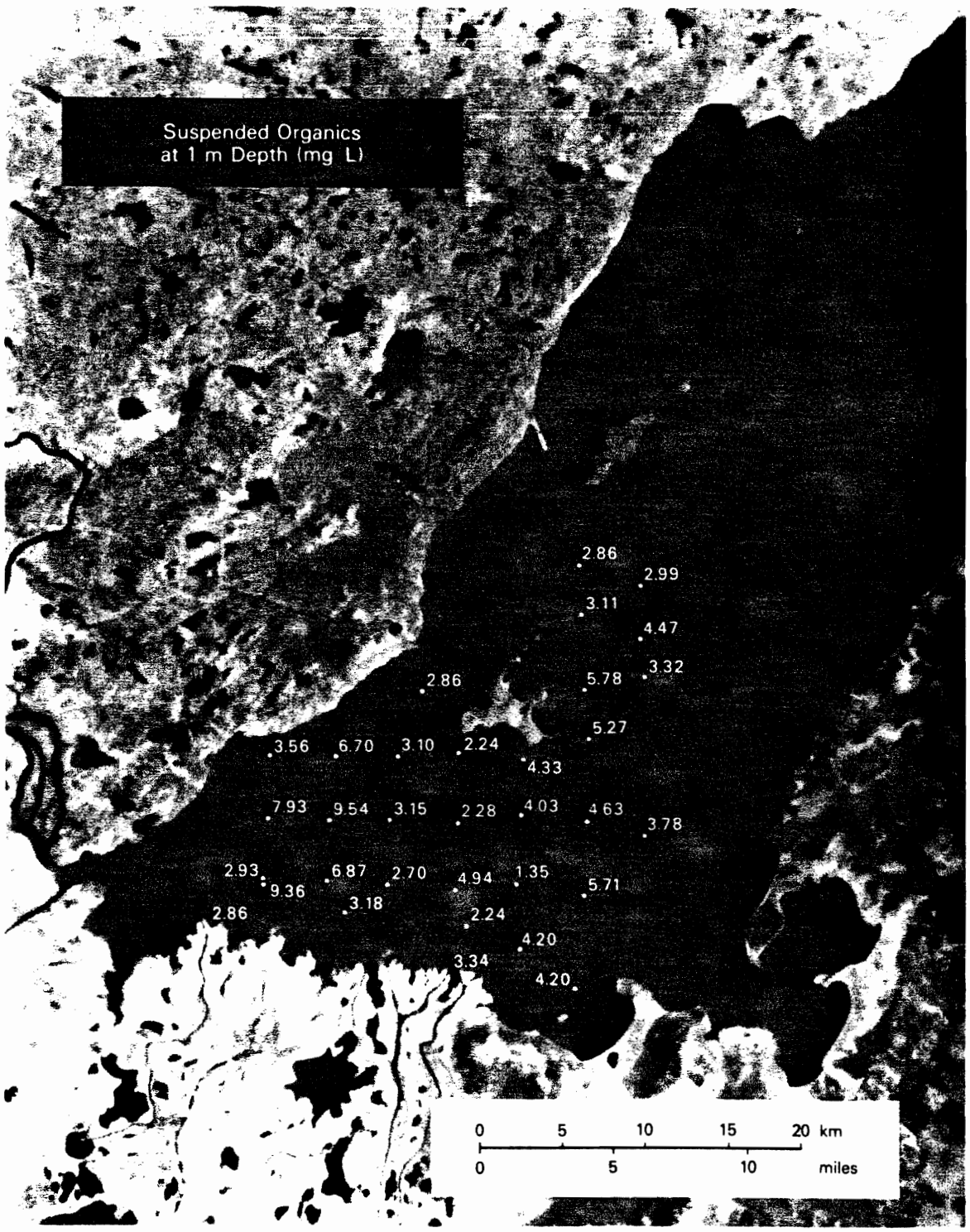

Figure 6. Continued

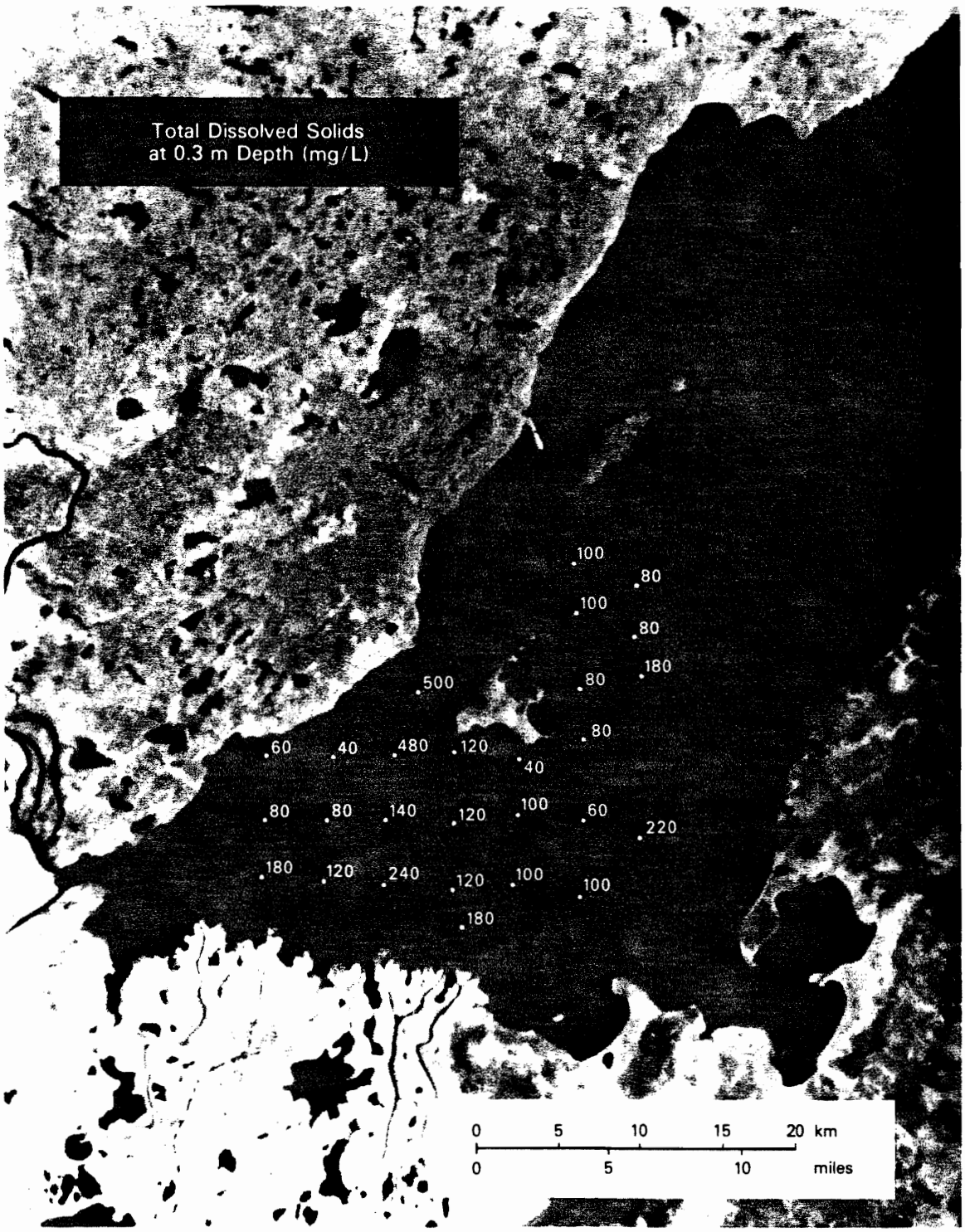

Figure 6. Continued

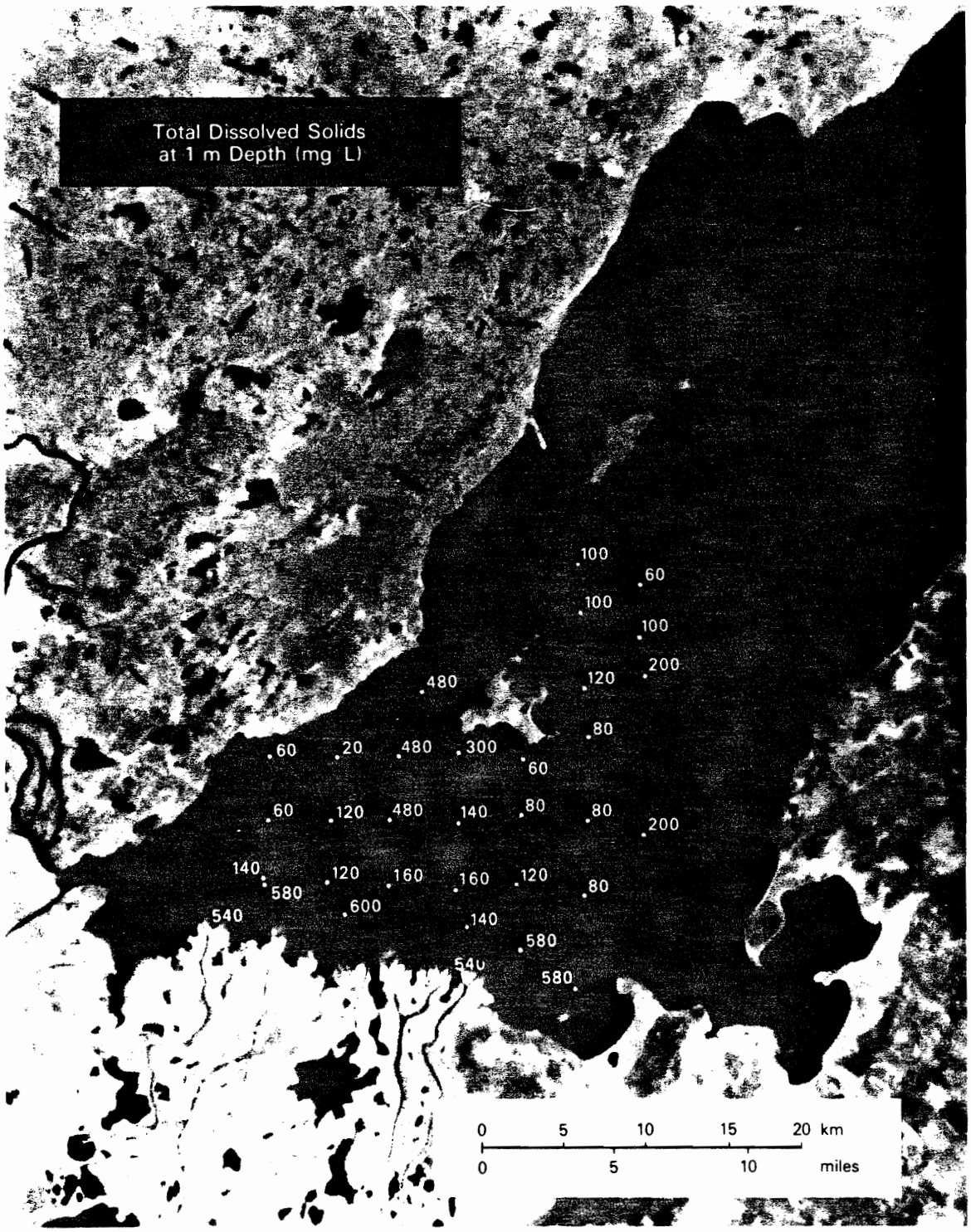

Figure 6. Conclusion

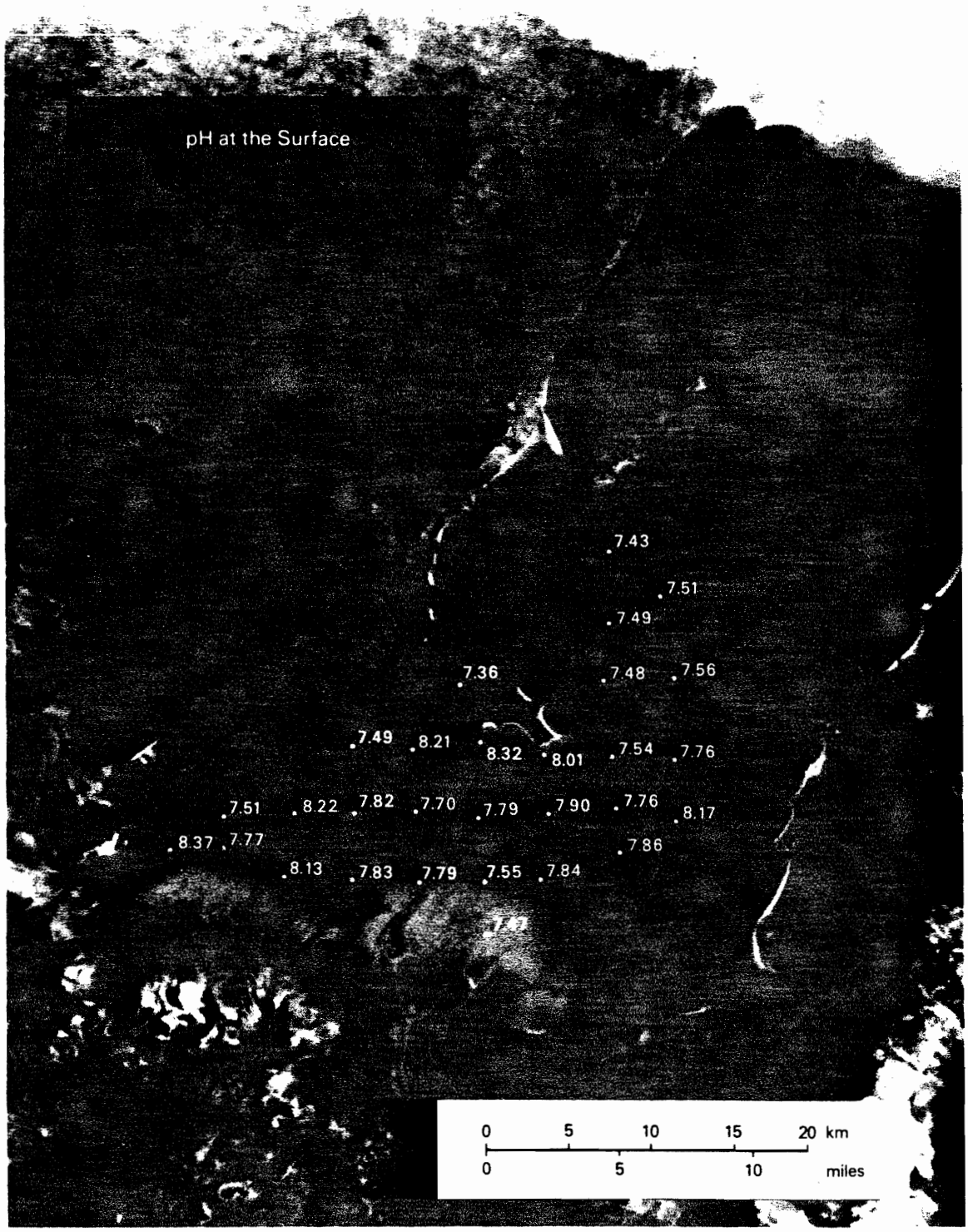

Figure 9. Water Quality Data, August, 1981
(continued from text)

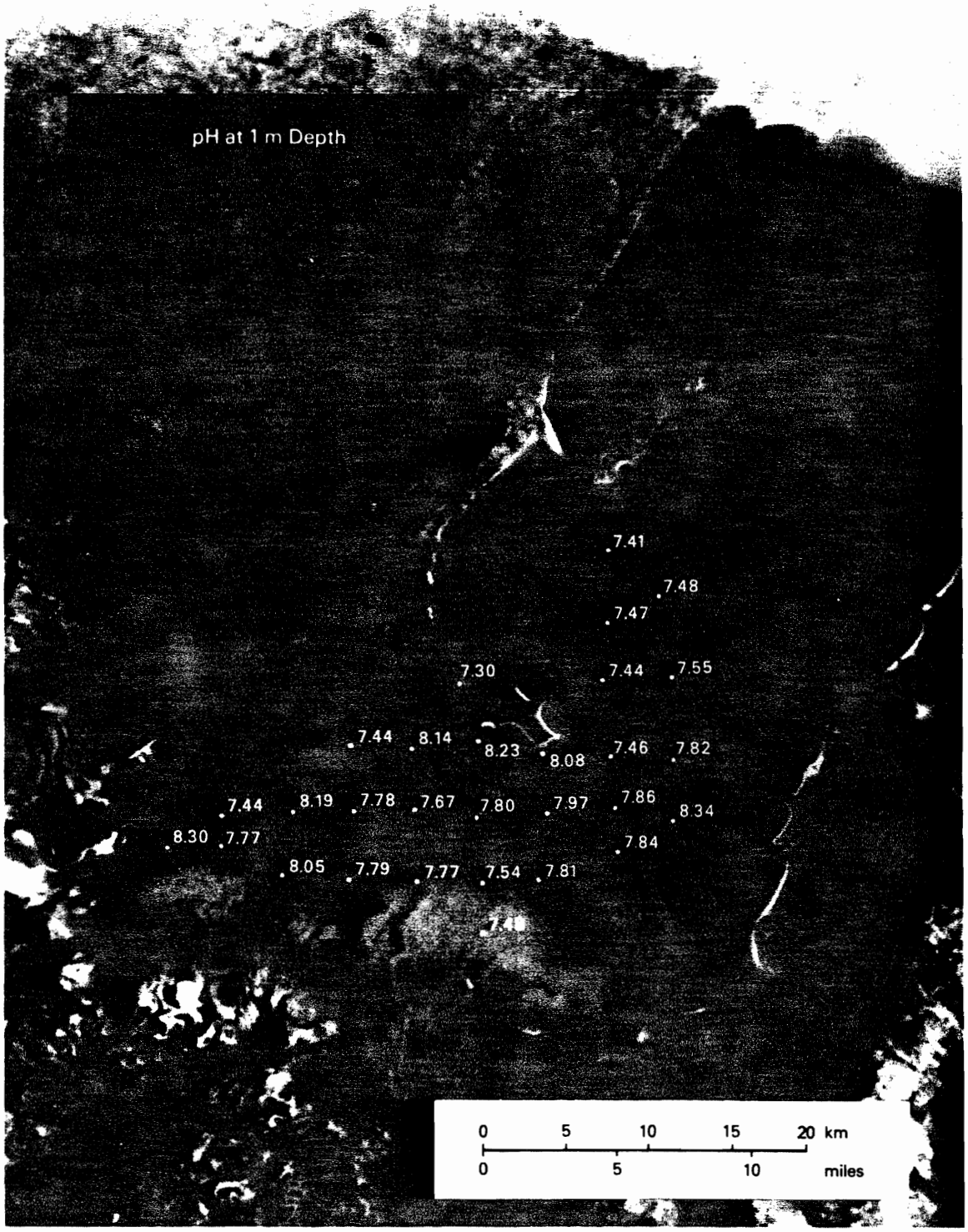

Figure 9. Continued

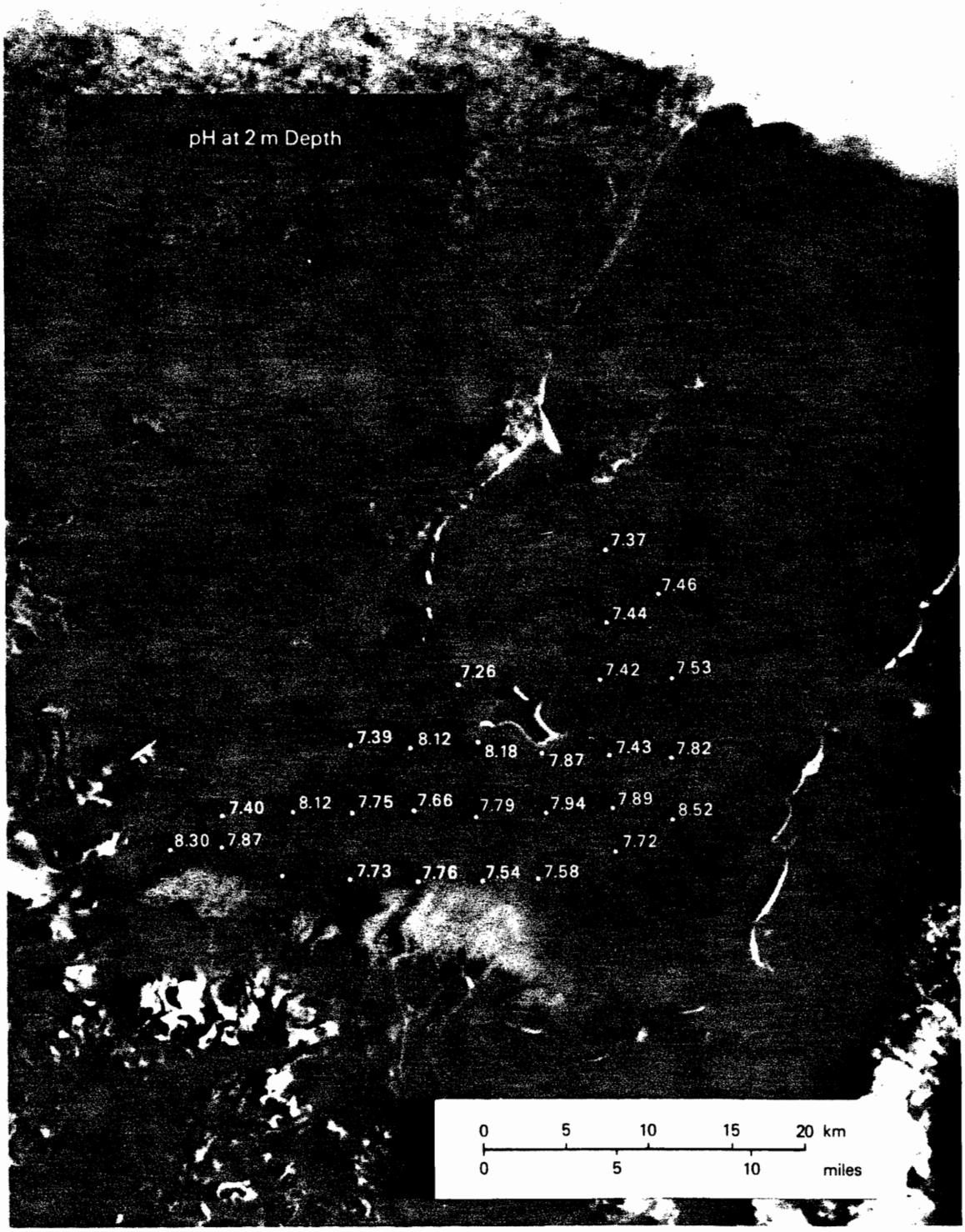

Figure 9. Continued

Figure 9. Continued

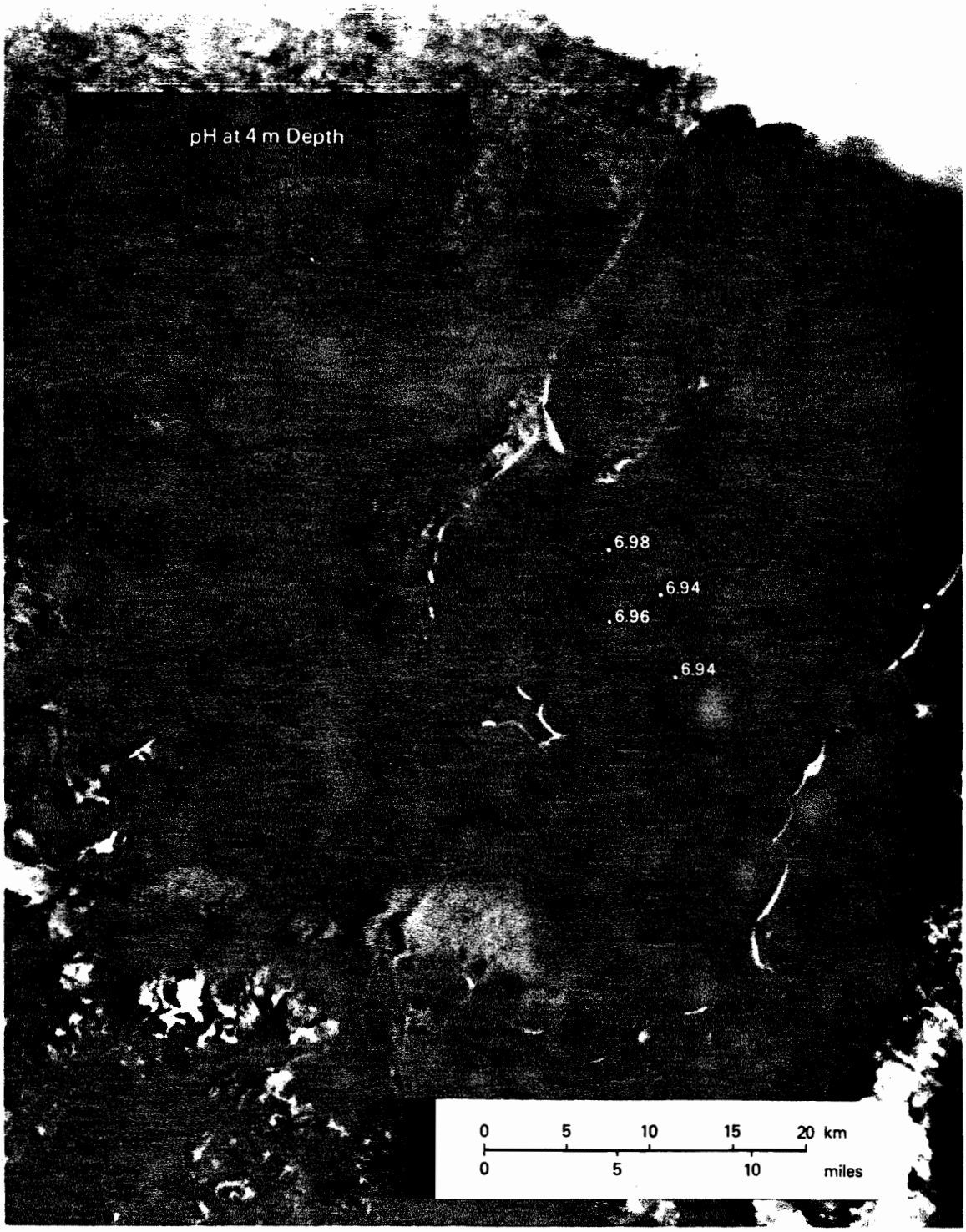

Figure 9. Continued

Figure 9. Continued

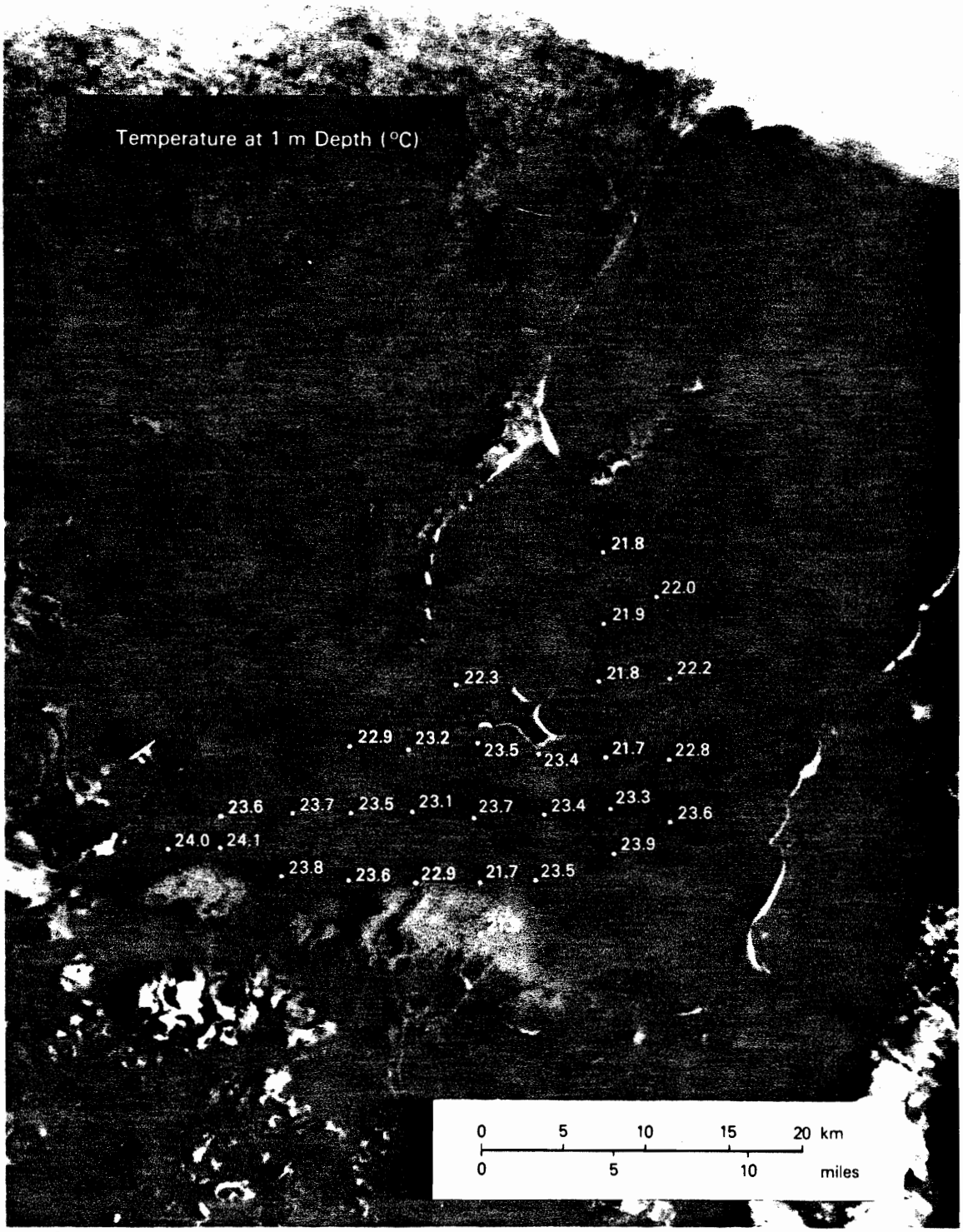

Figure 9. Continued

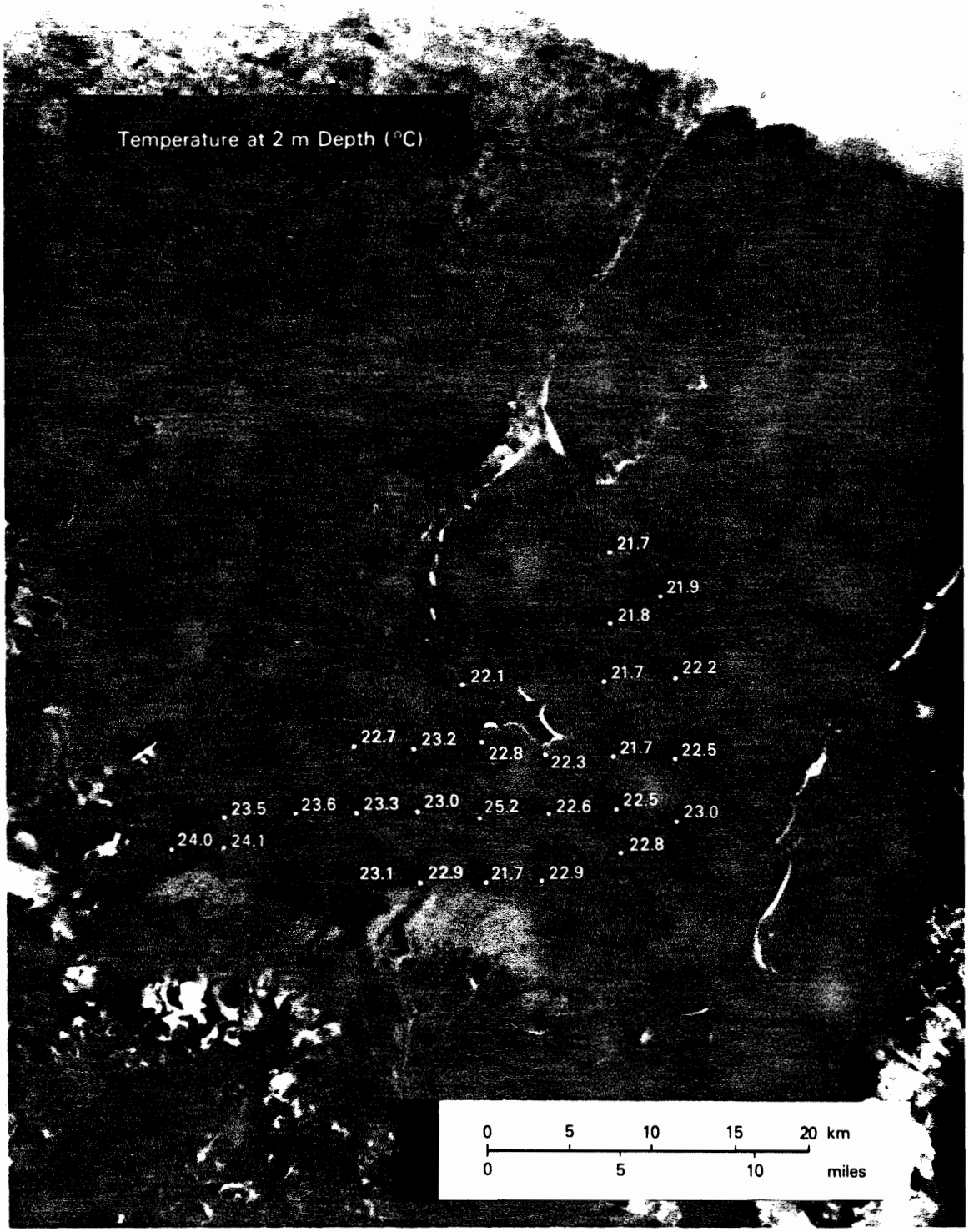

Figure 9. Continued

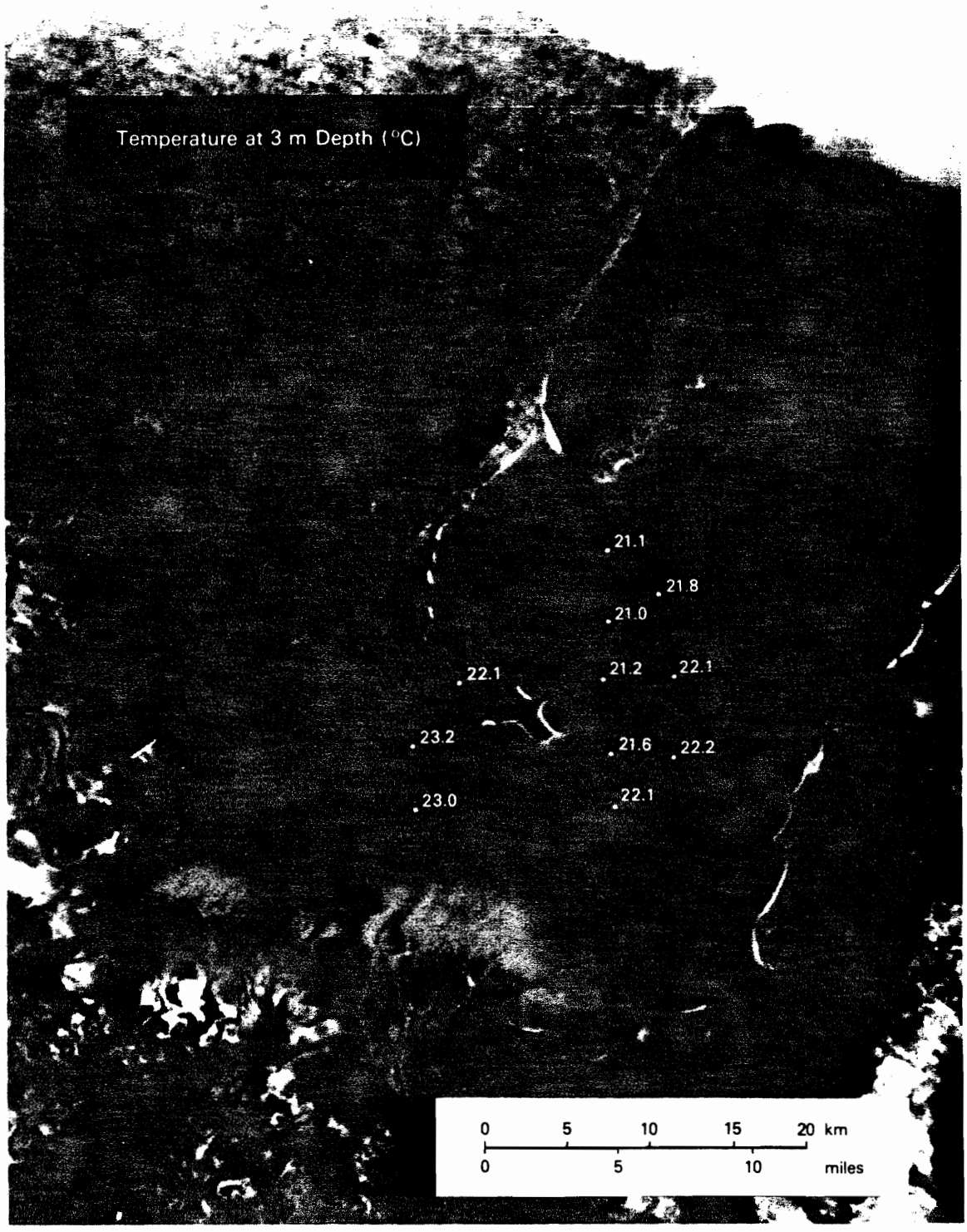

Figure 9. Continued

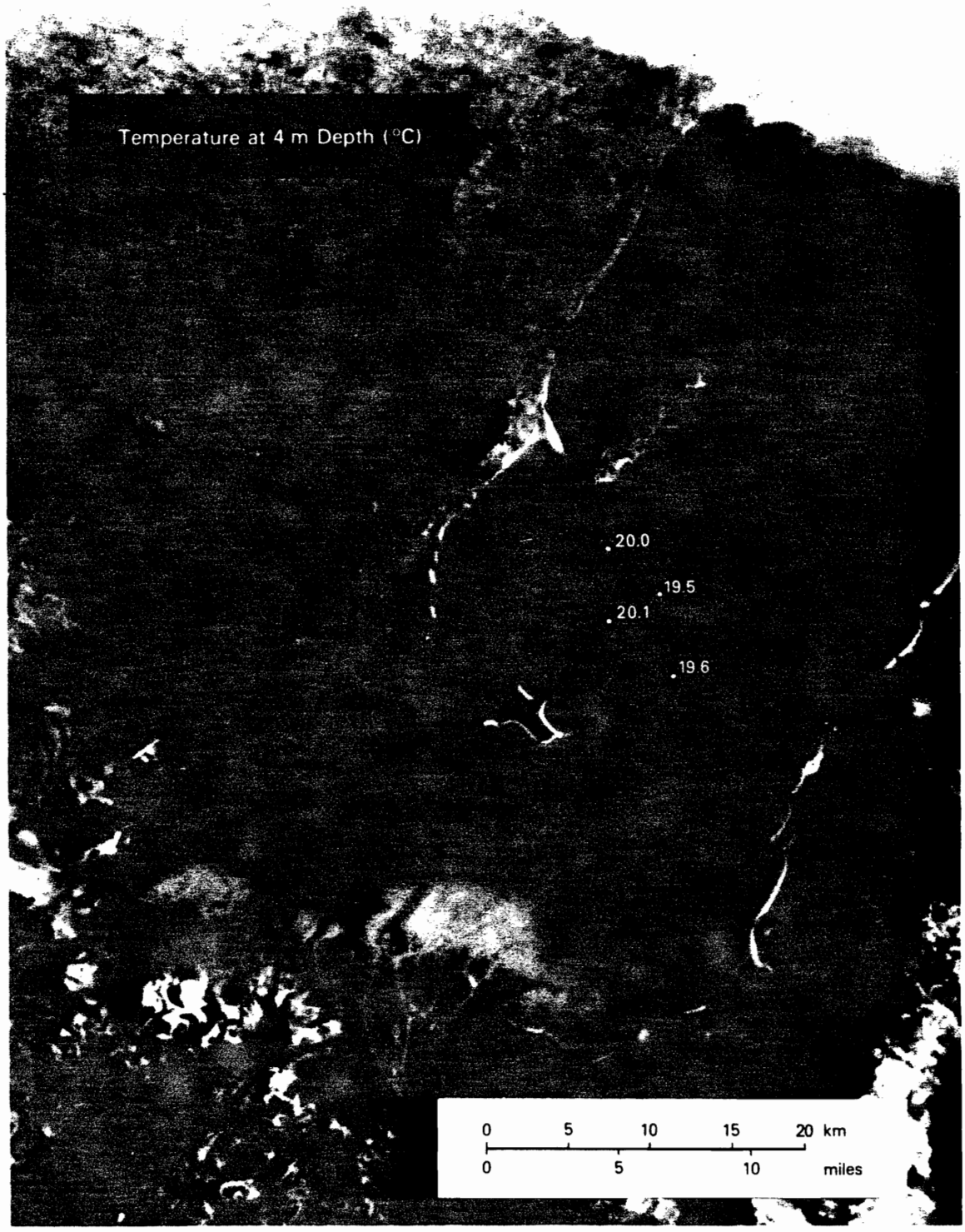

Figure 9. Continued

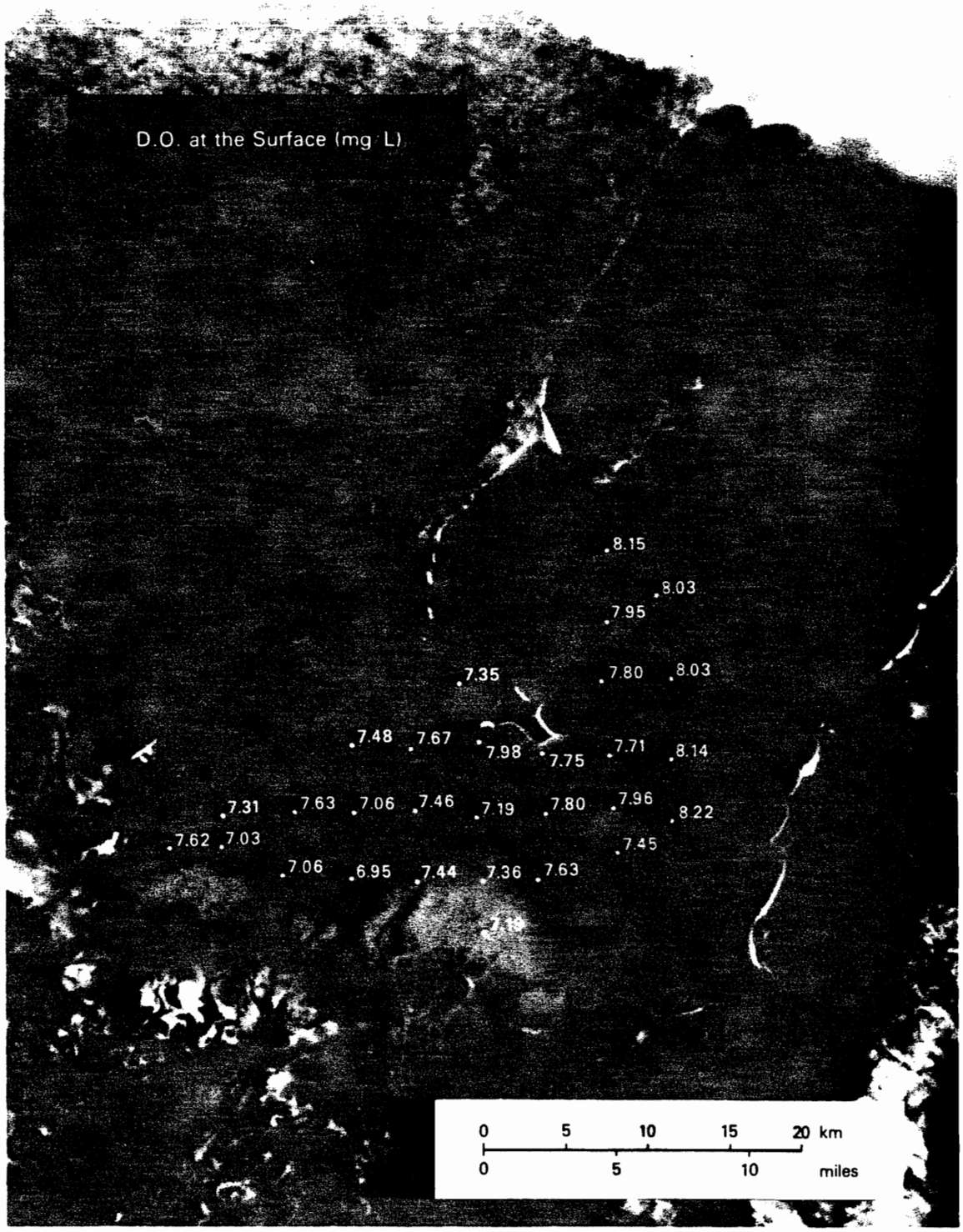

Figure 9. Continued

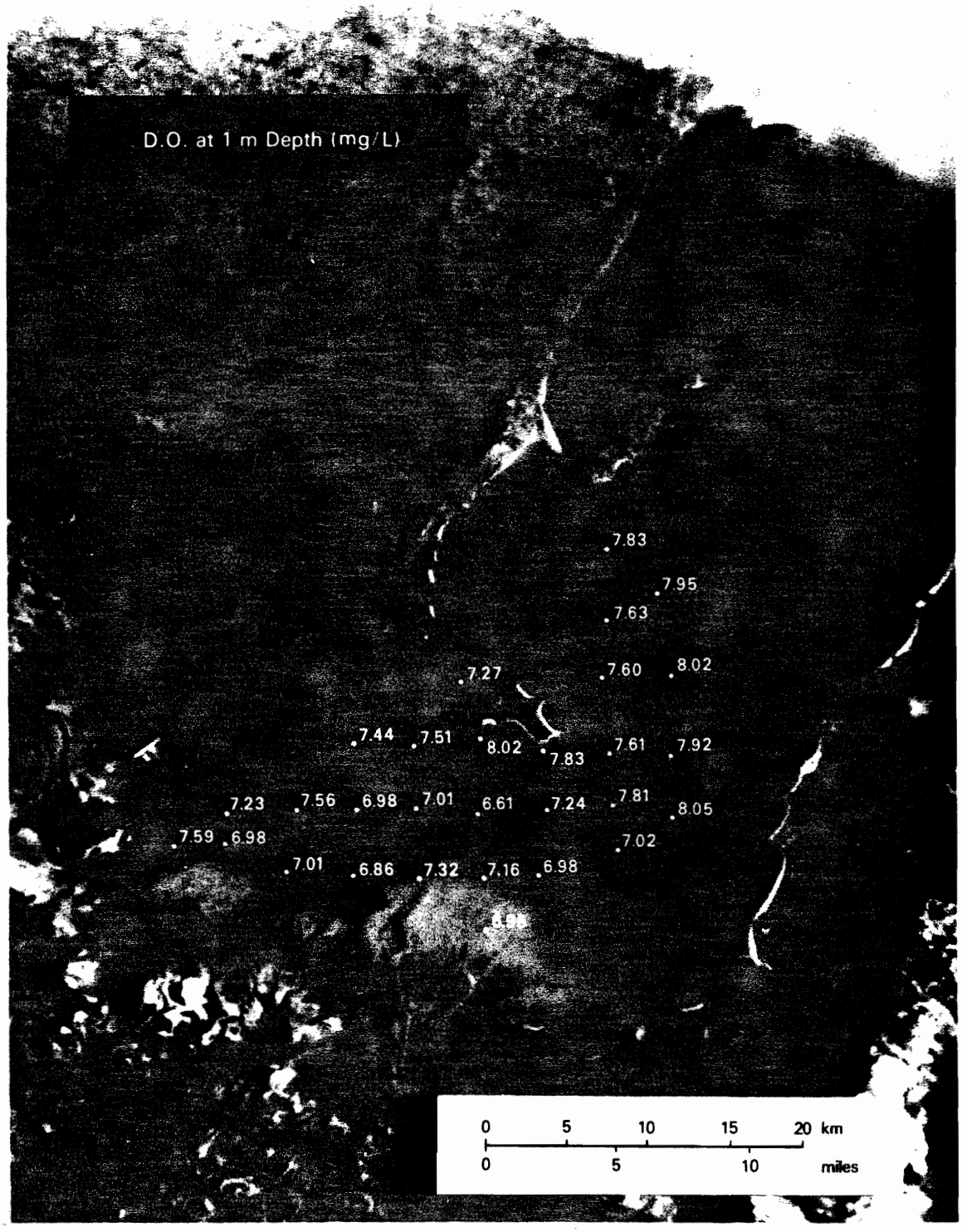

Figure 9. Continued

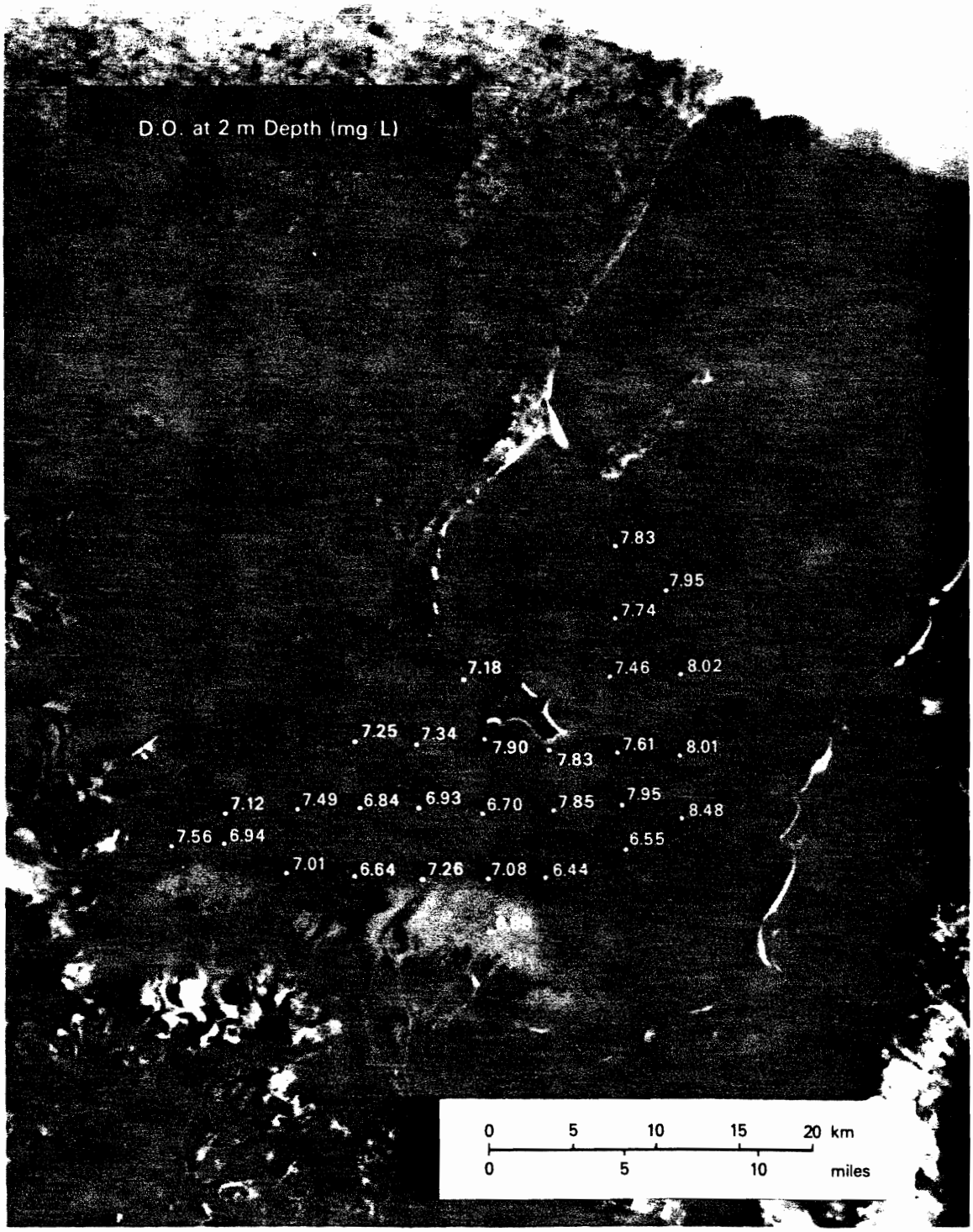

Figure 9. Continued

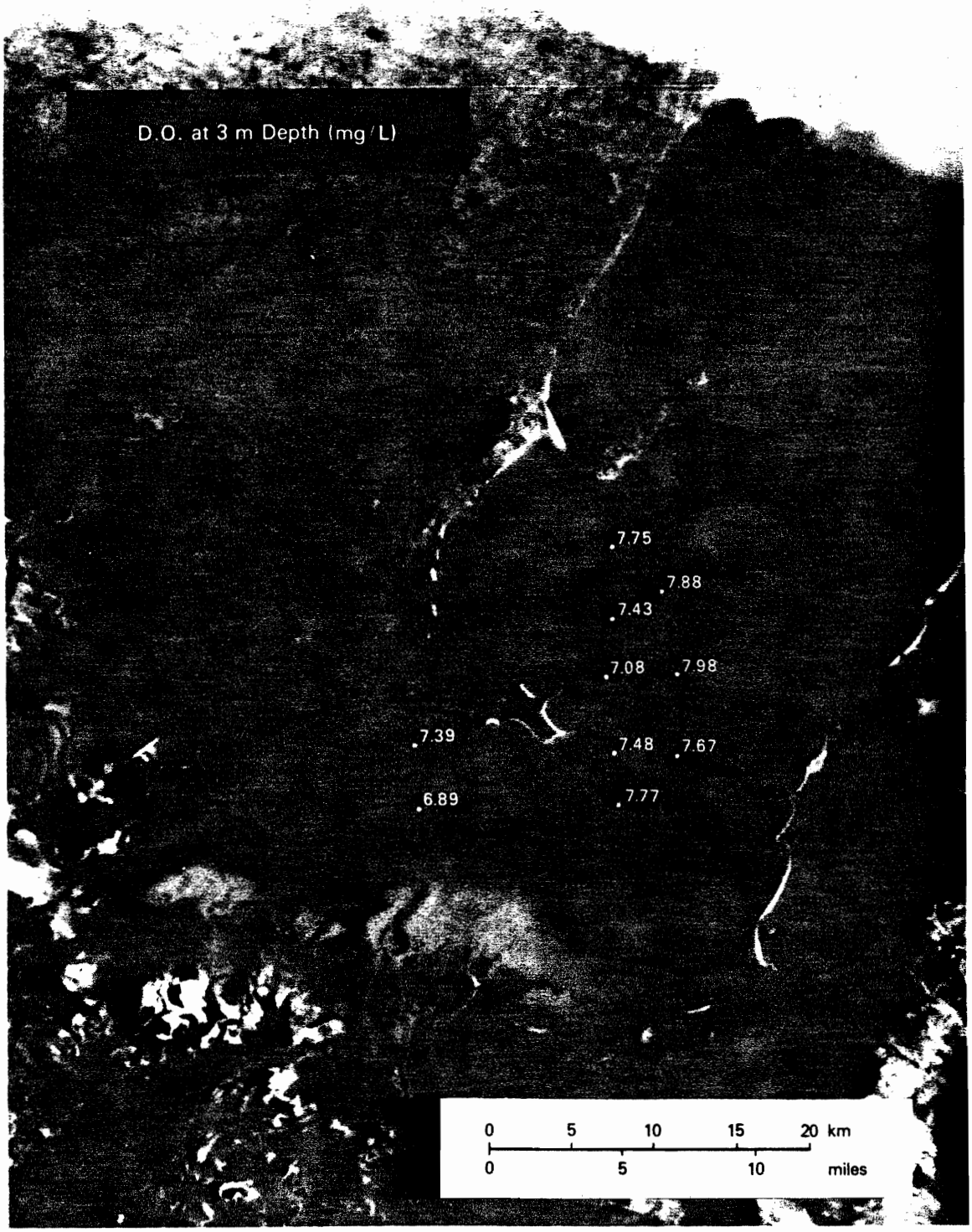

Figure 9. Continued

Figure 9. Continued

Figure 9. Continued

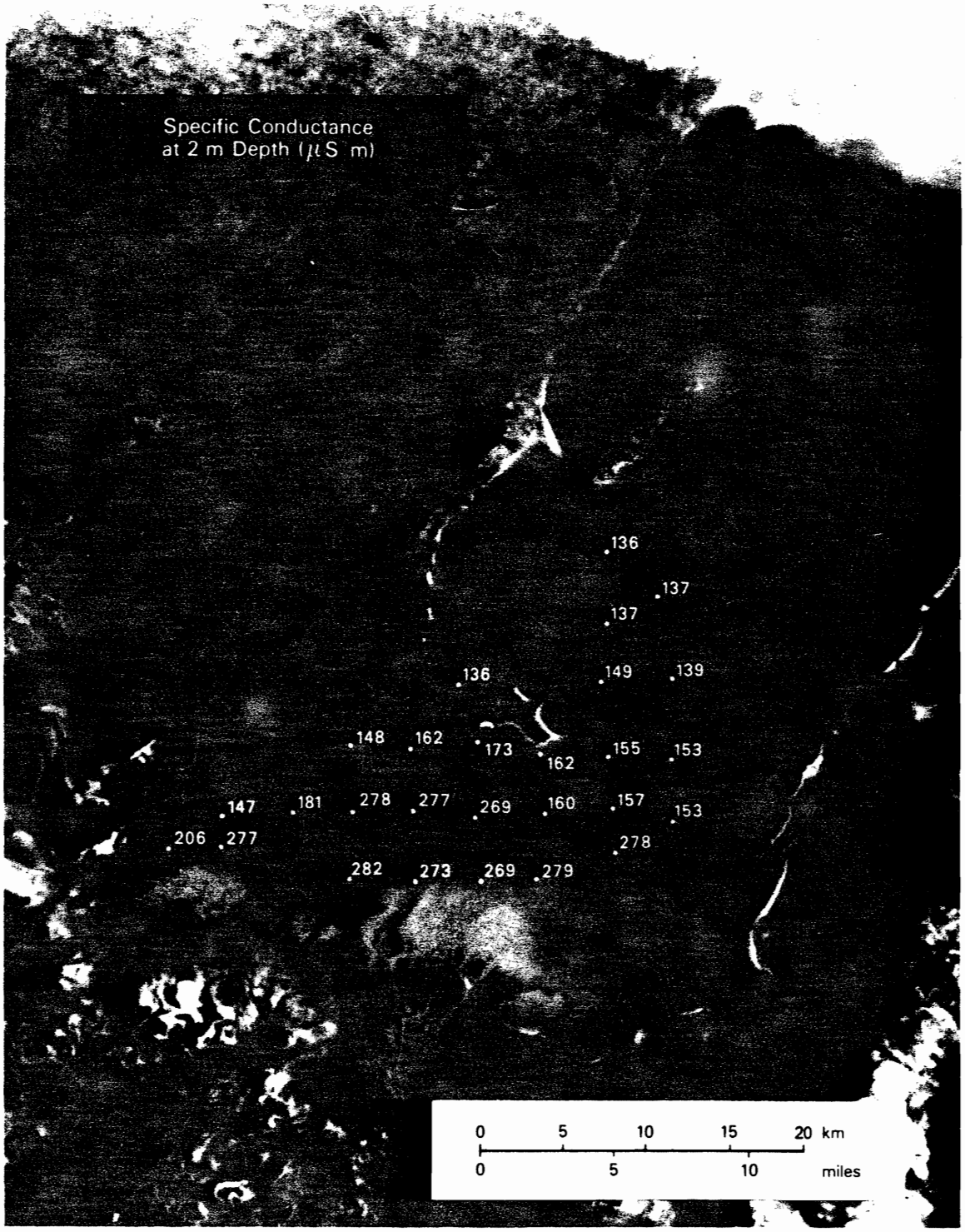

Figure 9. Continued

Figure 9. Continued

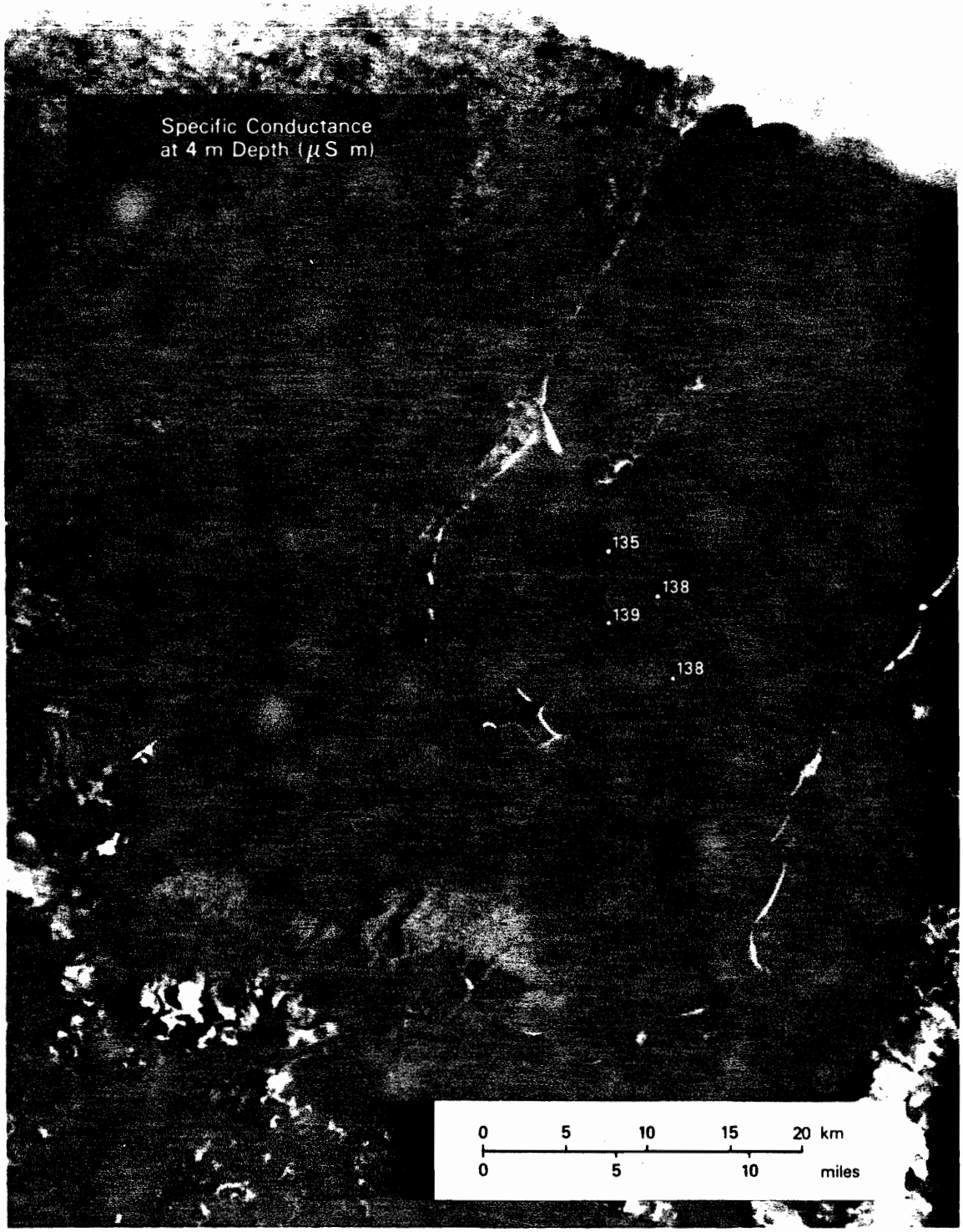

Figure 9. Continued

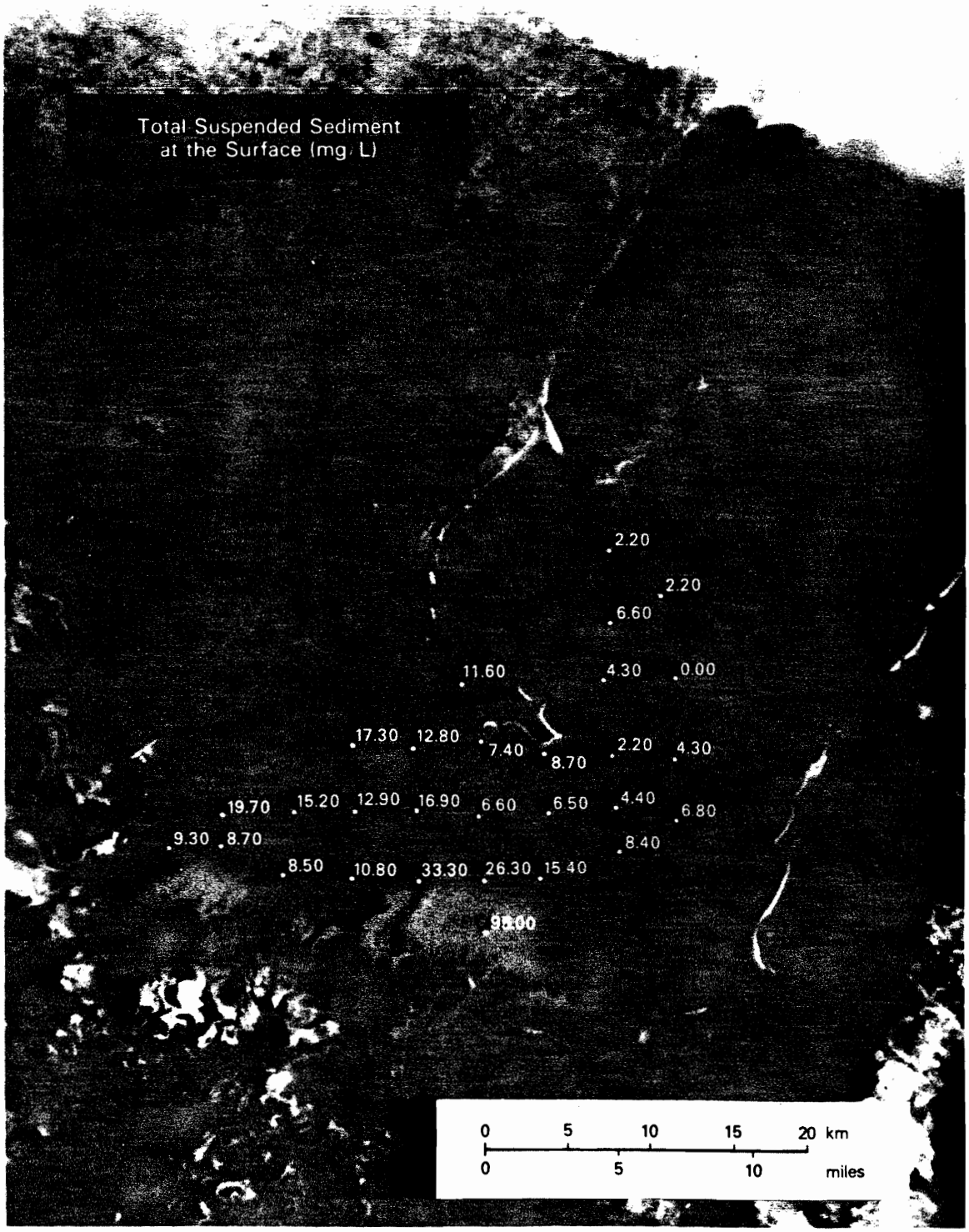

Figure 9. Continued

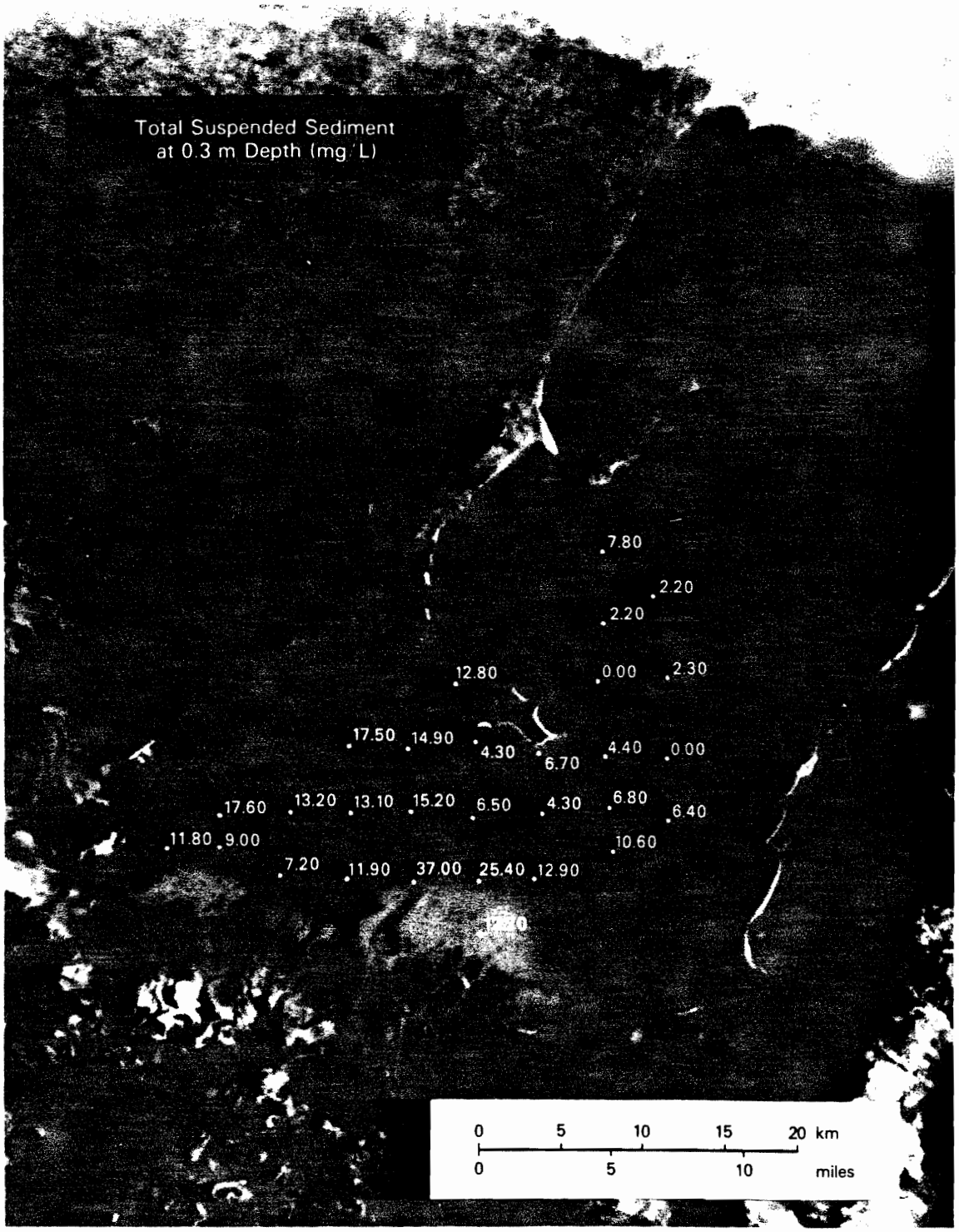

Figure 9. Continued

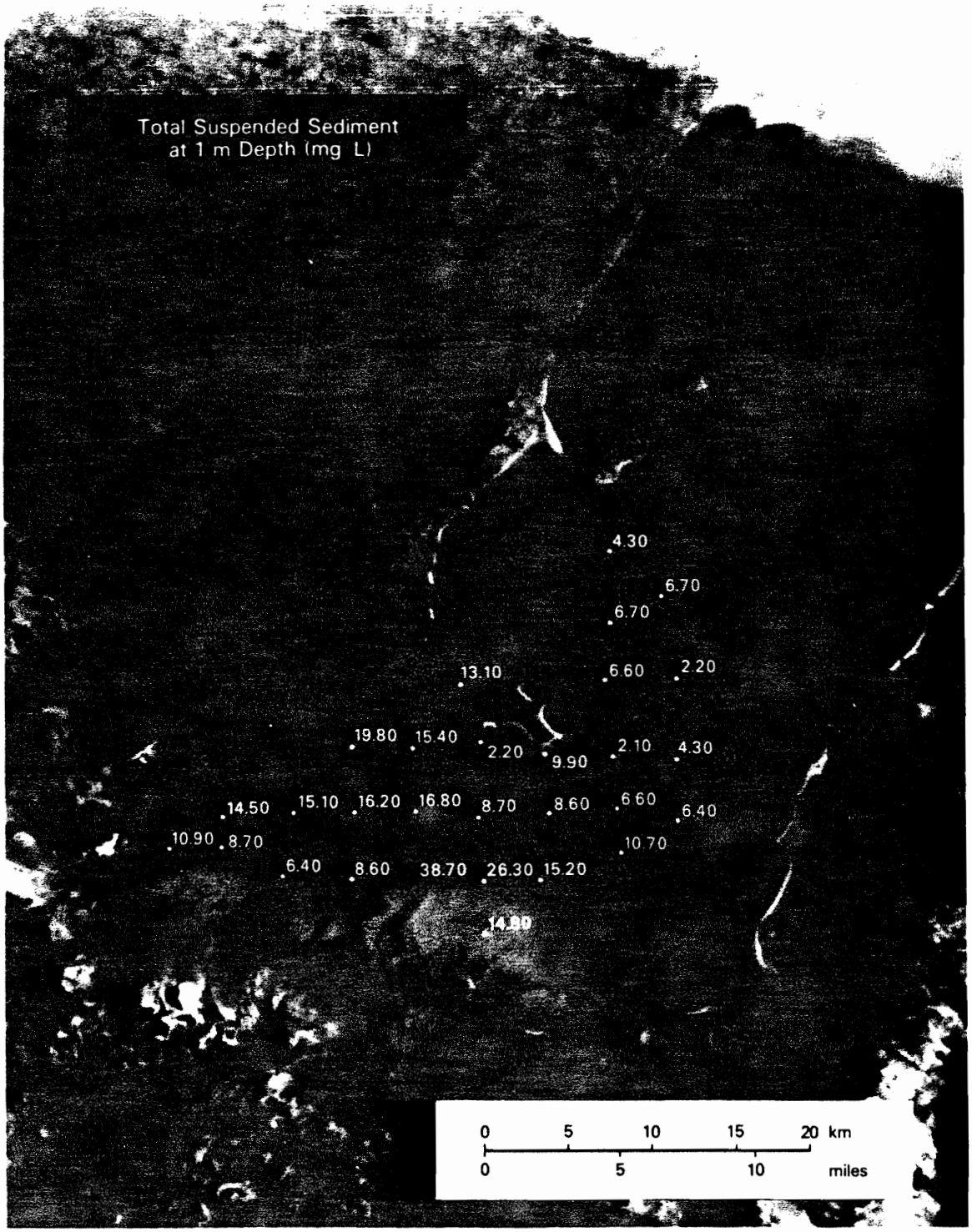

Figure 9. Continued

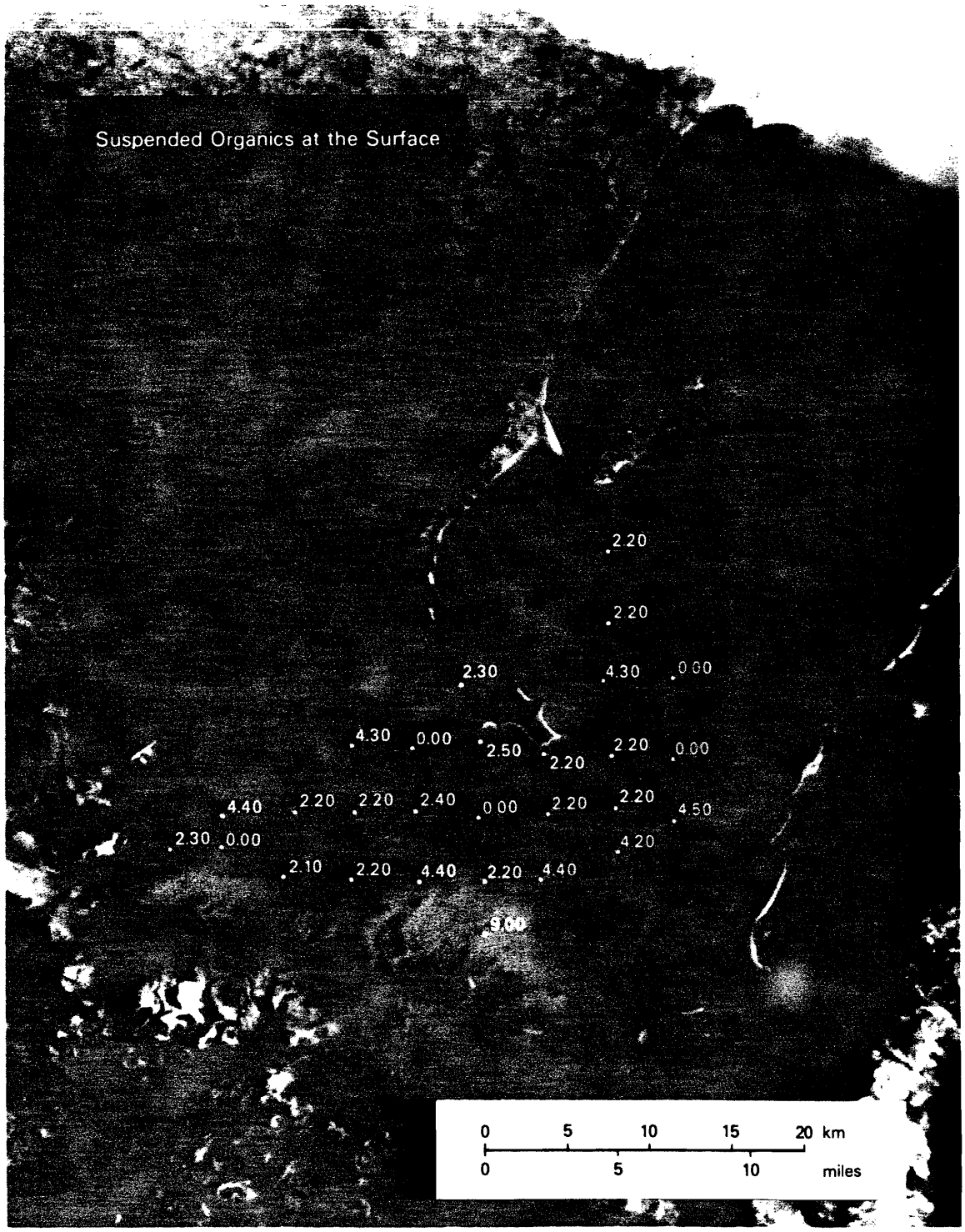

Figure 9. Continued

Figure 9. Continued

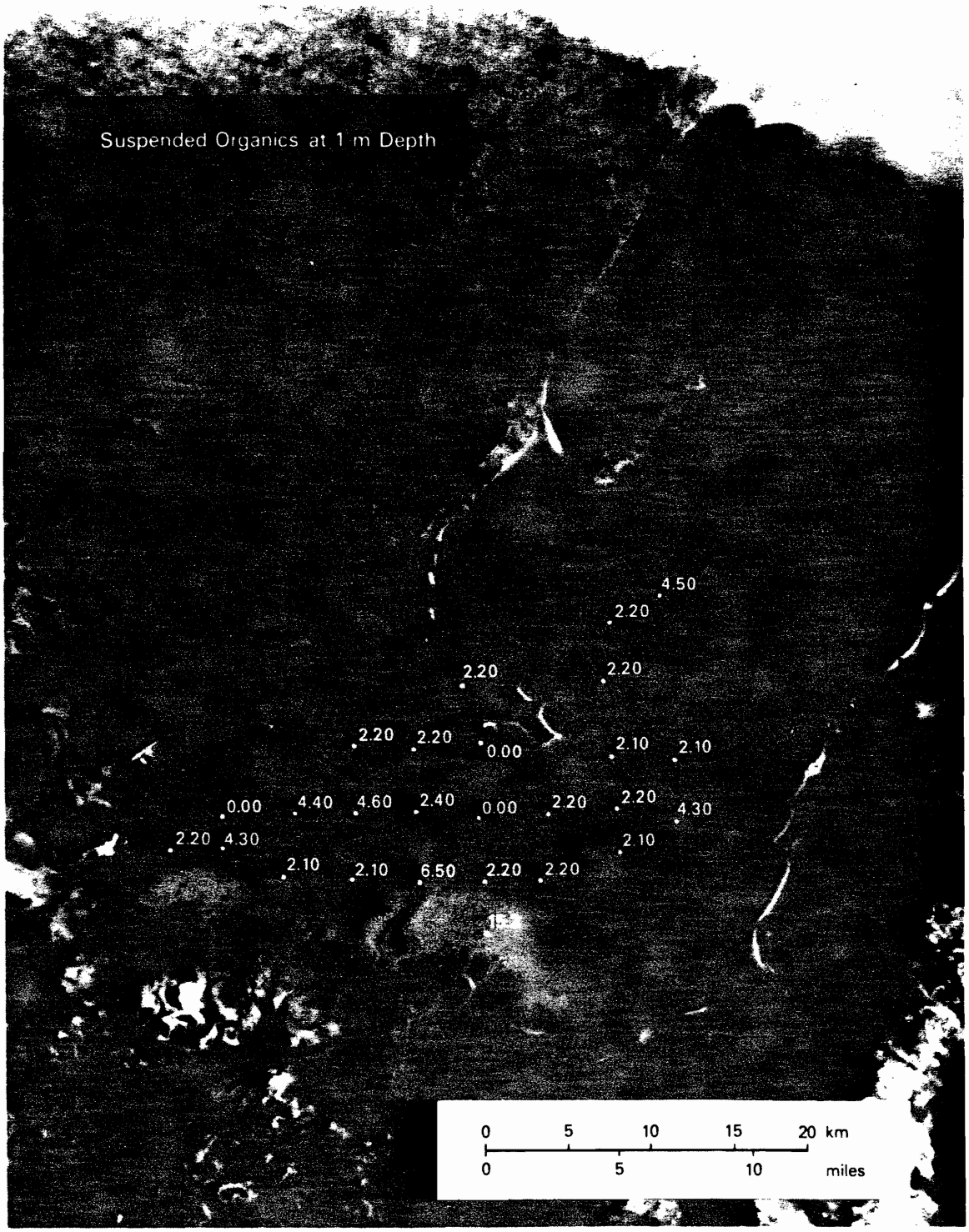

Figure 9. Continued

Figure 9. Continued

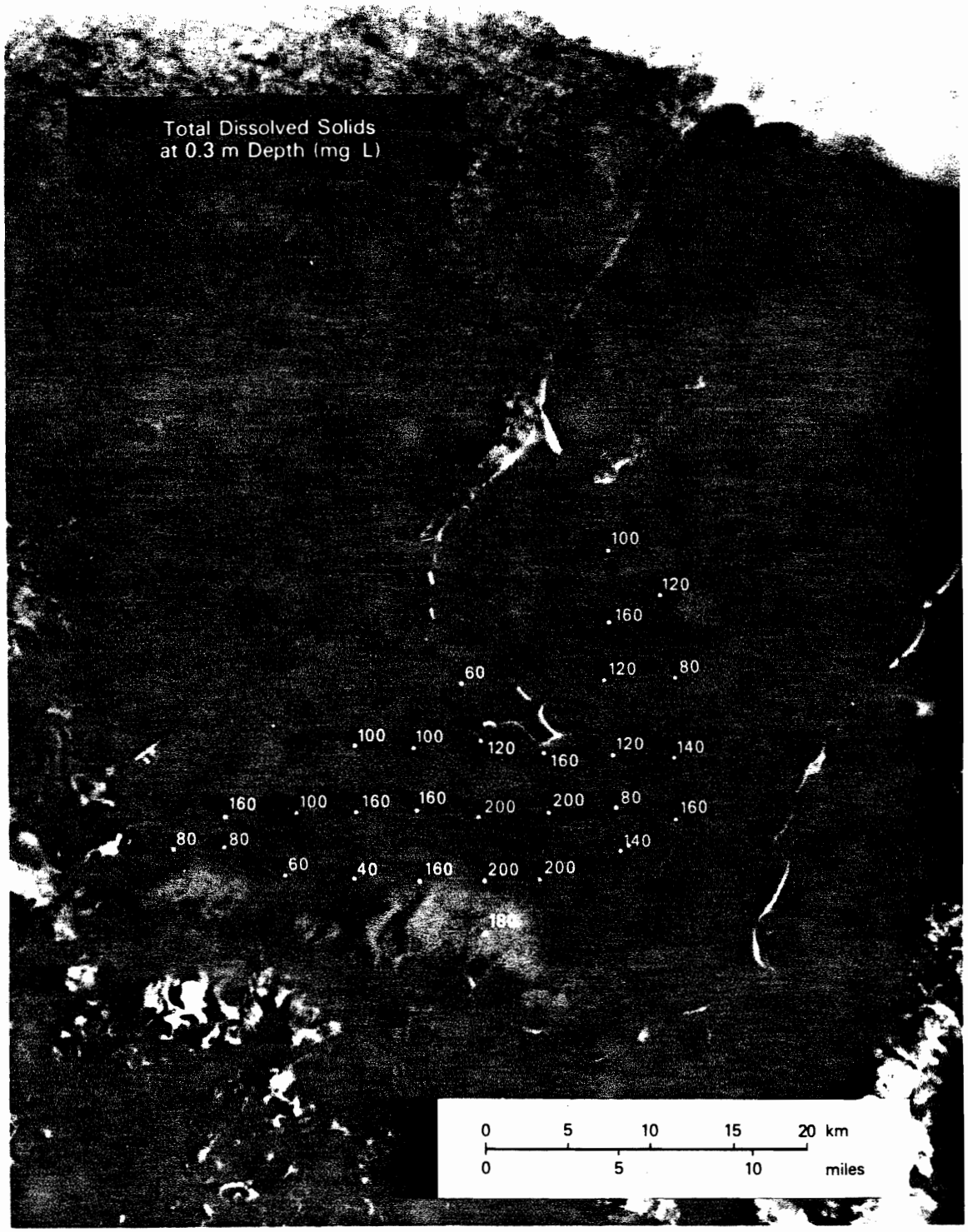

Figure 9. Continued

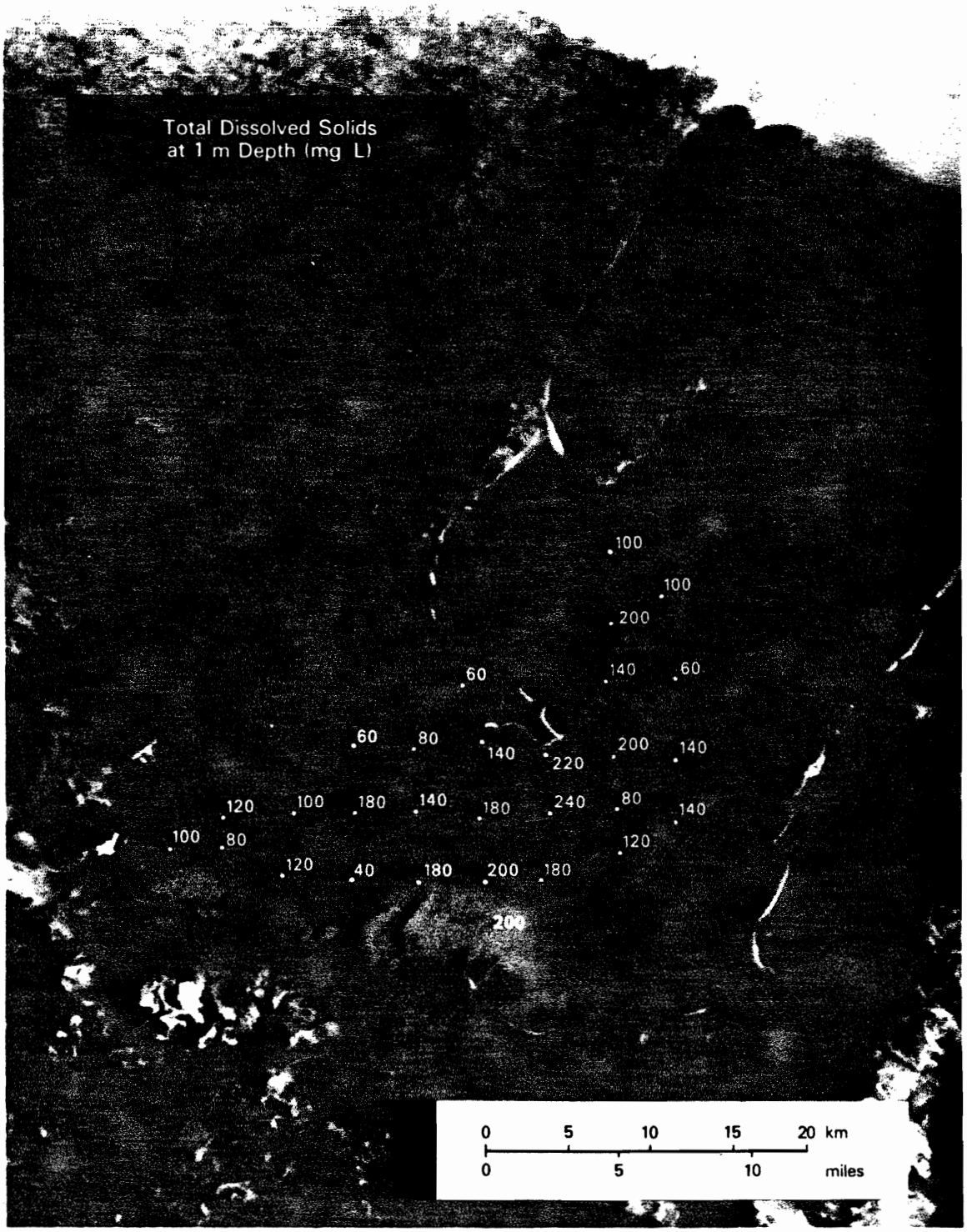

Figure 9. Continued

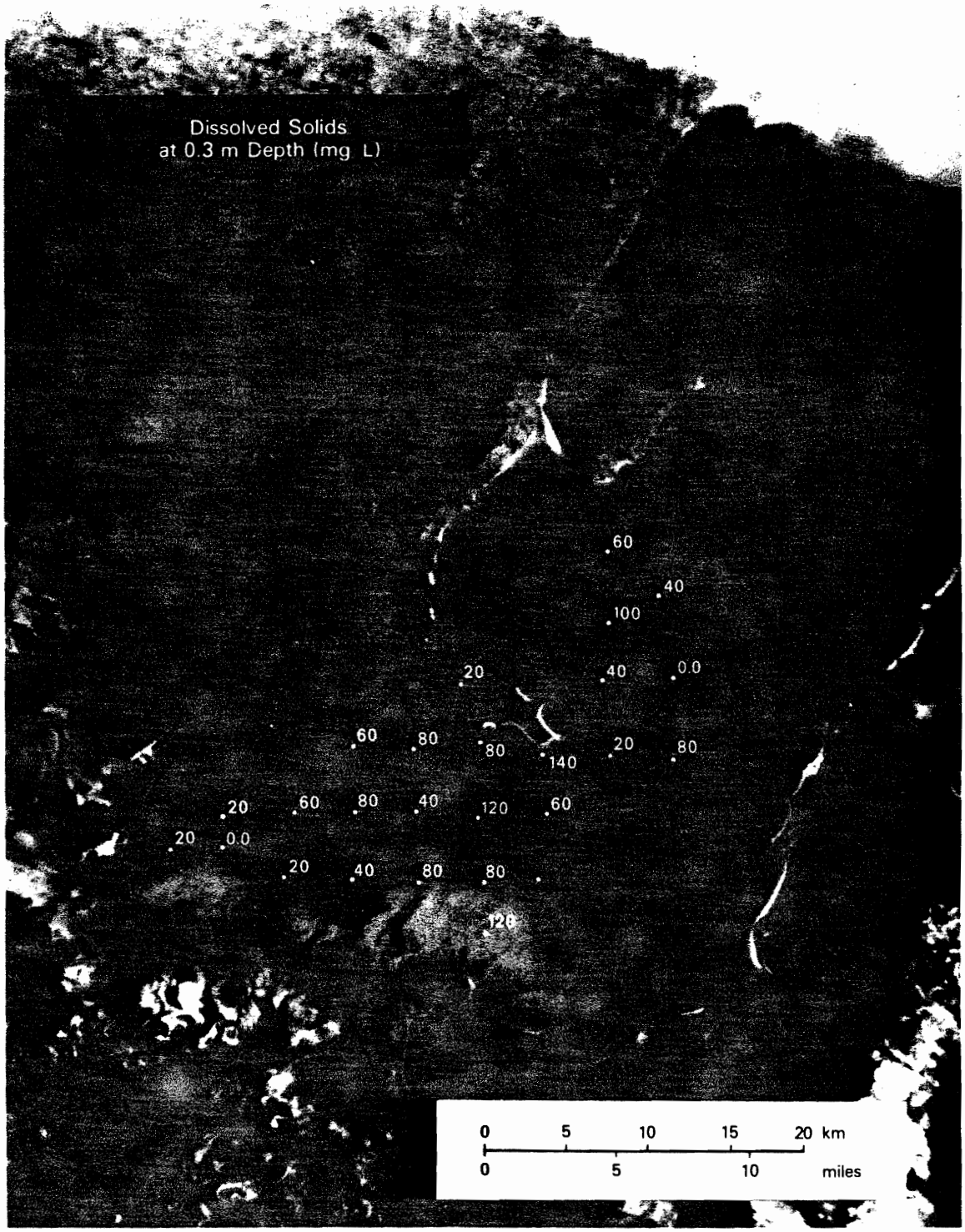

Figure 9. Continued

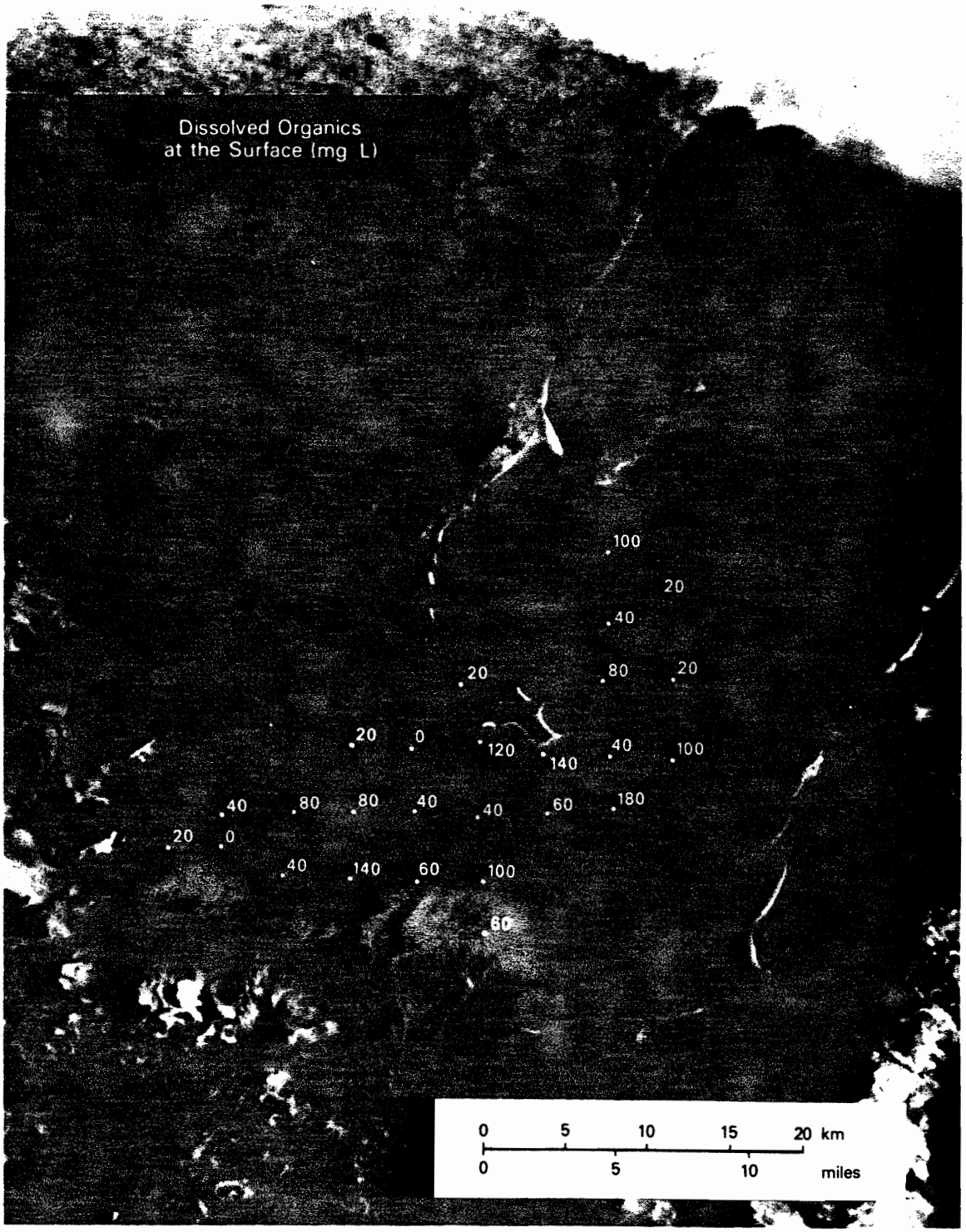

Figure 9. Continued

Figure 9. Conclusion